THÈSE

Pour obtenir le grade de

DOCTEUR DE L'UNIVERSITÉ GRENOBLE ALPES

École doctorale : MSTII - Mathématiques, Sciences et technologies de l'information, Informatique
Spécialité : Informatique
Unité de recherche : Laboratoire des Sciences pour la Conception, l'Optimisation et la Production de Grenoble

Plongements isométriques PL de surfaces plates

PL isometric embeddings of flat surfaces

Présentée par :

Florent TALLERIE

Direction de thèse :

Francis LAZARUS DIRECTEUR DE RECHERCHE, CNRS DELEGATION ALPES	Directeur de thèse

Rapporteurs :

XAVIER GOAOC
PROFESSEUR DES UNIVERSITES, UNIVERSITE DE LORRAINE
GABRIELA WEITZE-SCHMITHÜSEN
FULL PROFESSOR, UNIVERSITÄT DES SAARLANDES

Thèse soutenue publiquement le **10 octobre 2024**, devant le jury composé de :

REMI COULON, DIRECTEUR DE RECHERCHE, CNRS DELEGATION CENTRE-EST	Président
FRANCIS LAZARUS, DIRECTEUR DE RECHERCHE, CNRS DELEGATION ALPES	Directeur de thèse
XAVIER GOAOC, PROFESSEUR DES UNIVERSITES, UNIVERSITE DE LORRAINE	Rapporteur
GABRIELA WEITZE-SCHMITHÜSEN, FULL PROFESSOR, UNIVERSITÄT DES SAARLANDES	Rapporteure
ERWAN LANNEAU, PROFESSEUR DES UNIVERSITES, UNIVERSITE GRENOBLE ALPES	Examinateur
ALBA MARINA MALAGA SABOGAL, MAITRESSE DE CONFERENCES, UNIVERSITE DE LORRAINE	Examinatrice
THIERRY MONTEIL, CHARGE DE RECHERCHE, CNRS ILE-DEFRANCE VILLEJUIF	Examinateur
VINCENT BORRELLI, MAITRE DE CONFERENCES HDR, UNIVERSITE LYON 1 - CLAUDE BERNARD	Examinateur

À Imane

Remerciements

Je ne saurais initier ces remerciements par autre chose que d'exprimer ma profonde gratitude envers mon directeur de thèse, Francis Lazarus. Francis m'a accueilli et m'a guidé dans le monde merveilleux de la géométrie combinatoire avec toute l'exigence intellectuelle nécessaire à ma bonne formation et évolution dans le monde de la recherche, trouvant habilement le parfait équilibre dans son encadrement entre les directives que je devais suivre et les libertés qu'il me laissait. C'est avec un immense plaisir que je le considère désormais comme un ami, bien qu'il restera toujours pour moi l'exemple à suivre.

Je remercie également l'ensemble des membres de mon jury de thèse. Tout d'abord Gabriela Weitze et Xavier Goaoc qui m'ont fait l'immense honneur de rapporter sur ma thèse. J'exprime ma plus vive gratitude à l'égard de Vincent Borrelli, Rémi Coulon, Erwan Lanneau, Alba Málaga et Thierry Monteil pour avoir accepté de faire partie de mon jury de thèse.

Merci à tous les membres du laboratoire G-SCOP d'avoir apporté un peu de joie de vivre lors de ces trois laborieuses années. Les midis à la cafétéria à siroter mon café tout en échangeant, ou en jouant à la coinche ou au tarot, constituaient autant de pauses bienvenues. Merci ainsi à Ugo, Camille, Félix, Marco, Cléophée, Pascal, Astor, Sami, Ernest et tous ceux que je ne cite pas. Je remercie en particulier les membres de mon équipe de recherche, et tout particulièrement Louis Espéret notre chef d'équipe que je remercie pour sa patience et sa bienveillance. Je remercie de même mes actuels co-bureaux : Thomas Suzan, avec qui j'ai longuement échangé mathématiques ou informatique, Estefania avec qui j'ai expérimenté la fermentation sous les conseils avisés de Marthe Bonamy, mais aussi Ugo Giocanti qui a été mon compagnon de fortune au 5-B en première année.

Merci également aux membres de l'Institut Fourier qui m'ont accueilli malgré mon léger éloignement thématique, et en particulier à Julien Boulanger qui a été l'initiateur de mon itinérance entre le G-SCOP et l'IF.

Si j'ai eu l'occasion d'enseigner à l'université, c'est en grande partie grâce à Nadia Brauner qui m'a fait confiance alors que je n'étais qu'un petit doctorant en première année et je l'en remercie. Je remercie aussi Mario Cortes Cornax qui m'a reçu dans l'équipe pédagogique de bases de données et qui a été extrêmement présent et attentif afin que nous puissions proposer aux étudiants le meilleur encadrement possible.

Je tenais également à rendre grâce à mes collaborateurs et tous les enseignants-chercheurs avec qui j'ai discuté de mes travaux et qui ont partagé avec moi leur savoir. Ainsi, je remercie le trio Pierre Arnoux, Samuel Lelièvre et Alba Malaga pour avoir pris la patience de nous expliquer leur travaux sur les diplotores, Vincent Delecroix pour nous avoir pointé quelques références sur la compactification des espaces de modules de surfaces de translation, Martin Möller pour nous avoir expliqué la structure du bord de $\mathcal{H}(2)$ au

Résumé

Cette thèse porte sur les plongements isométriques PL de surfaces plates de petit genre ($g = 0, 1, 2$). Nous y présentons trois résultats originaux. Le premier concerne une méthode générique due à Burago et Zalgaller, détaillée dans leur article de 1995, pour plonger PL isométriquement une surface polyédrale quelconque. Alors qu'une des étapes de cette méthode repose sur le procédé non constructif de Nash-Kuiper, nous donnons une implémentation effective dans le cas des tores plats. La méthode de Burago et Zalgaller, bien que générique, ne permet pas de réaliser de manière uniforme, c'est-à-dire avec un nombre borné de sommets, une famille de surfaces polyédrales - par exemple la famille des tores plats. Nous construisons dans un second temps une triangulation universelle pour les tores plats, c'est-à-dire une triangulation T du tore qui, pour tout tore plat, admet une réalisation géométrique isométrique à ce tore plat, affine sur chaque triangle de T. Enfin, nous exhibons des plongements isométriques PL relativement simples de surfaces de translation de genre 2. Ces modèles peuvent être aisément utilisés à des fins de visualisation, et nous avons ainsi pu en réaliser par impression 3D ou par pliage papier. De manière générale, les surfaces de translation forment des espaces, dits de modules, stratifiés par le genre et la nature des singularités. La compréhension de ces espaces faisant intervenir des notions mathématiques délicates, nous avons choisi de présenter soigneusement les concepts utilisés dans le second chapitre. En genre 2, il n'y a que deux strates : $\mathcal{H}(2)$ et $\mathcal{H}(1, 1)$. Bien que nos modèles pour $\mathcal{H}(2)$ ne recouvrent pas la totalité de la strate, ils permettent de réaliser un ouvert de $\mathcal{H}(2)$ relativement important, comme il est décrit dans cette thèse.

Abstract

This thesis deals with PL isometric embeddings of flat surfaces of small genus ($g = 0, 1, 2$). We present inside three original results. The first one is about a generic method due to Burago and Zalgaller, which is detailed in their article of 1995, in order to PL isometrically embed any polyhedral surface. Although one of the steps of this method is based on the non constructive Nash-Kuiper process, we give an effective implementation in the case of flat tori. The method of Burago and Zalgaller, though generic, does not allow to uniformly realize, namely with a bounded number of vertices, a family of polyhedral surfaces - for instance the family of flat tori. We build in a second time a universal triangulation for flat tori, i.e. a triangulation T of the torus which, for every flat torus, admits a geometric realization isometric to this flat torus, linear in restriction to each triangle of T. Finally, we exhibit relatively simple PL isometric embeddings of genus 2 translation surfaces. This models can be easily used to visualization ends, and we were able to realize some ones by 3D printing or by paper folding. Generally, translation surfaces form spaces called moduli spaces, stratified by the genus and the nature of the singularities. Non trivial notions are involved to understand these spaces, and we chose to thoroughly present the concepts used in the second chapter. In genus 2, there is only two strata: $\mathcal{H}(2)$ and $\mathcal{H}(1, 1)$. Whereas our models for $\mathcal{H}(2)$ do not cover the entire strarum, they permit to realize a relatively important open subset of $\mathcal{H}(2)$, as we describe in this thesis.

Contents

Preface

This thesis gathers works on PL isometric embeddings of flat surfaces of small genus. While the mathematical background needed to understand this report is modest, it relies however on deep mathematical concepts about translation surfaces also known as Abelian differentials, and we chose to present in the Preliminaries a complete and almost self-contained introduction to our research field, often recalling well known definitions and constructions. The reader already aware of these mathematical foundations may skip this introductory chapter without inconvenience, going straight to chapter 3 for the state of the art, or to chapters 4, 5, 6 for our contribution, while the non familiar reader can benefit from our attempt to explain as well as possible such a rich and interesting theory, referring to the bibliography to deepen the discussion we just touch upon. These mathematical concepts turn out, though, to be if not essential, at least very useful to finalize the results presented in this thesis. Indeed, while the genus 1 case appeared to be relatively easily manageable, the case of flat surfaces of genus 2 is much harder and seems to rely on subtle theories that we did not yet fully exploit. In practice, we succeeded to reduce most of our problems to elementary geometry that nonetheless required a great deal of inventiveness. While at the beginning of this thesis, the experimental and algorithmic aspect was dominant, the need of profound mathematics became necessary and an entire program has emerged: to understand the geometry and topology of the stratum $\mathcal{H}(2)$ and its compactifications in order to find a universal triangulation for this stratum. Obvious generalizations to other strata and genera then arise. We hope our humble work will be useful to future researchers in order to complete the program that is taking shape.

Introduction en français

Problème du plongement isométrique (PL)

Une **surface** est un espace topologique qui ressemble localement au plan euclidien de dimension 2, $\mathbb{R}^2$. Un **plongement** d'une surface topologique dans une autre est une représentation fidèle de l'espace de départ dans l'espace d'arrivée.

On peut munir certains espaces topologiques d'une **métrique de longueur** qui permet de mesurer la longueur des chemins. Une **isométrie** entre deux surfaces topologiques est une application continue qui préserve la longueur des chemins.

Les notions précédentes s'adaptent dans le cas où la surface topologique admet une structure différentielle supplémentaire.

Dans cette thèse, nous nous intéresserons principalement au cas des surfaces orientables. Le fait que toute surface orientable se plonge dans $\mathbb{R}^3$ est un résultat bien connu. Le théorème de plongement de Whitney (1869) assure que toute variété de dimension n se plonge dans $\mathbb{R}^{2n}$.

Le théorème de plongement de Nash, démontré en 1954, et amélioré par Kuiper l'année suivante, affirme quant à lui que toute surface riemannienne (orientable), c'est-à-dire une surface lisse munie d'une métrique riemannienne, admet un plongement isométrique dans l'espace euclidien $\mathbb{E}^3$. C'est une amélioration importante du théorème de Whitney car, non seulement la structure différentielle, mais aussi la géométrie intrinsèque de la surface peut être réalisée dans $\mathbb{E}^3$. Cependant, le théorème de Nash-Kuiper n'est pas constructif : l'idée est de partir d'une application contractante, puis d'ajouter une suite infinie d'ondelettes de manière à s'approcher de la métrique cible, et de finalement l'atteindre à la limite. Ainsi, l'équipe Hévéa a réussi à produire un plongement isométrique C^1 du tore carré plat dans $\mathbb{E}^3$ [BJLT13].

Nos travaux portent quant à eux sur les structures plates. Une **surface polyédrale** est une surface obtenue par recollement de polygones euclidiens le long de leurs arêtes, deux arêtes identifiées devant être de même longueur. En général, il n'est pas possible de recoller ces polygones dans $\mathbb{E}^3$, afin d'obtenir une surface plongée, sans introduire de plis. Une application f d'une surface polyédrale dans $\mathbb{E}^3$ est dite **linéaire par morceaux** (ou **PL**) si les polygones de la surface polyédrale source peuvent être triangulés de manière à ce que f soit affine, c'est-à-dire préserve le barycentre, en restriction à chaque triangle.

Dans un article relativement récent [BZ95], Burago et Zalgaller montrent l'existence de plongements isométriques PL pour toute surface polyédrale orientable. Leur approche est la suivante : ils montrent d'abord comment plonger de manière PL et isométrique un triangle dans le voisinage d'un triangle plus petit. Cette *construction élémentaire* n'est possible qu'à condition que le triangle à plonger et sa plus petite version satisfassent certaines contraintes

géométriques. Dans une seconde étape, ils appliquent cette construction élémentaire à chaque triangle d'une triangulation aiguë de la surface polyédrale à plonger. Ils doivent traiter les singularités de manière à part afin d'obtenir le plongement isométrique désiré. De manière remarquable, leur construction repose sur le théorème de Nash-Kuiper.

En général, cette méthode recquiert un nombre très important de triangles : environ 170 000 pour le tore carré plat et plus de 2 millions pour le tore héxagonal lors de nos expérimentations.

Triangulation universelle pour une famille de surfaces

Soit $\mathcal{F}$ une famille de surfaces polyédrales admettant la même surface topologique S sous-jacente. On peut penser, par exemple, à la famille des tores plats bidimensionnels. Nous savons, qu'individuellement, chaque surface polyédrale de $\mathcal{F}$ peut être réalisée fidèlement dans $\mathbb{E}^3$. Afin d'apporter une notion "d'uniformité" au sein de ces réalisations, nous introduisons la définition suivante. Une **triangulation universelle** pour $\mathcal{F}$ est une triangulation abstraite $\mathcal{T}$ de S (un complexe simplicial de dimension 2) telle que, pour toute surface Σ de $\mathcal{F}$, $\mathcal{T}$ admet une *réalisation géométrique* isométrique à Σ, la réalisation étant affine sur chaque triangle de $\mathcal{T}$.

Intuitivement, $\mathcal{T}$ est une triangulation universelle pour $\mathcal{F}$ si $\mathcal{T}$ réalise toute surface de $\mathcal{F}$ sans besoin de subdiviser aucun triangle de $\mathcal{T}$.

Problèmes étudiés dans cette thèse

Dans cette thèse, nous présentons trois résultats qui ont trait aux plongements isométriques de surfaces polyédrales. Le premier est une implémentation explicite de la méthode de Burago et Zalgaller dans le cas des tores plats. Le second est une preuve contructive de l'existence d'une triangulation universelle pour les tores plats. Le dernier, dont nous espérons une utilité future dans une éventuelle preuve de l'existence de triangulations universelles pour d'autres familles de surfaces polyédrales, est une détermination explicite de plongements isométriques PL pour une large famille de surfaces polyédrales de genre 2.

Implémentation effective de la méthode de Burago et Zalgaller dans les cas des tores plats

La méthode de Burago et Zalgaller devient beaucoup plus simple dans le cas des tores plats que dans le cas général, vu qu'un tore plat n'admet aucune singularité. Étant donné un tore plat $\mathbb{T}$, la méthode comporte les étapes suivantes :

(i) calculer une triangulation de $\mathbb{T}$ dont les triangles sont tous aigus,

(ii) calculer un plongement quasi-conforme, f, de $\mathbb{T}$ dans $\mathbb{E}^3$,

(iii) Subdiviser de manière uniforme la triangulation aiguë de $\mathbb{T}$ de manière à ce que la construction élémentaire à laquelle nous avons fait allusion à la fin de la première section soit possible pour toute paire $(T, F(T))$, où T parcourt les triangles de la triangulation raffinée $\mathcal{T}$, et F est l'approximation polyédrale de f définie sur $\mathcal{T}$,

(iv) appliquer finalement la construction élémentaire à chaque paire $(T, F(T))$.

Dans le cas des tores plats, l'étape (i) devient facile, cf section 4.1. Pour l'étape (ii), nous avons choisi d'utiliser une construction due à Pinkall [Pin85] qui permet de plonger isométriquement n'importe quel tore plat dans $\mathbb{E}^4$. Il suffit ensuite de composer cette isométrie avec une projection stéréographique afin d'obtenir le plongement conforme voulu.

En particulier, cette méthode nous a permis, entre autres, d'obtenir de réalisations PL du tore carré plat, et du tore hexagonal.

Triangulation universelle pour les tores plats

Il est vain de croire que la méthode générique de Burago et Zalgaller puisse permettre de construire une triangulation universelle, du fait que la triangulation associée à un tel plongement dépend de manière importante de la géométrie du tore plat que l'on veut réaliser.

Nous choisissons d'utiliser deux constructions bien plus simples. La première est une méthode due à Zalgaller [Zal00] pour plonger des tores plats longs. Nous montrons que tout tore plat long admet une telle réalisation, tout en donnant des bornes explicites. La seconde est une (re-)découverte par Arnoux, Lelièvre et Màlaga de contructions appelées diplotores. Grâce à trois familles de diplotores, nous recouvrons les tores plats courts.

Il reste à superposer les deux triangulations correspondant aux tores plats longs et courts, ce afin d'obtenir finalement une triangulation universelle pour les tores plats.

Plongements isométriques PL de certaines surfaces de $\mathcal{H}(2)$ et $\mathcal{H}(1, 1)$

Nous passons ensuite aux surfaces polyédrales de genre 2. Plus spécifiquement, nous considérons la famille $\mathcal{H}(2)$ des surfaces polyédrales obtenues par recollement de 3 parallélogrammes selon le schéma donné en Figure 1. Le recollement partiel défini par σ_1 et σ_2 résulte en un polygone en forme de L épaissi, et nous nous référons à ce patron comme une **décomposition en L**.

Nous nous intéressons d'abord au cas où le parallélogramme central est rectangulaire. Nous donnons de simples réalisations pour de tels rectangles centraux qui sont de plus explicites. Nous plongeons ensuite les deux parallélogrammes périphériques qu'il reste, qui sont topologiquement des cylindres, grâce aux outils développés par Zalgaller dans [Zal00] afin de plonger un prisme droit selon une ligne brisée assez longue. Il est à noter que cette méthode impose une longueur minimale pour les parallélogrammes périphériques. Nous généralisons cette méthode à des déformations non rectangulaires du rectangle central. De cette manière, nous sommes en mesure de montrer l'existence d'une triangulation universelle pour un voisinage ouvert des surfaces de $\mathcal{H}(2)$ admettant une décomposition en L où le parallélogramme centrale est rectangulaire et les parallélogrammes périphériques assez longs.
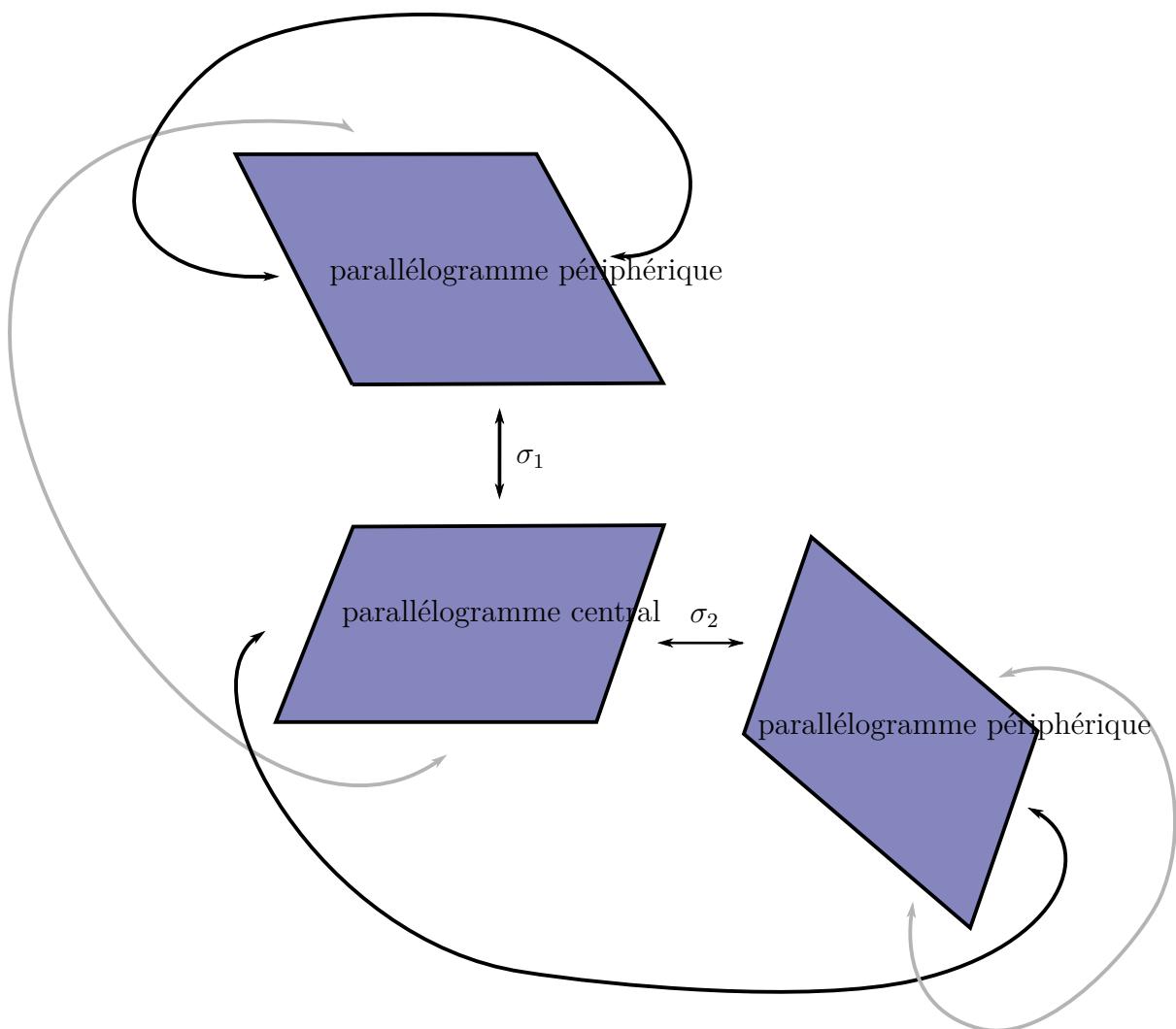
FIGURE 1 : Recollement typique de trois parallélogramme résultant en une surface de $\mathcal{H}(2)$.

Chapter 1

Introduction

1.1 (PL) Isometric embedding problem

A **surface** is a topological set such that every point admits a neighborhood which looks like the two-dimensional Euclidean plane $\mathbb{R}^2$. An **embedding** between two topological surfaces is a faithful representation of the source space in the arrival space.

Some topological surface can be endowed with a **length metric** which in turn enables to measure lengths of paths. An **isometry** between two metric topological surfaces is a continuous map that preserves lengths of paths.

If a topological surface is given a smooth structure, all the previous notions have a smooth version.

In this thesis, we will be mainly interested in orientable surfaces. It is well known that every orientable surface embeds into $\mathbb{R}^3$. The more general Whitney embedding theorem (1869) ensures that every manifold of dimension n embeds into $\mathbb{R}^{2n}$.

The theorem of embedding of Nash, demonstrated in 1954 and improved by Kuiper the year after, states that every (orientable) Riemannian surface, that is a smooth surface endowed with a smooth metric, admits a C^1 isometric embedding into the Euclidean space $\mathbb{E}^3$. It is a strong improvement over the previous Whitney theorem as, not only the differential structure, but also the intrinsic geometry of the surface can be realized in $\mathbb{E}^3$. Nonetheless, the Nash-Kuiper theorem is not constructive: the idea is to begin with a contracting map, and to add an infinite sequence of wavelets in order at each step to get closer to the aimed metric, and to finally reach it at the limit.
Thanks to more recent works, the Hévéa team succeeded in producing a C^1 isometric embedding of the square flat torus into $\mathbb{E}^3$ [BJLT13].

In this work, we shall focus on flat structures. A **polyhedral surface** is a surface obtained by gluing Euclidean plain polygons along edges which must be of the same length. In general, it is not possible to glue these polygons in $\mathbb{E}^3$ in order to obtain an embedded surface. A map f from a polyhedral surface into $\mathbb{E}^3$ is said to be **piecewise linear** (or **PL** in short) if the polygons of the polyhedral surface can be subdivided into triangles so that f is linear, that is preserves the barycenter, in restriction to each triangle.

In a relatively recent article [BZ95], Burago and Zalgaller show the existence of PL isometric embeddings for every orientable polyhedral surface. Their approach is the following: they first show how to embed PL isometrically a given triangle in the neighborhood of a smaller triangle. This *elementary construction* is only possible when

the triangle and its smaller version satisfy some geometric conditions. In a second step, they apply this construction to each triangle of an acute triangulation of the polyhedral surface we want to embed. They need to take care of singularities, to obtain the desired isometric embedding. Notably, their construction relies on the Nash-Kuiper theorem.

In general, this method requires a huge number of triangles, about 170,000 for the square flat torus and more than 2 millions for the hexagonal flat torus in our experimentations.

1.2 Universal triangulation for a family of surfaces

Let $\mathcal{F}$ be a family of polyhedral surfaces with the same underlying topological surface S. One may think, for instance, of the family of 2-dimensional flat tori. We know that, individually, every polyhedral surface in $\mathcal{F}$ can be realized faithfully in $\mathbb{E}^3$. In order to grasp some kind of "uniformity" in these realizations, we introduce the following definition. A **universal triangulation** for $\mathcal{F}$ is an abstract triangulation $\mathcal{T}$ of S (a 2-dimensional simplicial complex) such that, for every surface Σ in $\mathcal{F}$, $\mathcal{T}$ admits a *geometric realization* that is isometric to Σ, the realization being linear on each triangle of $\mathcal{T}$.

Roughly speaking $\mathcal{T}$ is a universal triangulation for $\mathcal{F}$ if $\mathcal{T}$ realizes every surface in $\mathcal{F}$ without the need of subdividing any triangle in $\mathcal{T}$.

1.3 Problems addressed in this thesis

In this thesis, we present three results on isometric embeddings of polyhedral surfaces. The first one is an explicit implementation of the method of Burago and Zalgaller in the case of flat tori. The second one is a constructive proof of existence of a universal triangulation for flat tori. The final one, which we hope will be useful to prove the existence of universal triangulations for other families of polyhedral surfaces, is the explicit computation of PL isometric embeddings for a large family of polyhedral surfaces of genus 2.

1.3.1 Implementation of the method of Burago and Zalgaller in the case of flat tori

The method of Burago and Zalgaller becomes much easier in the case of a flat torus than in the general case, as flat tori do not present any singularity. Given a flat torus $\mathbb{T}$, the method comprises the following steps:

(i) compute a triangulation of $\mathbb{T}$ whose triangles are acute,

(ii) compute an almost conformal embedding, f, of $\mathbb{T}$ in $\mathbb{E}^3$,

(iii) uniformly refine the acute triangulation of $\mathbb{T}$ in order for the elementary construction alluded to at the end of Section 1.1 to be possible for every pair $(T, F(T))$, where T is a triangle of the refined triangulation $\mathcal{T}$ and F is the polyhedral approximation of f defined on $\mathcal{T}$,

(iv) finally, apply the elementary construction to each pair $(T, F(T))$.

In the case of a flat torus, step (i) becomes easy, see Section 4.1. For step (ii), one can use the construction of Pinkall [Pin85] that gives an isometric embedding for any flat torus in $\mathbb{E}^4$. It suffices then to compose this isometry with a stereographic projection to obtain the desired conformal embedding.

In particular, this method allows us to obtain PL realizations of the square flat torus, and the hexagonal torus, among others.

1.3.2 Universal triangulation for flat tori

As previously stated, there is no hope to use the method of Burago and Zalgaller if one wants to obtain a universal triangulation for flat tori, as the triangulation associated to such an embedding depends heavily on the geometry of the flat torus we want to embed.

We choose to use two simple constructions. The first one is a method due to Zalgaller [Zal00] to embed long flat tori. We show that every long enough flat torus admits such a realization, and we give explicit bounds. The second one is a (re-)discovering by Arnoux, Lelièvre and Málaga [ALM21] of a construction called diplotorus. Thanks to three families of diplotori, we were able to cover short flat tori.

It remains to overlay the two triangulations corresponding to the long and the short flat tori, to obtain a universal triangulation for flat tori.

1.3.3 PL isometric embeddings of some surfaces in $\mathcal{H}(2)$ and $\mathcal{H}(1,1)$

We now turn to families of polyhedral surfaces of genus 2. Specifically, we consider the family $\mathcal{H}(2)$ of polyhedral surfaces obtained by gluing 3 parallelograms according to the gluin pattern below in Figure 2. The partial gluing defined by σ_1 and σ_2 gives a polygon with the shape of a thick L and we refer to this scheme as an **L decomposition**.

We first focus on the case where the central parallelogram is a rectangle. We provide a simple and explicit embedding for such central rectangles. Then we embed the two remaining peripheral parallelograms, which are topological cylinders, thanks to Zalgaller's machinery developed in [Zal00] to embed right prism according to a long enough broken line. Note that this method requires that the two peripheral parallelograms are long enough. We extend this method to non rectangular deformations of the central rectangle. This way we are able to show the existence of a universal triangulation for an open neighborhood of surfaces in $\mathcal{H}(2)$ admitting a L decomposition where the central parallelogram is a rectangle and with long enough peripheral parallelograms.
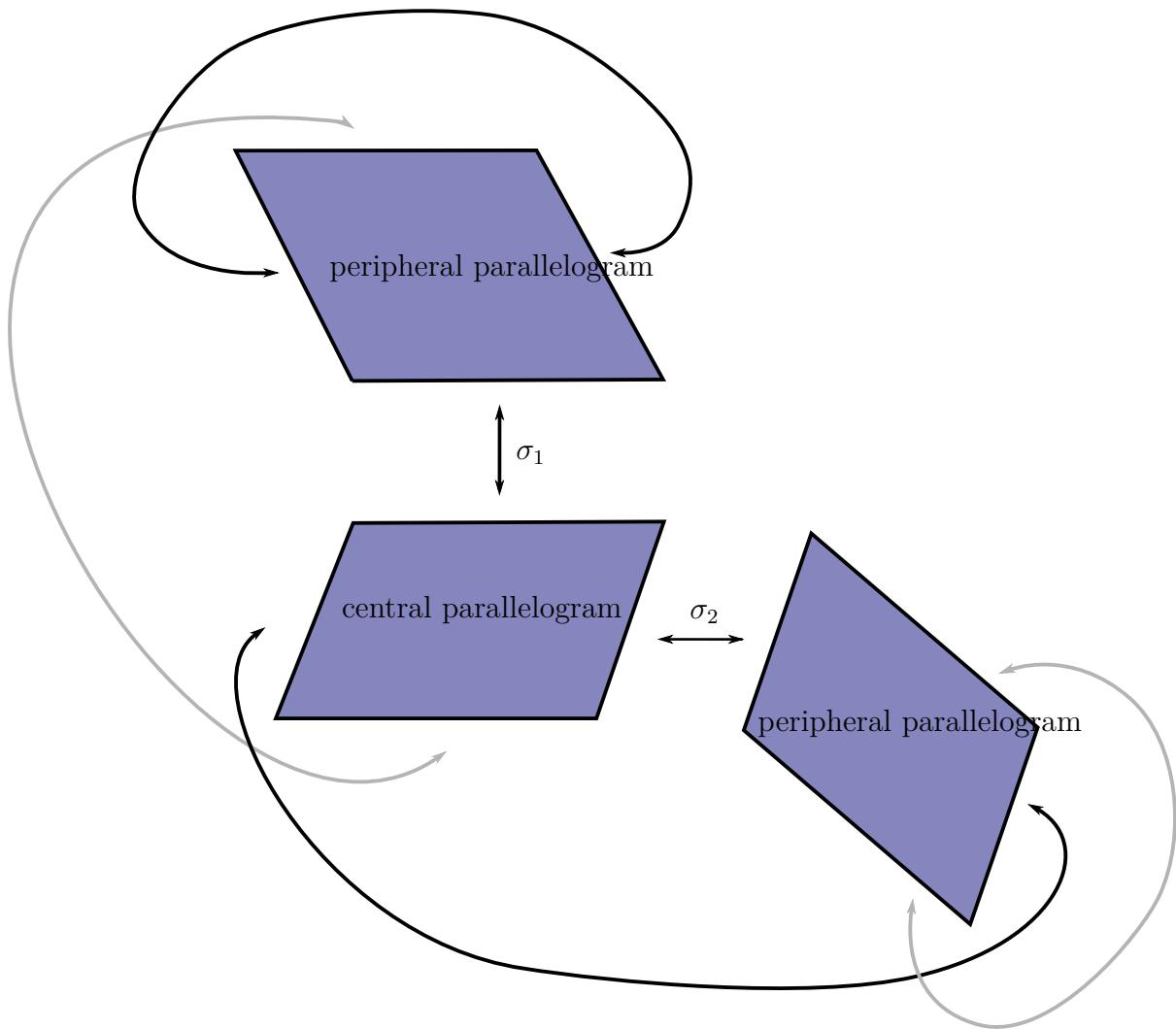
Figure 2: Typical gluing of three parallelograms resulting in a surface in $\mathcal{H}(2)$.

Chapter 2

Preliminaries

Résumé en français. Nous présentons dans ce chapitre les notions mathématiques nécessaires à la bonne compréhension du contenu de cette thèse. Après un rappel bref des définitions standards, nous nous concentrons sur les surfaces topologiques, polyédrales, différentiables, de Riemann puis enfin les surfaces de translation, ainsi que sur leurs espaces de modules et de Teichmüller.

In this chapter we present the mathematical notions necessary for a good understanding of the content of this thesis. After a brief reminder of the standard definitions, we focus on (topological, polyhedral, differential, Riemann) surfaces then finally translation surfaces, as well as their moduli spaces and Teichmüller spaces.

2.1 Basics

Topology. Given two topological spaces X and Y, a **homeomorphism** $\varphi : X \to Y$ between X and Y is a bicontinuous bijection that is a continuous bijection whose inverse is also continuous. A map $f : X \to Y$ is a **topological embedding** if its corestriction $X \to f(X)$ is a homeomorphism where $f(X)$ is given the topology induced by Y. A **topological immersion** $\iota : X \to Y$ is a map that is locally an embedding: every point in X admits a neighborhood U such that $\iota_{|U}$ is an embedding. An immersion is not necessarily injective. Moreover, an injective immersion is not always an embedding: for instance the immersion

$$\iota : \begin{array}{ccc} (-\pi, \pi) & \to & \mathbb{R}^2 \\ t & \mapsto & (\sin(2t), \sin(t)) \end{array}$$

is injective, but not an embedding as Figure 3 shows. However, an injective immersion of a compact space is always an embedding.
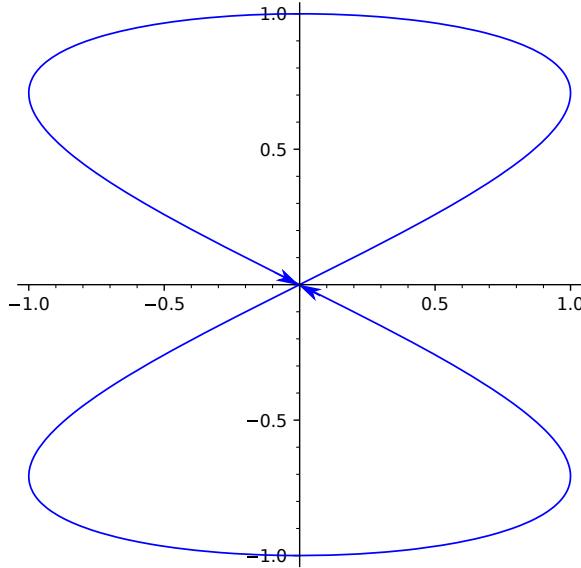
Figure 3: A lemniscate immersed in $\mathbb{R}^2$ but not embedded.

A **topological manifold** M of dimension n is a second countable, topological Hausdorff space that looks like $\mathbb{R}^n$ locally: every point in M admits a neighborhood that is homeomorphic to $\mathbb{R}^n$. In turn, a second countable topological space is a topological space M that admits a countable base for its topology: there exists a countable family $(U_i)_{i \geq 1}$ of open subsets such that any open set in M can be written as a union of U_i. A topological manifold M admits then a countable **atlas** $((U_i, \varphi_i))$ that is a countable open cover (U_i)

together with homeomorphisms $\varphi_i : U_i \to \varphi_i(U_i) \subseteq \mathbb{R}^n$ called **local charts**. Every chart φ_i can be written $\varphi_i = (x_1, ..., x_n)$ with $x_i : U_i \to \mathbb{R}$ continuous. The x_i are called **local coordinates**. That is why a chart is also called a **system of local coordinates**.

A topological manifold M of dimension n **with boundary** is a second countable, topological Hausdorff space that locally looks like $\mathbb{H}^n := \{x = (x_1, ..., x_n) : x_n \geq 0\}$: every point $x \in M$ admits a neighborhood that is homeomorphic to an open subset of $\mathbb{H}^n$. One can show that if a chart φ maps $p \in M$ into $\partial\mathbb{H}^n$, then so does every other chart defined at p. Hence $M = \mathring{M} \cup \partial M$, where $\partial M := \{p \in M : \exists \varphi \text{ chart s.t. } \varphi(p) \in \partial\mathbb{H}^n\}$ is the boundary of M and $\mathring{M} := M \setminus \partial M$ is the interior of M. One can easily see that a homeomorphism between two topological surfaces with boundary induces a homeomorphism between their boundaries.

Metrics. A **metric space** (X, d) is a topological space that is endowed with a **metric** $d : X \times X \to \mathbb{R}_+$ satisfying the following axioms:

- symmetry: $d(x, y) = d(y, x)$ for all $x, y \in X$,

- separation: $d(x, x) = 0$ for all $x \in X$,

- triangular inequality: $d(x, y) \leq d(x, z) + d(z, y)$ for all $x, y, z \in X$.

For our purpose, we will deal with possibly infinite distances, meaning that d satisfies the three preceding axioms, but can take the value ∞. Metric spaces are quite convenient, but not enough for our purpose. We rely on a slightly more restricted notion. To this end we follow the book [BBI$^+$01]. A **length structure** on a topological space X is a map $\ell : \mathcal{P}(X) \to \mathbb{R}_+ \cup \{\infty\}$ satisfying the following axioms, where $\mathcal{P}(X) \subseteq \mathcal{C}(X) := \{\gamma : [a, b] \to X \text{ continuous}\}$ are the continuous paths on X - typically $\mathcal{P}(X) = \mathcal{C}(X)$ or $\mathcal{P}(X) = \mathcal{C}^1_{pw}$ the set of piecewise C^1 paths on X when X is a differential manifold,

- $\ell(\gamma) = 0$ if γ is constant,

- juxtaposition: if $\gamma_0 : [a, b] \to X$ and $\gamma_1 : [b, c] \to X$ are such that $\gamma_0(b) = \gamma_1(b)$ then, denoting $\gamma_0 \cdot \gamma_1 : \begin{array}{ccc} t \in [a, b] & \mapsto & \gamma_0(t) \\ t \in [b, c] & \mapsto & \gamma_1(t) \end{array}$, $\ell(\gamma_0 \cdot \gamma_1) = \ell(\gamma_0) + \ell(\gamma_1)$,

- restriction: for all $\gamma : [a, b] \to X$, $t \mapsto \ell(\gamma_{|[a,t]})$ is continuous,

- reparametrization independence: if $\gamma : I \to X$ and $\phi : t \in J \mapsto \alpha t + \beta \in I$ is a linear bijection, then $\ell(\gamma \circ \phi) = \ell(\gamma)$,

- compatibility: for all $x \in X$ and all open neighborhood U containing x, there exists $r > 0$ such that for all $\gamma : [a, b] \to X$ with $\gamma(a) = x$ and $\gamma(b) \notin U$ satisfies $\ell(\gamma) > r$.

Given a length structure on X, one can define on (X, ℓ) the shortest path metric:

$$ d(x, y) = \inf_{\substack{\gamma \in \mathcal{P}(X) \\ \gamma(a) = x, \gamma(b) = y}} \ell(\gamma). $$

Every metric space can be given a length structure. Indeed, if (X, d) is a metric space,

we can define a length structure by giving to $\ell(\gamma)$ the value of the supremum, over all the subdivision $a = a_0 < ... < a_n = b$ of $[a,b]$ the interval of definition of γ, of $\sum_{i=1}^{n} d\left(\gamma(a_{i-1}), \gamma(a_i)\right)$. This endows X with an other metric induced by the length structure. We denote $\hat{d}$ the metric induced by this length structure. We say that the metric space X is a **length space** if $d = \hat{d}$.

Given a length space X we can thus talk about the length of a path, and the distance between two points that is equal to the shortest path length between the two points. An isometry $f : X \to Y$ between two length spaces X and Y is a length preserving continuous map: $\ell_Y(f \circ \gamma) = \ell_X(\gamma)$ for all $\gamma \in \mathcal{P}(X)$.

Quotient topology, gluing and link with metric. Let R be an equivalence relation on a topological space X. One can consider the canonical projection $\pi : X \to X/R$ which associates to an element in X its class under R. By definition, the quotient topology on X/R is the coarsest topology on X/R that makes the projection π continue. Open sets of X/R are thus subset $V \subseteq X/R$ such that $\pi^{-1}(V)$ is an open set in X.

An interesting class of quotient topologies are given by the topology obtained by gluing sides of polygons. Let $\mathcal{P}$ a family of plane Euclidean polygons. We denote by $E = E(\mathcal{P})$ the set of all edges of polygons in $\mathcal{P}$. Let $\sigma : E \to E$ be a **pairing** of the edges of polygons in $\mathcal{P}$, that means σ is an involution with $\sigma(e) \neq e$ for every edge e. We suppose given, for each pair $(e, \sigma(e))$, a homeomorphism $f_e : e \to \sigma(e)$ such that $f_{\sigma(e)} = f_e^{-1}$. Then the **gluing** of the family $\mathcal{P}$ according to the pairing σ with gluing maps $(f_e)_{e \in E}$ is the topological quotient space $\bigsqcup_{P \in \mathcal{P}} P/ \sim$ where $\sim$ is the equivalence relation *generated* by $p \sim f_e(p)$ for all $p \in e$ and all paired edge e. By generated, we mean the smaller equivalence relation containing the previous one.

Such a gluing admits a natural distance making it a length space. First note that the disjoint union admits a natural metric given by:

$$d : (x,y) \mapsto \begin{cases} d_{\mathbb{R}^2}(x,y) & \text{if } x, y \in P \\ \infty & \text{if } x, y \text{ belong to distinct polygons} \end{cases}.$$

Note that we allow d to take infinite values.

Let (X, d) be a topological space endowed with a **semi-metric** d, i.e. a map $d : X \times X \to \mathbb{R}_+$ that satisfies the symmetry and triangular inequality axioms of distances but possibly not the separation axiom. Define the equivalence relation R_d by: $x R_d y$ if $d(x, y) = 0$. The map d passes to the quotient over X/R_d. We denote by $\bar{d}$ this quotient, that is easily seen to be a metric.

Given a quotient $X/ \sim$ of a metric space (X, d), we can define a semi-metric on $X/ \sim$ by

$$d_\sim(x, y) := \inf \sum_{i=0}^{k} d(p_i, q_i) \tag{2.1}$$

where the infimum is taken aver all choices of $(p_i)_{i=0,...,k}$ and $(q_i)_{i=0,...,k}$ such that $p_0 \sim x$, $q_i \sim p_{i+1}$ for $i = 1, ..., k-1$ and $q_k \sim y$.
The space $(X/R_{d_\sim}, \overline{d_\sim})$ is a metric space called the **quotient metric space** of X under $\sim$.
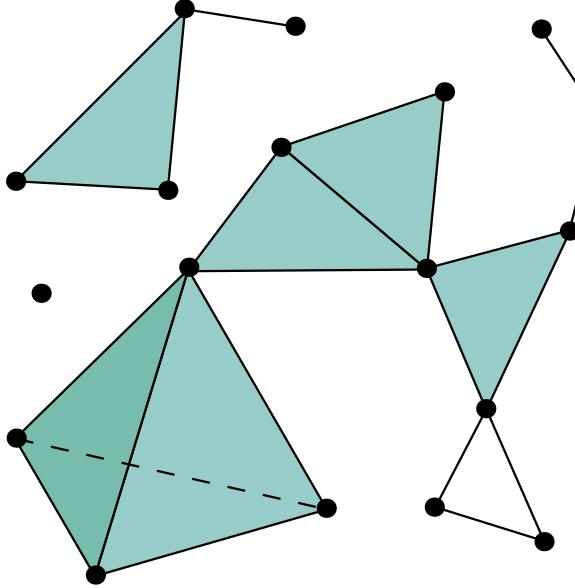
Figure 4: Example of a 3 dimensional simplicial complex - Wikipedia.

Suppose now that X is a length space. Recall that we denoted d the metric induced by the length structure, while $d_\sim$ is given by (2.1). Let us consider its quotient metric space $(X/R_{d_\sim}, \overline{d_\sim})$. Note first that $d_\sim \leq d$. Hence every d-continuous curve is $d_\sim$-continuous, and $\widehat{d_\sim} \leq \widehat{d} = d$. Now if $(p_i)_{i=0,\dots,k}$ and $(q_i)_{i=0,\dots,k}$ are as in the definition of $d_\sim$, one can construct a path from x to y whose length is almost equal to $\sum\limits_{i=0}^{k} d(p_i, q_i)$ by concatenating almost shortest paths from q_i to p_{i+1}. The projection of this concatenations in $X/\sim$ is continuous as $q_i \sim p_{i+1}$. Thus, the length of such a path can be made arbitrarily close to $\sum\limits_{i=0}^{k} d(p_i, q_i)$, and finally to $d_\sim(x,y)$. Hence $\widehat{\overline{d_\sim}} = \overline{d_\sim}$ and $X/R_{d_\sim}$ is a length space.

The interconnection between these two quotients is not obvious. For example, for $X = [0,1]$ and $x \sim y$ if $x = y$ or $x, y \in \mathbb{Q}$, we have that the topology of $X/\sim$ is non trivial, while $X/R_{d_\sim}$ is a point. Even if $X/\sim = X/R_{d_\sim}$ as sets, one has to be careful concerning the topologies. Nevertheless, when $X/\sim$ and $X/R_{d_\sim}$ coincide as sets while X is compact, one can show that the two previous topologies coincide.

Simplicial complexes. We now introduce some fundamental objects in combinatorial geometry. A n-**simplex** Δ is the convex hull of $n+1$ points affinely independent in some $\mathbb{R}^k$ called its **vertices**. A **face** of a simplex Δ is the convex hull of a subset of vertices of Δ. A **geometric simplicial complex** K is a family of simplices such that (see Figure 4):

- all faces of every simplices of K belongs to K,

- the intersection of two simplices are either empty, or a common face.

The dimension of a geometric simplicial complex K is the supremum of the dimension of its simplices seen as affine spaces.

The **polyhedron** - or **geometric realization** - associated to a geometric simplicial complex K is denoted $|K| := \bigcup\limits_{\Delta \subset K} \Delta$ and it is the union of all the simplices in K. If K is

finite and of finite dimension n, its polyhedron inherits a topology from $\mathbb{R}^n$.

Given a topological space X and a finite dimensional geometric simplicial complex K, we say that K **triangulates** simplicially X or that K is a **simplicial triangulation** of X if there exists a homeomorphism between $|K|$ and X.

2.2 Elements of algebraic topology

Fundamental group. Let X be a topological space and $x \in X$. We say that two continuous paths γ_0 and γ_1 starting at x and ending at $\gamma_0(1) = \gamma_1(1)$ are **homotopic** if there exists a **homotopy** $H : [0,1] \times [0,1] \to X$ between γ_0 and γ_1. In other terms H is continuous and verifies: $H(\cdot, 0) = \gamma_0$, $H(\cdot, 1) = \gamma_1$, $H(0, \cdot) \equiv x$ and $H(1, \cdot)$ is constant. We write $\gamma_0 \sim \gamma_1$ if γ_0 and γ_1 are homotopic. This is an equivalence relation. Then, by definition, the **fundamental group** of X based at x is $\pi_1(X, x) := \{\gamma : [0,1] \to X : \gamma \text{ is continuous and } \gamma(0) = \gamma(1) = x\} / \sim$ the set of all continuous loop of X based in x quotiented by homotopy. We denote $[\gamma]$ the class of a loop γ.

As its name indicates, $\pi_1(X, x)$ is a group. Let γ, γ_0 and γ_1 be three loops based in x. Then we define the **concatenation** of γ_0 and γ_1 by:

$$\gamma_0 \cdot \gamma_1 : \begin{array}{ccc} t \in [0, \frac{1}{2}] & \mapsto & \gamma_0(2t) \\ t \in [\frac{1}{2}, 1] & \mapsto & \gamma_1(2t - 1) \end{array}$$

and the **inverse** of γ by:

$$\bar{\gamma} : t \mapsto \gamma(1 - t).$$

One can check that the class of $\gamma_0 \cdot \gamma_1$ in $\pi_1(X, x)$ depends only on the classes of γ_0 and γ_1, and that the class of $\bar{\gamma}$ is independent on the representative $\gamma \in [\gamma]$. We can thus define the composition law on $\pi_1(X, x)$ by $[\gamma_0] * [\gamma_1] := [\gamma_0 \cdot \gamma_1]$. One verifies that $*$ is associative, that the neutral element is $[c_x]$ the constant path at x and that the inverse of $[\gamma]$ is $[\gamma]^{-1} = [\bar{\gamma}]$.

Suppose X is arcwise connected, and take two points $x_0, x_1 \in X$. Let α be a continuous path from x_0 to x_1. Then to every loop γ_0 based in x_0 corresponds a loop $\bar{\alpha} \cdot \gamma_0 \cdot \alpha$. The map $\rho_{\bar{\alpha}} : [\gamma] \mapsto [\bar{\alpha} \cdot \gamma \cdot \alpha]$ is then a homorphism of groups, whose inverse is ρ_α, hence it is an isomorphism (not canonical).

Given two pointed topological spaces (X, x) and (Y, y), a continuous map $f : X \to Y$ such that $f(x) = y$ induces a homorphism of groups:

$$f_* : \begin{array}{ccc} \pi_1(X, x) & \to & \pi_1(Y, y) \\ [\gamma] & \mapsto & [f \circ \gamma] \end{array}.$$

In turn, if f is a homeorphism, f_* is then an isomorphism.

Covering spaces. A **covering space** of a topological space X is a pair (Y, p) where Y is a topological space and $p : Y \to X$ is a continuous map such that for all $x \in X$ there exists a neighborhood U_x of x such that $p^{-1}(U_x) = \bigsqcup_{f \in F} V_f$, where F is a discrete space, and with the restriction $p_{|V_f} : V_f \to U_x$ being a homeomorphism for all $f \in F$. A typical example is given in Figure 5.
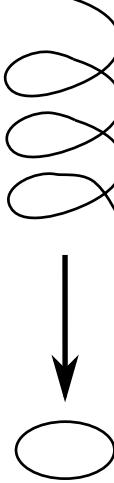
Figure 5: An infinite helix projecting to the unit circle, an example of covering space.

A morphism of covering spaces $p_1 : Y_1 \to X, p_2 : Y_2 \to X$ is a continuous map $f : Y_1 \to Y_2$ that makes the following diagram commutative:

$$
\begin{array}{ccc}
Y_1 & \xrightarrow{\ f\ } & Y_2 \\
& {\scriptstyle p_1} \searrow \quad \swarrow {\scriptstyle p_2} & \\
& X &
\end{array}
$$

.

In the case where $Y_1 = Y_2, p_1 = p_2$, and f is a homeomorphism, f is called a **deck transformation**. The set of deck transformations forms a group $\mathrm{Aut}(p)$.

X is said to be **semi-locally simply connected** if every point in X admits a neighborhood U such that every loop in U can be contracted to a simple point within X. Note that $\pi_1(U)$ need not to be trivial. Every semi-locally simply connected and path connected space X admits a so-called **universal cover** $\widetilde{X}$, i.e. a covering space such that for all other connected covering space Y of X, $\widetilde{X}$ is a covering space of Y. An equivalent characterization of universal covers is that they are simply connected - i.e. with trivial fundamental group. The universal cover of a space is unique up to isomorphism.

A covering space of X is called **Galois** is for each $x \in X$ and each pair of lifts $\widetilde{x}, \widetilde{x}'$ of x there is a deck transformation sending $\widetilde{x}$ on $\widetilde{x}'$. In other terms, p is Galois if $\mathrm{Aut}(p)$ acts transitively on the fibers of p. One can show that (Y, p) is normal if and only if $p_*(\pi_1(Y))$ is a normal subgroup of $\pi_1(X)$. In particular, as any universal cover $\widetilde{X}$ is simply connected, $\widetilde{X}$ must be Galois.

Euler's characteristic. Let K be a simplicial complex. Its **Euler characteristic** $\chi(K)$ is the alternating sum $\sum_n (-1)^n c_n$ where c_n denotes the number of n-faces in K. It is a topological invariant: it can be expressed as the alternating sum of the rank of the homology groups of the underlying topological space to K. By extension, we can define the Euler characteristic of any triangulated topological space. Finally, it can be shown that for an orientable closed surface S_g of genus g, we have $\chi(S_g) = 2 - 2g$. Moreover it can be shown that $\pi_1(S_g) \simeq \mathbb{Z}^{2g}$ where a basis of homotopy is given by the sides of the 4-gon from which S_g is a gluing (see next section).

2.3 Surfaces

The topic of this thesis are PL isometric embeddings of translation surfaces. We already saw what is an embedding and an isometry. We keep exploring topology and geometry in order to understand better the issue, focusing on the dimension 2 which is already very rich.

2.3.1 Topological surfaces

A **topological surface** is a 2-dimensional topological manifold.

Orientability. Let S be a topological surface. A strong theorem, proved by Radò, states that every topological surface can be simplicially triangulated (see [Tho92] or [DM68] for a proof). Let $\mathcal{T} \to S$ be a triangulation of S. An **orientation** o of a triangle $t = abc \in \mathcal{T}$ is a cyclic ordering of the vertices in t. An orientation of a triangle induces a natural orientation of its edges. Two orientations of two adjacent triangles are said to be **coherent** if they induced opposite directions on the common edge. A **coherent orientation** of a simplicial triangulation $\mathcal{T}$ is the assignment of an orientation to each triangle of $\mathcal{T}$ such that every two adjacent triangles have coherent orientations.
Finally S is said **orientable**, if it admits a triangulation $\mathcal{T}$ that can be given a coherent orientation. Such a surface S endowed with a coherent orientation is said oriented.

The notion of orientability can be made more concrete in the case of embedded differential surfaces in $\mathbb{R}^3$. A topological surface S embedded in $\mathbb{R}^3$ is orientable if and only if it admits a continuous **unit normal** $N : S \to \mathbb{S}^2$. This means that $N(p)$ is orthogonal to the tangent plane T_pS of S at p for every $p \in S$.

Moreover, in the case of a differential surface, its orientability is equivalent to the existence of an orientation preserving atlas, i.e. an atlas where all the chart transition maps have a positive Jacobian.

Two homeomorphic surfaces have the same orientability, as every triangulation of one surface gives rise to a triangulation of the other surface and vice-versa.

Triangulation of surfaces and canonical forms. We refer to [Mas19] and [GX$^+$13] for the detailed proofs and precisions about the two paragraphs that follow.
As stated before, every surface admits a simplicial triangulation. It is a key ingredient in the proof of the classification theorem of compact, connected surfaces - the topological part. References for a proof are [Tho92] and [DM68]. Hence every topological surface can be seen as a 2 dimensional simplicial complex. We can thus have a combinatorial viewpoint on any topological surface. The remaining of the work, to prove the classification theorem, consists in reducing the simplicial triangulation by elementary cut and paste operations in order to finally obtain a unique polygon (or a digon) whose sides are glued in some canonical way: according to a string of the form

$$a_1 b_1 a_1^{-1} b_1^{-1} ... a_g b_g a_g^{-1} b_g^{-1} c_1 h_1 c_1^{-1} ... c_k h_k c_k^{-1}, \quad g, k \in \mathbb{N} \tag{I}$$

in the orientable case, and of the form

$$a_1^2 ... a_g^2 c_1 h_1 c_1^{-1} ... c_k h_k c_k^{-1} \tag{II}$$

in the non orientable case. See Figure 6 for examples.
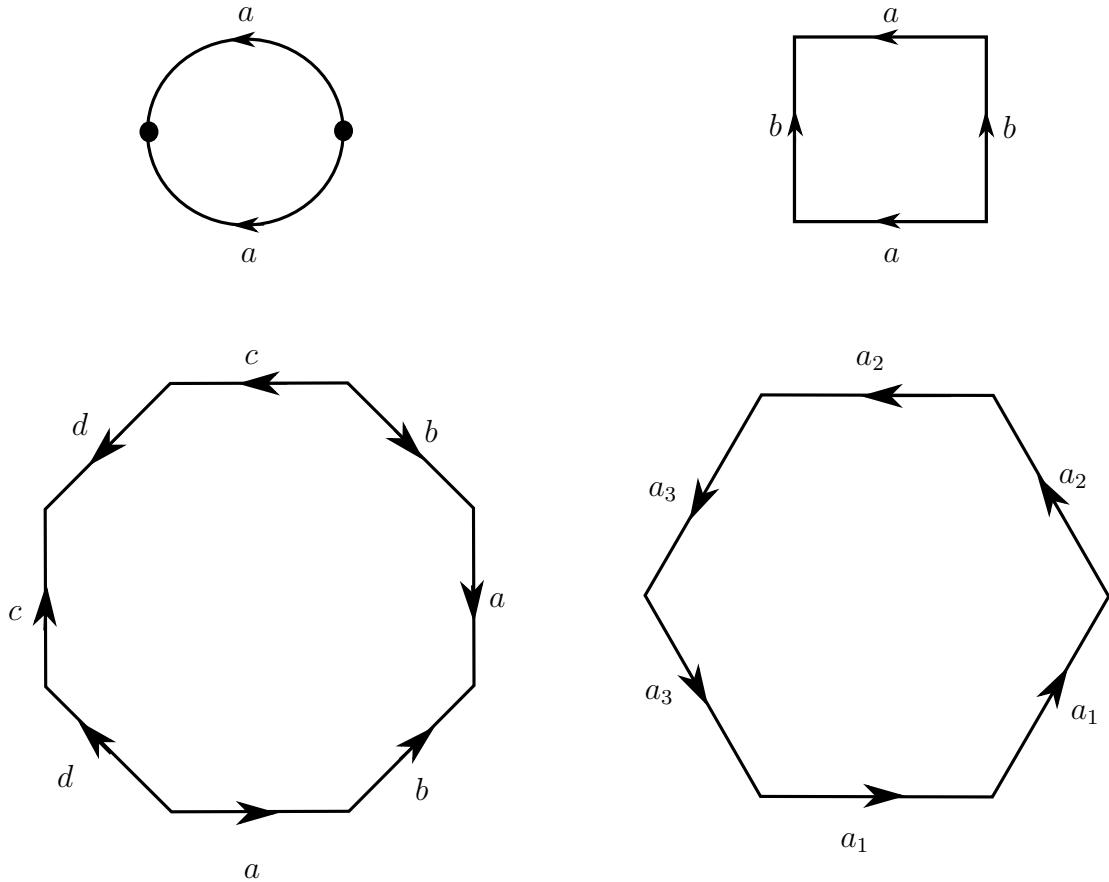
Figure 6: Examples of canonical glued polygons according to oriented edges (arrows), except the up left one which is not canonical. Up left: a sphere corresponding to the string aa^{-1}. Up right: a torus corresponding to the string $aba^{-1}b^{-1}$. Down left: a genus 2 orientable surface corresponding to the string $aba^{-1}b^{-1}cdc^{-1}d^{-1}$. Down right: a genus 3 non orientable surface corresponding to the string $a_1^2 a_2^2 a_3^2$.
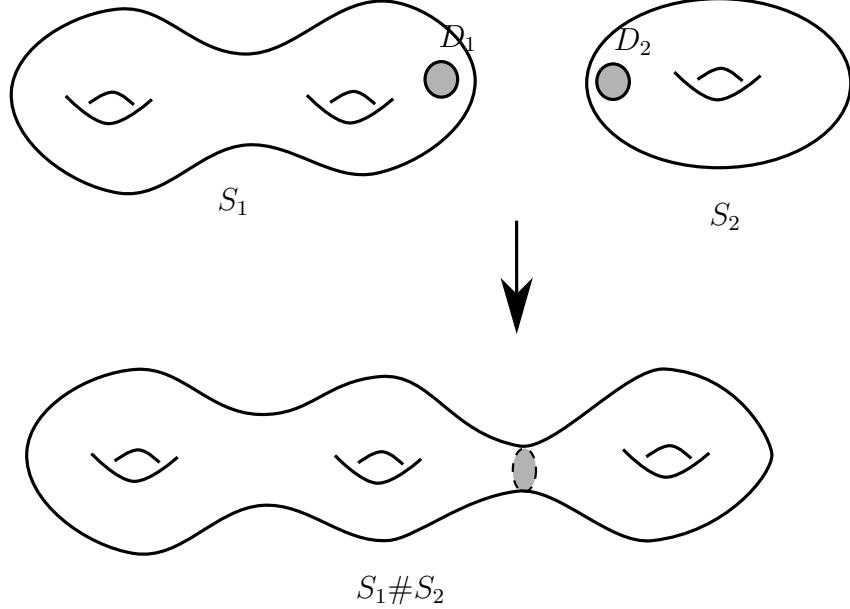
Figure 7: The connected sum of two surfaces S_1 and S_2.

The classification theorem of closed surfaces.

Connected sum and handles. Let S_1 and S_2 be two topological surface. Let $D_1 \subset S_1$ and $D_2 \subset S_2$ be two regions, both homeomorphic to a disk. The boundary ∂D_1 and ∂D_2 are thus both homeomorphic to a circle. Let $f : \partial D_1 \to \partial D_2$ be a homeomorphism. Then we define the connected sum $S_1 \# S_2$ to be the quotient space of $(S_1 \setminus \mathring{D}_1) \cup (S_2 \setminus \mathring{D}_2)/ \sim$, where $x \sim f(x)$ for $x \in \partial D_1$ (see Figure 7). One can show that $S_1 \# S_2$ does not depend of the regions D_1 and D_2 up to homeomorphism.

Thanks to the existence of a canonical form, we show that every surface can be obtained as a connected sum of tori possibly with boundary components. Of course, a torus is the topological surface obtained by identifying the opposite sides of a square without flip.

Indeed, suppose we are given a canonical form I: $a_1 b_1 a_1^{-1} b_1^{-1}...a_g b_g a_g^{-1} b_g^{-1} c_1 h_1 c_1^{-1}...c_k h_g c_k^{-1}$. As said before, we can realize it as a glued $(4g + 3k)$-gon, identification being done thanks to the labeling of the edges of the polygon. First, we can glue each edge labeled c_i with its corresponding one labeled c_i^{-1}, forcing h_i to be a loop - see Figure 8. Each loop, thus corresponds to a boundary component in the glued surface since h_i is not identified with any other edge. Consider the vertex v_i of the polygon at the begining of the path corresponding to the string $a_i b_i a_i^{-1} b_i^{-1}$. We cut the polygon through the diagonals joining v_1 to v_i for $1 \le i \le g$, taking care not to cross the loops. This results in 2 pentagons, realizing respectively the strings $a_1 b_1 a_1^{-1} b_1^{-1} d_1$ and $d_g' a_g b_g a_g^{-1} b_g^{-1}$, corresponding to tori with one boundary component, and $g - 2$ hexagons, each realizing a string of the form $d_i' a_i b_i a_i^{-1} b_i^{-1} d_i$, corresponding to tori having two boundary components - loops excluded. Moreover, we can suppose that all the loops are inside the first torus with one boundary component. Finally, it remains to glue the d_i and d_i' appropriately, which amounts to consider the connected sum of the tori. In the case where $g = 0$, one can show that we can introduce string of the form aa^{-1} while still obtaining the same surface. Hence $g = 0$ corresponds to a sphere with boundaries (a glued digon with loops inside).

21

Figure 8: Examples of realization of a orientable canonical form as a 11-gon - $g = 2$ and $k = 1$. After gluing the edge labeled c_1, we obtain a boundary component delimited by the loop made by h_1.
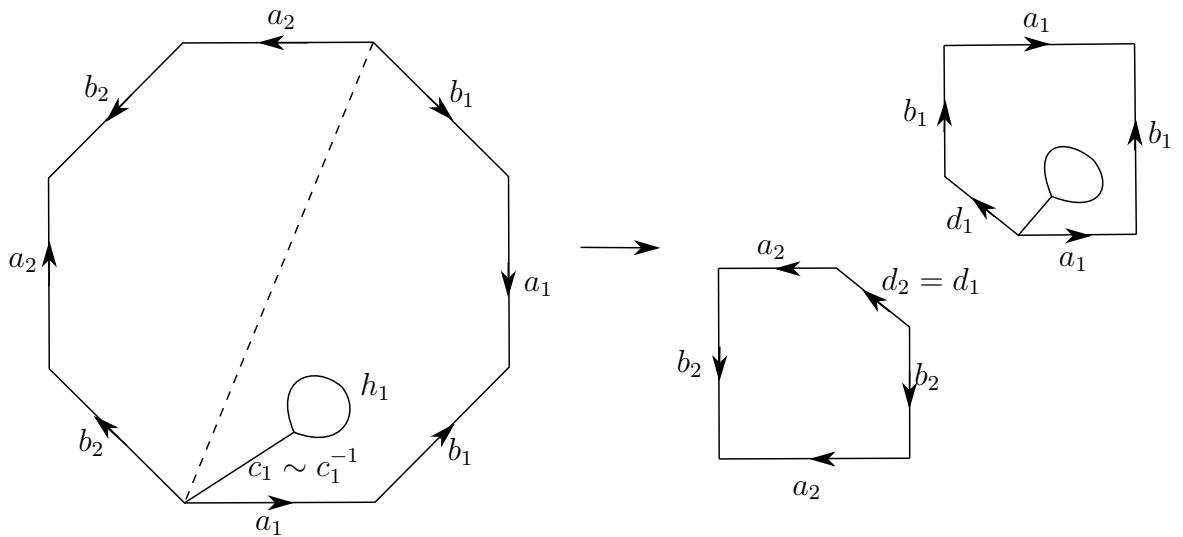
Figure 9: Examples 8 continued. The octagon in two to obtain two beveled squares corresponding to tori with a boundary component after edge gluing.

The same reasoning can be done for non orientable canonical forms II. The analog of handles are now called **cross-caps**, which are projective plane punctured at one point, and which correspond to strings of the form a^2. Every non orientable canonical form II is thus homeomorphic to a gluing of cross-caps with holes, i.e. a punctured connected sum of projective planes.

We can now state the classification theorem.

Theorem (classification of topological surfaces). *Let S be a topological surface.*

- *If S is orientable, then S is homeomorphic to the connected sum of $g \geq 0$ tori, with possibly some boundary components.*

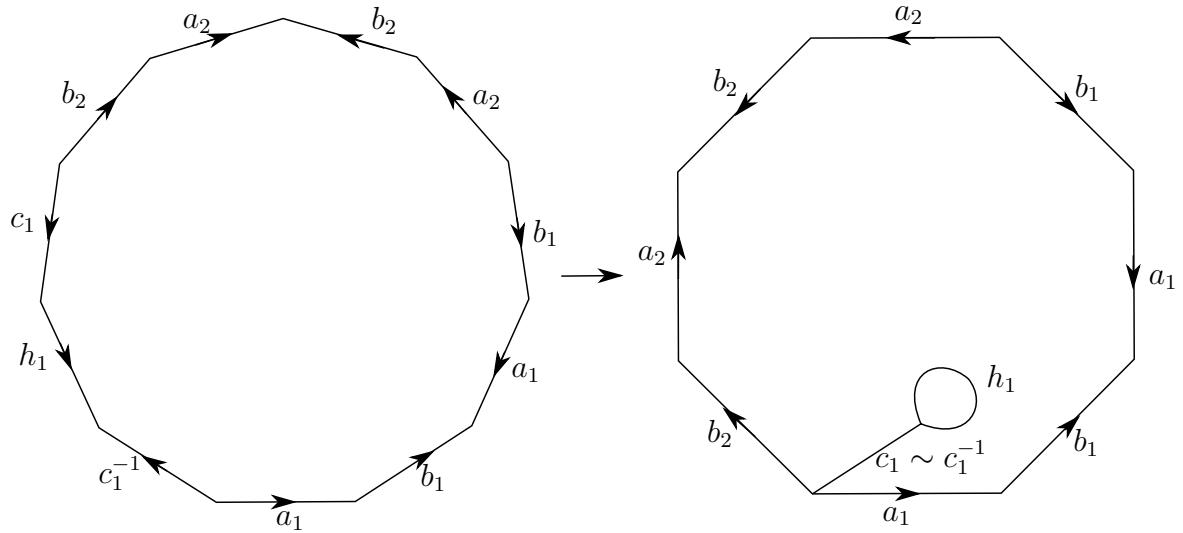- *If S is non orientable, then S is homemorphic to the connected sum of $g > 0$ projective planes, with possibly some boundary components.*

Thus, an orientable and **closed** - i.e. compact, connected, without boundary - topological surface is determined by the natural number g called its **genus**.

2.3.2 Polyhedral surfaces

There are two main ways to define (finite) polyhedral surfaces, a constructive one by gluing of polygons along isometrically paired edges, and a local one where each point admits a neighborhood isometric to a neighborhood of the apex of a Euclidean cone.

Let $\mathcal{P}$ be a finite family of compact Euclidean polygons, together with a partial pairing σ of their edges, and isometries $f_e : e \to \sigma(e)$ as gluing maps. This forces edges e and $\sigma(e)$ to be isometric - i.e. to have the same Euclidean length.

The gluing Σ of $\mathcal{P}$ according to σ with gluing maps $(f_e)_{e \in E}$ is called a **polyhedral surface**.

One can show that a polyhedral surface Σ is a topological surface, without boundary if the pairing is total.

As seen before, Σ is a length space whose intrinsic topology is the quotient topology. Let us keep the notations of section 2.1: $d_\sim$ being the semi-metric on $\Sigma = \mathcal{P}/\sim$ defined by Equation (2.1) and $\bar{d}$ the quotient of d over X/R_d. We can prove that $d_\sim$ is in fact a metric, and thus $\overline{d_\sim} = d_\sim$. Indeed, suppose that we are given two points $x \neq y$ in Σ. We thus have that $\pi^{-1}(x)$ is disjoint from $\pi^{-1}(y)$, and that both are closed and discrete in $\bigsqcup_{P \in \mathcal{P}} P$, thus finite. Hence, if $(p_i)_{i=0,...,k}$ and $(q_i)_{i=0,...,k}$ are as in the definition of $d_\sim$, then $\sum_{i=0}^{k} d(p_i, q_i) \geq d\left(\pi^{-1}(x), \pi^{-1}(y)\right) > 0$, hence $d_\sim(x, y) > 0$ and $d_\sim$ satisfies the separation axiom.

It appears that Σ is **flat** everywhere, except possibly at a finite number of points which are vertices of $\mathcal{P}$. A length space X is **flat** at a point p if p admits a neighborhood isometric to a plane disk in $\mathbb{R}^2$. Let p be a point in Σ which is not a vertex. If p belongs to the interior of some polygon P, then its Euclidean distance r to ∂P is positive, and then the Euclidean disk in P of radius $\frac{r}{2}$ centered at p provides a flat neighborhood at p. Otherwise, p is on an edge $e \subset P_e$, which is glued with an other edge $\sigma(e) \subset P_{\sigma(e)}$ and so the union of two sufficiently small half-disks of the same radius centered at p in P_e and $P_{\sigma(e)}$ glue together to form a disk centered at p in Σ.

Let v be a vertex in Σ. Its **conical angle** is the sum of all the incident angles to v. An angle being incident to v if it is the angle between two edges at some lift of v in some polygon. A vertex of conical angle 2π is flat: just glue parts of small enough disks of the same radius in the different polygon hitting v. On the contrary, if the conical angle at v is different from 2π, then Σ is not flat at v and v is called a **singularity**.

Let $\gamma : \mathbb{S}^1 \to \mathbb{S}^2$ be a rectifiable simple loop drawn in $\mathbb{S}^2 \subset \mathbb{R}^3$. The **Euclidean cone** C of apex O (the origin of $\mathbb{R}^3$) and directrix γ is the union of all the half-lines of origin O passing through a point of γ: $C = \left\{ x + t\overrightarrow{O\gamma(s)} : t \geq 0, s \in \mathbb{S}^1 \right\}$. The measure of its angle is the length of γ. Two directrices of the same length lead to isometric Euclidean cone. In particular, a Euclidean cone of angle 2π is isometric to a Euclidean plane. Indeed, setting $\varphi : O + te^{i\theta} \mapsto O + t\overrightarrow{O\widetilde{\gamma}(e^{i\theta})}$ yields the desired isometry between $\mathbb{C} \simeq \mathbb{R}^2$ and C.

Now, let p be a point in Σ. If Σ is flat at p, then p admits a neighborhood isometric to a Euclidean disk, and hence, by the previous discussion, isometric to a neighborhood of the apex of a Euclidean cone of angle 2π. If p is a singularity, we easily see, as in the flat case, that p has a neighborhood isometric to a neighborhood of the apex of a Euclidean cone whose angle is equal to the conical angle at p. By definition, this conical angle is $1/\varepsilon$ times the length of the circle of points at distance ε to p, for ε sufficiently small.

It can be shown conversely that a space endowed with a polyhedral metric is a polyhedral surface.

A **piecewise linear** or **PL** map $f : |T_1| \to |T_2|$ between simplicial triangulations is a continuous map such that for every triangle t of t_1, $f_{|t}$ maps t linearly into a triangle in T_2. We can extend this definition to polyhedral surfaces as the decomposition in polygon of a polyhedral surface Σ induces a simplicial triangulation of Σ by triangulating each polygons defining Σ. Thus, a **PL** map from a polyhedral surface Σ_1 to another Σ_2 is a map $f : \Sigma_1 \to \Sigma_2$ such that Σ_i admits a triangulation T_i, for $i = 1, 2$ with each $t_i \in T_i$ sent on a Euclidean triangle in Σ_i and with, for all triangle t_1 of T_1, $f_{|t_1}$ linearly mapping t_1 into a triangle in T_2.

2.4 Riemann surfaces and their moduli space

The references for this section are [IT12], [Sik18] and [Wel16].

Smooth differential surfaces and Riemann surfaces. Let M be a Hausdorff second countable topological space.

A **smooth atlas** on M is the data of a family of **charts** $(U_\alpha, \varphi_\alpha)$ where (U_α) is an open cover of M and $\varphi_\alpha : U_\alpha \to V_\alpha \subset \mathbb{R}^n$ are a homeomorphisms, such that the **chart transition** maps $\varphi_\beta \circ \varphi_\alpha^{-1} : \varphi_\alpha(U_\alpha \cap U_\beta) \to \varphi_\beta(U_\alpha \cap U_\beta)$ are C^∞ diffeomorphisms for all α, β. M equipped with a smooth atlas is called a **smooth manifold** of dimension n.

A map $f : U \subseteq \mathbb{C}^n \to V \subseteq \mathbb{C}^n$ between two open sets of $\mathbb{C}^n$ is said to be **holomorphic** if it is C^1 and if its real differential $df(z)$ is $\mathbb{C}$ linear[1] at each z in $\mathbb{C}^n$, where the action of $\mathbb{C}$ is viewed thanks to the identification $\mathbb{C}^n \overset{\iota}{\simeq} \mathbb{R}^{2n}$.

A **holomorphic atlas** on M is the data of a family of **charts** $((U_\alpha, \varphi_\alpha))$ where (U_α) is an open cover of M and $\varphi_\alpha : U_\alpha \to V_\alpha \subset \mathbb{C}^n$ are homeomorphisms, such that the

---

[1]Formally: $d(\iota \circ f)(\iota(a \cdot v)) = a \cdot \iota \circ df(\iota(v))$ for $a \in \mathbb{C}$ and $v \in \mathbb{C}^n$.

chart transition maps $\varphi_\beta \circ \varphi_\alpha^{-1} : \varphi_\alpha(U_\alpha \cap U_\beta) \to \varphi_\beta(U_\alpha \cap U_\beta)$ are biholomorphisms for all α, β. The manifold M equipped with such a holomorphic atlas is called a **complex manifold** of dimension n.

A **smooth differential surface** is a smooth manifold of dimension 2, while a **Riemann surface** is a complex manifold of dimension 1.

A **holomorphic** (resp. **smooth**) map f between two Riemann surfaces (resp. smooth differential surfaces) is a map that is holomorphic (resp. C^∞) when read through charts. A **meromorphic** function $f : \mathbb{C} \to \mathbb{C}$ is a function that is holomorphic except possibly at isolated **singularities** of finite order. A **meromorphic** map between two Riemann surfaces is a map that is meromorphic when read through charts.

Let $f : S_1 \to S_2$ be a holomorphic (resp. smooth) map between Riemann surfaces (resp. smooth differentiable surfaces), and $(U_i, \varphi_i), (V_j, \psi_j)$ atlases of S_1 and S_2. Then f defines a family of holomorphic (resp. smooth) maps $f_{i,j} = \varphi_i \circ f \circ \psi_j^{-1} : \psi_j(V_j) \cap \varphi_i(U_i) \to U_{i,j} := \psi_j(V_j) \cap U_i$ which agree on overlapping charts: if $U_i \cap U_k \neq \emptyset$ and $V_j \cap V_l \neq \emptyset, f_{i,j|U_{i,j}\cap U_{k,l}} = f_{k,l|U_{i,j}\cap U_{k,l}}$. Conversely, if we are given holomorphic (resp. smooth) maps $f_{i,j} : U_{i,j} \to U_{i,j}$ such that $f_{i,j|U_{i,j}\cap U_{k,l}} = f_{k,l|U_{i,j}\cap U_{k,l}}$ whenever $U_{i,j} \cap U_{k,l} \neq \emptyset$, they glue together to define a unique holomorphic (resp. smooth) map $f : S_1 \to S_2$.

Every Riemann surface is in particular a smooth differential surface. Furthermore, as the Jacobian $J_z\varphi$ of a biholomorphism φ is equal to $|\varphi'(z)|^2$ by Cauchy-Riemann equations, every Riemann surface is canonically oriented.

Tangent space at a point. Let S be a Riemann surface (resp. a smooth differentiable surface) and $x \in S$. Let φ be some chart near x. φ is said to be centered at x if $\varphi(x) = 0$. We define the **tangent space of S at x** denoted $T_x S$ as

$$T_x S = \left\{ (\varphi, v) : \varphi \text{ chart centered at } x, v \in \mathbb{C} \simeq \mathbb{R}^2 \right\} / \sim$$

where $(\varphi_1, v_1) \sim (\varphi_2, v_2)$ if $d(\varphi_1 \circ \varphi_2^{-1})(0) \cdot v_2 = v_1$. $T_x S$ inherits a structure of complex vector space of dimension 1 (resp. real vector space of dimension 2) via $[(\varphi_1, v_1)] + \lambda[(\varphi_2, v_2)] = [(\varphi_1, v_1 + \lambda d(\varphi_1 \circ \varphi_2^{-1})(0) \cdot v_2)]$.

Differential. Let $f : S_1 \to S_2$ be a smooth map between smooth differentiable surfaces, $x \in S_1$ and φ, ψ charts of S_1 at x and of S_2 at $f(x)$ respectively. We define the differential of f at x by

$$df(x) \cdot [(\varphi, v)] = [(\psi, d(\psi \circ f \circ \varphi^{-1})(\varphi(x)) \cdot v)].$$

This is well defined because if $(\varphi_1, v_1) \sim (\varphi_2, v_2)$ then by the chain rule $d(\psi \circ f \circ \varphi_1^{-1})(\varphi_1(x)) \cdot v_1 = d(\psi \circ f \circ \varphi_2^{-1})(\varphi_2(x)) \circ d(\varphi_2 \circ \varphi_1^{-1})(\varphi_1(x)) \cdot v_1 = d(\psi \circ f \circ \varphi_2^{-1})(\varphi_2(x)) \cdot v_2$. Note that for a holomorphic map, $df(x)$ is $\mathbb{C}$-linear at every x, and is thus the multiplication by a scalar denoted $f'(x) \in \mathbb{C}$.

Vector bundles. Let $\mathbb{K} = \mathbb{R}$ or $\mathbb{C}$. A vector bundle is a 4-tuple $\left(E, X, \pi, \mathbb{K}^k \right)$ where:

i) X and E are topological spaces, named respectively the **base space** and the **total space**,

ii) $\pi : E \to X$ is a continuous surjection called the **bundle projection**,

iii) the **fiber** $E_x := \pi^{-1}(x)$ is a finite dimensional $\mathbb{K}$ vector space for all $x \in X$,

iv) at every point x, π admits a **local trivialization** (U, φ), where U is an open neighborhood of x and $\varphi : \pi^{-1}(U) \to U \times \mathbb{K}^k$ is a homeomorphism such that:

- the diagram
$$
\begin{array}{ccc}
\pi^{-1}(U) & \xrightarrow{\varphi} & U \times \mathbb{K}^k \\
\downarrow{\scriptstyle \pi} & \swarrow{\scriptstyle \pi_1} & \\
U & &
\end{array}
$$
is commutative, where π_1 denote the projection on the first coordinate,

- the map $v \in \mathbb{K}^k \mapsto \varphi^{-1}(x, v) \in \pi^{-1}(U)$ is a linear isomorphism.

Given a vector bundle as before, and two local trivialization (U, φ) and (V, ψ), the composite $\varphi^{-1} \circ \psi : (U \cap V) \times \mathbb{K}^k \to (U \cap V) \times \mathbb{K}^k$ is of the form $\varphi^{-1} \circ \psi(x, v) = (x, g_{UV}(x).v)$ for some continuous map $g_{UV} : U \cap V \to GL_k(\mathbb{K})$. The g_{UV} are called the **transition functions**. They satisfy

$$g_{UU} = id \text{ and } g_{UV} = g_{UW} \circ g_{WV}. \tag{$*$}$$

In fact, the data of an open cover $\mathcal{U}$ of the topological space X and a family of continuous maps $(g_{UV} : U \cap V \to GL_k(\mathbb{K}))$ satisfying the cocycle condition ($*$) define a structure of vector bundle of base space X. Indeed, one can consider $E = \bigsqcup_{\mathcal{U}} U \times \mathbb{K}^k / \sim$ the disjoint union of the spaces $U \times \mathbb{K}^k$ quotiented by the equivalence relation $(U, x, v) \sim (V, x, g_{VU}(x).v)$ for all $x \in U \cap V$ and all $v \in \mathbb{K}^k$. The projection π is then the quotient of the second projection, and local trivializations are given by inverses of quotient of the injection $U \times \mathbb{K}^k \hookrightarrow \bigsqcup_{\mathcal{U}} U \times \mathbb{K}^k$.

If $\pi : E \to X$ is a vector bundle, its **dual** $\pi^* : E^* \to X$ is defined as follows:

- $E^* = \bigsqcup_{x \in X} E_x^*$ where F^* denotes the dual of the vector space F,

- π^* sends each E_x^* on $x \in X$,

- For each local trivialization $\varphi : \pi^{-1}(U) \to U \times \mathbb{K}^k$ of π, we define a local trivialization for π^*:
$$
\varphi^* : \begin{array}{ccc}
\pi^{*-1}(U) & \to & U \times \mathbb{K}^k \\
\lambda & \mapsto & \left(p, (\varphi_{|E_x}^t)^{-1} \cdot \lambda \right)
\end{array} .
$$

The associated transition functions defined then a structure of vector bundle.

Similarly, if E, F are vector bundles over a same base space X, their **tensor product** $E \otimes F$ is the vector bundle defined by the transition functions $g_{\alpha\beta} \otimes h_{\alpha\beta}$, where $g_{\alpha\beta}$ (resp. $h_{\alpha\beta}$) runs through the transition functions of E (resp. F). In particular, setwise, $E \otimes F = \bigsqcup_{x \in X} E_x \otimes F_x$.

A section of a vector bundle, is a map $s : X \to E$ such that $\pi \circ s = id_X$. Note that a section ω of the dual bundle E^* acts on each fiber of E by $\omega \cdot v = \omega_x(v)$ for $v \in E_x$ as $\omega_x \in E_x^*$. For the same reason, an element of $E \otimes E$ acts on each fiber of $E \oplus E$.

Vector bundles can be endowed with additional structures. If $\mathbb{K} = \mathbb{R}$, a **smooth** vector bundle is a vector bundle such that the transition maps are C^∞. If $\mathbb{K} = \mathbb{C}$, a **holomorphic** vector bundle is a vector bundle whose transition maps are holomorphic.

Let $\pi : E \to X$ be a topological (resp. smooth, holomorphic) fiber bundles. Let $s : X \to E$ a continuous (resp. smooth, holomorphic) section and (U_i) an open cover of X. Then s defines a family of continuous (resp. smooth, holomorphic) sections $s_i : U_i \to E$ by restriction that agree on overlaps: $s_{i|U_i \cap U_j} = s_{j|U_i \cap U_j}$ for all i, j. Conversely, if (s_i) is a family of continuous (resp. smooth, holomorphic) sections $s_i : U_i \to E$ such that $s_{i|U_i \cap U_j} = s_{j|U_i \cap U_j}$, then they glue together to define a unique section $s : X \to E$.

Tangent bundle, cotangent bundle, and Riemannian metrics. Let S be a Riemann surface (respectively a smooth differential manifold).

The **tangent bundle** TS of S is the holomorphic (respectively smooth) vector bundle whose transition maps are given by the differential of the chart transition maps $\varphi_{\alpha\beta} : x \mapsto d(\varphi_\beta \circ \varphi_\alpha^{-1})(x)$. It can be seen setwise as the disjoint union of the tangent spaces T_pS.

A holomorphic (resp. smooth) section $X : S \to TS$ is called a **vector field**. Let $\varphi = (x, y) : U \to \mathbb{R}^2$ a system of local coordinates on a smooth surface S at p. Note that, by definition, φ is itself a differential map. We define the vector fields $\frac{\partial}{\partial x}$ and $\frac{\partial}{\partial y}$ on U by

$$\left(\frac{\partial}{\partial x}\right)_p := (d\varphi(p))^{-1} \cdot (1, 0) \text{ and } \left(\frac{\partial}{\partial y}\right)_p := (d\varphi(p))^{-1} \cdot (0, 1).$$

The family $\left(\left(\frac{\partial}{\partial x}\right)_p, \left(\frac{\partial}{\partial y}\right)_p\right)$ is then a basis of T_pS at each $p \in U$, which depends smoothly of p. Every smooth vector field X can thus be written, locally on U, $X_p = \tilde{f}(p)\left(\frac{\partial}{\partial x}\right)_p + \tilde{g}(p)\left(\frac{\partial}{\partial y}\right)_p$ for all $p \in U$ and for some smooth functions $f, g : U \to \mathbb{R}$. We often write $X = f(x, y)\frac{\partial}{\partial x} + g(x, y)\frac{\partial}{\partial y}$ for $f = \tilde{f} \circ \varphi$ and $g = \tilde{g} \circ \varphi$ smooth.

Similarly, if S is a Riemann surface, and if $\varphi = z : U \to \mathbb{C}$ is a local coordinate of S at p, we define:

$$\left(\frac{\partial}{\partial z}\right)_p = (d\varphi(p))^{-1} \cdot 1.$$

$\left(\frac{\partial}{\partial z}\right)_p$ is a basis of T_pS at each $p \in U$ which depends analytically of p. As previously, every holomorphic vector field X reads through φ, locally on U, as $X = f(z)\frac{\partial}{\partial z}$ where f is holomorphic on U.

The **cotangent bundle** T^*S of S is the dual of the tangent bundle TS. A holomorphic (respectively meromorphic, smooth) section $\omega : S \to T^*S$ of T^*S is called a **holomorphic 1-form** (respectively a **meromorphic 1-form**, a **smooth differential 1-form**). We denote $\Omega(S)$ the space of 1-forms on S.

Let $\zeta : U \to \mathbb{C}$ a local coordinate of a Riemann surface S at p. We define the holomorphic 1-form on $U, d\zeta = \zeta^* dz = \zeta' dz$ by

$$d\zeta_p = d\zeta(p) = \zeta'(p) \cdot$$

where we denoted $dz = id_\mathbb{C}$, and $f^*(\omega) : p \mapsto \omega_{f(p)}(df(p)\cdot)$. We have $d\zeta_p \neq 0$ for all $p \in U$. Hence every holomorphic 1-form ω reads through ζ as $\omega = f(\zeta)d\zeta$ for some holomorphic function f.

Similarly, if S is a smooth surface and $\varphi = (x, y) : U \to \mathbb{R}^2$ is a local coordinate of S at

x, denote (e_x^*, e_y^*) the dual basis of the canonical basis of $\mathbb{R}^2$. We define smooth 1-form $dx = \varphi^* e_x^*, dy = \varphi^* e_y^*$ on U by:

$$dx_p = e_x^* \circ d\varphi(p), \quad dy_p = e_y^* \circ d\varphi(p).$$

We have that (dx_p, dy_p) is a basis of $T^*S_p \otimes T^*S_p$ that depends smoothly of p. Hence every smooth 1-form ω reads through φ as $\omega = f(x, y)dx + g(x, y)dy$ for some smooth functions f, g.

A holomorphic **quadratic differential** $q : S \to T^{*2}S$ is a holomorphic section of the vector bundle $T^{*2}S := T^*S \otimes_{\mathbb{C}} T^*S$ that takes value in $\mathrm{Sym}T^{*2}S$ the sub-bundle formed by symmetric $\mathbb{C}$-bilinear forms.

A **Riemannian metric** $g : S \to T^{*2}S$ is a smooth section of the smooth vector bundle $T^{*2}S := T^*S \otimes_{\mathbb{R}} T^*S$ such that for all $p \in S$, $g_p := g(p)$ is a symmetric definite positive $\mathbb{R}$-bilinear form on T_pS.
Every Riemannian manifold (M, g) is a length space. Given a piecewise C^1 path $\gamma : I \to M$, we can define its length by $\ell(\gamma) = \int_I \sqrt{g_{\gamma(t)}(\gamma'(t), \gamma'(t))}dt$. The distance between two points in M is then defined as the shortest path distance. This metric endows M with a length space structure.

Link between complex structures and conformal structures. Let (M, g) and (N, h) be two Riemannian manifolds. A **conformal map** from M to N is a diffeomorphism $f : M \to N$ such that the **pull back** $f^*h : m \in M \mapsto h_{f(m)}(df(m)\cdot, df(m)\cdot)$ of h under f is equal to $e^\varphi g$ where φ is a smooth real-valued function on M. M and N are said to be **conformally equivalent** or to have the same **conformal structure** if such a conformal map exists.

Intuitively, f is conformal if it locally preserves oriented angles: for every point $m \in M$ and every smooth paths γ_1, γ_2 through m, the oriented angle $\angle((f \circ \gamma_1)'(0), (f \circ \gamma_2)'(0))$ is equal to $\angle(\gamma_1'(0), \gamma_2'(0))$.

Suppose now f is a conformal map between two open subsets U, V of $\mathbb{C}$. Then $df(z)$ preserves angles, that is $df(z)$ is a direct similarity, for all z. Hence, f satisfies Cauchy-Riemann equations and so is holomorphic. Conversely, every holomorphic function between open subsets of $\mathbb{C}$ is conformal as its differential at z is the multiplication by $f'(z)$ which preserves angles.

The latter fact is actually general. First, it can be shown that every Riemannian manifold can be endowed a natural complex structure - and conversely every complex manifold admits a Riemannian metric. Then, a map $f : (M, g) \to (N, h)$ between two Riemannian surfaces is conformal if and only if it is biholomorphic between the underlying Riemann surfaces.

Moduli spaces. A **holomorphic**, or **conformal**, map $f : S_1 \to S_2$ from a Riemann surface S_1 to another Riemann surface S_2 is a map that is holomorphic when read in charts: $\varphi_2 \circ f \circ \varphi_1^{-1}$ is holomorphic for all chart φ_1 of S_1 and φ_2 of S_2. A **biholomorphism** $f : S_1 \to S_2$ between S_1 and S_2 is a bijective holomorphic map whose inverse is holomorphic. We say that two Riemann surfaces S_1 and S_2 are **biholomorphically equivalent**, are **conformally equivalent**, have the same **complex structure** or have the same **conformal structure** if there exists a biholomorphism between S_1 and S_2.

Now, let S_g be the closed orientable topological surface of genus $g \geq 0$. S_g can be endowed with a lot of different complex structures. See Section 2.5 for a classification of all complex structures in genus 1. It is thus helpful to define:

$$\mathcal{M}_g := \{\text{biholomorphic classes } [S] \text{ of closed Riemann surfaces of genus } g\}.$$

$\mathcal{M}_g$ is called the **moduli space** of Riemann surfaces of genus g. It can be shown that $\mathcal{M}_g$ is reduced to a point if $g = 0$, and admits a complex structure making it a complex manifold of dimension $3g - 3$ if $g \geq 2$. We will describe explicitly $\mathcal{M}_1$ in the next section.

Uniformisation theorem. The uniformisation theorem is a central result in the theory of Riemann surfaces. It permits to classify compact closed Riemann surfaces up to biholomorphism. Let us state the theorem. We refer to the Section 2.5 for details about the Riemann sphere and the upper half-plane.

Theorem (Uniformisation). *Every simply connected Riemann surface is biholomorphic to one of the following:*

1. *the Riemann sphere $\widehat{\mathbb{C}}$,*

2. *the complex plane $\mathbb{C}$,*

3. *the upper half-plane $\mathbb{H}^2$.*

This implies that if Σ is a connected Riemann surface, then its universal cover $\begin{smallmatrix} \widetilde{\Sigma} \\ \downarrow{\scriptstyle \pi} \\ \Sigma \end{smallmatrix}$ is

biholomorphic to one of $\widehat{\mathbb{C}}, \mathbb{C}$ or $\mathbb{H}^2$.

In the following, Σ denotes a compact and closed Riemann surface.

If the genus of Σ is equal to $g = 0$, then Σ is homeomorphic to $\widehat{\mathbb{C}}$ as a topological surface thus the only possibility is that Σ is biholomorphic to $\widehat{\mathbb{C}}$.

Now suppose $g \geq 1$. We can transfer the analytic structure on Σ by π and endow $\widetilde{\Sigma}$ with the analytic atlas $\{(V, \varphi \circ \pi) : V \text{ sheet of } \pi \text{ over } U \text{ and } (U, \varphi) \text{ chart on } \Sigma\}$. This is in fact the only complex structure on $\widetilde{\Sigma}$ making π holomorphic. For this complex structure, every deck transformation γ of $\widetilde{\Sigma}$ is a biholomorphism: for $(V, \varphi_1 \circ \pi)$ and $(V_2, \varphi_2 \circ \pi)$ charts of $\widetilde{\Sigma}$ we have $(\varphi_2 \circ \pi) \circ \gamma \circ (\varphi_1 \circ \pi)^- 1 = \varphi_2 \circ (\pi \circ \gamma) \circ \pi^{-1} \circ \varphi_1^{-1} = \varphi_2 \circ \pi \circ \pi^{-1} \circ \varphi_1^{-1} = \varphi_2 \circ \varphi_1^{-1}$ which is holomorphic. Denote by Γ the group of deck transformations of the universal cover $\widetilde{\Sigma}$. Now, by the theory of covering, the universal covering is Galois, and we can define $f : \begin{array}{ccc} \Sigma & \to & \widetilde{\Sigma}/\Gamma \\ s & \mapsto & [\tilde{s}] \text{ where } \pi(\tilde{s}) = s \end{array}$. We have then the following commutative diagram:

$$\begin{array}{ccc} \widetilde{\Sigma} & & \\ \downarrow{\scriptstyle \pi} & \searrow^{\pi_0} & \\ \Sigma & \xrightarrow{f} & \widetilde{\Sigma}/\Gamma \end{array} \qquad \text{where we denoted } \pi_0 = [\cdot] : \widetilde{\Sigma} \to \widetilde{\Sigma}/\Gamma \text{ the canonical projection, which}$$

shows that f is surjective. Moreover, if $f(s_1) = f(s_2)$ then for any $\tilde{s_1} \in \pi_0^{-1}(s_1)$ and $\tilde{s_2} \in \pi_0^{-1}(s_2)$ we have $\tilde{s_2} = \gamma \cdot \tilde{s_1}$ for some $\gamma \in \Gamma$, so $s_2 = \pi(\tilde{s_2}) = (\pi \circ \gamma)(\tilde{s_1}) = \pi(\tilde{s_1}) = s_1$ and f is bijective. Moreover, as π and π_0 are both continuous and open, so is f which

is thus a homeomorphism $f : \Sigma \to \widetilde{\Sigma}/\Gamma$. This defines a complex structure on $\widetilde{\Sigma}/\Gamma$ by transfer via f^{-1}, and for this structure the canonical projection π_0 is holomorphic. One can show that Γ acts discontinuously on $\widetilde{\Sigma}$: every $\tilde{s} \in \widetilde{\Sigma}$ admits a neighborhood V such that $V \cap \gamma \cdot V = \emptyset$ for all $\gamma \in \Gamma \setminus \{id\}$. This implies in particular that Γ acts without fixed point on $\widetilde{\Sigma}$.

If $\widetilde{\Sigma} = \mathbb{C}$, then as we will show in Section 2.5.3, Γ is a subgroup of $\mathrm{Aut}(\mathbb{C}) = \{z \mapsto az + b : a, b \in \mathbb{C}, a \neq 0\}$. If $\gamma : z \mapsto az + b$ with $a \neq 1$, then $\frac{b}{1-a}$ is a fixed point. Hence $a = 1$ for every chart of Γ, and Γ is a group of translations identified with an additive subgroup of $\mathbb{C}$. Γ is thus a discrete subgroup of $\mathbb{C}$, implying that Γ is either trivial, infinite monogene, or a lattice. As Σ is compact, Γ must be a lattice, and $\Sigma \simeq \mathbb{C}/\Gamma$ is a torus (cf Section 2.5.1).

We have just proved that, if $\widetilde{\Sigma} = \mathbb{C}$, then $g = 1$.

Finally, if $\widetilde{\Sigma} = \mathbb{H}^2$, Γ is a subgroup of $\mathrm{Aut}(\mathbb{H}^2) = \mathrm{PSL}_2(\mathbb{R}) = \mathrm{Isom}^+(\mathbb{H}^2, ds^2_{\mathbb{H}^2})$ and the metric $ds^2_{\mathbb{H}^2}$ - see section 2.5.2 - descends to a metric ds^2_Σ in such a way that $(\Sigma, ds^2_{\Sigma^2})$ is locally isometric to $(\mathbb{H}^2, ds^2_{\mathbb{H}^2})$. Its curvature is then -1, implying that the genus of Σ is different from 1.

It results from this discussion the following classification theorem:

Theorem (Classification of closed Riemann surfaces). *Let Σ be a closed Riemann surface of genus g. Then:*

0. if $g = 0$, then Σ is biholomorphic to the Riemann sphere $\widehat{\mathbb{C}}$,

1. if $g = 1$, then Σ is biholomorphic to a flat torus $\mathbb{C}/\Gamma$,

2. if $g \geq 2$, Σ is biholomorpic to a quotient $\mathbb{H}^2/\Gamma$ of $\mathbb{H}^2$ by a Fuschian group $\Gamma < PSL_2(\mathbb{R})$.

2.5 Moduli space of flat tori: the modular curve $\mathcal{M}_1$

In this section we recall the determination of the moduli space of flat tori, also called the modular curve. We first give two definitions of flat tori. We give then some basics about hyperbolic geometry in the upper half plane. We finally compute the modular curve. The main reference for this section is [JS87] that we follow carefully.

2.5.1 Definition(s) of geometric flat tori

A **geometric flat torus** $\mathbb{T}$ is the polyhedral surface obtained by gluing the opposite edges of a parallelogram (isometries between edges being given by translations). It is a polyhedral surface of genus 1.

Suppose that the (non degenerated) parallelogram $P = \mathrm{ConvHull}(0, v_1, v_2, v_1 + v_2)$ defining $\mathbb{T}$ is embedded in the plane. Then, we can associate to $\mathbb{T}$ the lattice $\Gamma = \mathbb{Z}v_1 \oplus \mathbb{Z}v_2$. It appears that $\mathbb{T} \simeq \mathbb{C}/\Gamma$ as length spaces.

Conversely, given a lattice $\Gamma = \mathbb{Z}v_1 \oplus \mathbb{Z}v_2$ we can associate the parallelogram $P = \mathrm{ConvHull}(0, v_1, v_2, v_1 + v_2)$.

Moreover, we also have that $\mathbb{T} \simeq \mathbb{C}/\Gamma$ as Riemann surfaces. Indeed, first note that a geometric flat torus has no singularity. Hence, decomposing P in two overlapping parts
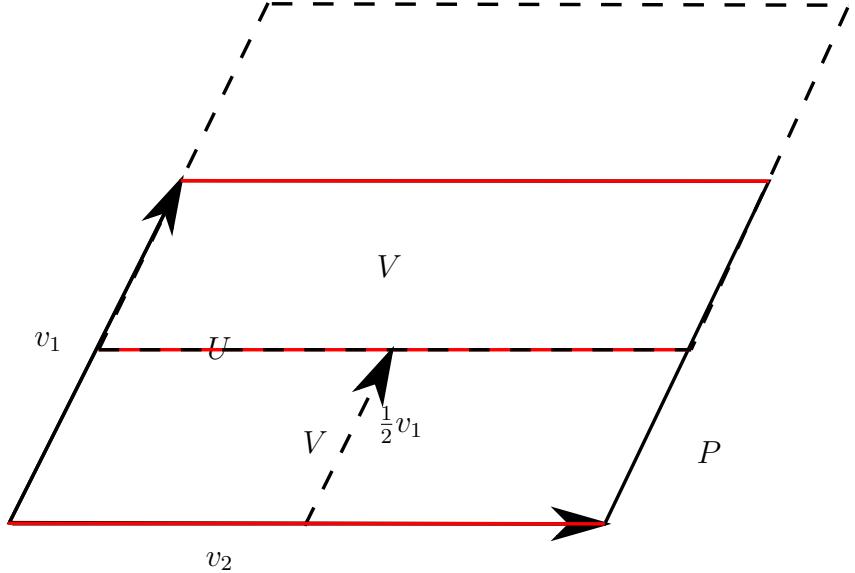
Figure 10: The parallelogram P, and the chart open sets U and V. Red segments represent removed parts.

$U = \pi(P \setminus [0,1]v_2)$ and $V = \pi(P \setminus [0,1](v_2 + \frac{1}{2}v_1))$ as in Figure 10 which consists of $\mathbb{T}$ with a latitude circle removed, we obtain an atlas of $\mathbb{T}$ in two charts: the canonical projection realizing a biholomorphism between any of the two previous sub-regions and an open annulus in $\mathbb{R}^2$. The chart transition maps are then given by the translations of vector $\pm\frac{1}{2}v_1$. Hence chart transition maps are holomorphic.

For $\mathbb{C}/\Gamma$, posing

$$U = \pi\left(\{\lambda_1 v_1 + \lambda_2 v_2 : 0 \leq \lambda_1, \lambda_2 \leq 1 \text{ and } \lambda_1 \neq 0, 1\}\right) \text{ and}$$

$$V = \pi\left(\left\{\lambda_1 v_1 + \lambda_2 v_2 : 0 \leq \lambda_1, \lambda_2 \leq 1 \text{ and } \lambda_1 \neq \frac{1}{2}\right\}\right)$$

gives charts with also translations as chart transition functions.

Finally, the identity id_P passes to quotient in both side to give a biholorphism between $\mathbb{T}$ and $\mathbb{C}/\Gamma$.

2.5.2 Hyperbolic geometry of the upper half plane $\mathbb{H}^2$

Metric. The upper half plane $\mathbb{H}^2 = \{z = x + iy \in \mathbb{C} \mid \Im(z) := y > 0\}$ is a Riemann surface as an open subset of $\mathbb{C}$. We can define a Riemannian metric on $\mathbb{H}^2$ by:

$$ds^2_{z=x+iy} := \frac{|dz|^2}{\Im(z)^2} = \frac{dx^2 + dy^2}{y^2}$$

where dx, dy are the linear forms of $\mathbb{C} \simeq \mathbb{R}^2$ dual of the canonical basis (x, y). As we saw before, this induces a structure of length space $(\mathbb{H}^2, d_{\mathbb{H}^2}, \ell_{\mathbb{H}^2})$ on $\mathbb{H}^2$.

Figure 11: A topological picture explaining the decomposition of a flat torus in two charts.
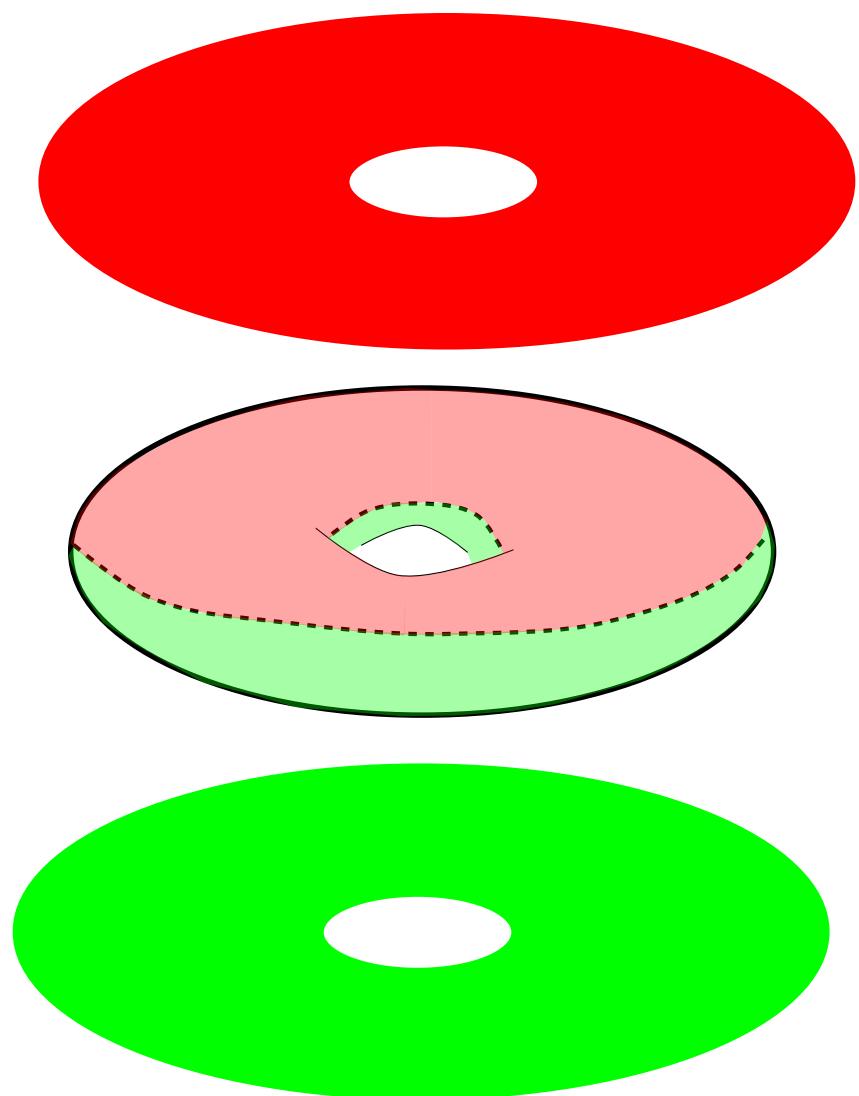
Isometries. First note that $SL_2(\mathbb{R})$ acts transitively on $\mathbb{H}^2$ by homography: $\begin{pmatrix} a & b \\ c & d \end{pmatrix} \cdot z :=$ $\frac{az+b}{cz+d}$, since $\Im \frac{az+b}{cz+d} = \frac{ad-bc}{|cz+d|^2} \Im z$. The kernel of this action being equal to homotheties, it induces a free and transitive group action of $\mathrm{PSL}_2(\mathbb{R}) \curvearrowright \mathbb{H}^2$.

Let $\gamma = (x,y) : I \to \mathbb{H}^2$ be a piecewise C^1 path, and let $A = \begin{pmatrix} a & b \\ c & d \end{pmatrix} \in \mathrm{PSL}_2(\mathbb{R})$. We will show that $\ell_{\mathbb{H}^2}(A \cdot \gamma) = \ell_{\mathbb{H}^2}(\gamma)$. Note $A \cdot z = u(z) + iv(z)$. One computes $v(z) = \frac{y}{|cz+d|^2}$ and $A'(z) = \frac{1}{(cz+d)^2}$, hence $A'(z) = \frac{v(z)}{y}$ and

$$\ell_{\mathbb{H}^2}(A \cdot \gamma) = \int_I \frac{|(A \circ \gamma)'(t)|}{v \circ \gamma(t)} dt = \int_I \frac{|\frac{v \circ \gamma}{y}(t)||\gamma'(t)|}{v \circ \gamma(t)} dt = \int_I \frac{|\gamma'(t)|}{y(t)} dt = \ell_{\mathbb{H}^2}(\gamma).$$

We thus show that every elements of $\mathrm{PSL}_2(\mathbb{R})$ is an isometry of $\mathbb{H}^2$.

Digression about the Riemann sphere $\widehat{\mathbb{C}}$ and its Möbius transformations. By definition, the **Riemann sphere** $\widehat{\mathbb{C}} = \mathbb{C} \cup \{\infty\}$ is the Alexandrov's completion of $\mathbb{C}$. $\widehat{\mathbb{C}}$ can be endowed a structure of Riemann surface compatible with its topology by the atlas $((U_i, \varphi_i))_{i=1,2}$ where $U_1 = \mathbb{C}$, $U_2 = \widehat{\mathbb{C}} \setminus \{0\}$ and $\varphi_1 = id_{\mathbb{C}}$, $\varphi_2 = id_{\widehat{\mathbb{C}} \setminus \{0\}}$. Thus the chart transition map is $\begin{array}{ccc} \mathbb{C}^* & \to & \mathbb{C}^* \\ z & \mapsto & \frac{1}{z} \end{array}$ which is holomorphic.

In fact, let us endow $\mathbb{S}^2$ with the complex structure given by the standard atlas $((U_N, \pi_N), (U_S, \pi_S))$ where $U_N = \mathbb{S}^2 \setminus \{N := (0,0,1)\}$, $U_S = \mathbb{S}^2 \setminus \{S := (0,0,-1)\}$, and π_N (resp. π_S) is the stereographic projection from the North pole N (resp. from the South pole S): $\pi_N : (x,y,z) \in \mathbb{S}^2 \setminus \{N\} \mapsto \frac{x+iy}{1-z} \in \mathbb{C}$ (resp. $\pi_S : (x,y,z) \in \mathbb{S}^2 \setminus \{S\} \mapsto \frac{x-iy}{1+z} \in \mathbb{C}$). See Figure 12. Inverses are given by $\pi_N^{-1} : z \in \mathbb{C} \mapsto \left(\frac{2z}{1+|z|^2}, \frac{|z|^2-1}{|z|^2+1} \right)$ and $\pi_S^{-1} : z \in \mathbb{C} \mapsto \left(\frac{2\bar{z}}{1+|z|^2}, \frac{1-|z|^2}{1+|z|^2} \right)$. The chart transition maps are given by $\pi_N \circ \pi_S^{-1} : z \in \mathbb{C}^* \mapsto \frac{1}{z} \in \mathbb{C}^*$ - and its inverse. It now follows easily that the map $f : \begin{array}{ccc} z \in \mathbb{C} & \mapsto & \pi_N^{-1}(z) \in \mathbb{S}^2 \setminus N \\ \infty & \mapsto & N \end{array}$ is a biholomorphism examining how f and f^{-1} read in charts. Indeed, for example, $\pi_N \circ f \circ \varphi_1 : z \mapsto z$, while $\pi_S \circ f \circ \varphi_1 = \pi_S \circ \pi_N^{-1} \circ (\pi_N \circ f \circ \varphi_1) : z \mapsto \frac{1}{z}$, and by the same kind of manipulation as before $\pi_N \circ f \circ \varphi_2 : z \mapsto \frac{1}{z}$ and $\pi_S \circ f \circ \varphi_2 : z \mapsto z$.

Now, note that $GL_2(\mathbb{C})$ acts on $\widehat{C}$ by homography:

$$\begin{pmatrix} a & b \\ c & d \end{pmatrix} \cdot z = \begin{cases} \frac{az+b}{cz+d} & \text{if} & z \neq \frac{-d}{c}, \infty \\ \infty & \text{if} & z = \frac{-d}{c} \\ \frac{a}{c} & \text{if} & z = \infty \end{cases} \quad \text{if } c \neq 0,$$

$$\begin{pmatrix} a & b \\ c & d \end{pmatrix} \cdot z = \begin{cases} \frac{az+b}{cz+d} & \text{if} & z \neq \infty \\ \infty & \text{if} & z = \infty \end{cases} \quad \text{if } c = 0.$$

This action being invariant by homothety, it defines a free action $\mathrm{PSL}_2(\mathbb{C}) \curvearrowright \widehat{\mathbb{C}}$. It can be shown that this is a meromorphic action and that $Aut(\widehat{\mathbb{C}})$, the set of meromorphic bijections of $\widehat{\mathbb{C}}$, identifies with $\mathrm{PSL}_2(\mathbb{C})$. They are called **Möbius transformations**. Now we define a **circle** of $\widehat{\mathbb{C}} \simeq \mathbb{S}^2$ the intersection of $\mathbb{S}^2$ with a Euclidean plane Π not tangent to $\mathbb{S}^2$. We will show that a Möbius transformation sends circles on circles. If Π
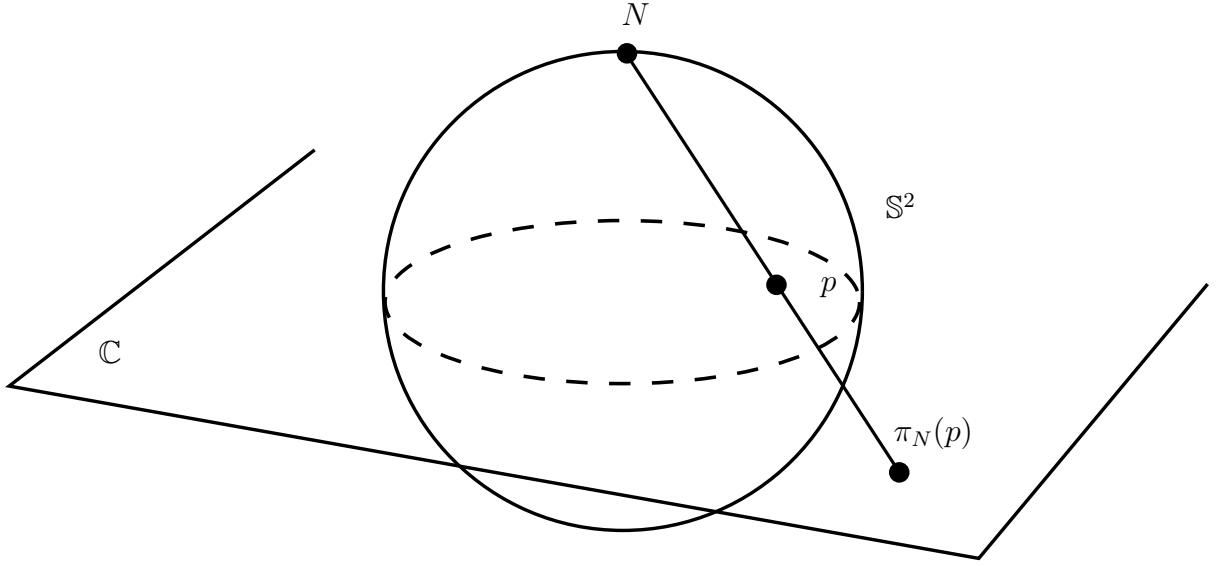
Figure 12: The stereographic projection π_N from the North pole N. π_N is the intersection point of the half-line from N through p with the plane (O, x, y).

admits the equation $\alpha x_1 + \beta x_2 + \gamma x_3 = \delta$ with $\alpha, \beta, \gamma, \delta \in \mathbb{R}$, then the circle it defines on $\widehat{\mathbb{C}}$ is $\pi_N(\Pi \cap \mathbb{S}^2)$ that has for equation

$$2\alpha x + 2\beta y + \gamma(|z|^2 - 1) = \delta(|z|^2 + 1), \quad z = x + iy.$$

Denoting $a = \gamma - \delta \in \mathbb{R}, b = \alpha - i\beta \in \mathbb{C}$ and $c = -(\gamma + \delta) \in \mathbb{R}$, this becomes:

$$az\bar{z} + bz + \bar{b}\bar{z} + c = 0.$$

Let $h = \begin{pmatrix} a_1 & a_2 \\ a_3 & a_4 \end{pmatrix}$ be a Möbius transformation, and C a circle with equation $az\bar{z} + bz + \bar{b}\bar{z} + c = 0$. Then $h^{-1}(C)$ is the set of solutions of the equation $ah(z)\overline{h(z)} + bh(z) + \overline{bh(z)} + c = 0$ that can be rearranged as $\tilde{a}z\bar{z} + \tilde{b}z + \bar{\tilde{b}}\bar{z} + \tilde{c} = 0$, with $\tilde{a} = |a_1|^2 a + 2\Re(a_1\bar{a_3}b) + |a_3|^2 c \in \mathbb{R}$ and $\tilde{c} = a|a_2|^2 + 2\Re(ba_2\bar{a_4}) + c|a_4|^2 \in \mathbb{R}$. Hence $h^{-1}(C)$ is a circle of $\widehat{\mathbb{C}}$.

Finally, let $h = \begin{pmatrix} a & b \\ c & d \end{pmatrix}$ be a Möbius transformation of $\widehat{\mathbb{C}}$. We know that h is meromorphic. We show that h is in fact conformal. Let us read h through charts. Let us recall the notation φ_1, φ_2 of the two introduced charts of $\widehat{\mathbb{C}}$, and $J : z \mapsto \frac{1}{z}$ be the chart transition map as seen before. We denote $h_{i,j} : z \mapsto \varphi_i \circ h \circ \varphi_j^{-1}(z)$ for $i, j = 1, 2$. Then $h_{1,1}(z) = h(z) = \frac{az+b}{cz+d}$, which has as derivative $h'_{1,1}(z) = \frac{ad-bc}{(cz+d)^2} = \frac{1}{(cz+d)^2} \in \mathbb{C}^*$ for all $z \neq \frac{-d}{c}$. Hence $h_{1,1}$ is conformal on $\mathbb{C} \setminus \{\frac{-d}{c}\}$. Hence so is h. It remains to check conformality at ∞ and $\frac{-d}{c}$.

If $c = 0$, then $a \neq 0$, $\frac{-d}{c} = \infty$ and $h_{2,2}(z) = J \circ h_{1,1} \circ J(z) = \frac{c+dz}{a+bz}$ satisfies $h'_{2,2}(z) = \frac{1}{(a+bz)^2} \in \mathbb{C}^*$ for all $z \neq \frac{-a}{b}, 0$. In particular, $h'_{2,2}$ admits a holomorphic continuation near 0, which is conformal. Consequently, $J(0) = \infty$ is a erasable singularity in one chart, hence in all charts, and h is conformal at ∞, and thus everywhere.

If $c \neq 0$, let us take a look at ∞. We have: $h_{1,2}(z) = \frac{a+bz}{c+dz}$ and $h'_{1,2}(z) = \frac{-1}{(c+dz)^2} \in \mathbb{C}^*$ for all $z \neq \infty, 0$, hence h is conformal at $J(0) = \infty$. Finally, at $\frac{-d}{c} \neq \infty$, we have $h_{2,1}(z) = \frac{cz+d}{az+b}$

34

and $h'_{2,1}(z) = \frac{-1}{(az+b)^2} \in \mathbb{C}^*$ for all $z \neq \frac{-d}{c}, 0$, so $h_{2,1}$ admits a conformal continuation at $\frac{-d}{c}$ and so h is conformal.

Geodesics. A **geodesic** between two points in $\mathbb{H}^2$ is a path of shortest length between these two points. We will show that given two points z_1, z_2 in $\mathbb{H}^2$, there is a unique geodesic between them.

Suppose first that $z_1 = x_0 + ia$ and $z_2 = x_0 + ib$ have the same real part. Let $\gamma = (x_0, y)$: $[0,1] \to \mathbb{H}^2$ the segment $x_0 + [ia, ib]$ so that $y(0) = a$, $y(1) = b$ and $y'(t) > 0$. We have:

$$\ell_{\mathbb{H}^2}(\gamma) = \int_0^1 \frac{|y'(t)|}{y(t)} dt = \int_a^b \frac{dy}{y} = \ln\left(\frac{b}{a}\right).$$

Moreover, if $\tilde{\gamma} = (\tilde{x}, \tilde{y}) : [0,1] \to \mathbb{H}^2$ is an other piecewise C^1 path on $\mathbb{H}^2$, then:

$$\ell_{\mathbb{H}^2}(\tilde{\gamma}) = \int_0^1 \frac{\sqrt{\tilde{x}'(t)^2 + \tilde{y}'(t)^2}}{\tilde{y}(t)} dt \geq \int_0^1 \frac{|\tilde{y}'(t)|}{\tilde{y}(t)} dt \geq \int_0^1 \frac{\tilde{y}'(t)}{\tilde{y}(t)} dt = \ell_{\mathbb{H}^2}(\gamma).$$

Equality holds if and only if $\tilde{x}' = 0$ and $\tilde{y}' \geq 0$. Hence $\tilde{\gamma}$ is the Euclidean segment joining $z_1 = x_0 + ia$ to $z_2 = x_0 + ib$.

Now suppose that z_1 and z_2 have not the same real part. The perpendicular bisector of the Euclidean segment joining z_1 and z_2 cuts the real axis in a point r which is the center of the unique Euclidean circle C through z_1 and z_2 and orthogonal to the real axis. Suppose that C intersects $\mathbb{R}$ at z_1^* and z_2^*. The action $\mathrm{PSL}_2(\mathbb{R}) \curvearrowright \mathbb{R} \cup \{\infty\}$ being 2-transitive, there exists $h \in \mathrm{PSL}_2(\mathbb{R})$ such that $h(z_1^*) = 0$ and $h(z_2^*) = \infty$. But, as a Möbius transformation, h sends C to a circle of $\widehat{\mathbb{C}}$ orthogonal to the real axis. Hence $h(C)$ is the imaginary axis. But we just saw that the geodesic between $h(z_1^*)$ and $h(z_2^*)$ is the Euclidean segment joining them. Hence, the geodesic between z_1^* and z_2^* is the arc of C in $\mathbb{H}^2$ joining these two points.

We thus showed that geodesics in $\mathbb{H}^2$ are given by straight vertical lines and half-circles centered in the real horizontal axis. We adjoin a point ∞ to vertical geodesics. By this way, any geodesic admits two end points in $\mathbb{R} \cup \{\infty\}$. We saw that $\mathrm{PSL}_2(\mathbb{R})$ sends geodesics on geodesics. In fact, this gives a transitive action of $\mathrm{PSL}_2(\mathbb{R})$ on the set of geodesics in $\mathbb{H}^2$. Indeed, if C, C' are two such geodesics, and if C (resp. C') has endpoints $s, t \in \mathbb{R} \cup \{\infty\}$ (resp. $s', t' \in \mathbb{R} \cup \{\infty\}$), then there exists $h \in \mathrm{PSL}_2(\mathbb{R})$ such that $h(s) = s'$ and $h(t) = t'$ as the action of $\mathrm{PSL}_2(\mathbb{R})$ on $\mathbb{R} \cup \{\infty\}$ is 2-transitive. It follows that $h(C) = C'$ as the endpoints of a geodesic determine it uniquely.

Generators for $\mathrm{PSL}_2(\mathbb{C})$. We showed that $\mathrm{PSL}_2(\mathbb{C})$ and $\mathrm{PSL}_2(\mathbb{R})$ appear as subgroups of isomorphisms of some geometric space, the Riemann surface $\widehat{\mathbb{C}}$ for the first and the Riemannian manifold $(\mathbb{H}^2, ds^2)$ for the second. We now give generators for $\mathrm{PSL}_2(\mathbb{C})$.

Note that similarities $S_\alpha = \begin{pmatrix} \alpha & 0 \\ 0 & 1 \end{pmatrix} : z \mapsto \alpha z, \alpha \in \mathbb{C}^*$, the inversion $J = \begin{pmatrix} 0 & 1 \\ 1 & 0 \end{pmatrix} : z \mapsto \frac{1}{z}$ and translations $T_t = \begin{pmatrix} 1 & t \\ 0 & 1 \end{pmatrix} : z \mapsto z + t, t \in \mathbb{C}$, are all Möbius transformations.

Conversely, it appears that they generate $\mathrm{PSL}_2(\mathbb{C})$. Indeed, let $h = \begin{pmatrix} a & b \\ c & d \end{pmatrix} \in \mathrm{PSL}_2(\mathbb{C})$.

If $c = 0$, then $h(z) = \frac{a}{d}z + \frac{b}{d} = T_t \circ S_\alpha(z)$ with $t = \frac{b}{d}$ and $\alpha = \frac{a}{d} \in \mathbb{C}^*$. If $c \neq 0$, then $h(z) = \frac{a}{c} - \frac{bc-ad}{a(cz+d)} = (T_t \circ J)\left(\frac{c^2z+cd}{bc-ad}\right)$ with $t = \frac{a}{c}$. Applying the case $c' = 0$ to $\frac{a'z+b'}{c'z+d'}$ with $a' = c^2, b' = cd, d' = bc - ad$, we see that h can be expressed thanks to similarities, translations and the inversion J.

2.5.3 Classification of flat tori

Let $\mathbb{T} = \mathbb{C}/\Gamma$ be a geometric flat torus, with $\Gamma = \mathbb{Z}v_1 \oplus \mathbb{Z}v_2$ its associated lattice. Exchanging v_1 and v_2 if necessary, we can suppose that (v_1, v_2) forms a direct basis. Then, the similarity by multiplication by v_1^{-1} sends Γ to $\Gamma_\tau = \mathbb{Z} \oplus \mathbb{Z}\tau$, where $\tau = \frac{v_2}{v_1} \in \mathbb{H}^2$, and descends into a biholomorphism between $\mathbb{T}$ and $\mathbb{C}/\Gamma_\tau$. We can thus suppose that Γ is of the form Γ_τ for some $\tau \in \mathbb{H}^2$. We denote $\mathbb{T}_\tau = \mathbb{C}/\Gamma_\tau$

Now given two geometric flat tori $\mathbb{T}_\tau$ and $\mathbb{T}_{\tau'}$, we want conditions on τ and τ' for them to be conformally equivalent. Assume so that there is a biholomorphism $f : \mathbb{T}_{\tau'} \to \mathbb{T}_\tau$. Considerations of algebraic topology - the fact that $\mathbb{C}$ is a holomorphic universal cover of any flat torus $\mathbb{T}$, and the existence and uniqueness of the lift of a path - implies that f lifts into a continuous map $\tilde{f} : \mathbb{C} \to \mathbb{C}$ satisfying $\pi_\tau \circ \tilde{f} = f \circ \pi_{\tau'}$. But since $\pi_{\tau'}$ is a local biholomorphism, in the neighborhood of a point $z_0 \in \mathbb{C}$, we have $\tilde{f} = \sigma_{z_0,\tau} \circ f \circ \pi_{\tau'}$ where $\sigma_{z_0,\tau}$ is a local holomorphic inverse of π near z_0. Hence, $\tilde{f}$ is holomorphic.
Now, as $\pi_\tau \circ \tilde{f} = f \circ \pi_{\tau'}$ we have that for all $z \in \mathbb{C}$ and $\gamma' \in \Gamma_{\tau'} : \tilde{f}(z + \gamma') = \tilde{f}(z) + \gamma_z$ for some $\gamma_z \in \Gamma_\tau$. But $z \in \mathbb{C} \mapsto \gamma_z \in \Gamma_\tau$ is continuous (even holomorphic) and so is constant by connectedness. Differentiating the previous equality yields $f'(z + \gamma') = \tilde{f}(z)$ for all $\gamma' \in \Gamma_{\tau'}$. We infer that $\tilde{f}'$ is holomorphic and $\Gamma_{\tau'}$ periodic and thus bounded on $\mathbb{C}$, it is hence constant by Liouville's theorem. Finally, $\tilde{f}(z) = \alpha z + \beta$ for some $\alpha \in \mathbb{C}^*$ and $\beta \in \mathbb{C}$.
Then, $\tilde{f}(1) \equiv \tilde{f}(\tau') \equiv \tilde{f}(0) = \beta \mod \Gamma_\tau$ which amounts to the existence of $a, b, c, d \in \mathbb{Z}$ verifying

$$\tilde{f}(\tau') = \alpha\tau' + \beta = a\tau + b + \beta,$$
$$\tilde{f}(1) = \alpha + \beta = c\tau + d + \beta.$$

Finally, we obtain:

$$\tau' = \frac{a\tau + b}{c\tau + d}.$$

Applying the same reasoning to f^{-1} gives integers a', b', c', d' satisfying $\tau' = \frac{a'\tau+b'}{c'\tau+d'}$. But, the previous formulas define in fact an action of $GL_2(\mathbb{Z})$ on $\mathbb{C}$ by homography given by $\begin{pmatrix} a & b \\ c & d \end{pmatrix} \cdot z := \frac{az+b}{cz+d}$. Hence, $\begin{pmatrix} a & b \\ c & d \end{pmatrix} \in SL_2(\mathbb{Z})$. Moreover, we compute $\Im(\tau') = \frac{ad-bc}{|c\tau+d|^2}\Im\tau > 0$. It follows that $ad - bc = 1$ and $\begin{pmatrix} a & b \\ c & d \end{pmatrix} \in GL_2{}^+(\mathbb{Z}) = SL_2(\mathbb{Z})$ the connected component of id in $GL_2(\mathbb{Z})$. The action $GL_2(\mathbb{Z}) \curvearrowright \mathbb{C}$ induces an action $\mathrm{PSL}_2(\mathbb{Z}) \curvearrowright \mathbb{H}^2$ as the computation of $\Im\tau'$ shows.

Conversely, if $\tau' = \frac{a\tau+b}{c\tau+d}$ for some $\begin{pmatrix} a & b \\ c & d \end{pmatrix} \in SL_2(\mathbb{Z})$, then $f : \begin{array}{ccc} \mathbb{T}_{\tau'} & \mapsto & \mathbb{T}_\tau \\ [z] & \mapsto & [(c\tau + d)z] \end{array}$ is a well defined holomorphic map with inverse $f^{-1} : [z] \mapsto [\frac{z}{c\tau+d}]$.

We can thus state the following theorem.

Theorem (Classification of flat tori). *Let $\mathbb{T}$ and $\mathbb{T}'$ be two flat tori with respective associated lattices $\Gamma = \mathbb{Z}v_1 \oplus \mathbb{Z}v_2$ and $\Gamma = \mathbb{Z}v_1' \oplus \mathbb{Z}v_2'$. We can suppose that $\frac{v_1}{v_2}, \frac{v_1'}{v_2'} \in \mathbb{H}^2$, relabeling if necessary. The following assertions are equivalent.*

1. *$\mathbb{T}$ and $\mathbb{T}'$ are conformally equivalent,*

2. *Γ and Γ' are similar, i.e. $\Gamma' = \lambda\Gamma$ for some $\lambda \in \mathbb{C}'$,*

3. *denoting $\tau = \frac{v_1}{v_2}$ (respectively $\tau' = \frac{v_1'}{v_2'}$) the **modulus** of $\mathbb{T}$ (respectively $\mathbb{T}'$), we have*
   $$\tau' = \frac{a\tau + b}{c\tau + d} =: \begin{pmatrix} a & b \\ c & d \end{pmatrix} \cdot \tau \text{ for some } \begin{pmatrix} a & b \\ c & d \end{pmatrix} \in PSL_2(\mathbb{Z}).$$

2.5.4 Modular curve

The previous discussion shows that the moduli space of flat tori $\mathcal{M}_1$ can be identified with the quotient space $\mathscr{M} := \mathbb{H}^2 / PSL_2(\mathbb{Z})$.

Note that $PSL_2(\mathbb{Z})$ is a discrete subgroup of $PSL_2(\mathbb{R})$, a so-called **Fuschian group**. A **fundamental region** for a topological group action $G \curvearrowright X$ is a closed set F such that

- $\bigcup_{g \in G} g \cdot F = X$,

- $\mathring{F} \cap g \cdot \mathring{F} = \emptyset$ for all $g \in G \setminus \{1\}$.

We want to find a fundamental region F for the action of $PSL_2(\mathbb{Z})$ on $\mathbb{H}^2$. Define $D_p(PSL_2(\mathbb{Z})) := \{z \in \mathbb{H}^2 : d_{\mathbb{H}^2}(z, p) \leq d_{\mathbb{H}^2}(z, h(p)) = d_{\mathbb{H}^2}(h(z), p) \text{ for all } h \in PSL_2(\mathbb{Z})\}$ the **Dirichlet region** for $PSL_2(\mathbb{Z})$ at p. We have that $p \in D_p(PSL_2(\mathbb{Z}))$ and as the action is discrete, $D_p(PSL_2(\mathbb{Z}))$ contains a neighborhood of p. Let $h_0 \in PSL_2(\mathbb{Z})$. The equality $d_{\mathbb{H}^2}(z, p) = d_{\mathbb{H}^2}(z, h(p))$ describes the hyperbolic orthogonal bisector of the geodesic through p and $h_0(p)$. Hence the inequality $d_{\mathbb{H}^2}(z, p) \leq d_{\mathbb{H}^2}(z, h(p))$ corresponds to a hyperbolic half-plane containing p. $D_p(PSL_2(\mathbb{Z}))$ is thus an intersection of hyperbolic half planes and is consequently a hyperbolically convex region - a hyperbolic polygon if there are finitely many of such half planes. The rest of the discussion aims at showing the following lemma.

Lemma. *The Dirichlet region of any point not fixed by $PSL_2(\mathbb{Z})$ is a fundamental region.*

Proof. Let $z_1 \in \mathbb{H}^2$ and z_0 be a point of least hyperbolic distance to p in the $PSL_2(\mathbb{Z})$-orbit of z_1. Such a z_0 exists: the orbit O_{z_1} of z_1 is discrete, so there exists a hyperbolic disk $\Delta(z_1, \varepsilon)$ centered at z_1 and of radius ε that contains no other point of O_{z_1} except z_1. We have thus an open cover $\bigcup_{h \in PSL_2(\mathbb{Z})} h\left(\Delta(z_1, \varepsilon)\right)$ of O_{z_1} in pairwise disjoint open subsets each containing exactly one element of O_{z_1}. Let r be sufficiently large so that the compact hyperbolic disc $\overline{\Delta}(p, r)$ contains at least one element of O_{z_1} with its surrounding hyperbolic disc of radius $\frac{\varepsilon}{2}$. By compactness, there is only finitely many elements of O_{z_1} within this disc. It suffices to choose then an element z_0 closest to p in this finite family. We have $d_{\mathbb{H}^2}(z_0, p) \leq d_{\mathbb{H}^2}(h(z_0), p)$ for all $h \in PSL_2(\mathbb{Z})$ by construction. Hence $D_p(PSL_2(\mathbb{Z}))$ contain at least one point of each $PSL_2(\mathbb{Z})$-orbit. Next, we want to show that two distinct points z_1, z_2 in the interior of $D_p(PSL_2(\mathbb{Z})$ cannot lie in the same $PSL_2(\mathbb{Z})$-orbit. If a

point z in $D_p(\mathrm{PSL}_2(\mathbb{Z}))$ satisfies $d_{\mathbb{H}^2}(z,p) = d_{\mathbb{H}^2}(h(z),p)$ for some $h \in \mathrm{PSL}_2(\mathbb{Z}), h \neq id$, then z lies in the boundary of $D_p(\mathrm{PSL}_2(\mathbb{Z}))$ - more precisely on the orthogonal bisector of the geodesic segment through p and $h(p) \neq p$. Hence interior points cannot belong to the same orbit. Finally, we showed that $D_p(\mathrm{PSL}_2(\mathbb{Z}))$ is a connected fundamental region. $\square$

An explicit computation of the metric shows that in fact

$$D_p(\mathrm{PSL}_2(\mathbb{Z})) = \left\{ z \in \mathbb{H}^2 : |\frac{h(z) - p}{z - p}| \geq \frac{1}{|cz + d|} \text{ for all } h = \begin{pmatrix} a & b \\ c & d \end{pmatrix} \in \mathrm{PSL}_2(\mathbb{Z}) \right\}. \quad (2.2)$$

We now want to determine $D_p(\mathrm{PSL}_2(\mathbb{Z}))$ for a suitable choice of $p \in \mathbb{H}^2$. Let $k > 1$. We first show that ki is not fixed by a nontrivial $h \in \mathrm{PSL}_2(\mathbb{Z})$. Indeed, if $h = \begin{pmatrix} a & b \\ c & d \end{pmatrix} \in \mathrm{PSL}_2(\mathbb{Z})$, we have $h(ki) = \frac{aki+b}{cki+d} = \frac{ack^2+bd+(ad-bc)ki}{c^2k^2+d^2}$, hence if ki is a fixed point of h, we have $c^2k^2 + d^2 = 1$ so $c = 0, d = \pm 1$ and $h(ki) = aki + b = ki$ so $a = 1$ and $b = 0$, i.e. $h = \pm id$. Let us determine $D_{ki}(\mathrm{PSL}_2(\mathbb{Z}))$. Let $z \in D_{ki}(\mathrm{PSL}_2(\mathbb{Z}))$. Putting $h = T : z \mapsto z + 1$ or $h = T^{-1} : z \mapsto z - 1$ in (2.2) gives $|z \pm 1 - ki| \geq |z - ki|$ which shows z is closer to ki than to $ki \pm 1$ (for the standard Euclidean metric). Therefore $D_{ki}(\mathrm{PSL}_2(\mathbb{Z})) \subseteq \left\{ z \in \mathbb{H}^2 : -\frac{1}{2} \leq \Re z \leq \frac{1}{2} \right\}$. Moreover let $h = S : z \mapsto \frac{-1}{z}$. Then $\frac{|\frac{-1}{z} - ki|}{|z - ki|} \geq \frac{1}{|z|}$ so $|1 + kiz|^2 \geq |z - ki|^2$ which leads to, after expanding, $(k^2 - 1)|z|^2 \geq k^2 - 1$. Finally: $D_{ki}(\mathrm{PSL}_2(\mathbb{Z})) \subseteq F := \left\{ z \in \mathbb{H}^2 : |z| \geq 1, |\Re z| \leq \frac{1}{2} \right\}$.

In fact the previous inclusion is an equality. Indeed, first note that $D_{ki}(\mathrm{PSL}_2(\mathbb{Z}))$ is symmetric with respect to the imaginary axis. For, let $\sigma : z \mapsto -\bar{z}$. As σ sends geodesics on geodesics, it is an isometry. And for all $h \in \mathrm{PSL}_2(\mathbb{Z})$, as $\sigma \circ h \circ \sigma \in \mathrm{PSL}_2(\mathbb{Z})$: $d_{\mathbb{H}^2}(\sigma(z), h(ki)) = d_{\mathbb{H}^2}(\sigma(z), h \circ \sigma(ki)) = d_{\mathbb{H}^2}(z, \sigma \circ h \circ \sigma(ki)) \geq d_{\mathbb{H}^2}(z, ki) = d_{\mathbb{H}^2}(\sigma(z), ki)$. Therefore $\sigma(z) \in D_{ki}(\mathrm{PSL}_2(\mathbb{Z}))$ for all $z \in D_{ki}(\mathrm{PSL}_2(\mathbb{Z}))$. We claim that the following lemma is true.

Lemma. *Let $z, w \in F$. Moreover, suppose that there exists $h \in PSL_2(\mathbb{Z}) \setminus \{id\}$ such that $h(z) = w$. Then $w = z$ or $w = \sigma(z)$ and in the latter case $z, w \in \partial F$.*

Proof. Indeed, if $h = \begin{pmatrix} a & b \\ c & d \end{pmatrix} \in \mathrm{PSL}_2(\mathbb{Z})$ maps z to $w = h(z)$ then:

$$\begin{aligned} |cz + d|^2 &= c^2|z|^2 + 2cd\Re z + d^2 \\ &\geq c^2 - cd + d^2 = (c - d)^2 + cd \\ &\geq 1. \end{aligned}$$

This shows that $\Im w = \frac{\Im z}{|cz+d|^2} \leq \Im z$. By interchanging the roles of $z = h^{-1}(w)$ and w, we obtain $\Im z \leq \Im w$. Thus $\Im z = \Im w$ and $|cz + d|^2 = 1$ and all the previous inequalities are equalities. It follows that

$$(c - d)^2 + cd = 1 \quad (2.3)$$

and

$$c^2(|z|^2 - 1) + cd(2\Re z + 1) = 0. \quad (2.4)$$
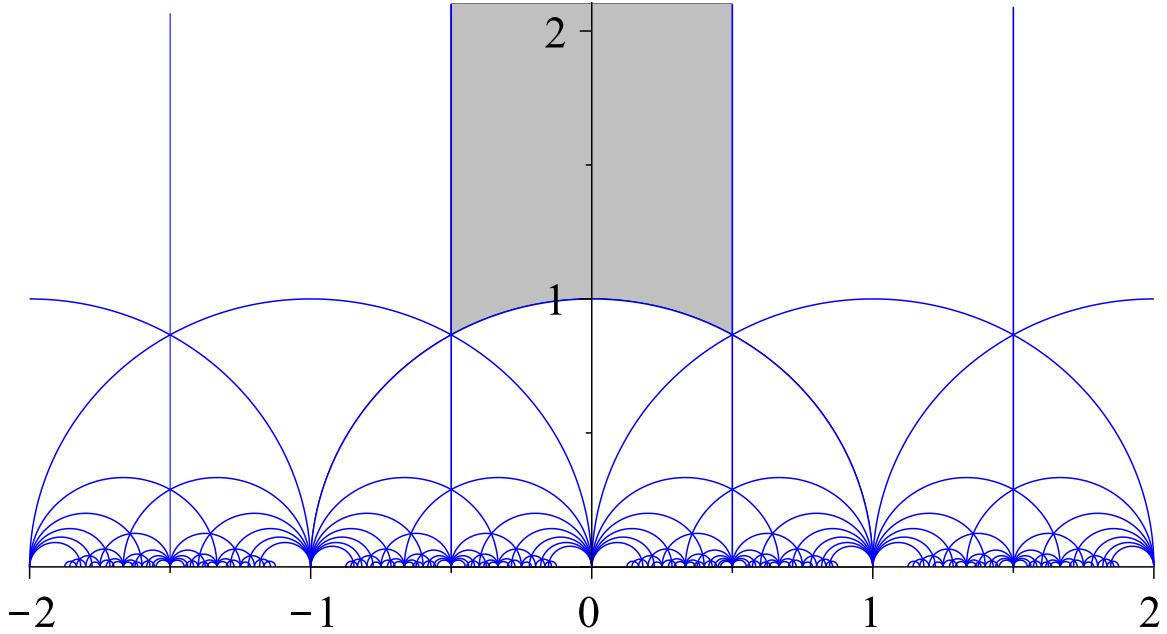
There are three possibilities:

Figure 13: In blue: (part of) the triangulation induced by the action $\mathrm{PSL}_2(\mathbb{Z}) \curvearrowright \mathbb{H}^2$. Each triangle of this triangulation is a fundamental region. In grey: the fundamental region $F = \left\{ z : |z| \geq 1, |\Re z| \leq \frac{1}{2} \right\}$ for this action. Wikipedia.

i) $c = 0$ and $d = \pm 1$, so $h = T^{\pm 1}$ and so z, w lie on the two vertical half-line of the boundary of F.

ii) $c = \pm 1, d = 0$ which implies that $|z| = 1$ by equation (2.4). We have then $h : z \mapsto \frac{az \mp 1}{\pm z} = \pm a - \frac{1}{z} = \pm a - \bar{z}$ with $a = 0, -1$ or 1 because $h(z) \in F$. If $a = 0$ then $h = S$ which acts as σ on $\mathbb{S}^1 \ni z, w$. If $a = \pm 1$, then $z = \frac{\pm 1 + i\sqrt{3}}{2} = \{e^{i\frac{\pi}{3}}, e^{2i\frac{\pi}{3}}\}$ and z is fixed by h.

iii) $c = d = \pm 1$ which implies by equation (2.4) that $|z| = 1$ and $\Re z = \frac{-1}{2}$ and so $z = e^{2i\frac{\pi}{3}}$. Then, as $h(z) \in F$ and as it has the same imaginary part as z, we have $h(z) = z$ or $h(z) = e^{i\frac{\pi}{3}} = \sigma(z)$.

$\square$

Finally, if $z \in F$, as $D_{ki}(\mathrm{PSL}_2(\mathbb{Z}))$ is a fundamental region, there exists $h \in \mathrm{PSL}_2(\mathbb{Z})$ with $h(z) \in D_{ki}(PSL_2(\mathbb{Z})) \subseteq F$. By the previous discussion, $z = h(z)$ or $z = \sigma \circ h(z)$. In both cases, we have $z \in D_{ki}(\mathrm{PSL}_2(\mathbb{Z}))$.

We thus showed that $\mathcal{M}$ is the quotient of F by the modular group $\mathrm{PSL}_2(\mathbb{Z})$ generated by $T : z \mapsto z + 1$ and $S : z \mapsto \frac{-1}{z}$. F being delimited by three incident geodesics, it is thus a hyperbolic triangle with vertices $e^{\pm 2i\frac{\pi}{3}}$ and an ideal vertex at ∞. It induces thus a hyperbolic tiling of $\mathbb{H}^2$ given by F and all its images by elements of $\mathrm{PSL}_2(\mathbb{Z})$ with interiors pairwise disjoint. Some representation of F and its image under some element of $\mathrm{PSL}_2(\mathbb{Z})$ are given in Figure 13.

One can show that $\mathcal{M}$ can be endowed with a complex structure and is thus a Riemann surface. We can easily show that $\mathcal{M}$ is not compact. Indeed, consider the sequence $(ki)_{k \geq 1}$.

Then every element of this sequence admits a unique representative in F, namely itself. Hence, for every point $z \in F$, Taking the image in $\mathscr{M}$ of a Euclidean open disk of radius $\frac{1}{2}$ surrounding z, we see that ki does not belong eventually to this neighborhood of z. Hence $(ki)_{k \geq 1}$ does not admit an accumulation point and $\mathscr{M}$ is not compact.

In fact, one can show that $\mathscr{M}$ admits a compactification $\overline{\mathscr{M}}$ with a unique **point at infinity**: $\overline{\mathscr{M}} \setminus \mathscr{M}$ is reduced to a point.

2.6 Links between topological, PL and smooth structures on a surface

In this section, we investigate the links between topological, PL and smooth structures one can put on a surface. It appears that they are all equivalent in some sense.

2.6.1 Topological and PL structures

First, every polyhedral surface admits a canonical topological structure as a metric space.

Conversely, the theorem of triangulation of Radò shows that every topological space admits a PL structure. A PL structure being a topological atlas where transition maps are PL.

The link between the two can even be made stronger. Every *PL* homeomorphism between polyhedral surfaces induces a homeomorphism as topological surfaces. There is a converse to this statement, the Hauptvermutung for surfaces: every homeomorphism of triangulated topological surfaces can be approximated by PL homeomorphisms (for the C^0-norm). Therefore, a topological structure on a surface induces a unique PL structure - and vice-versa.

The idea of a proof is the following, and can be found in [Moi13]. Suppose we are given a homeomorphism between two topological surfaces $f : S_1 \to S_2$ and $\varepsilon > 0$. As S_1 and S_2 admit triangulations, it is not restrictive to suppose that $S_1 = |T_1|$ and $S_2 = |T_2|$ are the geometric realizations of simplicial triangulations T_1 and T_2 respectively. Let T_i^1 be the **1-skeleton** of T_i, i.e. the collection of all the edges and vertices of T_1. $|T_1^1|$ is thus a geometric graph. Then f restricts to a homeomorphism $f_1 := f_{||T_1^1|} : |T_1^1| \to f(|T_1^1|) \subset S_2$. We want to approximate f_1 by a PL homeomorphism $F_1 : |T_1^1| \to S_2$ such that $F_{||T_1^0|} = f_{||T_1^0|}$, where T_1^0 stands for the vertices of T_1. The idea is to first subdivide T_1 (for example uniformly) so that the diameter of the image of each edge is sufficiently small (less than $\varepsilon/3$). Then to consider small discs surrounding the image of each vertex of T_1, and a regular neighborhood $N_{\varepsilon'}(e') := \{x : d(x, e') < \varepsilon'\}$ of the images of each edge. Finally using the fact that each such neighborhood is brokenline-wise connected, and with some technicalities, it is possible, for each edge e joining vertices v and w, to approximate its image by a broken line at distance at most ε of $f(e)$ in such a way that two broken lines associated to different edges can only intersect at end points. It suffices then to define F_1 to be the PL (homeomorphism) sending each edge e onto the broken line associated to e.

Let T_1' be a subdivision of T_1. We can construct F_1 as before, and for each $t \in T_1'$, each $F_{1|\partial t}$ can be extended to give a PL homeomorphism $F_{2,t}$. We want to chose T_1' and ε so that the PL homeomorphism $F_{2,t}$ fit together to give a PL homeomorphism $F_2 : |T_1'| \to |T_2|$ at distance at most ε to f. Subdividing T_1 sufficiently, we can suppose that the diameter of

the image of each triangle of T_1' is at most $\varepsilon/3$. We chose then F_1 to be a ε'-approximation of $f_{||T_1'^1|}$ where ε' is less than $\varepsilon/3$ and less than the minimum distance between the images of two vertices. Then, we extend F_1 into $F_{2,t}$ for all $t \in T_1'^1$ giving a PL continuous map F_2. As $F_2(t) \subset N_{\varepsilon/3}(f(t))$, we have that F_2 is an ε-approximation of f. It remains to show that F_2 is a homeomorphism. To do this, it suffices to show that F_2 is injective that is the sets $\mathrm{Int}F_2(t)$ are pairwise disjoint. But if $t_1 \neq t_2$, then t_2 has a vertex v which does not lie in t_1 and we have $F_2(t_1) \subset N_{\varepsilon'}(f(t_1))$ with $\varepsilon' \leq d(f(v), f(w))$ for all vertex w of t_1. Hence $v \notin F_2(t_1)$ and as $F_{2||T_1'|^1}$ is bijective, it ensures that $\mathrm{Int}F_2(t_1)$ and $\mathrm{Int}F_2(t_2)$ are disjoint.

2.6.2 Topological and smooth structures

Every smooth differential surface is by definition a topological surface.

Conversely, one can show that every topological surface admits a smooth structure. Moreover, the smooth structure is essentially unique as it can be shown that every homeomorphism between smooth surface is isotopic - i.e. can be continuously deformed - to a smooth diffeomorphism. We will sketch the proof of these two assertions. We refer to the very well written paper by Hatcher [Hat13] for further details.

We will admit the following theorem, which is central in the proof.

Theorem (Handle Smoothing)**.** *Let S be a smooth surface. Then:*

0. A topological embedding $\mathbb{R}^2 \to S$ can be isotoped to a smooth embedding in a neighborhood of the origin, staying fixed outside a larger neighborhood of the origin.

1. Denote $D^1 = [0,1]$. A topological embedding $D^1 \times \mathbb{R} \to S$ which is a smooth embedding near $\partial D^1 \times \mathbb{R}$ can be isotoped to a smooth embedding near a neighborhood of $D^1 \times \{0\}$, staying fixed outside a larger neighborhood of $D^1 \times \{0\}$ and near $\partial D^1 \times \mathbb{R}$.

2. A topological embedding $D^2 \to S$ which is a smooth embedding in a neighborhood of ∂D^2 can be isotoped to be a smooth embedding on all of D^2, staying fixed in a smaller neighborhood of ∂D^2.

Let S be a topological surface without boundary, together with a countable atlas $(V_i, \varphi_i)_{i \in \mathbb{N}}$. Denote $h_i = \varphi_i^{-1}$ local parametrizations of S. As every simply connected open subset of $\mathbb{R}^2$ is homeomorphic to $\mathbb{R}^2$, we can suppose $h_i : \mathbb{R}^2 \to S$. We will construct smooth parametrizations of $U_n := \cup_{i=0}^n h_i(\mathbb{R}^2)$ by induction. For $n = 0$ there is nothing to do as h_0 is a local parametrization of $U_0 = V_0$. Consider the induction step of extending a smooth structure from U_{n-1} to U_n. Let $W = h_n^{-1}(U_{n-1})$. This is an open set in $\mathbb{R}^2$. One can show that W admits a triangulation $\mathcal{T}$. Then, by using 0 at each vertex of $\mathcal{T}$, we obtain a new topological embedding h_n that is smooth on a neighborhood of the 0-skeleton $\mathcal{T}^0$ of $\mathcal{T}$. Then, every edge of $\mathcal{T}$ admits a tubular neighborhood in W that is homeomorphic to $D^1 \times \mathbb{R}$. We can thus apply 1 on each such tubular neighborhood to get a new embedding h_n which is smooth on a neighborhood of the 1-skeleton $\mathcal{T}^1$ of $\mathcal{T}$ - since h_n remains fixed in a neighborhood of each edge. Finally, applying 2 to each triangle of $\mathcal{T}$, we get a global smooth embedding $h_{n|W} : W \to U_{n-1}$. The new h_n thus constructed gives a compatible local parametrization for U_n. This shows that S admits a smooth structure.

If S has a non empty boundary, then it is possible to construct a (collar) neighborhood of ∂S that admits a smooth structure. Then it suffices to apply the method in the non boundary case to extend this smooth structure on all of S.

In fact, the smoothing procedure previously described can be applied to every homeomorphism $f : S \to S$ of the smooth surface S, if S has an empty boundary. Using once again a collar neighborhood of ∂S, this extends to every surface. Hence every homeomorphism of a smooth surface is isotopic to a smooth diffeomorphism.

2.7 Translation surfaces

In this section, we discuss some basic definitions and properties about translation surfaces which are polyhedral surfaces of a certain type: they are gluing of polygons where gluing maps are translations. We give some equivalent definitions that enable to handle them better from a complex analytic and algebraic point of view. We then define their moduli space and give several useful properties about them. Finally, we focus on genus 2 translation surfaces, and give canonical decompositions for them: they are either the gluing of a L polygonal shape, or a Z polygonal shape. References for this section include [DHV24], [FM13], [Hub06], [Mas22], [Mum71], [McM], [Pet24], [Tro86], [Vee86], [Vee90], [Wri15] and [Yoc10].

2.7.1 Definitions

Constructive definition. A **translation surface** Σ is an orientable polyhedral surface where all the polygons are given in a same Euclidean plane and gluing maps are taken to be translations. For example, every flat torus is a translation surface. As a polyhedral surface, a translation surface is flat except at possible singularities. Let v be a singularity of Σ. We will show that it has conical angle $\alpha_v = 2k_v\pi$ for some $k_v \in \mathbb{N}^*$. Indeed, consider a reciprocal image $w \in \mathbb{R}^2$ of v by the canonical projection. Let e, e' be the edges incident to w in the plane. Consider the equivalence relation on oriented edges induced by: $e \sim e'$ if e and e' contain both a vertex that projects to a same point in Σ which is the source of e and e'. Clearly $e \sim \sigma(e)$ for all edge e where orientation is reversed, and the same holds for two adjacent edges. Now denoting $\mathcal{O}_v = \{e_0, ..., e_m\}$ the equivalence class of oriented edges that contain a vertex that projects to v as a source, labeling such that e_i and e_{i+1} are adjacent, we have $\alpha_v = \sum\limits_{i=0}^{m} \angle(\overrightarrow{e_i}, \overrightarrow{e_{i+1}})$ where indices are taken modulo m. But as $e \sim \sigma(e)$ - with orientation reversed - the sum is of the form $\sum\limits_{k=0}^{k_v} \overrightarrow{e_k}\overrightarrow{\sigma(e_k)}$ by Chasles' relations. As e and $\sigma(e)$ are translates of each other, the previous sum is equal to $2k_v\pi$. The number $k_v - 1$ is called the **order** of the singularity v.

Analytic definition. Let Σ be a translation surface obtained from the gluing of a family $\mathcal{P}$ of polygons. Given an edge e belonging to some polygon $P_e \in \mathcal{P}$, consider the (non empty) set $\mathcal{T}_e$ of all triangles that contain the edge e as one of their edges and such that their third vertex is a vertex of P_e. Now let e, e' be paired edges, and let τ be the translation sending e on e'. Then $t \cup \tau(t') \subset \mathbb{R}^2 \simeq \mathbb{C}$ is a planar quadrilateral whose interior is denoted $V_{t,t'}$. Denote also $U_{t,t'}$ the interior of the image of $t \sqcup t'$ in Σ. $V_{t,t'}$ is

naturally in bijection with $\mathring{t} \cup e \sqcup \mathring{t}'$ which is itself in bijection with $U_{t,t'}$ by the canonical projection. The inverse of this bijective map from $V_{t,t'}$ to $U_{t,t'}$ is denoted $\varphi_{t,t'} : U_{t,t'} \to V_{t,t'}$. It is a homeomorphism.

Denote $V(\Sigma)$ the (finite) set of vertices of Σ (singularities or not). Then the domains $U_{t,t'}$ form an open cover of $\Sigma \setminus V(\Sigma)$. And the transition map $\varphi_{t_1,t_1'} \circ \varphi_{t_0,t_0'}^{-1}$ is equal to the composition $\tau_1 \circ \tau_0^{-1}$ of the translations defining the $V_{t_i,t_i'}$. Hence this defines a complex structure on $\Sigma \setminus V(\Sigma)$. Now let $v \in V(\Sigma)$, and let U_v be an open disc surrounding v such that the U_v are pairwise disjoint. Its preimage under the canonical projection is a union of circular sectors $S_1, ..., S_l$ where S_i surrounds a vertex v_i whose angle at v_i is θ_i. Suppose that we label the S_i such that their straight boundaries are delimited by edges e_i, f_i with f_i parallel to e_{i+1}. Denoting $\Theta_i = \sum_{j=1}^{i-1} \theta_i$, we define a map on each S_i by $\varphi_v^i(v_i + \rho e^{i(\Theta_i + \theta)}) = \rho e^{\frac{1}{k_v}(\Theta_i + \theta)}$, for $0 \le \rho \le r, 0 \le \theta \le \theta_i$. The φ_v^i match together to define a homeomorphism $\varphi_v : U_v \to D(0, r)$ where $D(0, r)$ denote the Euclidean disk of center 0 and radius r. Adjoining the charts (U_v, φ_v) to the atlas $(U_{t,t'}, \varphi_{t,t'})$ gives an atlas on the whole Σ. The transition maps are either the previous translations, the $\varphi_{t,t'} \circ \varphi_v^{-1} : z \mapsto (z - z_0)^p + z_1$ and the $\varphi_v \circ \varphi_{t,t'}^{-1} : z \mapsto (z + z_0)^{\frac{1}{p}} + z_1$ which are all holomorphic - the last one is holomorphic since it is defined on $\pi^{-1}(U_v) \cap V_{t,t'}$ which is an angle sector whose apex is v hence a branch of logarithm can be holomorphically defined.

Σ can thus be endowed with a complex structure and is a Riemann surface. Moreover, by pulling back the canonical holomorphic 1-form dz on $\mathbb{C}$ via the charts $\varphi_{t,t'}$, we obtain compatible - as transition maps are translation and thus have trivial derivative - 1-forms that glue together to form a holomorphic 1-form ω on $\Sigma \setminus V(\Sigma)$. If v is a flat vertex, it is possible to cut and paste the polygons defining Σ so that v lie now in the interior of a polygon - recall that every polygon can be triangulated. So ω is in fact well defined on $\Sigma \setminus \mathrm{Sing}(\Sigma)$. We impose $w_v \equiv 0$ at a singularity v. This defines a holomorphic 1-form. Indeed, ω is holomorphic when read through charts of the form $\varphi_{t,t'}$, and at a singularity v, we have: $F_{v*}\omega : z \mapsto \omega_{F_v^{-1}(z)}(dF_v^{-1}\cdot)$. But, $\omega_{F_v^{-1}(z)} = \varphi_{t,t'}^* dz$ and $dF_v^{-1} = d\varphi_{t,t'}^{-1} \cdot d(\varphi_{t,t'} \circ F_v^{-1}) : z \mapsto d\varphi_{t,t'}^{-1} \cdot (k_v z^{k_v - 1})$. Hence, $F_{v*}\omega : z \mapsto k_v z^{k_v - 1} dz$ and ω is holomorphic at v which is a zero of order $k_v - 1$.

Conversely it can be shown that given a pair (Σ, ω) where Σ is a Riemann surface and ω is a holomorphic 1-form, Σ is a polyhedral surface with an atlas on $\Sigma \setminus \mathrm{Sing}(\Sigma)$ whose transition maps are translations. It is thus a translation surface as defined previously. A nice proof can be found in [DHV24]. The idea is to construct an atlas of $\Sigma \setminus \mathrm{Sing}(\Sigma)$ by integrating ω in charts. The transition maps of the new atlas are then translations. Then, it suffices to triangulate Σ by flat Euclidean triangles with $\mathrm{Sing}(\Sigma)$ being a subset of the vertices of the triangulation. All the difficulty lies in the construction of such a triangulation.

Geometric definition. As we saw, in the constructive definition of a translation surface Σ, there is an atlas $(U_{t,t'}, \varphi_{t,t'})$ of $\Sigma \setminus \mathrm{Sing}(\Sigma)$ whose transition maps are translations. Moreover, we saw that all $v \in \mathrm{Sing}(\Sigma)$ admits a local chart (U_v, φ_v) that reads through the $\varphi_{t,t'}$ as $z \mapsto z^{1/k_v}$. This atlas is called a **translation structure** on Σ.

Conversely, if such an atlas exists, then as before this defines a complex structure on Σ. Moreover, we can as previously glue the $\varphi_{t,t'}^* dz$ to obtain a holomorphic 1-form on

$\Sigma \setminus \mathrm{Sing}(\Sigma)$ that extends entirely on Σ, with a zero of order $k_v - 1$ at each singularity v.

2.7.2 Moduli spaces

The equivalence between the geometric and analytic definitions enables us to have an algebraic point of view on the family of all possible translation surfaces of a given genus g.

Definition of $\mathcal{H}(\mu)$ and $\mathcal{H}_g$. Let $g \geq 0$ be a natural number and S_g the orientable and closed topological surface of genus g. Let also $\mu = (m_1, ..., m_n)$ be a multi-index of natural number. We define:

$\mathcal{H}_G(\mu) := \{\text{maximal translation structures on } S_g \text{ with } n \text{ singularities of order } m_1, ..., m_n\} / \sim_g$

$\mathcal{H}_A(\mu) := \{(\Sigma, \omega) : \Sigma \text{ Riemann surface of genus } g \text{ and } \omega \text{ holomorphic 1-form on } \Sigma \text{ with}$
$\qquad n \text{ zeros of order } m_1, ..., m_n\} / \sim_a$

where we identify two maximal translation structures $\mathscr{T}_1$ and $\mathscr{T}_2$ for $\sim_g$ if there is homeomorphism $f : S_g \to S_g$ preserving orientation such that $f^* \mathscr{T}_2 := \{(f^{-1}(U), \varphi \circ f) : (U, \varphi) \in \mathscr{T}_2\} = \mathscr{T}_1$. Note that $\mathscr{T}_1 \sim_g \mathscr{T}_2$ implies that those two atlases have the same number of singularities, and each singularity and its image have the same order. In turn, we identify two pairs (Σ_1, ω_1) and (Σ_2, ω_2) for $\sim_a$ if there exists a biholomorphism $f : \Sigma_1 \to \Sigma_2$ such that $f^* \omega_2 = \omega_1$.

We show that, in fact, $\mathcal{H}_G(\mu)$ and $\mathcal{H}_A(\mu)$ are in bijection. We denote by $\mathcal{H}(\mu)$ the common space they represent. The following is devoted to demonstrating this bijection.

Let (Σ, ω) be a pair composed by a Riemann surface and a holomorphic 1-form. The complex structure together with the holomorphic 1-form allows to define a translation structure. Indeed, for p_0 away from the zeroes of ω, take a simply connected neighborhood U_{p_0} of p_0 and define $\varphi_{p_0} : p \in U_{p_0} \to \int_{p_0}^p \omega$. For $p \in U_{p_0} \cap U_{p_1}$, we have then: $\varphi_{p_0}(p) = \int_{p_0}^{p_1} \omega + \varphi_{p_1}(p)$. Hence transition maps are translations. Moreover, near a zero p of ω, by local normalization (see [Sik18]), ω reads through a chart (U, φ) near p as $\omega := f(z)^{k-1} dz$ where $f : \varphi(U) \to D(0, r)$ is a biholomorphism with $f(0) = 0$ ($r > 0$) and $k \geq 2$. We look for a biholomorphism g satisfying $g_*(\omega) = z^{k-1} dz$ which is equivalent to $z^{k-1} = f \circ g^{-1}(z)^{k-1} \times \frac{1}{g' \circ g^{-1}(z)}$ or $g(z)^{k-1} g'(z) = f(z)^{k-1}$. This solves to $g^k(z) = kF(z)$ where F is any primitive of f^{k-1}. It suffices to take the k-th root of F - which can be built holomorphically as F is bounded - to find a biholomorphism g such that ω reads $z^{k-1} dz$ in the chart $g \circ \varphi =: \psi$. Hence, for every other chart φ_0 defined away from a singularity, we have $\psi_* \cdot \omega = z^{k-1} dz = (\psi \circ \varphi_0^{-1} \circ \varphi_0)_* \cdot \omega = (\psi \circ \varphi_0^{-1})_* \cdot dz$. Hence $(\varphi_0 \circ \psi^{-1})'(z) = z^{k-1}$ and $\varphi_0 \circ \psi^{-1}(z) = z^k$ assuming it sends the origin to itself. Finally, we defined a translation structure on Σ.

Now, suppose we are given two Riemann surface endowed with 1-forms (Σ_1, ω_1) and (Σ_2, ω_2) which have maximal translation structures equivalent through a homeomorphism f. Then, f reads through charts φ_1 of Σ_1 and φ_2 of Σ_2 as $\varphi_2 \circ f \circ \varphi_1^{-1}$ which is a transition map, and hence is holomorphic. The same holds for f^{-1}, which is therefore a biholomorphism. Now, for $v \in \Sigma_1 \setminus \mathrm{Sing}(\Sigma_1)$, we have by construction a chart φ_2 of $\Sigma_2 \setminus \mathrm{Sing}(\Sigma_2)$ near $f(v)$ such that: $(f^* \cdot \omega_2)_v = f^* \varphi_2^* \cdot dz = (\varphi_2 \circ f)^* \cdot dz = \omega_{1v}$. Hence $f^* \cdot \omega_2 = \omega_1$ on $\Sigma_1 \setminus \mathrm{Sing}(\Sigma_1)$. It follows that f must send $\Sigma_1 \setminus \mathrm{Sing}(\Sigma_1)$ on $\Sigma_2 \setminus \mathrm{Sing}(\Sigma_2)$. Hence f is a bijection from $\mathrm{Sing}(\Sigma_1)$ to $\mathrm{Sing}(\Sigma_2)$. Finally, near a singularity v of Σ_1, for some local coordinates z

near v and w near $f(v)$: $(f^*\omega_2)_v = f'(v)\omega_{2f(v)} = f'(v)w^{k_{f(v)}-1}dw = \omega_{1v} = z^{k_v-1}dz$. Hence f sends zeros of ω_1 onto zeros of ω_2 preserving multiplicities.

Conversely, if there exists a biholomorphism $f : \Sigma_1 \to \Sigma_2$ such that $f^*\omega_2 = \omega_1$, then f is a orientation preserving homeomorphism $(\Sigma_1, \mathscr{T}_1) \to (\Sigma_2, \mathscr{T}_2)$ - where $\mathscr{T}_i$ is a maximal translation structure on Σ_i. Moreover, $f^*\mathscr{T}_2$ is a subatlas of $\mathscr{T}_1$. Indeed, for all charts (U_2, φ_2), (V_2, ψ_2) in $\mathscr{T}_2$, $f^{-1}(U_2)$ is open and $(\varphi_2 \circ f) \circ (\psi_2 \circ f)^{-1} = \varphi_2 \circ \psi_2^{-1}$ are transition maps of $\mathscr{T}_2$ hence translations or of the form $z \mapsto z^k$ or its inverse. Hence $f^*\mathscr{T}_2 \subseteq \mathscr{T}_1$ by maximality. The same reasoning applied to f^{-1} shows that $f^{-1*}\mathscr{T}_1 \subseteq \mathscr{T}_2$. Thus $f^*\mathscr{T}_2 = \mathscr{T}_1$ and $\mathscr{T}_1 \sim_g \mathscr{T}_2$.

Finally, we show that we can associate to a translation structure $\mathscr{T}$ a pair (Σ, ω) composed of a Riemann surface and a holomorphic one-form, and vice-versa, and that two translation structures $\mathscr{T}_1$ and $\mathscr{T}_2$ are identified in $\mathcal{H}_G(\mu)$ if and only if their associated pairs satisfy $(\Sigma_1, \omega_1) \sim_a (\Sigma_2, \omega_2)$.

Now let $\Sigma \in \mathcal{H}(\mu)$ be a translation surface of genus g obtained by gluing a family $\mathcal{P} = \{P_1, ..., P_p\}$ of polygons with translated and facing paired edges. By cutting the polygons in $\mathcal{P}$ if necessary, we can suppose P_i convex for all i - for example a triangle. Denote by $2N$ the total number of edges of the polygons, n_i the number of vertices of P_i. We have that $2N = \sum_{i=1}^p n_i$. By padding μ with 0's, to account for the vertices with angle 2π "resulting from the P_i", we may assume that n is equal to the number of vertices after identification of the paired edges. On the one hand, we have by counting the total angle at every conical point: $\sum_{i=1}^n 2(m_i + 1)\pi = \sum_{j=1}^p (n_j - 2)\pi$. On the other hand, Euler formula gives: $\chi(\Sigma) = n - N + p = n - \frac{1}{2}\sum_{i=1}^p n_i + p = 2 - 2g$. Hence:

$$\sum_{i=1}^n m_i = 2g - 2. \tag{2.5}$$

We define then the moduli space of all translation structures, up to equivalence, on the closed orientable surface S_g of genus g:

$$\mathcal{H}_g = \bigcup_{\substack{\mu = (m_1, ..., m_n) \\ \sum_{i=1}^n m_i = 2g - 2}} \mathcal{H}(\mu).$$

Teichmüller space of translation structures. Let (Σ, ω) be a translation surface with underlying topological surface S_g, μ a multi-index which represents the multiplicities of the zeros of ω, and denote $\text{Diff}^0(S_g)$ the group of diffeomorphisms of S_g homotopic to the identity and $Z = \{x_1, ..., x_n\} \subset S_g$ the set of zeros of ω. We have an action of the group $\text{Diff}^0(S_g, Z)$, formed by the elements of $\text{Diff}^0(S_g)$ fixing the zeros of ω, on the space $\mathscr{C}(S_g, Z, \mu)$ of translation structures of S_g with singularities Z of order given by μ, given by pushing forward via $f \cdot (\Sigma, \omega) = (f_*\Sigma, f_*\omega)$ where $f_*\Sigma$ denotes the Riemann surface endowed with the atlas over S_g: $\{(f(U), \varphi \circ f^{-1}) : (U, \varphi) \text{ atlas of } \Sigma\}$. We define then the Teichmüller space of translation surfaces of type (S_g, Z, μ) the quotient space

$$\mathscr{Q}(S_g, Z, \mu) := \mathscr{C}(S_g, Z, \mu)/\text{Diff}^0(S_g).$$

Fix a universal cover $\pi : (\widetilde{S_g}, \tilde{x}) \to (S_g, x)$ of S_g. To each translation structure (Σ, ω) on S_g we can associate a continuous map, the **developing map**

$$D_{\Sigma,\omega} : (\widetilde{S_g}, \tilde{x}) \to (\mathbb{C}, 0), \tilde{p} \mapsto \int_{\tilde{x}}^{\tilde{p}} \pi^* \omega.$$

Suppose $D_{\Sigma,\omega} = D_{\Sigma',\omega'}$. Then by change of variables: $0 = \int_{\tilde{x}}^{\tilde{p}} \pi^* \omega - \pi^* \omega' = \int_{\tilde{x}}^{\tilde{p}} \pi^* (\omega - \omega') = \int_{\gamma} \omega - \omega'$ for all $\tilde{p} \in \widetilde{S_g}$, where γ is the projection of a path from $\tilde{x}$ to $\tilde{p}$. This in turn implies that $\omega = \omega'$ as one can see easily in local coordinates. Moreover, if $f \in \mathrm{Diff}^0(S_g)$, we have $D_{f^*\Sigma, f^*\omega}(\tilde{p}) = \int_{\tilde{x}}^{\tilde{p}} \pi^* f^* \omega = \int_{\tilde{x}}^{\tilde{p}} (f \circ \pi)^* \omega = \int_{f \circ \gamma} \omega = \int_{\gamma} \omega = D_{\Sigma,\omega}(\tilde{p})$ as f is homotopic to identity. Finally, we have a well defined map $D : \mathscr{Q}(S_g, Z, \mu) \to \mathcal{C}^0(\widetilde{S_g}, \mathbb{C}), [(\Sigma, \omega)] \mapsto D_{\Sigma,\omega}$. We transport the compact-open topology from $\mathcal{C}^0(\widetilde{S_g}, \mathbb{C})$ to $\mathscr{Q}(S_g, Z, \mu)$ thanks to D.

We saw, in the previous paragraph, that $\mathcal{H}(\mu) = \mathcal{H}_A(\mu)$, where the identification $(\Sigma, \omega) \sim_a (\Sigma', \omega')$ is given by the action of $\mathrm{Diff}_+(S_g)$ on $\mathscr{C}(S_g, Z, \mu)$. It follows that $\mathcal{H}(\mu) = \mathscr{C}(S_g, Z, \mu)/\mathrm{Diff}_+(S_g) \simeq \mathscr{Q}(S_g, Z, \mu)/\mathrm{MCG}(S_g)$ where we denoted $\mathrm{MCG}(S_g) := \mathrm{Diff}_+(S_g)/\mathrm{Diff}^0(S_g)$ the **mapping class group** of S_g. Hence $\mathcal{H}(\mu)$ inherits the quotient topology.

Period coordinates. Let (Σ, ω) be a translation surface of genus g with n singularities $x_1, ..., x_n \in \Sigma$ in the Teichmüller space $\mathscr{Q}(S_g, Z = \{x_1, ..., x_n\}, \mu)$. A **period** of ω is a integral of the form $\int_{\gamma} \omega$ where γ is a piecewise C^1 path on S_g. Denote $\alpha_1, ..., \alpha_{2g}$ piecewise C^1 representatives of a basis of $\pi_1(S_g, x_1)$, and c_i a piecewise C^1 simple path from x_1 to x_{i+1}, $1 \leq i \leq n-1$. We define the **period coordinates** of Σ with respect to the basis $\mathcal{B} := (\alpha_1, ..., \alpha_{2g}, c_1, ..., c_{n-1})$ to be the complex numbers:

$$\Phi_{\mathcal{B}}(\omega) := \left(\int_{\alpha_1} \omega, ..., \int_{\alpha_{2g}} \omega, \int_{c_1} \omega, ..., \int_{c_{n-1}} \omega \right).$$

Note that, if $(\Sigma_2, \omega_2) \sim (\Sigma_1, \omega_1)$ in $\mathscr{Q}(S_g, Z, \mu)$ and if $f \in \mathrm{Diff}^0(S_g)$ is such that $f^* \omega_2 = \omega_1$, then by change of variables formula: $\Phi_{\mathcal{B}}(f^* \omega_2) = \Phi_{f(\mathcal{B})}(\omega_2)$. Indeed, as f is homotopic to the identity, $f_* = id$ and thus $f(\mathcal{B}) = \mathcal{B}$. Note that this is generally not the case if f is only supposed to be a biholomorphism between Σ_1 and Σ_2.

This defines a family of local charts for $\mathscr{Q}(S_g, Z, \mu)$. A proof using so-called zippered rectangle constructions can be found in [Yoc10]. Moreover, this zippered rectangle constructions allows to canonically associate a Riemann surface Σ_ω to a holomorphic one-form ω so that Σ_ω is biholomorphic to $\Sigma_{\omega'}$ if and only if there exists $f \in \mathrm{Diff}_+(S_g)$ pulling back ω' to ω.

These charts can be used to endow $\mathscr{Q}(S_g, Z, \omega)$ with a complex structure of complex dimension $2g + n - 1$. This enables to define a structure of complex orbifold on $\mathcal{H}(\mu)$, that is roughly speaking a structure of complex manifold with isolated singularities.

Moreover, these period charts can also be used to define the topology of $\mathcal{H}(\mu)$. A basis for the topology is given by the $\pi \circ \Phi_{\mathcal{B}}^{-1}(U)$ where U runs over all open subset of $\mathbb{C}^{2g+n-1}$ sufficiently small so that $\Phi_{\mathcal{B}}^{-1}$ is well defined on U, and $\pi : \mathscr{Q}(S_g, Z, \mu) \to \mathcal{H}(\mu)$ is the above quotient map.

Digression: link between quadratic differentials on a Riemann surface and the cotangent space to Riemann surfaces Teichmüller space. We give in this

paragraph an alternate description of the topology of $\mathcal{Q}(S_g, Z, \mu)$ and $\mathcal{H}(\mu)$. We refer to [FM13] and [Hub06] for this paragraph. Let S_g be the topological closed orientable surface of genus g - we recall that S_g admits a unique smooth structure. We define the **Teichmüller space** of S_g by

$$\mathcal{T}_g = \left\{ (\Sigma, f) : \begin{array}{ll} \Sigma & \text{a Riemann surface,} \\ f : S_g \to \Sigma & \text{an orientation preserving diffeomorphism} \\ & \text{homotopic to identity} \end{array} \right\} / \sim$$

where $\sim$ identifies (Σ_1, f_1) and (Σ_2, f_2) if there exists a biholomorphism $\varphi : \Sigma_1 \to \Sigma_2$ so that $f_2^{-1} \circ \varphi \circ f_1 : S_g \to S_g$ is homotopic to the identity. The moduli space $\mathcal{M}_g$ identifies with a quotient of $\mathcal{T}_g$. Indeed, let $\Phi : \mathcal{T}_g \to \mathcal{M}_g, [(\Sigma, f)] \mapsto [\Sigma]$ be the natural projection. Φ is clearly surjective, and $\Phi([\Sigma, f]) = \pi([\Sigma, g])$ for all $f, g \in \mathrm{Diff}_+(S_g)$. Hence, denoting $\mathrm{MCG}(S_g) = \mathrm{Diff}_+(S_g)/\mathrm{Diff}_+^0$ the mapping class group of S_g, we have the identification $\mathcal{M}_g \simeq \mathcal{T}_g/\mathrm{MCG}(S_g)$ where $\mathrm{MCG}(S_g)$ acts on $\mathcal{T}_g$ by $[h] \cdot [(\Sigma, f)] = [(\Sigma, f \circ h)]$.

A **Beltrami differential** on a Riemann surface Σ is a section of $\mathcal{M}(\Sigma) := L_*^\infty(T\Sigma, T\Sigma)$ the subbundle of (almost everywhere and norm) bounded antilinear maps of the tangent bundle $T\Sigma$ that is (almost everywhere) less than 1 for the L^∞ operator norm. Here, a map g is antilinear if g satisfies $g(u + \lambda v) = g(u) + \bar{\lambda} g(v)$ for all vectors u, v and all complex scalar λ. Hence, a Beltrami differential μ reads in a local coordinate ζ as $\nu(\zeta) \frac{d\bar{\zeta}}{d\zeta}$ where $\left(\nu(\zeta) \frac{d\bar{\zeta}}{d\zeta} \right) \left(w(\zeta) \frac{\partial}{\partial \zeta} \right) = \nu(\zeta) \overline{w(\zeta)} \frac{\partial}{\partial \zeta}$. The space of $\mathbb{R}$-linear functions from $\mathbb{C}$ to $\mathbb{C}$ is of complex dimension 2 and admits for $\mathbb{R}$-basis $(dz : z \mapsto z, d\bar{z} : z \mapsto \bar{z})$. By this way, the differential df_x at a point x of an application $f : \Sigma_1 \to \Sigma_2$ between two Riemann surfaces, seen as a $\mathbb{R}$-linear map from $T_x\Sigma_1$ to $T_{f(x)}\Sigma_2$, decomposes on this basis into $\left(\frac{\partial f}{\partial \bar{z}}(x), \frac{\partial f}{\partial z}(x) \right)$ so that $df = \frac{\partial f}{\partial \bar{z}} dz + \frac{\partial f}{\partial z} d\bar{z}$. Typically, if $f : \Sigma_1 \to \Sigma_2$ is a smooth homeomorphism between two Riemann surfaces such that for all $x \in \Sigma_1$ in a local chart z at x, $\kappa(f, x) := \frac{\frac{\partial f}{\partial \bar{z}}(x)}{\frac{\partial f}{\partial z}(x)}$ is bounded by a fixed constant $0 \leq k < 1$ - we say that f is **quasi-conformal**, then $\mu_x = \kappa(f, x) \frac{d\bar{z}}{dz}$ glue together to define a Beltrami differential denoted μ_f. It can be shown that every orientation preserving smooth diffeomorphism is quasi-conformal. Intuitively, quasi-conformal maps are those whose differentials send infinitesimal circles into infinitesimal ellipses of eccentricity that fits into an interval $0 < a < b < \infty$. The measurable Riemann mapping theorem gives a converse on $\mathbb{C}$: if μ is a bounded measurable function defined on some open set $U \subseteq \mathbb{C}$ and if μ has module (almost everywhere) less than 1, then there exists a quasi-conformal solution $f^\mu : U \to \mathbb{C}$ to the Beltrami equation $\frac{\partial f}{\partial \bar{z}} = \mu \frac{\partial f}{\partial z}$ unique up to post-composition by an injective conformal map. In particular, it implies that given a Beltrami differential μ on a Riemann surface Σ with an atlas (U_i, φ_i), writing $\mu_{|U_i} = \varphi_i^* \left(\mu_i \frac{dz}{d\bar{z}} \right)$ for some smooth functions μ_i, the Beltrami equations $\frac{\partial \psi}{\partial \bar{z}} = \mu_i \frac{\partial \psi}{\partial z}$ admits quasi-conformal solutions $\psi_i : \varphi_i(U) \to \mathbb{C}$. The charts $(U_i, \psi_i \circ \varphi_i)$ defines then a complex structure on Σ because if $U_i \cap U_j \neq \emptyset$, ψ_i and $\psi_j \circ \varphi_j \circ \varphi_i^{-1}$ are both solution of the same Beltrami equation, hence $\psi_i = f \circ \psi_j \circ \varphi_j \circ \varphi_i^{-1}$ for some injective holomorphic function f and it follows that the transition map $\psi_i \circ \varphi_i \circ \varphi_j^{-1} \circ \psi_j^{-1} = f$ is holomorphic. Moreover, uniqueness up to conformal map implies that this complex structure is independent of the choice of the initial atlas (U_i, φ_i). Let us denote Σ_μ the so built complex structure, and fix a complex structure Σ_g on S_g. We have a well defined natural projection $\Phi : \mathcal{M}(\Sigma_g) \to \mathcal{T}_g, \mu \mapsto [(\Sigma_\mu, id : \Sigma_g \to \Sigma_\mu)]$, where we recall that $\mathcal{M}(\Sigma_g)$ denotes the

Beltrami differentials on Σ_g which is an infinite dimensional unit ball of a Banach manifold and hence whose topology is understood. One can show that there exists a unique complex structure on $\mathcal{T}_g$ such that Φ is holomorphic. In turn, the complex structure on $\mathcal{T}_g$ allows to provide the moduli space $\mathcal{M}_g$ with the quotient topology. Moreover, the local coordinates computation enables to show that the cotangent spaces $T^*_{[\tau]}\mathcal{T}_g$ identifies with the vector bundle $\mathcal{Q}(\Sigma_\tau) = \mathrm{Sym}(T^*\Sigma_\tau \otimes T^*\Sigma_\tau)$ formed by the holomorphic quadratic differentials. Denote $\rho : T^*\mathcal{T}_g \to \mathcal{T}_g$ the canonical projection. The Teichmüller space identifies naturally with the space of all complex structures on S_g up to pull back by an element of $\mathrm{Diff}^0_+(S_g)$ via the correspondences $[(\Sigma, f)] \mapsto [\Sigma]$ and $[\Sigma] \mapsto [(\Sigma, id : \Sigma_g \to \Sigma)]$. If $\mathcal{A}$ is a complex structure on S_g, then for all $\varphi \in \mathrm{Diff}_+(S_g)$: $\varphi : (S_g, \mathcal{A}) \to (S_g, \varphi^{-1*}\mathcal{A})$ is holomorphic and $\varphi^*\mathcal{Q}(\varphi^{-1*}\mathcal{A}) = \mathcal{Q}(\mathcal{A})$. Moreover, if $g \geq 2$, the action of $\mathrm{Diff}^0_+(S_g)$ on the family of all complex structures on S_g is free, i.e. for all $\varphi \in \mathrm{Diff}^0_+(S_g) \setminus \{id_{S_g}\}$ and all complex structures $\mathcal{A}$ we have $\varphi^*\mathcal{A} \neq \mathcal{A}$. Hence, if $g \geq 2$, $\rho^{-1}([\mathcal{A}])$ is naturally identified with $\mathcal{Q}(\mathcal{A}')$ for any $\mathcal{A}' \sim \mathcal{A}$. Finally, the map
$$\begin{array}{ccc} \mathscr{Q}(S_g, Z, \mu) & \to & \mathcal{Q}(\Sigma) \simeq \rho^{-1}(\Sigma) \subset T^*\mathcal{T}_g \\ [(\Sigma, \omega)] & \mapsto & \omega \otimes \omega \end{array}$$
enables us to identify $\mathscr{Q}(S_g, Z, \mu)$ with a subspace of $T^*\mathcal{T}_g$ which inherits its topology.

For this topology, if two translation moduli (Σ_1, ω_1) and (Σ_2, ω_2) are "close" then the Teichmüller moduli $(\Sigma_1, \varphi_{\omega_1})$ and $(\Sigma_2, \varphi_{\omega_2})$ are close too for the topology previously mentioned on $\mathcal{T}_g$ where φ_{ω_1} and φ_{ω_2} are quasi conformal maps naturally associated to ω_1 and ω_2. Indeed, for $g \geq 2$, by uniformization theorem, $\Sigma_i \simeq \mathbb{H}^2/\Gamma_i$ where $\Gamma_i < \mathrm{PSL}_2(\mathbb{R})$ is a Fuschian group. Denote $\pi_i : \mathbb{H}^2 \to \Sigma_i$ the canonical projection - in fact this is the universal cover of Σ_i. Then π_i is a local diffeomorphism thus π_i^* identifies $\mathcal{M}(\Sigma_i) \simeq \mathcal{M}^{\Gamma_i}(\mathbb{H}^2)$ where $\mathcal{M}^{\Gamma_i}(\mathbb{H}^2)$ denotes the space of Γ_i-invariant Beltrami differential. Here, we have to define what we mean by the pull back of a Beltrami differential. Given $f : \Sigma_1 \to \Sigma_2$ quasi conformal between Riemann surfaces and μ a (bounded by 1 in norm) Beltrami differential on Σ_2, let z, w be respective local charts on Σ_1 and Σ_2 such that μ reads $\mu = [\mu]\frac{d\bar{w}}{dw}$. The pullback is given by the formula

$$f^*\mu = \frac{\frac{\partial f}{\partial \bar{z}} + [\mu] \circ f \overline{\frac{\partial f}{\partial z}}}{\frac{\partial f}{\partial z} + [\mu] \circ f \overline{\frac{\partial f}{\partial \bar{z}}}} \frac{d\bar{z}}{dz}.$$

One can verify that $g^*\mu_f = \mu_{f \circ g}$. Let $\mu \in \mathcal{M}^{\Gamma_i}(\mathbb{H}^2)$. Then $\hat{\mu} : z \mapsto \begin{cases} \mu_z & \text{if } z \in \mathbb{H}^2 \\ 0 & \text{if } z \in \mathbb{H}^{2*} \cup \mathbb{R} \cup \{\infty\} \end{cases}$
defines a Γ_i-invariant Beltrami differential on $\widehat{\mathbb{C}}$, where we denoted $\mathbb{H}^{2*}$ the lower half plane. There exists then a unique solution $f^{\hat{\mu}}$ of the Beltrami equation associated to $\hat{\mu}$ fixing $0, 1, \infty$: the group action $\mathrm{Aut}(\widehat{\mathbb{C}}) \curvearrowright \widehat{\mathbb{C}}$ of Möbius transformations on $\widehat{\mathbb{C}}$ is sharply 3-transitive. By connectedness, we have a conformal map $f^{\hat{\mu}}_{|\mathbb{H}^{2*}} : \mathbb{H}^{2*} \to \mathbb{H}^{2*}$, and a quasi conformal map $f^{\hat{\mu}}_{|\mathbb{H}^2} : \mathbb{H}^2 \to \mathbb{H}^2$ which projects to a quasi conformal map $\tilde{\varphi}_i := \pi_i \circ f^{\hat{\mu}}_{|\mathbb{H}^2} : \mathbb{H}^2 \to \Sigma_i$. Moreover, since $\hat{\mu}$ is Γ_i-invariant, we have for all $h \in \Gamma_i : (f^{\hat{\mu}} \circ h \circ f^{\hat{\mu}-1})^*\mu_0 = f^{\hat{\mu}-1*}h^*f^{\hat{\mu}*}\mu_0 = f^{\hat{\mu}-1*}h^*\mu = f^{\hat{\mu}-1*}\mu = \mu_0$, where we denoted $\mu_0 \equiv 0$. Hence φ is a Möbius transformation, and it follows that $\tilde{\varphi}_i \cdot \Gamma_i := \tilde{\varphi}_i \circ \Gamma_i \circ \tilde{\varphi}_i^{-1}$ is a Fuschian group. Then, one can associate to the conformal map $f^{\hat{\mu}}_{|\mathbb{H}^{2*}} : \mathbb{H}^{2*} \to \mathbb{H}^{2*}$ a quadratic differential $\mathcal{S}\{f^{\hat{\mu}}_{|\mathbb{H}^{2*}}\}$ on $\mathbb{H}^{2*}$ - its Schwarzian derivative - which is Γ_i-invariant in such a way that $\Phi(\mu) = \Phi(\nu)$ in $\mathcal{T}_g$ if and only if $\mathcal{S}\{f^{\hat{\mu}}_{|\mathbb{H}^{2*}}\} = \mathcal{S}\{f^{\hat{\nu}}_{|\mathbb{H}^{2*}}\}$. Hence it defines a map $\Psi_{id} : \mathcal{T}_g \to \mathcal{Q}^{\Gamma_i}(\mathbb{H}^{2*})$ which can be used to give a topology to $\mathcal{T}_g$ com-

patible with its complex structure. In fact, given any quasi conformal $\tilde{\varphi} : \mathbb{H}^2 \to \mathbb{H}^2$, $\mathcal{M}^{\tilde{\varphi} \cdot \Gamma_i}(\mathbb{H}^2) \simeq \mathcal{M}^{\Gamma_i}(\mathbb{H}^2)$ where $\tilde{\varphi} \cdot \Gamma_i = \tilde{\varphi} \circ \Gamma_i \circ \tilde{\varphi}^{-1}$ and we obtain by the same process $\Psi_{\tilde{\varphi}} : \mathcal{T}_g \to \mathcal{Q}^{\tilde{\varphi} \cdot \Gamma_i}(\mathbb{H}^*)$ continuous. These are the local coordinates on $\mathcal{T}_g$.

We can even endow $\mathcal{T}_g$ with a compatible metric, the Teichmüller metric:

$$d([(\Sigma_1, f_1)], [(\Sigma_2, f_2)]) = \inf_f \ln K_f$$

where $K_f = \sup \frac{\frac{\partial f}{\partial \bar{z}}}{\frac{\partial f}{\partial z}}$ and the infimum is taken over all orientation preserving diffeomorphism $f : \Sigma_1 \to \Sigma_2$ such that $f_2 = f \circ f_1$.

The stratum $\mathcal{H}(0)$. Let (Σ, ω) a representative of a modulus in $\mathcal{H}(0)$. We have then $2g - 2 = 0$ by equation (2.5), i.e. $g = 1$. Hence Σ is a flat torus. We have thus a forget map $\Phi_0 : \begin{array}{ccc} \mathcal{H}(0) & \to & \mathcal{M}_1 \\ [(\Sigma, \omega)] & \to & [\Sigma] \end{array}$. Conversely, given any flat torus $\mathbb{T} = \mathbb{C}/\Gamma$, denoting $\pi : \mathbb{C} \to \mathbb{T}$ the universal cover and (U_i, φ_i) an analytic atlas on the torus, we can define $\omega_i = \varphi_i^* dz_{|U_i}$. If $U_i \cap U_j \neq \emptyset$, we have $\omega_{i|U_i \cap U_j} = \varphi_i^* dz_{|U_i \cap U_j} = (\varphi_i \circ \varphi_j^{-1} \circ \varphi_j)^* dz_{|U_i \cap U_j} = \varphi_j^* dz_{|U_i \cap U_j} = \omega_{j|U_i \cap U_j}$ as $\varphi_i \circ \varphi_j^{-1}$ is a translation. Hence the ω_i glue together to give a holomorphic 1-form ω on Σ. And if ω' is an other holomorphic 1-form on Σ, then $\pi^* \omega$ and $\pi^* \omega'$ are two Γ-invariant holomorphic 1-form on $\mathbb{C}$, so they are constant by the maximum principle. Let $a \in \mathbb{C}^*$ such that $\pi^* \omega = a \pi^* \omega' = \pi^*(a \omega')$. We have thus $\pi^*(\omega - a \omega') = 0$ and $\omega - a \omega' = 0$ by injectivity of π^* - π being submersion ensures that π^* is injective. Finally, posing $\tilde{f} : \begin{array}{ccc} \mathbb{C} & \to & \mathbb{C} \\ z & \mapsto & az \end{array}$ and denoting $\Gamma' = f(\Gamma)$, f induces a biholomorphism $f : \Sigma = \mathbb{C}/\Gamma \to \mathbb{C}/\Gamma' \simeq \Sigma$ such that $\pi^* f^* \omega' = (f \circ \pi)^* \omega' = (\pi \circ \tilde{f}) \omega' = \tilde{f}^* \pi^* \omega' = \pi^*(a \omega') = \pi^* \omega$ thus $f^* \omega' = \omega$. Finally, we showed that Φ_0 is bijective and in fact it gives a homeomorphism:

$$\mathcal{H}(0) \simeq \mathcal{M}_1.$$

Mumford's compactness criterion. For simplicity, we will deal with translation surfaces of normalized total area (equal to 1). Denote $\mathcal{Q}^{(1)}(S_g, Z, \mu)$ the corresponding moduli subspace, which is a real hyperspace of $\mathcal{Q}(S_g, Z, \mu)$. First note that as the period map is continuous, it is lower bounded on any compact subset $K \subset \mathcal{Q}^{(1)}(S_g, Z, \mu)$. Hence, for a family of translation surfaces to be compact, their periods must be lower bounded.

For the converse, Mumford proved a very useful characterization of compact subset of $\mathcal{M}_g$ when $g \geq 2$.

Theorem. *Let $g \geq 2$ and let $\mathcal{M}_g$ be the moduli space of Riemann surfaces of genus g. For all $\varepsilon > 0$, the subset:*

$$\{[\Sigma] \in \mathcal{M}_g : \text{ all complete geodesics on } \Sigma \text{ have hyperbolic length } \geq \varepsilon\}$$

is compact.

We have to explain what we mean by hyperbolic length. Let $\pi : \mathbb{H}^2 \to \Sigma$ be the universal cover of Σ and Γ denotes its group of deck transformations. As $\Gamma < \mathrm{PSL}_2(\mathbb{R}) = \mathrm{Isom}^+(\mathbb{H}^2)$ is a Fuschian group, we have $\gamma^* ds^2_{\mathbb{H}^2} = ds^2_{\mathbb{H}^2}$ for all $\gamma \in \Gamma$. Morevoer, we know that the analytic structure on Σ is given by an atlas of the form $(\pi(U_i), \pi^{-1}_{|\pi(U_i)} : \pi(U_i) \to U_i)$

where $U_i \subset \mathbb{H}^2$ is an elementary open set for the cover. Hence, the transition map on σ are given by deck transformations. Finally, the metric $ds^2_{\mathbb{H}^2}$ being Γ-invariant, it descends into a metric d_Σ on Σ such that π realizes an isometry between $(\mathbb{H}^2, ds^2_{\mathbb{H}^2})$ and (Σ, ds^2_Σ).

Mumford's criterion enables us to characterizes compact subset of $\mathscr{Q}^{(1)}(S_g, Z, \mu)$. Indeed, let $\varepsilon > 0$, and $[(\Sigma, \omega)] \in \mathscr{Q}^{(1)}(S_g, Z, \mu)$. The Riemannian metric $|\omega|^2$ is well defined on $\Sigma \setminus Z$ outside the zeros Z of ω. As (Σ, ds^2_Σ) and $(\Sigma, |\omega|^2)$ defines the same conformal structure outside the zeros of Σ, we must have $|\omega|^2 = \lambda ds^2_{\mathbb{H}^2}$ for some smooth strictly positive function λ on Σ. As Σ is compact, λ is upper bounded by some constant M. Let γ be a closed complete geodesic on Σ. We thus deduce that $\ell_{|\omega|^2}(\gamma) \leq M\ell_{ds^2_\Sigma}(\gamma)$.

Note now that for two equivalent pair $(\Sigma, \omega) \sim (\Sigma', \omega')$, if $\omega' = f^*\omega$, for some biholomorphism $f : \Sigma' \to \Sigma$ homotopic to identity, and γ is a path on Σ', we have $\int_\gamma |\omega'| = \int_{f\circ\gamma} |\omega| = \int_\gamma |\omega|$ by substitution of variables. Hence, for all $M > 0$,

$$
\begin{aligned}
K_{\varepsilon/M} = \quad & \left\{ [(\Sigma, \omega)] \in \mathscr{Q}^{(1)}(S_g, Z, \mu) : \text{ all closed complete geodesics on } \Sigma \text{ have } |\omega|^2 \text{ length } \geq \frac{\varepsilon}{M} \right\} \\
\subseteq \quad & \left\{ ([\Sigma, \omega]) \in \mathscr{Q}^{(1)}(S_g, Z, \mu) : \text{ all complete geodesics on } \Sigma \text{ have hyperbolic length } \geq \varepsilon \right\},
\end{aligned}
$$

is well defined and is included in some subset of $\mathscr{Q}^{(1)}(S_g, Z, \mu)$ which is similarly defined as the compact subsets characterized by Mumford's criterion.

Thus, it is reasonable to pretend that $\pi(K_{\varepsilon/M})$ is relatively compact. It remains to show that $\pi(K_{\varepsilon/M})$ is compact to conclude that it is compact.

Finally we state:

Theorem (Compactness criterion, [Mas22])**.** *Let $g \geq 2$. A subset $K \subset \mathcal{H}^{(1)}(\mu)$ is compact if and only if there exists $\varepsilon > 0$ such that for all $[(\Sigma, \omega)] \in K$ there exists a representative $[\Sigma', \omega']$ in $\mathscr{Q}^{(1)}(S_g, Z, \mu)$ with the $|\omega'|^2$-length of any complete geodesic on Σ' being greater or equal than ε.*

Note that we can replace complete geodesic with saddle connection in the previous theorem characterizing compact subsets of $\mathcal{H}^{(1)}(\mu)$.

2.7.3 L decomposition for surfaces in $\mathcal{H}(2)$ and Z decomposition for surfaces in $\mathcal{H}(1,1)$

In this section, we give explicit simple polygonal decompositions in the genus 2 case.

We will use the fact that every genus 2 translation surface (Σ, ω) admits a hyperelliptic involution ρ, i.e. a holomorphic involutive and isometric automorphism of Σ acting as -1 on homology and which sends every simple geodesic closed curve to a simple geodesic closed curve, fixes the singularities of Σ among a finite number of fixed points. The metric being given by the integral of $|\omega|^2$. Moreover we will use the fact that any maximal collection of **saddle connections** - i.e. geodesics connecting two singularities - that do not intersect each other in their interior is a triangulation.

L decomposition of an element of $\mathcal{H}(2)$. Let $[(\Sigma, \omega)] \in \mathcal{H}(2)$, and let ρ a hyperelliptic involution of Σ. Denote $\mathcal{T}$ a geodesic triangulation of Σ made of saddle connection. Then not every **saddle connection** is mapped to itself by ρ. Otherwise, we would have that each triangle of the triangulation would be mapped to itself. Now, let t be such a triangle

delimited by simple geodesic curves α, β, γ. We have that ρ maps each boundary curve to itself, and that the morphism induced by ρ in homology satisfies: $\rho_* = -1$. This implies, denoting ι the intersection form: $\iota(\alpha, \gamma) = \iota(\rho(\alpha), \rho(\gamma)) = -\iota(\alpha, \gamma)$. Indeed, as ρ is isometric and only has a finite number of fixed points, $\rho(\alpha) = \alpha$ and $\rho(\gamma) = \gamma$. Hence $\iota(\alpha, \gamma) = 0$ contradicting that t is a triangle. Let c be a saddle connection not mapped to itself by ρ. Then the homology classes of c and $\rho(c)$ are opposite as $\rho_* = -1$, and $\rho(c)$ is a saddle connection. Finally, assuming that c and $\rho(c)$ only intersect at the singularity, $c \cup \rho(c)$ is a separating curve for Σ. Cutting Σ along c and $\rho(c)$ separates Σ into two components - as c and $\rho(c)$ are homologous and only intersects at the singularity - one of which is a cylinder and the other a torus with a slit. Indeed, as ρ acts as -1 on homology, $c \cup \rho(c)$ is separating. Denote by C_1 and C_2 the closure of the components bounded by this curves. Consider a tubular neighborhood of $c \cup \rho(c)$ in these two components. Necessary, there is a component, denote it C_1, such that the corresponding tubular neighborhood admits 1 boundary component. While the tubular neighborhood in the other component, denote it C_2, admits 2 boundary component. Otherwise, Σ would not be a manifold near its singularity.It follows by inclusion-exclusion formula: $-2 = \chi(\Sigma) = \chi(C_1 \cup C_2) = \chi(C_1) + \chi(C_2) - \chi(C_1 \cap C_2)$. But $C_1 \cap C_2 = c \cup \rho(c) \simeq \mathbb{S}^1 \vee \mathbb{S}^1$. Hence $\chi(C_1 \cap C_2) = -1$. Finally, denoting g_i the genus of C_i, we have: $\chi(C_1) = 2 - 2g_1 - 1, \chi(C_2) = 2 - 2g_2 - 2$ and we deduce that $g_1 + g_2 = 1$. All together, this gives a L decomposition of Σ (see Figure 14).

Z decomposition of an element of $\mathcal{H}(1,1)$. The same way as in the previous paragraph, if $[(\Sigma, \omega)] \in \mathcal{H}(1,1)$, consider a geodesic triangulation of Σ made of saddle connections. Pick a triangle of this triangle t of this triangulation that connects the two singularities. Then, the singularity that appears once as a vertex of t is fixed by the hyperelliptic involution ρ. At most one of the edges of t is fixed by ρ by the same reasoning as previously, hence t admits an edge c that connects the two singularities and that is not fixed by ρ. Cutting Σ along c and $\rho(\bar{c})$ decomposes the surface into two tori, and Σ is obtained by the slit torus construction. Indeed, using again inclusion-exclusion formula with the fact that $C_1 \cap C_2 = c \cup \rho(c) \simeq \mathbb{S}^1$ and that $c \cup \rho(c)$ corresponds to one boundary component of C_1 and C_2, we deduce that $g_{C_1} + g_{C_2} = 2$. Hence Σ admits a Z shape decomposition (see Figure 15).

Other arguments to show the existence of a L decomposition. We give an alternative method to prove the existence of the previous L and Z decompositions, detailing the case of $H(2)$.

Fix (Σ, ω) a translation surface of $\mathcal{H}(2)$. Let p be a Weierstrass point of Σ, i.e. a fixed point of ρ, that is not a singularity of Σ. Consider a geodesic closed segment I obtained, from p, by aiming at the singularity of Σ and going straight, with 2π angle between its extremities. Let $\theta \in \mathbb{S}^1$, and consider the subset $M_\theta \subset \Sigma$ of points reached by a geodesic starting from a point of I in the direction θ. If $M_\theta \subsetneq \Sigma$, then its boundary must be made of saddle connections. Indeed, first, every geodesic starting from a point x of I either reaches a singularity or returns to I. This is because, otherwise, the geodesic transportation of a small geodesic segment containing x would be of infinite area, contradicting the compactness of Σ. By this remark, if a point y in the boundary of M_θ does not belong to a saddle connection, it is reached by a geodesic starting from a point in I that is not a
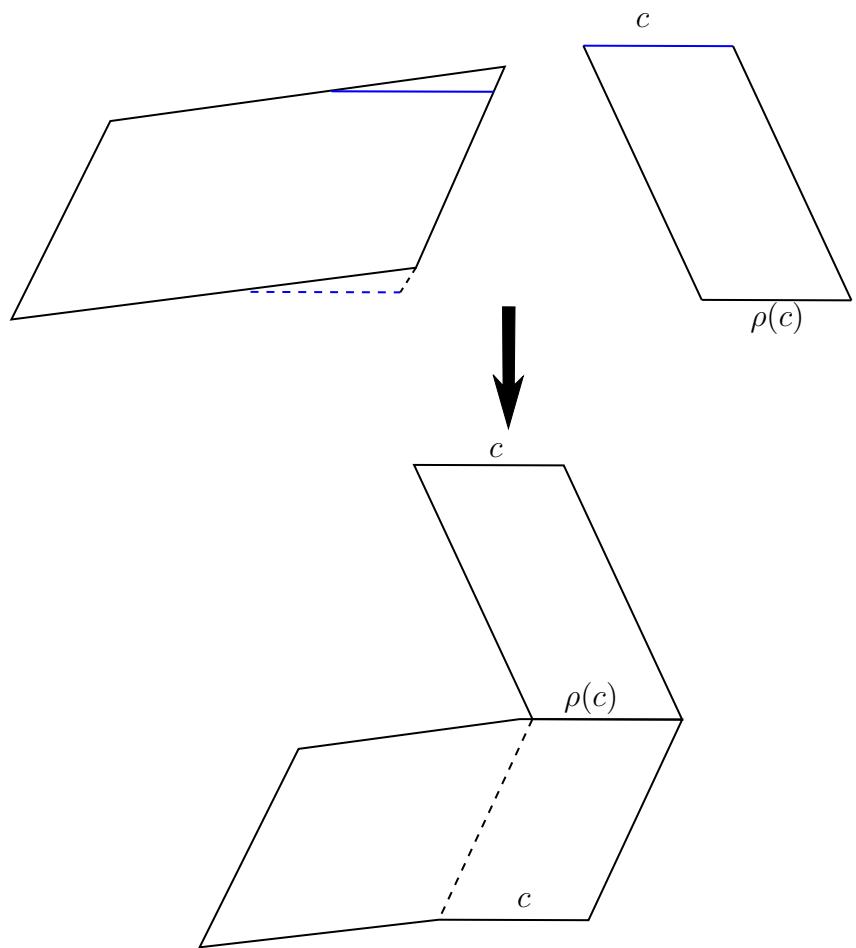
Figure 14: L decomposition of a surface in $\mathcal{H}(2)$. Blue segments represent slits.
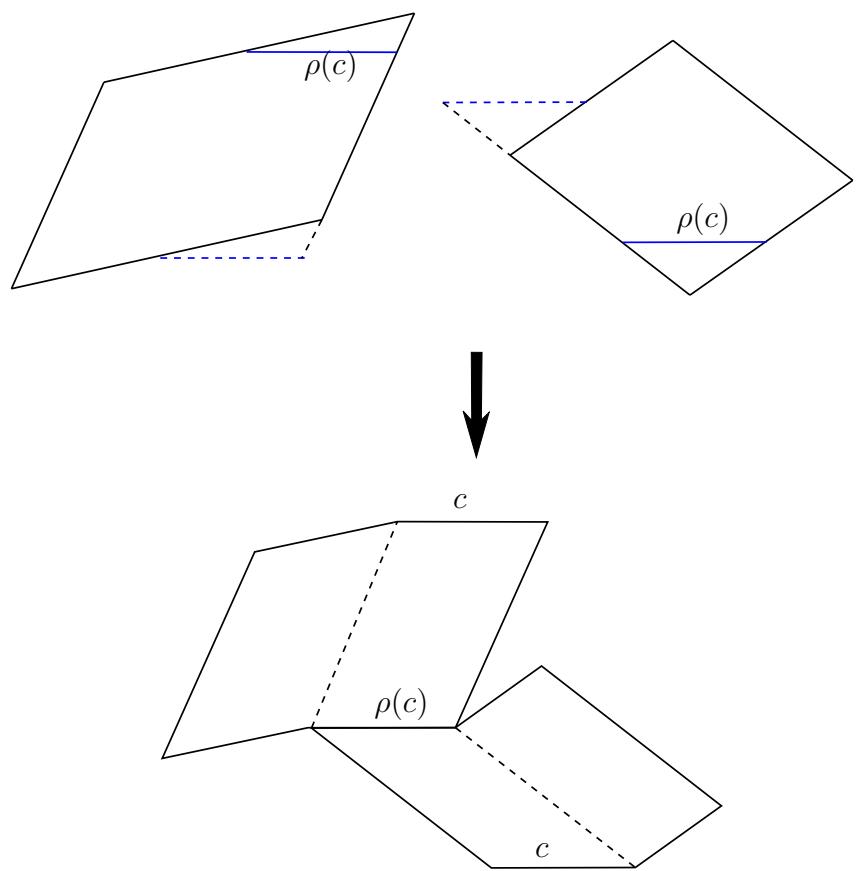
Figure 15: Z decomposition of a surface in $\mathcal{H}(1,1)$. Blue segment represent slits.
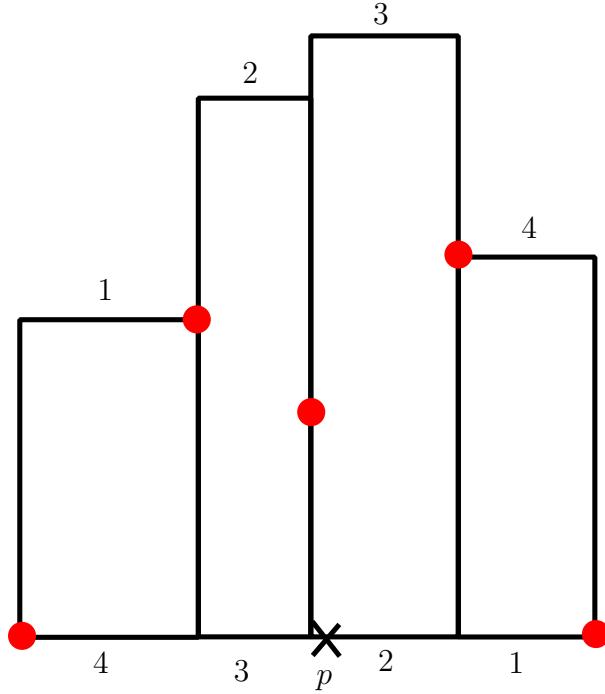
Figure 16: The zippered rectangle construction in the case of a surface in $\mathcal{H}(2)$. The singularity is in red. Numbers indicate the gluing procedure.

singularity. We could thus take a small neighborhood of y in I which would imply that y belongs to the interior of M_θ, a contradiction. Hence, by choosing θ not in the at most countable subset of directions of all possible saddle connections, we can suppose $M_\theta = \Sigma$. It can be shown, using the geometric properties of (Σ, ω), that it is obtained by four zippered rectangles as in Figure 16. By pasting and gluing, one obtains an octagon as in Figure 17. Finally, it suffices again to glue and paste parts of this octagon to obtain the L shape decomposition, see Figure 18.
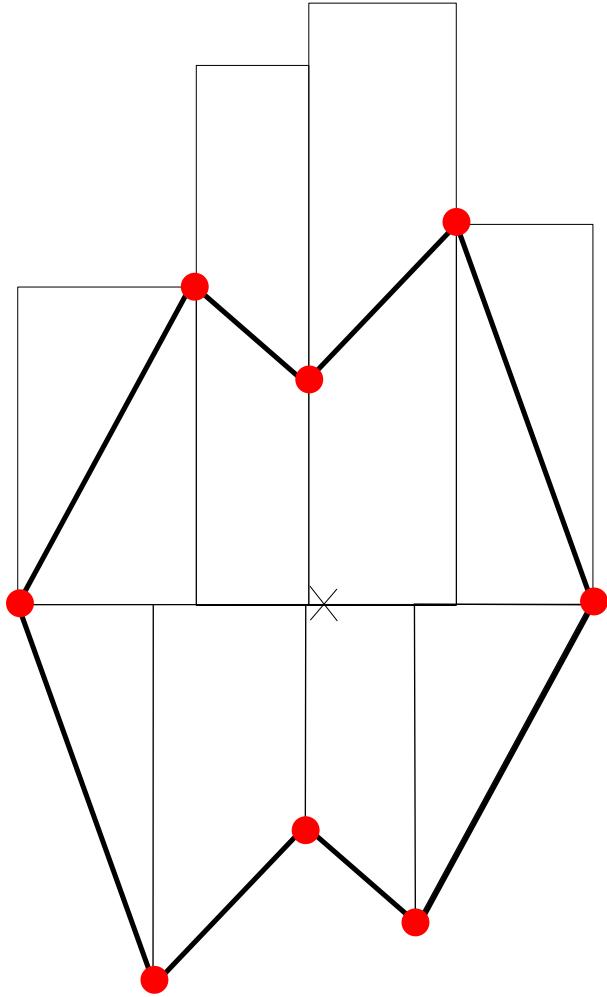
Figure 17: Masur-Yoccoz octagon decomposition of a surface in $\mathcal{H}(2)$ obtained by gluing and pasting parts of the zippered rectangles decomposition.
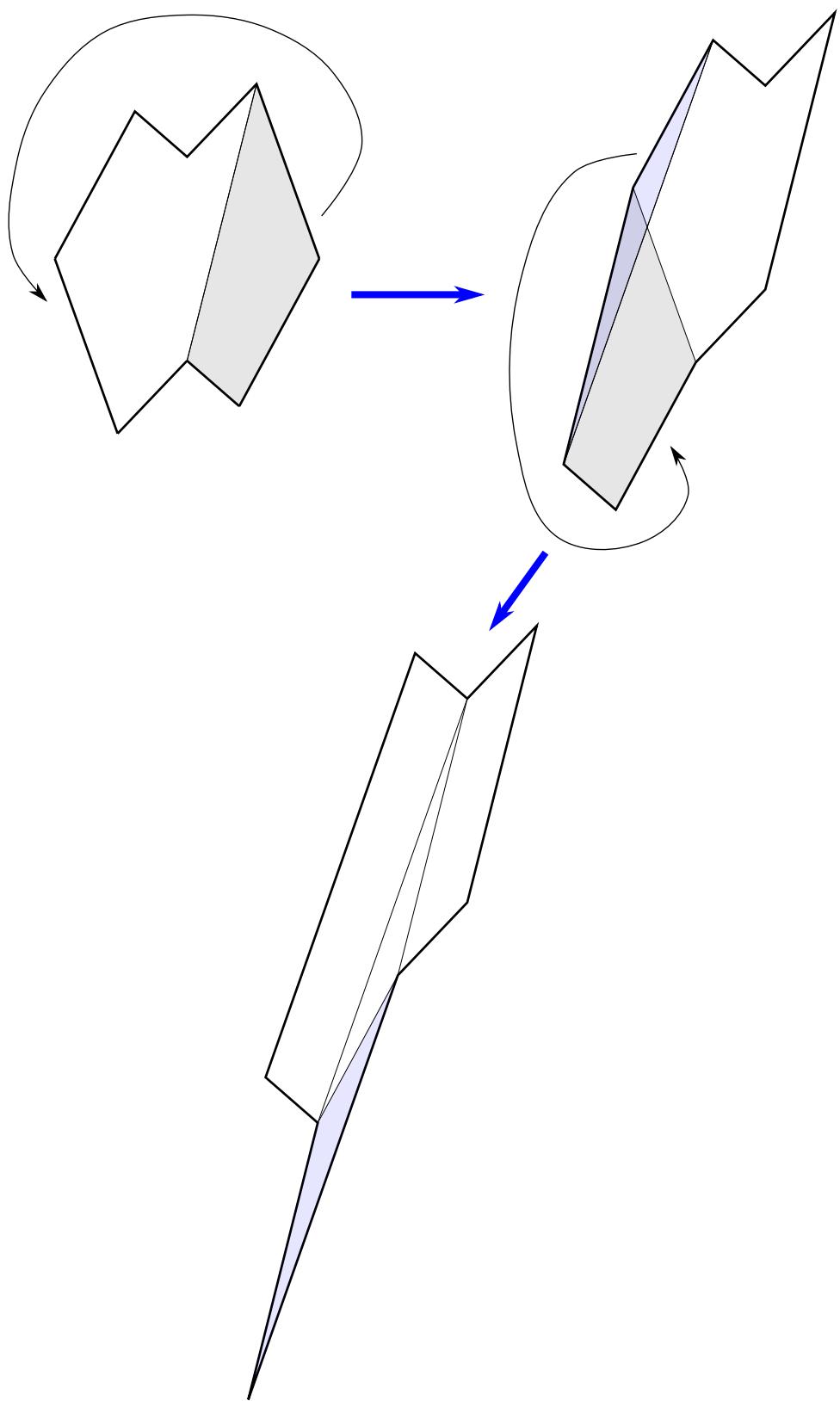
Figure 18: Gluing and pasting a Masur-Yoccoz octagon to obtain a L decomposition.

Chapter 3

PL isometric embeddings: previous works

Résumé en français.   Nous rappelons dans ce chapitre l'état de l'art sur les plongements isométriques PL de surfaces polyédrales. Nous commençons par énoncer le théorème d'Alexandrov sur la réalisation des métriques plates à singularités convexes (d'angle au plus 2π) de la sphère, et donnons une application de ce théorème à l'existence de triangulation universelle en genre 0. Nous rappelons ensuite le théorème de Burago et Zalgaller, analogue PL du théorème de Nash-Kuiper, qui portent sur les plongements isométriques PL de surfaces polyédrales. Nous donnons enfin deux constructions que nous utiliserons au chapitre 5 pour construire une triangulation universelle pour les tores plats. La première est dû à Zalgaller et permet de réaliser tous les tores plats suffisamment longs. La deuxième, qui présente une histoire complexe, a été rédécouverte récemment par Arnoux, Lelièvre et Màlaga et porte le nom de diplotore.

In this chapter we recall previous results about isometric embeddings of surfaces. First, we state Alexandrov's theorem about the existence of realizations of polyhedral metric of conical angles less than 2π on the sphere and give some application to the existence of a universal triangulation in genus 0 with a number of fixed conical angles. We then present the theorem of Burago and Zalgaller about PL isometric embeddings of surfaces. Finally, we end the section with three elementary constructions for flat tori. The first one can realize any long flat torus, long meaning that the ratio of its area by the square of the length of its systole is large, and is used in our construction of flat surfaces of genus 2. The second enables to realize any flat torus but is harder to generalize in higher genus.

3.1 Alexandrov's theorem

We refer to [Ale06] for this section.

Let $\mathbb{S}$ denote the unit sphere. A polyhedral metric ρ on $\mathbb{S}$ admits a polygonal scheme, i.e. a family of polygons whose gluing is isometric to ρ. Indeed, pick some vertex A_1 and draw the geodesic lines from A_1 to the other vertices $A_2, ..., A_n$ - such geodesics can be shown to exist. Cutting the sphere along these shortest arcs, we obtain a polygon Q with $2(n-1)$ sides, which can be glued to obtain the metric ρ.

It appears that every convex polyhedral metric on the sphere, i.e. a metric with conical angles less than 2π, can be realized in ambient space as a convex polyhedron in 3-space. The proof's plan developed by Alexandrov is the following.

A polygonal scheme of the sphere as the one given in the previous paragraph can be triangulated. By this way, fixing the underlying combinatorial triangulation, the geometry of the scheme is characterized by the lengths of its edges. Denote by n the common number of vertices of the triangulations, which is equal to the number of singularities of the metric. By Euler's formula, it is easily seen that the number of edges is $3n-6$. Hence the space of polygonal scheme realizing a metric with n given singularities is $3n-6$ dimensional. On the other hand, a convex polyhedron is entirely determined by the coordinates of its vertices as it is the convex hull of its vertices. Considering polyhedron up to rigid motions, we can fix 6 coordinates of its vertices (for instance, we may fix one vertices entirely top be the origin, two coordinates of an other vertices so that it lies in the $\{y = z = 0, x > 0\}$ half-line, and the coordinate of a last one so that it belongs to the $\{z = 0, y > 0\}$ half-plane). This gives $3n-6$ variables characterizing a convex polyhedron, with n vertices. Hence the space of polyhedra with n vertices and the space of polygonal schemes of polyhedral metrics with n singularities have the same dimension.

A convex polyhedron admits a natural triangulation. Consider such a triangulation. By a deformation we mean a small change of the edge length of this triangulation. It appears that there exists a neighborhood of this triangulation that can be realized by convex polyhedra. Then Alexandrov shows that every metric ρ_1 can be connected to a realizable metric ρ_0 through a continuous family of metric ρ_t. He next proves then that every metric close to a realizable metric is also realizable. It followss that ρ_1 is realizable by connectedness.

However, it may happen that the metric is realized by a double covered polygon. Igor Pak, in [Pak06], found a method to embed doubly covered polygons. Let $\mathcal{P}$ be a doubly covered polygon obtained by gluing two copies of a polygon P. For each vertex v of P
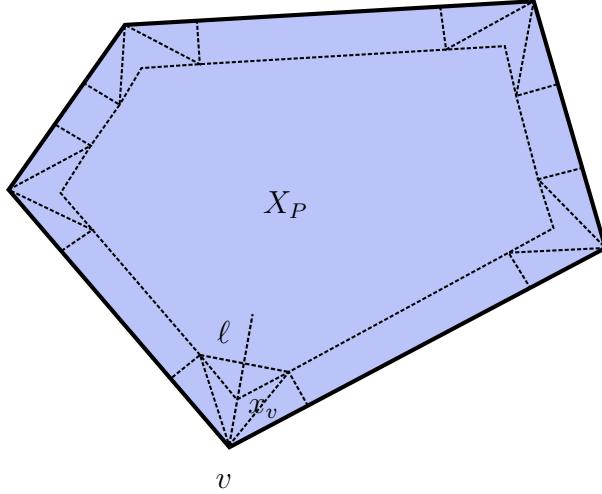
Figure 19: The polygons P and X_P, and the procedure to obtain a polygonal scheme of P which allows to embed $\mathcal{P}$ into $\mathbb{R}^3$.
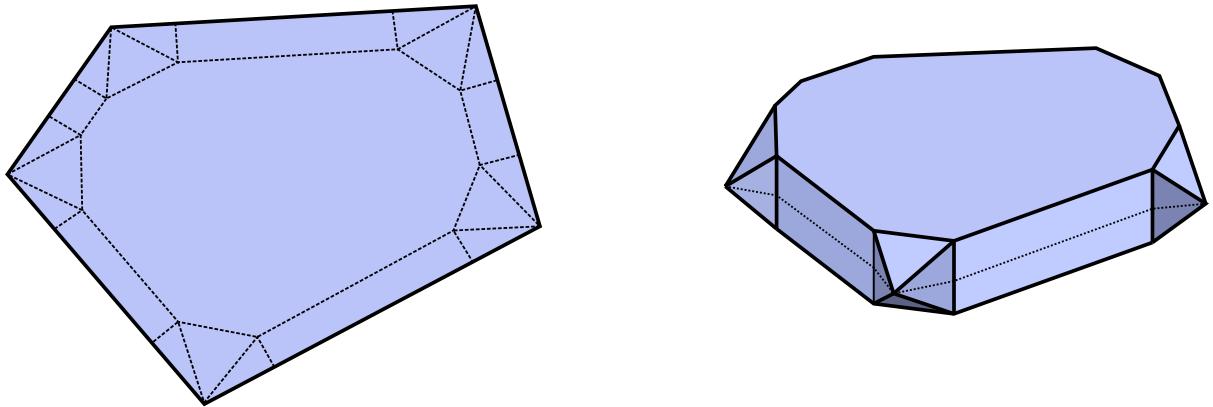

Figure 20: Isometric embedding with $5n$ vertices of a doubly covered n-gon as described by Igor Pak in [Pak06] (here $n = 5$).

incident to two edges e and e', denote x_v a point at distance ε from e and e', and X_P the polygon whose vertices are the x_v. Refer to Figure 19. Then, for every vertex v of P, cut P with a line $\ell \perp (v, x_v)$ at distance $|vx_v|$ from x_v. Connect the two points of intersection of ℓ and X_P to v, and drop perpendiculars to the sides of P. We obtain finally a decomposition of P into a large polygonal region in the interior of P, rectangles (one per side), and triangles around vertices (three per vertex). It remains to bend the rectangles at right angle with respect to X_P, and to bend the triangles to form a pyramid whose apex v project to x_v. Reflecting the obtained surface through the horizontal plane containing the vertices v gives the desired embedding. See Figure 20 for an example.

We can now state a complete Alexandrov's theorem:

Theorem (Alexandrov). *Let ρ be a metric on the sphere $\mathbb{S}$ with n conical angles less than 2π. Then there exists a convex polyhedron $\mathcal{P} \subset \mathbb{R}^3$ with n vertices, possibly degenerated into a doubly covered polygon, and a PL isometry $(\mathbb{S}, \rho) \to \mathcal{P}$.*

This theorem can be used in turn to build a universal triangulation for polyhedral

metrics with a fixed number of singularities. Indeed, the number of triangulations on the sphere with n vertices is finite. We then consider a common refinement of all such triangulations to obtain a fixed triangulation that realizes every polyhedral metric of positive "curvature" with n singularities.

3.2 Theorem of Burago and Zalgaller

In this section we state the theorem of Burago and Zalgaller about PL isometric embeddings of polyhedral surfaces and sketch its proof, following the paper [BZ95].

We begin by the theorem in itself, and then move to the proof.

Here, **short** means contractant and the approximation part has to be understood in the space of continuous mappings for the uniform convergence norm.

Theorem 1 (Burago and Zalgaller). *Let Σ be a polyhedral surface. Let $f : \Sigma \to \mathbb{R}^3$ be a short and C^2 embedding. Then for all $\varepsilon > 0$, there exists a PL isometric embedding $g : \Sigma \to \mathbb{R}^3$ such that $\sup_{x \in \Sigma} |f(x) - g(x)| < \varepsilon$.*
In other words, every short and C^2 embedding in $\mathbb{R}^3$ of a polyhedral surface can be approximated by a PL isometric embedding.

Embedding a triangle above a smaller one. We first describe the main building block of the construction of Burago and Zalgaller. It gives a pleating of an acute triangle - acute meaning that the triangles admits only acute angles - in the half prism delimited by a smaller acute triangle. Moreover, the construction extends to the case where the 3 sides of the prism are slightly tilted. More formally, we have the following lemma:

Lemma 2. *Let $T = A_1 A_2 A_3$ and $t = a_1 a_2 a_3$ be Euclidean triangles such that:*

- *(i) T and t are acute,*

- *(ii) $|a_i a_j| < |A_i A_j|$ for $1 \le i, j \le 3; i \ne j$,*

- *(iii) the distance of the circumcenter ω of t to each side $a_i a_j$ is smaller than the distance of the circumcenter Ω of T to the corresponding side $A_i A_j$.*

Assume that t lies in the horizontal plane xy of $\mathbb{R}^3$. Denote by m_{ij} the point vertically above $a_i a_j$ at equal distance from a_i and a_j. Then T has a PL isometric embedding in the prism above t with the boundary condition that each side $A_i A_j$ is sent to the broken line $a_i m_{ij} a_j$. Moreover, each face of the prism can be slightly rotated so that the construction remains possible.

Proof. The triangles T and t being acute, they contain their circumcenters Ω and ω in their interior. We let ω' be the point vertically above ω such that $|a_1 \omega'| = |A_1 \Omega|$ - see Figure 22. In other words: $\omega' = \omega + z' e_z$. Note that ω' is well defined since by assumption the circumradius $|A_1 \Omega|$ of T is larger than the circumradius $|a_1 \omega|$ of t.

We first subdivide T into three subtriangles $\Omega A_i A_j$. The goal is to fold each $\Omega A_i A_j$ above $\omega a_i a_j$ with the boundary condition for $A_i A_j$ as in the lemma, and so that the boundary edges ΩA_i, ΩA_j are sent respectively to the segments $\omega' a_i$ and $\omega' a_j$. To this end,
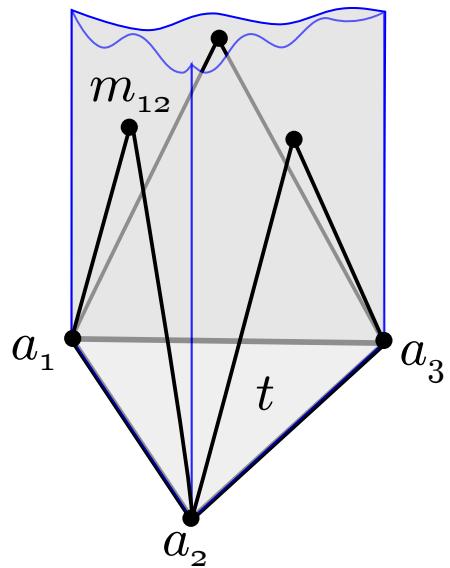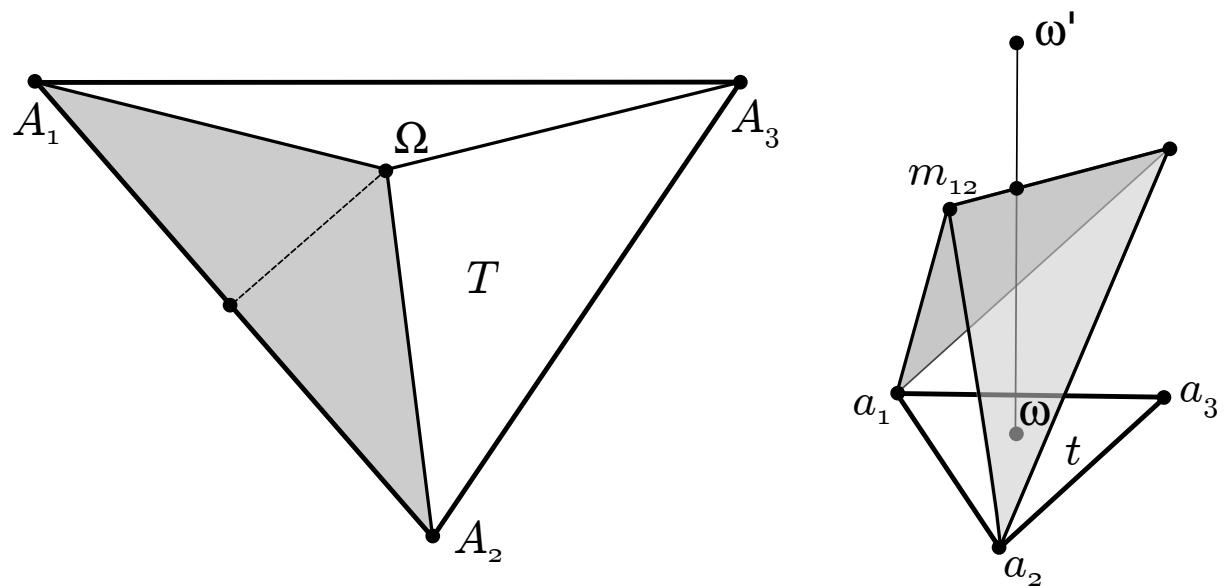
Figure 21: The prism above t.

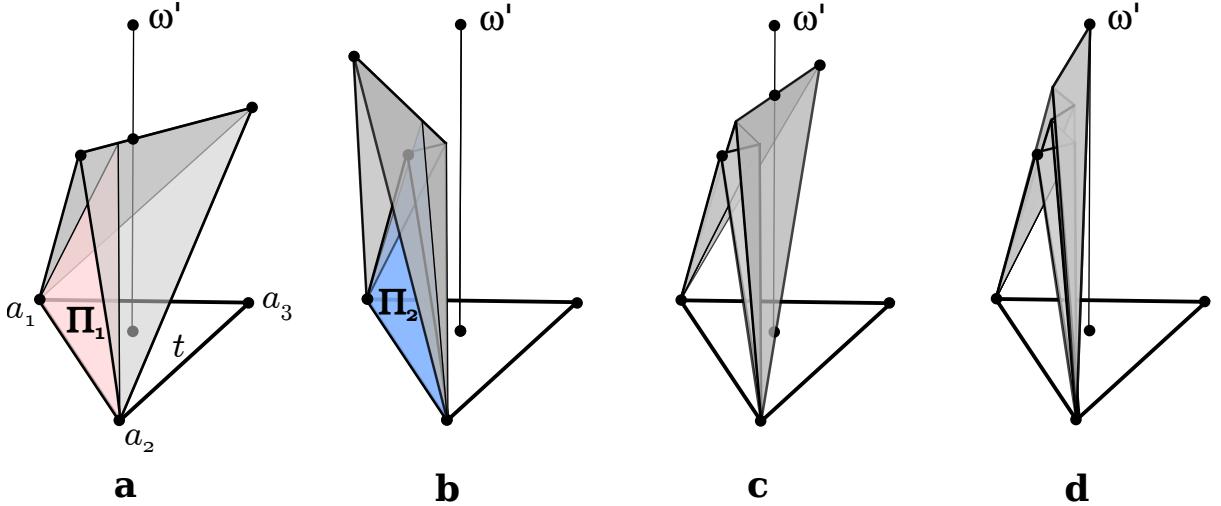Figure 22: The subtriangle $\Omega A_1 A_2$ is folded above t.

Figure 23: a - the reflection plane Π_1. b - after reflection in Π_1, and the plane Π_2. c - reflection in Π_2. d - after an even number of reflections the point Ω is sent to ω'.

we first fold $\Omega A_1 A_2$ along its altitude from Ω and place the resulting two-winged shape above t, as in Figure 22, so that the side $A_1 A_2$ is folded onto the broken line $a_1 m_{12} a_2$. We next consider a plane Π_1 in the pencil of planes through $a_1 a_2$ to reflect the part of the two-winged shape lying to the right of that plane. See Figure 23. Another plane Π_2 in the same pencil of planes is then chosen to reflect part of the already reflected part. Choosing Π_1 and Π_2 appropriately, it is not hard to see that after an even number of reflections the point Ω in $\Omega A_1 A_2$ can be sent to ω', cf Figure 23 d. We finally apply the same construction to the two other subtriangles $\Omega A_2 A_3$ and $\Omega A_3 A_1$ and paste them to form a folding of T above t as desired. □

Note 3. *As previously stated, this pleating of T admits some flexibility. In particular, the boundary conditions can be modified so that each boundary wedge $a_i m_{ij} a_j$ is tilted around the axis $a_i a_j$. This modification is needed in order to paste the constructions above two adjacent triangles that are non coplanar as illustrated in Figure 24.*

Embedding of a closed polyhedral surface Σ. Denote by $f_0 : \Sigma \to \mathbb{R}^3$ the original short $\mathcal{C}^2$ embedding as in Theorem 1. We first modify f_0 near small neighborhoods of the singularities of Σ to obtain a $\mathcal{C}^2$ short embedding f_1 such that every singularity admits a neighborhood that is sent to a small Euclidean disk in the tangent plane in order to apply some constructions. Without entering into the details, the modifications are such that f_1 is conformal near singularities of conical angle less than 2π, and so that f_1 is isometric on the radial segments and uniformly contracting on the circles centered at the singularity with conical angle greater than 2π. See [BZ95]. We then surround the singularities of Σ by small disjoint polygonal neighborhoods which depend on f_1. Denote U the union of such neighborhoods. The strategy for the proof of Theorem 1 is the following:

(a) Compute an acute triangulation $\mathcal{T}$ of $\Sigma \setminus U$, where each triangle is acute, and such that there exist a uniform lower and upper bound on the angles of all the triangles.
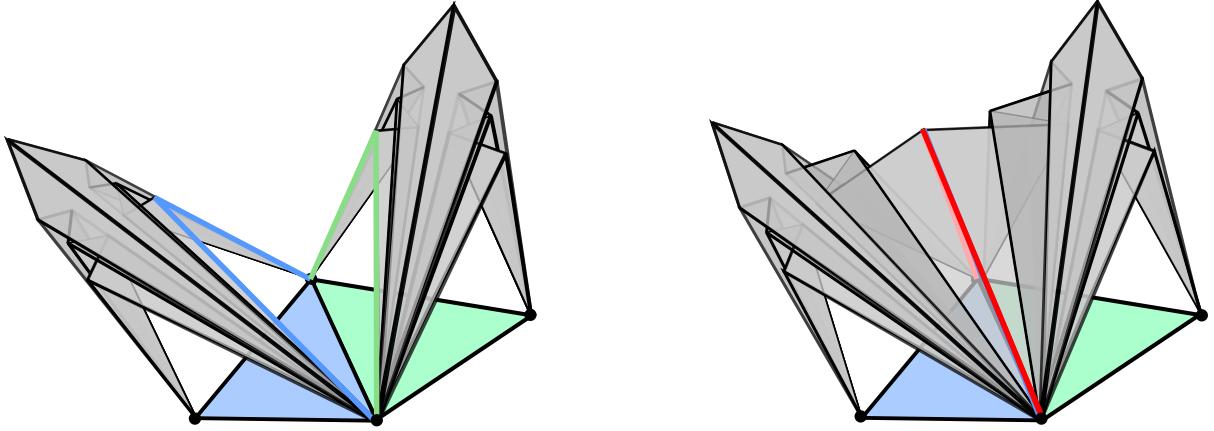
Figure 24: Pasting two foldings of large triangles sharing an edge above small triangles that are non coplanar.

(b) Compute an approximation f_2 of f_1 that is almost conformal outside a small neighborhood $U_{>2\pi}$ of the singularities with conical angle greater than 2π and stays short and $\mathcal{C}^2$ on Σ.

(c) Refine the acute triangulation of $\Sigma \setminus U$ uniformly to obtain an acute triangulation with small triangles, and propagate it to the entire Σ. The meaning of *small* depends on the geometric properties of f_2 and the flexibility in Note 3.

(d) Replace f_2, outside $U_{>2\pi}$, by its PL approximation F mapping linearly each triangle $T = A_1 A_2 A_3$ of $\mathcal{T}$ to the triangle $F(T) := f(A_1)f(A_2)f(A_3)$ in $\mathbb{R}^3$.

(e) Apply the construction in the previous paragraph to every pair $(T, F(T))$, using the tilted version in Note 3 in order to paste the constructions of adjacent triangles.

(f) Fill the gaps near singularities of conical angle greater than 2π with specific construction as described in [BZ95].

Computing an acute triangulation as required in step (a) is a non trivial task. If Σ is obtained from a gluing of Euclidean triangles, it was shown how to compute an acute refinement of reasonable size [BZ60, Zam13]. Step (b) is the most challenging and relies on the Nash-Kuiper theorem [Nas54, Kui55]. The idea is to apply this theorem in order to approximate f_1 by an almost isometric map with respect to a metric homothetic to the metric on Σ but slightly smaller. This provides the map f_2 that is at the same time short and almost conformal. This almost conformality combined with the uniform subdivision in step (c) implies that any triangle T of $\mathcal{T}$ is sent by the PL approximation F of step (d) to an almost similar triangle $F(T)$. Since f_2 and its PL approximation are short, this in turn implies that the pair $(T, F(T))$ satisfies the three conditions of Lemma 2. The previous arguments work outside U. Near a vertex A of conical angles θ less than 2π, the polygonal neighborhood $Q(A)$ is chosen to be a regular hexagon centered at the singularity composed of six isosceles with apical angle $\theta/6$, further refined into isosceles triangles according to the uniform refinement of $\Sigma \setminus U$, see Figure 25. The map f_1 is chosen so that first the vertices of each isosceles triangle T composing $Q(A)$ are sent to vertices of acute
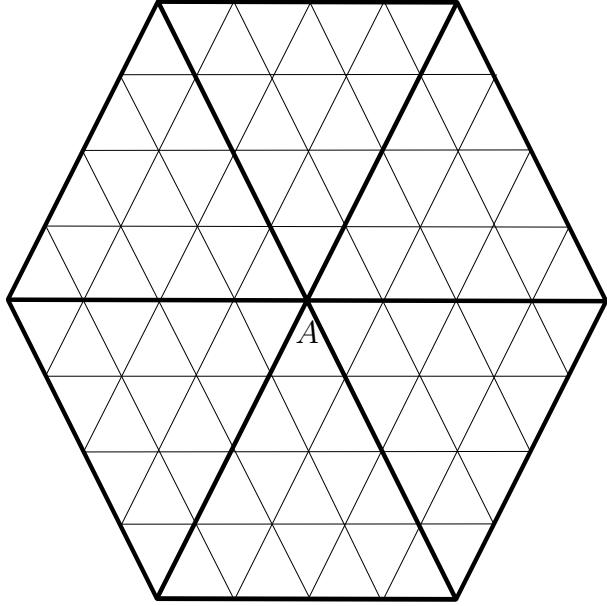
Figure 25: The hexagonal neighborhood of a singularity A of conical angle less than 2π. Here, the triangulation has been refined on the edges and has been propagated.

triangles t in the tangent plane of $f_1(\Sigma)$ at $f_1(A)$. Moreover, it is also chosen such that the coefficient of contraction is so large that the conditions of Lemma 2 are fulfilled. This ensures the possibility to apply the Lemma 2 to every triangles outside $U_{>2\pi}$. Moreover, the fact that the triangles in $\mathcal{T}$ are small together with the smoothness of f_2 ensure that F maps adjacent triangles to almost coplanar triangles. We can thus apply the building block of Lemma 2 and its tilted version as in Note 3 to perform step (e). This eventually leads to a PL isometric embedding of $S \setminus U_{>2\pi}$. It remains to embed appropriately $U_{>2\pi}$ as required by step (f) to complete the construction.

This can be done the following way. Recall that, by construction, at a singularity B of conical angle θ greater than 2π, f_1 sends a circular disk V_0 of B into a plane sector in the tangent plane at $f_0(B)$. We also know that the map is isometric on the radial segments and uniformly contracting on the circles centered at B. We split the boundary $V = \partial V_0$ into N_0 equal arcs, each arc being the base of an isosceles "triangle" in the exterior of V. As a result we obtain a "cogged" polygon $Q(B)$ - see Figure 26. It is possible to propagate the refinement of the triangulation $\mathcal{T}$ of $\Sigma \setminus U$ so that the "cogs" of the polygon $Q(B)$ become smaller and more numerous, see Figure 27. Given a refinement of the complementary of U, this splits the boundary of the circular neighborhood V_0 into $N \geq N_0$ arcs of equal length. Denote $F_1, ..., F_N$ the splitting points, and E_i the midpoint if the chord $F_i F_{i+1}$. Then the polygon $V(B) = F_1...F_N$ can be isometrically and piecewise linearly embedded above the tangent plane P_B at $f_1(B)$ as a radially creased surface as shown in Figure 28. If the refined triangulation $\mathcal{T}$ is sufficiently thin, every broken line $F_i E_i F_{i+1}$ lie in a plane almost perpendicular to P_B, and it is possible to apply the arguments of Note 3 to make coincide the broken line $F_i E_i F_{i+1}$ with the side $F_i F_{i+1}$ of an adjacent triangle T of the refined triangulation.
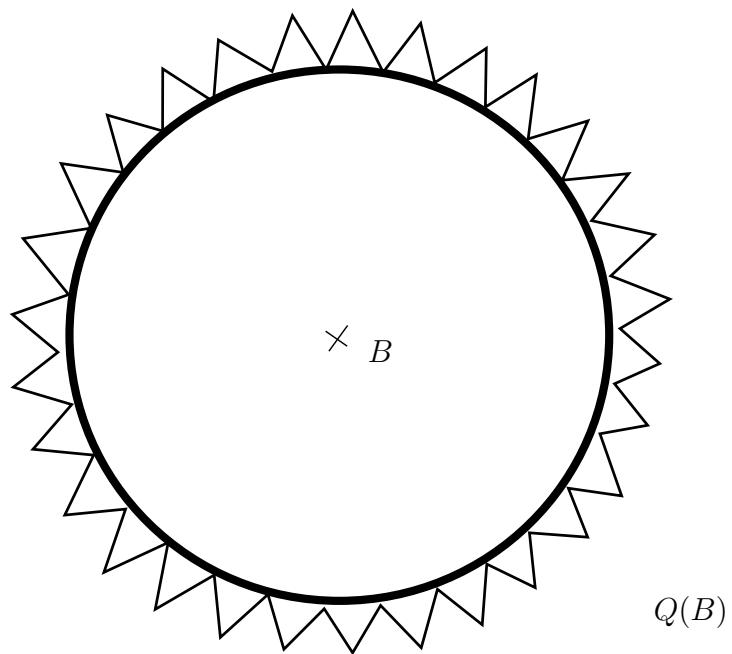
Figure 26: A typical cogged polygon $Q(B)$ surrounding a singularity of conical angle greater than 2π.
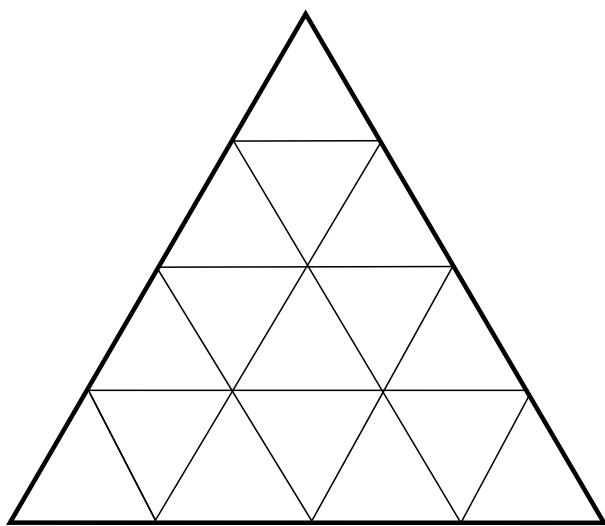

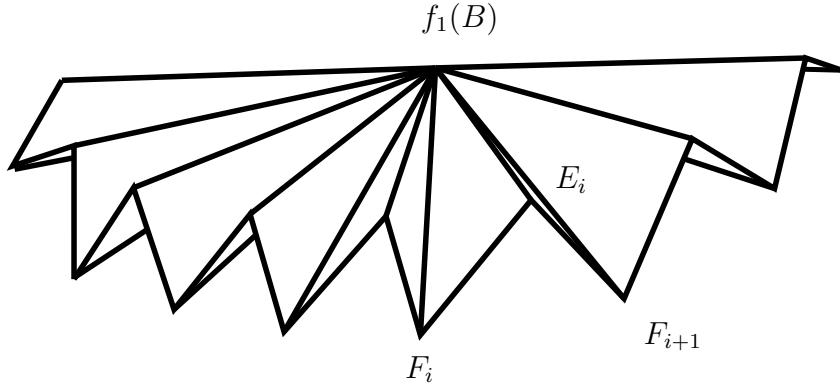Figure 27: The refinement propagated to a cog.

Figure 28: The creased embedding of the circular neighborhood V_0 of a singularity B of conical angle greater than 2π. If the triangulation is sufficiently fine, each adjacent triangle $F_i F_{i+1} A_i$ to V_0 can be embedded thanks to Lemma 2 so that the boundary condition matches with the broken line $F_i E_i F_{i+1}$.

3.3 Zalgaller's long flat tori

Any flat torus can be obtained by identifying abstractly the top and bottom boundaries of a right circular cylinder. Non rectangular tori are obtained by shifting circularly the top boundary before identification. We can moreover cover all the torus moduli by varying the ratio between the height and the length of its boundaries. A torus is said long when this ratio is large. In [Zal00], Zalgaller proposes an origami style folding of long flat tori, much simpler than the general construction of Burago and Zalgaller [BZ95]. Instead of a circular cylinder, Zalgaller starts with a polyhedral cylinder in $\mathbb{R}^3$, namely a right prism with equilateral triangular basis, that he bends at several places to make the boundaries coincide, allowing their geometric identification. A twist is also applied before the bending so as to simulate a circular shift of the top boundary. To do so, and to rotate the cross-section of the prism without rotating its "material", Zalgaller introduces what he calls a **gasket**.

How to bend a triangular prism. Consider a right prism $\mathcal{P}$ with triangular basis and an orthogonal cross section $CC'D$. A **bending at angle φ with cutting angle λ** along the **rib** CC' is obtained by (see Figure 29)

(a) cutting two isosceles triangles ACB and $AC'B$ out of $\mathcal{P}$, where A, B lie on the generatrix of the prism through D, and the angle at C (and C') is 2λ,

(b) bending the cut prism at angle $0 \leq \varphi < \pi$,

(c) folding ACB and $AC'B$ appropriately to fit them back on the bended prism.

Let A_1, B_1 be the respective positions of points A, B after bending and let $\angle A_1 C B_1 = 2\mu$. In order for the construction not to overlap, one should have $\mu > 0$, hence λ should satisfy $\lambda_0(\varphi) < \lambda < \frac{\pi}{2}$ where $\lambda_0(\varphi)$ is the angle for which, after bending, the triangles $A_1 CC'$ and $B_1 CC''$ coincide. Looking at the right angled triangles ADC and ADV, one
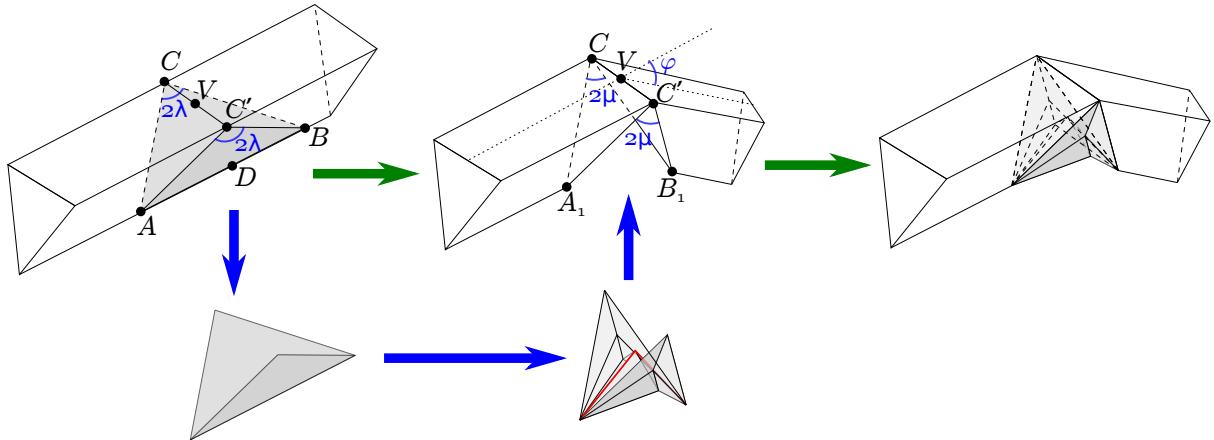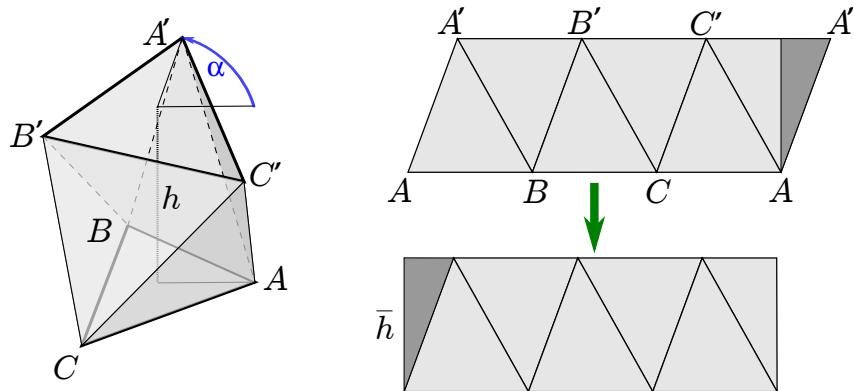
Figure 29: Bending of a prism.

Figure 30: Left, a gasket with turn α and height h. Right, the gasket is unfolded in the plane. Cutting and pasting a small triangular piece shows that the gasket has the geometry of a right prism.

easily computes

$$\lambda_0(\varphi) = \arctan\left(\frac{\sqrt{3}}{2}\tan\frac{\varphi}{2}\right). \tag{3.1}$$

We postpone the study of prism bending to Section 5.1. In particular, we will show that it is possible to bend a right prism introducing only 12 triangles in step (c).

Rotating a cross section with a gasket. The ribs of the prism $\mathcal{P}$ may have only three possible directions. This prevents to bend $\mathcal{P}$ in an arbitrary direction. To circumvent this rigidity, Zalgaller introduces a simple construction that he calls a gasket. Consider an equilateral triangle ABC in the horizontal plane and a vertical translate $A'B'C'$ at height h. Rotate $A'B'C'$ by an angle α about the central vertical axis. The **gasket with turn α and height h** is the polyhedral cylinder formed by the six congruent triangles $ABA', A'BB', B'BC, B'CC', C'CA, AA'C'$. See Figure 30. This gasket is embedded for every $\alpha \in (-\pi/3, \pi)$ independently of $h > 0$.

By pasting two prisms at the boundaries of a gasket, we obtain a polyhedral cylinder with triangular boundaries, where the two boundaries are turned at the angle α with
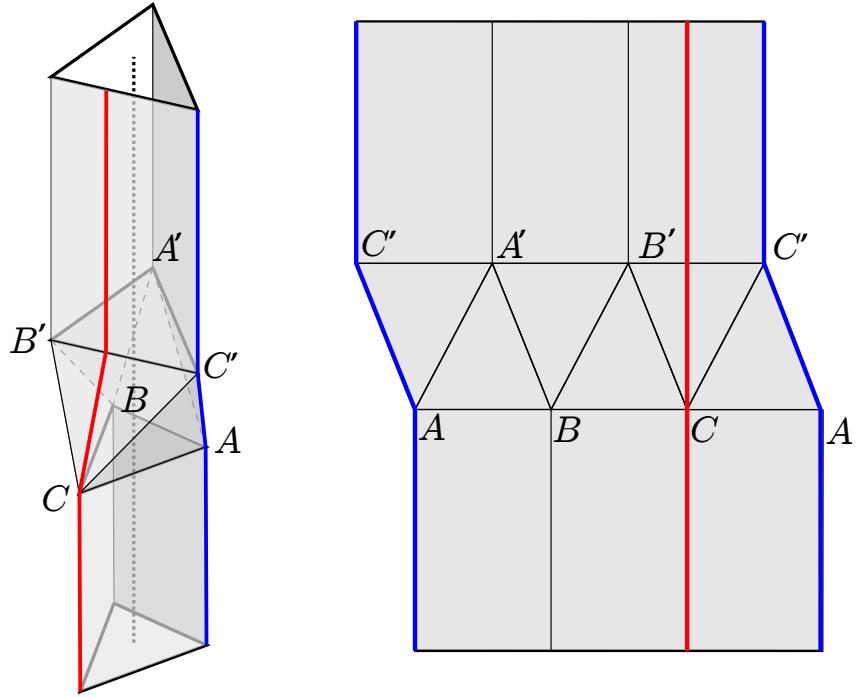
Figure 31: Joining a gasket with two prisms to rotate their ribs. Right, unfiolding of the construction showing the line of cut (in blue) and a generatrix (in red) of the polyhedral cylinder.

respect to each other, cf Figure 31.

Note. *The top and bottom prisms in Figure 31 have the same central axis. This allows to rotate the rib of a prism at an angle $\alpha \in (-\pi/3, \pi)$ before applying a bending.*

Note 4. *By joining k gasket in a row, we can rotate the rib of a prism at an angle $\alpha \in (-k\pi/3, k\pi)$.*

We will study in details gasket in Section 5.1, where we quantify how much "material" is needed to realize a gasket of height h with turn α.

Twisting a prism. Replacing a portion of a prism by a gasket with turn α allows to turn the top boundary of the prism with respect to the bottom one but does not *twist* the prism: the gasket makes generatrices going through a vertex on the bottom triangle not go through the corresponding vertex in the top. In order to twist the prism so that the top endpoint of this geodesic indeed turns with the boundary, Zalgaller introduces yet an other construction that he calls a *helical twist*. This construction takes advantage of the holonomy of parallel transport on the sphere: consider a unit sphere of center O with a spherical triangle PQR (see Figure 32). If one parallel transports an object from P to P following the sides of the triangle PQR, then the object is rotated by a certain angle around the axis OP that is equal to the signed area of the spherical triangle PQR. In order to twist a prism with axis directed by $\overrightarrow{OP}$ by an angle θ we may thus bend the prism successively in the directions $\overrightarrow{OQ}, \overrightarrow{OR}$ and $\overrightarrow{OP}$. Each bending at angle φ indeed corresponds to a transport along a spherical geodesic of length φ. Each portion of prism
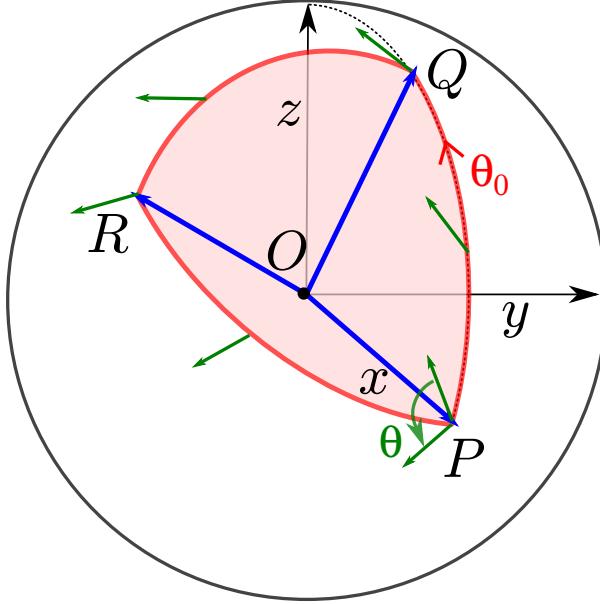
Figure 32: The green tangent vector is transported along the spherical triangle PQR. The angle θ is equal to the area of PQR, while the angle θ_0 is given by L'Huillier's formula.

between two bends should include two gaskets to orient its rib properly. Indeed, by Note 4, two gaskets allow to turn by an angle in $(-2\pi/3, 2\pi)$, which cover all possible orientations.

A **helical twist of angle** θ consists of a sequence of gaskets and bends according to the pattern $(g^2b)^5g^2 = (g^2b)^3(g^2b)^2g^2$, where b, g stands respectively for bends and gaskets. The prefix $(g^2b)^3$ in the pattern is used to simulate the parallel transport as described above, assuming that the central axis of the initial cross section is already aligned with $\overrightarrow{OP}$. The next factor $(g^2b)^2$ allows to return on the central axis of the initial cross section. Since $\overrightarrow{OP}$ is aligned with this central axis, the changes of direction due to the factor $(g^2b)^2$ happen in the same plane. The resulting holonomy is thus trivial, which ensures that the first and last cross sections of this portion are parallel. Finally, the last two gaskets allows to turn the cross section by any angle in $(-2\pi/3, 2\pi]$ - see Figure 33

We refer to Section 5.1 to see a possible implementation and our choice for P, Q, R leading to an effective construction of the helical twist. Moreover, we also quantify how much "length" is needed to realize a helical twist.

Putting the pieces together. Consider a flat torus with modulus $\tau = \tau_1 + i\tau_i \in \left\{ z : |z| \geq 1, |\Re z| \leq \frac{1}{2} \right\}$. It can be obtained from a cylinder of height τ_i and boundary length 1, identifying the boundaries after a circular shift at angle $2\pi\tau_1$. Zalgaller constructs his PL isometric embeddings of long tori, assuming that τ_i is large, as follows. He first replaces the circular cylinder by an isometric equilateral triangular prism that is bent 6 times at angle $\pi/3$ to form a hexagonal tube. If the torus is rectangular, that is if $\tau_1 = 0$, then the initial and final cross-sections coincide geometrically, and their identification provides the desired embedding. Otherwise, Zalgaller replaces one side of the hexagon by a helical twist of angle $2\pi\tau_1$ in order to glue the boundaries of the prism with the correct angular shift. We use a slightly different construction that allows to get shorter tori. Starting from a helical twist of angle θ, we add 4 bends at angle $\pi/2$ and 3 portions
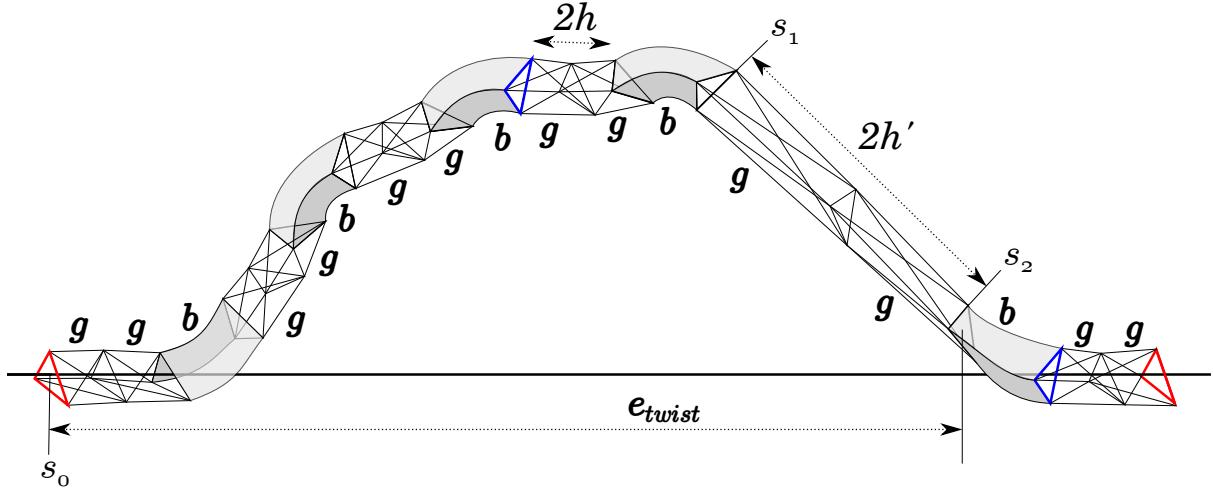
Figure 33: The cross section (in blue) after the last bending of a helical twist is rotated by an angle θ about the central axis with respect to the initial cross section (in red). The last two gaskets allow to turn the last cross section (in red) to be a translate of the initial one.
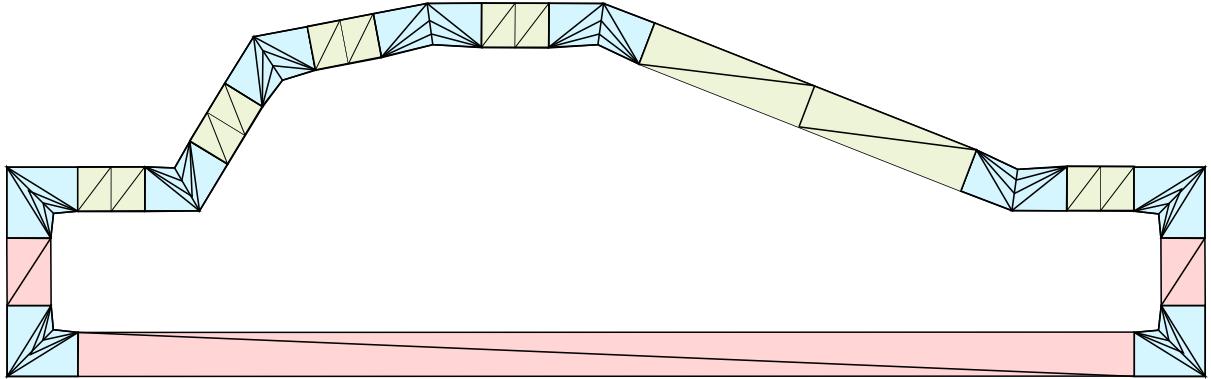

Figure 34: Our construction decomposed into bends (in light blue), gaskets (in light green) and triangular prisms (in pink).

of right prisms as illustrated in Figure 34 to form a torus with rectangle shape.

3.4 Diplotori

The previous construction allows to realize a flat torus only if it is long enough. We describe in this section a construction that can be used to realize any flat torus according to the parameters one chooses.

It was only recently that Arnoux, Lelièvre and Málaga [ALM21, not yet published], and Tsuboi [Tsu20], independently (re-)discovered very simple geometric realizations of flat tori. Arnoux, Lelièvre and Málaga are able to prove that their construction, called **diplotorus**, allows to realize all flat tori. However, one cannot cover all rectangular flat tori using a fixed combinatorics.

The diplotorus $\mathcal{D}_{n,d}^{a,h}$ with parameter n, d, a, h is defined as follows. Let $A_k = \left(e^{i\frac{2k\pi}{n}}, 0 \right)$
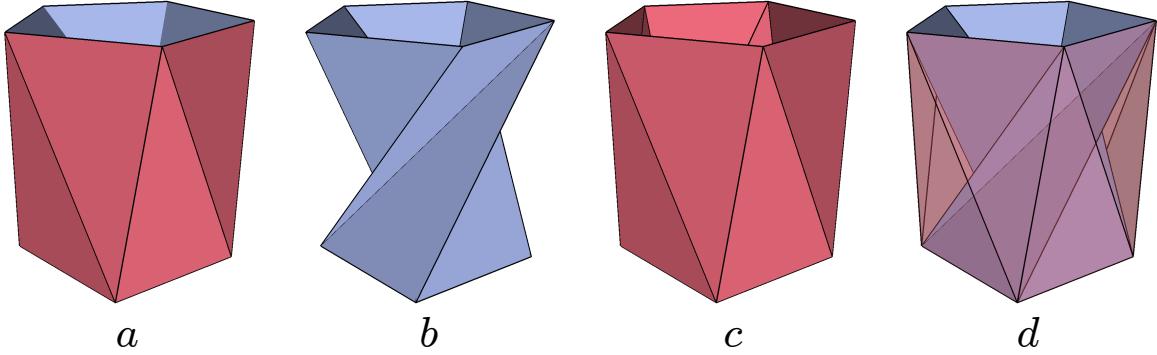
Figure 35: View of the diplotorus $\mathcal{D}_{5,2}^{3.5,2}$ (a) with its internal (b) and external (c) ploids. (d), an other view of $\mathcal{D}_{5,2}^{3.5,2}$ with a transparent external ploid.

be the vertices of the regular n-gon in the horizontal coordinate plane. Let $B_k = \left(e^{i\frac{\pi}{n}(a+1+2k)}, h\right)$ be the vertices of the vertical translate by h of this n-gon, turned by an angle $(a+1)\frac{\pi}{n}$. Then $\mathcal{D}_{n,d}^{a,h} = \mathcal{P}_{int} \bigcup \mathcal{P}_{ext}$ is the union of two twisted prisms, called **ploids**, where $\mathcal{P}_{int}$ is the union of triangles $\{A_k A_{k+1} B_k\}_{0 \leq k < n}$ and $\{B_k A_{k+1} B_{k+1}\}_{0 \leq k < n}$, and $\mathcal{P}_{ext}$ is the union of triangles $\{A_k A_{k+1} B_{k-d}\}_{0 \leq k < n}$ and $\{B_{k-d} A_{k+1} B_{k+1-d}\}_{0 \leq k < n}$. Of course, all indices should be considered modulo n. Note that a ploid with $n = 3$ is nothing but a gasket. Figure 35 shows the diplotorus $\mathcal{D}_{5,2}^{3.5,2}$.

We postpone to Section 5.2 more involved considerations about diplotori. In particular, the realization theorem of Arnoux, Lelièvre and Málaga which we use later in our construction of a universal triangulation for flat tori.

Chapter 4

Implementation of the method of Burago and Zalgaller in the case of flat tori

Résumé en français. La méthode de Burago et Zalgaller, bien que générique, n'est pas totalement constructive car repose sur le procédé de Nash-Kuiper à l'étape (b). Cependant, dans le cas des tores plats, il est possible d'adapter la méthode pour obtenir un algorithme effectif, ce que nous faisons dans ce chapitre.
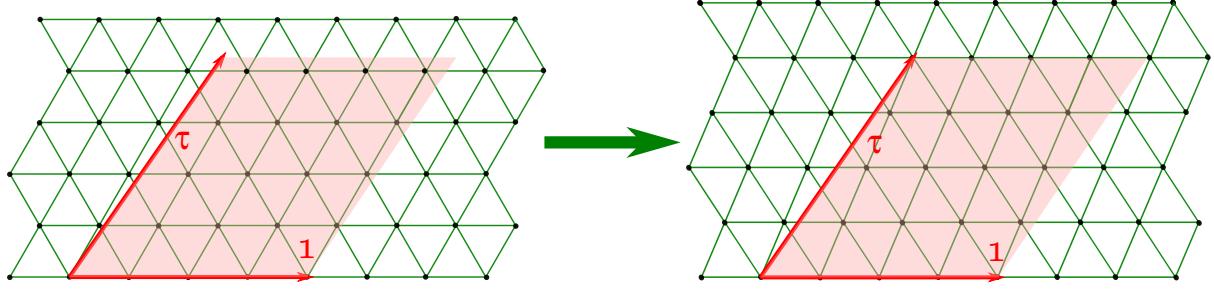
Figure 36: The equilateral lattice (here $n = 4$) is deformed to fit the lattice of $\mathbb{T}$.

In this chapter we present our implementation of the method of Burago and Zalgaller in the case of flat tori. Let $\mathbb{T} = \mathbb{T}_\tau$ a flat torus of modulus $\tau \in \left\{ z : |z| \geq 1, |\Re z| \leq \frac{1}{2} \right\}$. As a flat torus has no singularity by Gauss-Bonnet theorem, we can set the neighborhood of the singularities U to be empty in the last paragraph of Section 3.2. We recall that we have to compute an acute triangulation of $\mathbb{T}$, and then we have to choose a short and smooth embedding we will have to modify in order to make it quasi-conformal. These steps become relatively simple in the case of flat tori.

4.1   Simple acute triangulation of a flat torus

Itoha and Yuan [iIY09] have shown that every flat torus can be triangulated into at most 16 acute triangles. However, since we need a fine triangulation as in step (c) with a good control on the acuteness, we use the following triangulation, which is conceptually simpler. We consider the equilateral triangular lattice generated by $\frac{e^{i\frac{\pi}{3}}}{n}$ and $\frac{1}{n}$ for some positive integer n. This lattice comes with a regular triangulation $\mathcal{T}_e$ by equilateral triangles. Let $p_{a,b} = a\frac{e^{i\pi/3}}{n} + \frac{b}{n}$ with $a, b \in \mathbb{Z}$, be a point in this lattice that is closest to τ, the modulus of $\mathbb{T}$. In particular, $|\tau - p_{a,b}| \leq \frac{1}{n\sqrt{3}}$. We deform $\mathcal{T}_e$ by a linear transformation ℓ defined by $1 \mapsto 1$ and $p_{a,b} \mapsto \tau$. By the previous inequality and for n large enough, ℓ is close to the identity. The triangles in $\ell(\mathcal{T}_e)$ are thus close to equilateral. Now, the lattice $\mathbb{Z} + \mathbb{Z}\tau$ leaves $\ell(\mathcal{T}_e)$ invariant, so that $\ell(\mathcal{T}_e)/(\mathbb{Z} + \mathbb{Z}\tau)$ is a well defined triangulation of $\mathbb{T}$ by almost equilateral triangles. See Figure 36.

4.2   Conformal embedding of a flat torus

In the case of flat tori, we can directly provide short and conformal embeddings.

The case of rectangular flat tori.   Let us identify $\mathbb{R}^3$ with $\mathbb{C} \times \mathbb{R}$. First observe that the standard embedding of the square flat torus $\mathbb{T}_1$ as a torus of revolution,

$$f : \left\{ \begin{array}{ll} \mathbb{T}_1 & \to \mathbb{R}^3 \\ (u, v) & \mapsto \quad ((R + r\cos(2\pi u))e^{i2\pi v}, r\sin(2\pi u)) \end{array} \right.$$

is never conformal as the ratio of the lengths of the partial derivative is non-constant. The partial derivatives are nonetheless orthogonal and when the torus is rectangular, i.e.,
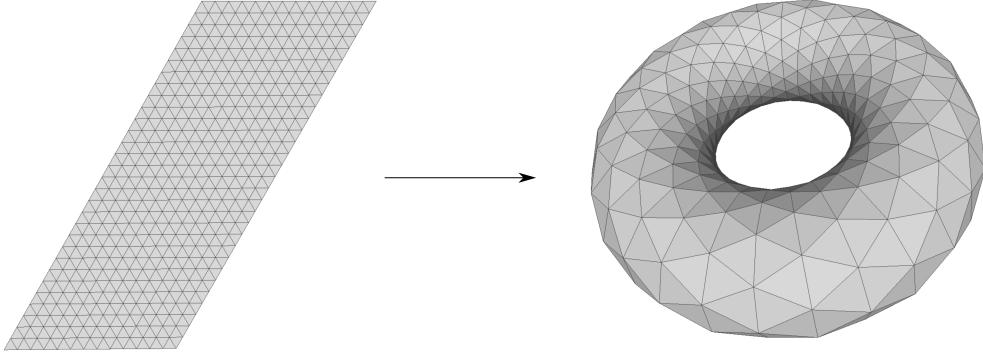
73

Figure 37: Left, the fundamental domain of the rectangular torus $\mathbb{T}_{2i}$ is chosen to be aligned with an almost equilateral tiling as in Section 4.1. Right, PL approximation of the conformal embedding f_{2i}.

when $\tau = i\tau_i$ is pure imaginary, there are conformal maps of the form

$$f_{i\tau_i} : \begin{cases} \mathbb{T}_{i\tau_i} & \to & \mathbb{R}^3 \\ (u,v) & \mapsto & f(\alpha(u), v/\tau_i) \end{cases}$$

for some 1-periodic function α. Indeed, when α satisfies the differential equation $\tau_i \alpha' = \cos(2\pi\alpha) + \frac{R}{r}$, one easily checks that the partial derivatives of $f_{i\tau_i}$ with respect to u and v have the same norm (and are orthogonal). This differential equation solves to

$$\alpha(u) = \frac{1}{\pi} \arctan\left(\sqrt{\frac{R+r}{R-r}} \tan\left(\frac{\sqrt{R^2 - r^2}}{\tau_i r} \pi u \right) \right) \quad \text{with } \frac{R}{r} = \sqrt{\tau_i^2 k^2 + 1}$$

for some integer k. In practice we chose $k = r = 1$, leading to the conformal map:

$$f_{i\tau_i}(u,v) = \left(\left(\sqrt{\tau_i^2 + 1} + \cos(2\pi\alpha(u)) \right) e^{i2\pi v/\tau_i}, \sin(2\pi\alpha(u)) \right)$$

with $\alpha(u) = \frac{1}{\pi} \arctan\left(\sqrt{\frac{\sqrt{\tau_i^2+1}+1}{\sqrt{\tau_i^2+1}-1}} \tan(\pi u) \right)$. It remains to compose $f_{i\tau_i}$ with a contracting homothety to get a short conformal embedding of $\mathbb{T}_{i\tau_i}$. See Figure 37 for an example.

The general case. In order to embed non rectangular tori conformally, we rely on the Hopf tori developed by Pinkal [Pin85]. These are based on the Hopf fibration

$$p : \begin{cases} \mathbb{S}^3 & \to & \mathbb{S}^2 \\ (x,y,z,t) & \mapsto & (2xz + 2yt, 2xt - 2yz, x^2 + y^2 - z^2 - t^2) \end{cases} ,$$

which is a circle bundle of the 3-sphere $\mathbb{S}^3$ onto the 2-sphere $\mathbb{S}^2$. Pinkall proves that if γ is a simple closed curve on $\mathbb{S}^2$, then $p^{-1}(\gamma)$ endowed with the metric inherited from $\mathbb{R}^4$ is a flat torus isometric to $\mathbb{T}_\tau$, with $\tau = \frac{A+iL}{4\pi}$, where L is the length of γ and A is the oriented area delimited by γ on $\mathbb{S}^2$, choosing the side of γ so that $A \in [-2\pi, 2\pi)$. Since this torus lies in $\mathbb{S}^3 \subset \mathbb{R}^4$, it remains to apply a stereographic projection, say from the South pole $(0,0,0,-1)$, assuming it does not lie on the torus, to obtain a conformal embedding of $\mathbb{T}_\tau$ in $\mathbb{R}^3$. In coordinates: $(x,y,z,t) \mapsto \frac{(x,y,z)}{t+1}$.

Banchoff [Ban88] revisited Pinkall's approach to give explicit parametrizations of the Hopf-Pinkall tori. On $\mathbb{S}^2$, Banchoff considers a curve of the form $\gamma_\tau(\theta) = (\sin\phi(\theta)e^{i\theta}, \cos(\phi(\theta)))$ given in spherical coordinates, where the polar angle $0 < \phi < \pi$ is a smooth function of the azimuthal angle $0 \leq \theta \leq 2\pi$. He next defines $L(\theta) = \int_0^\theta |\gamma_\tau'(t)|dt$ to be the length of the curve portion $\gamma_\tau([0,\theta])$ and $A(\theta) = \int_0^\theta (1 - \cos\phi(t))dt$ the area on $\mathbb{S}^2$ swept by the arc of meridian linking the North pole to the point on γ_τ up to θ. The conformal embedding $f_\tau : \mathbb{T}_\tau \to \mathbb{R}^3$ is then given by $f_\tau = f \circ g^{-1}$ with

$$f : \left\{ \begin{array}{ccc} (\mathbb{R}/2\pi\mathbb{Z})^2 & \to & \mathbb{R}^3 \\ (\theta,\psi) & \mapsto & \left(\sin\frac{\phi(\theta)}{2}e^{i(\theta+\psi)}, \cos\psi\cos\frac{\phi(\theta)}{2}\right) / \left(1 + \sin\psi\cos\frac{\phi(\theta)}{2}\right) \end{array} \right. , \text{ and}$$

$$g : \left\{ \begin{array}{ccc} (\mathbb{R}/2\pi\mathbb{Z})^2 & \to & \mathbb{T}_{-1/\tau} \sim \mathbb{T}_\tau \\ (\theta,\psi) & \mapsto & \left(\frac{L(\theta)}{2}, \frac{A(\theta)}{2} + \psi\right) \end{array} \right. .$$

In other words,

$$f_\tau(u,v) = \left(\sin\frac{\phi(\theta)}{2}e^{i(\theta+u-A(\theta)/2)}, \cos(u - A(\theta)/2)\cos\frac{\phi(\theta)}{2}\right) / \left(1 + \sin(u - A(\theta)/2)\cos\frac{\phi(\theta)}{2}\right),$$

where θ satisfies $L(\theta) = 2v$ and $(u,v) \in \mathbb{R}^2/(\mathbb{Z}2\pi i + \mathbb{Z}2\pi i/\tau)$

We chose ϕ of the form $\phi(\theta) = a + b\sin(n\theta)$ for $a < b, 0 \leq b < \pi - a$ and $n \in \mathbb{N}$. in order to represent the modulus $\tau = \tau_1 + i\tau_i$, the parameters a, b, n should satisfy $A(2\pi) = 4\pi\tau_1$ and $L(2\pi) = 4\pi\tau_i$ or equivalently:

$$J_0(b)\cos a = 1 - 2\tau_1 \text{ and } \int_0^{2\pi} \sqrt{n^2b^2\cos^2(nt) + \sin^2(a + b\sin(nt))}dt = 4\pi\tau_i,$$

where $J_0(b) = \frac{1}{\pi}\int_0^\pi \cos(b\sin t)dt$ denotes the 0-th Bessel function of the first kind. The condition on the total area implies $0 \leq \tau_1 \leq 1$. Nevertheless, it is still possible to obtain a conformal embedding in the case of $\tau_1 < 0$ by first reflecting the torus along one of its boundary edge and applying a reflexion of the image torus in $\mathbb{R}^3$. We can thus cover the whole moduli space.

4.3 Final construction

We now have all the pieces to produce PL isometric embeddings of flat tori. Given a modulus τ, we first compute a quasi-equilateral triangulation of $\mathbb{T}_\tau$ as in Section 4.1. We then compute a PL approximation F_τ of the conformal map f_τ defined in Section 4.2 and finally apply the construction in the first paragraph of Section 3.2 to every pair of triangle $(T, F_\tau(T))$. Figures 38 and 39 show some results.

4.4 Limitations and discussion

The construction of Burago and Zalgaller, though generic, gives rise to triangulations with a huge number of triangles, moreover distinct for every initial short and smooth embedding f_0. Nevertheless, by the flexibility of the construction mentioned in the first paragraph of Section 3.2, in a small neighborhood of a flat torus $\mathbb{T}$ in the moduli space
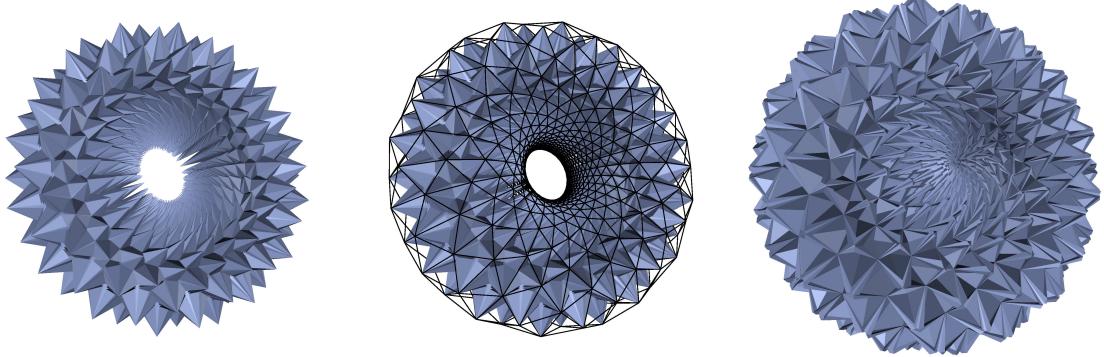
Figure 38: Left, PL isometric embedding of the square flat torus with 170,040 triangles. Middle, the mesh with black edges shows the PL approximation of the initial conformal embedding. Each of its triangle is replaced with a construction (in blue) as in Section 3.2 oriented toward the interior of the initial embedding. Right, the construction is oriented towards the outside, giving another isometric immersion of the square flat torus - this last model present self-intersections; a finer triangulation should be used to avoid them.
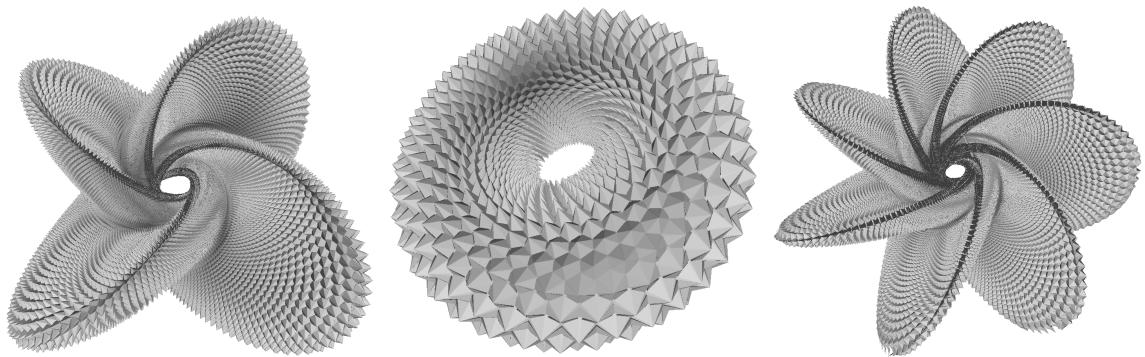
Figure 39: Isometric immersion of $\mathbb{T}_\tau$ with, form left to right $\tau = e^{i\pi/3}, (1+i)/2, (1+3i)/2$. The left immersion is a hexagonal flat torus. While the subdivisions of the left and right tori already have more than 7 millions triangles, they present self-intersections. Finer triangulations should be used to get embeddings.

$\mathcal{M}$ of flat tori, it is possible to use the same PL approximation of a short and conformal embedding (for example the one of $\mathbb{T}$) as a common frame for all the flat torus in the neighborhood in order to apply Lemma 2. In other words, locally in $\mathcal{M}$, we can fix a triangulation that realizes geometrically and linearly, i.e. without the need of subdividing it, any flat torus in a small neighborhood. This suffices to show the existence of a universal triangulation for any compact subset of $\mathcal{M}$. $\mathcal{M}$ being not compact, this is not enough for our purpose. However, as $\mathcal{M}$ admits only one point at infinity, it is enough to realize a neighborhood of this point at infinity with a fixed triangulation to conclude about the existence of a universal triangulation for all of $\mathcal{M}$. The next section is devoted to the construction of such a triangulation. While the flat tori near infinity, which correspond to long flat tori - i.e. flat tori $\mathbb{T}_\tau$ with a large $|\tau|$ where $\tau \in \left\{ z : |z| \geq 1, |\Re z| \leq \frac{1}{2} \right\}$, are dealt with Zalgaller's construction, we go further and use three families of diplotori to cover the remaining compact subset that remains to realize.

Chapter 5

Universal triangulation for flat tori

Résumé en français. L'algorithme du chapitre 4 permet de réaliser tous les tores plats de manière individuelle. Nous nous intéressons, dans ce chapitre, à l'aspect uniforme de telles réalisations. Plus précisément, nous introduisons la notion de **triangulation universelle** pour une famille $\mathcal{F}$ de surfaces polyédrales de genre g. Une triangulation $\mathcal{T}$ de la surface topologique orientable fermée S_g est dite **universelle** pour $\mathcal{F}$ si, pour tout élément $\Sigma \in \mathcal{F}$, $\mathcal{T}$ admet une réalisation géométrique dans $\mathbb{R}^3$ isométrique à Σ, la réalisation étant affine en restriction à chaque triangle de $\mathcal{T}$. Le chapitre est dévolu à la démonstration du Théorème 5, qui démontre de manière constructive l'existence d'une triangulation universelle pour la famille $\mathcal{M}$ des tores plats comportant 2434 triangles. La démonstration comporte trois parties. Tout d'abord, par une étude fine des tores longs de Zalgaller, nous démontrerons l'existence d'une triangulation universelle pour la partie $\mathcal{M}^{long}$ de $\mathcal{M}$ formée des modules de partie imaginaire supérieure ou égale à 33. Nous exhibons ensuite trois familles de diplotores qui suffisent à réaliser le complémentaire $\mathcal{M}^{short}$ de $\mathcal{M}^{long}$ dans $\mathcal{M}$, et en déduisons une triangulation universelle pour $\mathcal{M}$. Enfin, nous procédons à la superposition des deux triangulations précédentes pour obtenir la triangulation universelle de $\mathcal{M}$ désirée.

In this chapter we revisit and take a deeper look at Zalgaller's long flat tori, and at dipotori described in the previous chapter in order to build a universal triangulation for flat tori. While Zalgaller's construction is used to realize long flat tori, that is the subset

$$\mathscr{M}_{long} := \left\{ [\tau] : |\tau| \geq 1, |\Re\tau| \leq \frac{1}{2}, \Im\tau \geq 33 \right\} \subset \mathscr{M}$$

we use three families of diplotori to cover the complementary

$$\mathscr{M}_{short} = \mathscr{M} \setminus \mathscr{M}_{long} \subset \mathscr{M}.$$

It is then enough to overlay the two corresponding triangulations to obtain a universal triangulation for $\mathscr{M}$. The following sections will permit to state the following statement:

Theorem 5. *There exists an abstract triangulation $\mathcal{T}$ of the torus with 2434 triangles that admits for each flat torus an embedding in $\mathbb{R}^3$ which is linear on each triangle of $\mathcal{T}$, and which is isometric to this flat torus. Moreover, every flat torus has an isometric PL embedding in $\mathbb{R}^3$ with at most 270 triangles.*

5.1 A deeper look at Zalgaller's tori: universal triangulation for long flat tori

In this section we show the following proposition.

Proposition 6. *There exists an abstract triangulation with 270 triangles, which admits linear embeddings isometric to every flat torus with modulus in $\mathscr{M}_{long}$.*

The proof amounts to add fine and precise quantitative bounds to the various step in Zalgaller's construction of Section 3.3. The main difficulty remains to identify what "long" means in mathematical terms, i.e. to find a good candidate for $\mathscr{M}_{long}$ that was not known a priori.

Bending a right prism introducing 12 triangles. We will show that it is always possible to bend a right prism by introducing 12 triangles to the initial triangulation. More precisely, we show the following Lemma.

Lemma 7. *Let $\mathcal{P}$ be an infinite right prism. For every $\varphi \in (0, \pi)$ and for every $\lambda \in (\lambda_0(\varphi), \pi/2)$, there is an embedded bending of $\mathcal{P}$ at angle φ with cutting angle λ introducing 12 triangles.*

Proof. Recall the first paragraph of Section 3.3. We only have to check that ACB and $AC'B$ can be folded appropriately in step (c) introducing only 12 triangles. To do so, we first fold CAB along its altitude from C to reduce the angle $\angle ACB$ from 2λ to 2μ. The side AB is mapped onto a broken line $A_1\tilde{D}B_1$ and the goal is to rotate this broken line so that it is contained in the "vertical" plane through A_1, B_1, V, where V is the middle of CC'. See Figures 29 and 40. Denote by Π_0 the plane spanned by A_1, B_1, C. Also denote by Π_θ the plane in the pencil of planes through A_1B_1, making an angle θ with Π_0. Let
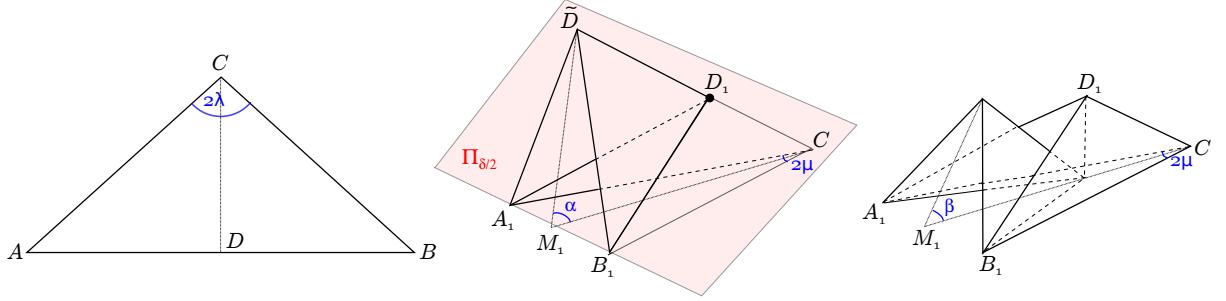
Figure 40: Folding of triangle ACB.

α, β be such that Π_α contains $\tilde{D}$ and Π_β contains V. Because the triangles $C\tilde{D}M_1$ and CVM_1 - where M_1 is the middle of A_1B_1 - are right angled at $\tilde{D}$ and V, we easily deduce

$$\alpha = \arcsin \frac{\cos \lambda}{\cos \mu} \text{ and } \beta = \arcsin \frac{\cos \lambda}{2 \cos \mu}.$$

Set $\delta = \alpha - \beta$. The plane $\Pi_{\delta/2}$ cuts $C\tilde{D}$ in D_1. We first reflect across $\Pi_{\delta/2}$ the pieces of triangles $A_1C\tilde{D}$ and $B_1C\tilde{D}$ lying above $\Pi_{\delta/2}$. We next reflect across Π_0 the part of the reflected part lying below Π_0. As a result, $A_1\tilde{D}B_1$ is rotated in Π_β as desired. The resulting folding is composed of 6 triangles as illustrated on Figure 41. Moreover, if $\beta > \delta/2$, then the resulting folding of ACB lies inside the "top" quadrant delimited by Π_β and Π_0. As a consequence, we can fold $AC'B$ according to the symmetric image across Π_β of the folding of ACB; the two triangle foldings join along the folding of AB in Π_β and they fit inside the tetrahedron A_1B_1CC' without creating intersection with the rest of the bended prism. They comprise 12 triangles in total.

Zalgaller [Zal00] also considers the case $\beta \le \delta/2$ that forces him to use an a priori unbounded number of triangles for bending a prism. We claim that there is no need for this second case and that we indeed have $\beta > \delta/2$ for every $\varphi \in (0, \pi)$ and for every $\lambda \in (\lambda_0(\varphi), \pi/2)$. This inequality is equivalent to $F\left(\frac{\cos \lambda}{\cos \mu}\right) > 0$ for $F(x) = 3 \arcsin \frac{x}{2} - \arcsin x$. We have $F(0) = F(1) = 0$ and a simple computation shows that the derivative of F cancels only once on $[0, 1]$ at $x = \sqrt{5/8}$. Since $F(\sqrt{5/8}) > 0$, we infer that F is positive on $(0, 1)$. We finally remark that $\mu < \lambda$, implying $\frac{\cos \lambda}{\cos \mu} \in (0, 1)$, which allows us to conclude the demonstration of Lemma 7. $\qquad\square$

For further reference, we call a **bend** a bent prism cut along the orthogonal cross section through A_1 and B_1. See Figure 41.

The intrinsic length of a gasket. We quantify how much "material" is needed to realize a gasket with unit length basis. More precisely, we have:

Lemma 8. *For every $\alpha \in (-\pi/3, \pi)$, the gasket with turn α and height h is isometric to a right prism of length $\bar{h}$ with*

$$\bar{h}^2 = h^2 + \frac{2}{27}(\sin^2 \frac{\alpha}{2} + \sin^2(\frac{\pi}{3} - \frac{\alpha}{2})) - \frac{4}{81}(\sin^2 \frac{\alpha}{2} - \sin^2(\frac{\pi}{3} - \frac{\alpha}{2}))^2 - \frac{1}{36}$$
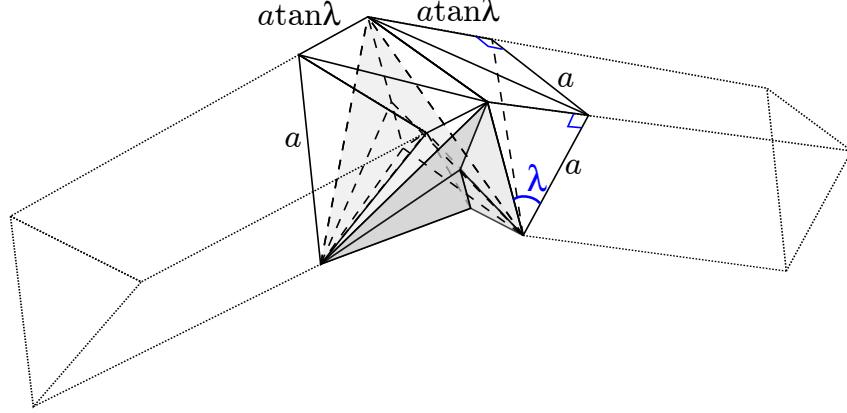$$< h^2 + \frac{1}{9}.$$

80

Figure 41: A bend is isometric to a right prism of length $2a \tan \lambda$. It comprises 20 triangles.

Proof. By unfolding the gasket in the plane, it is seen to be isometric to a Euclidean rectangle after identifying its vertical sides, see Figure 30. It is thus isometric to a right prism of length $\bar{h}$, where $\bar{h}$ is the height of the rectangle. Fix the coordinates of A, B, C to be respectively $\left(\frac{1}{3\sqrt{3}}, 0\right)$, $\left(\frac{e^{i2\pi/3}}{3\sqrt{3}}, 0\right)$ and $\left(\frac{e^{-i2\pi/3}}{3\sqrt{3}}, 0\right)$ in $\mathbb{R}^3 = \mathbb{C} \times \mathbb{R}$. Then the coordinates of A', B', C' are respectively $\left(\frac{e^{i\alpha}}{3\sqrt{3}}, h\right)$, $\left(\frac{e^{i(\alpha+2\pi/3)}}{3\sqrt{3}}, h\right)$ and $\left(\frac{e^{i(\alpha-2\pi/3)}}{3\sqrt{3}}, h\right)$. The three sides of the congruent triangles are given by

$$|AB| = 1/3, \quad |A'A| = \sqrt{\frac{4}{27}\sin^2(\alpha/2) + h^2}, \quad |BA'| = \sqrt{\frac{4}{27}\sin^2(\pi/3 - \alpha/2) + h^2}.$$

From Heron's formula, we have $\bar{h} = 2\frac{\sqrt{p(p-|AB|)(p-|BA'|)(p-|AA'|)}}{|AB|}$ with p the half-perimeter of ABA', and we obtain

$$\bar{h}^2 = h^2 + \frac{2}{27}\left(\sin^2\frac{\alpha}{2}6\sin^2(\frac{\pi}{3} - \frac{\alpha}{2}) - \frac{4}{81}(\sin^2\frac{\alpha}{2} - \sin^2(\frac{\pi}{3} - \frac{\alpha}{2}))^2 - \frac{1}{36}.$$

Since

$$\sin^2\frac{\alpha}{2} + \sin^2(\frac{\pi}{3} - \frac{\alpha}{2}) = \frac{3}{4} - \sin\frac{\alpha}{2}\sin(\frac{\pi}{3} - \frac{\alpha}{2}) < 7/4,$$

it follows that

$$\bar{h}^2 < h^2 + \frac{2}{27} \times \frac{7}{4} - \frac{1}{36} < h^2 + \frac{1}{9}.$$

$\square$

Minimal length to realize a helical twist. In practice, to construct a helical twist of angle $\theta \in (-\pi, \pi]$, we choose an equilateral triangle PQR on the unit sphere, with area θ. Moreover, we fix $P = (1, 0, 0)$, and we take Q in the plane Oxz with positive z coordinate. Then, R is the unique point making PQR equilateral and counterclockwise. Denote θ_0 the angle between the vectors $\overrightarrow{OP}$ and $\overrightarrow{OQ}$. L'Huillier's formula relates the area $\mathcal{A}$ of a geodesic triangle on the unit sphere with its side lengths a, b, c by

$$\tan\frac{\mathcal{A}}{4} = \sqrt{\tan\left(\frac{p}{2}\right)\tan\left(\frac{p-a}{2}\right)\tan\left(\frac{p-b}{2}\right)\tan\left(\frac{p-c}{2}\right)},$$

where p is the half-perimeter. It follows that θ_0 satisfies the equation

$$\theta = 4\arctan\left(\sqrt{\tan(\frac{3\theta_0}{4})\tan^3(\frac{\theta_0}{4})}\right).$$

This equation has an explicit solution for $|\theta| \leq \pi$:

$$\theta_0 = 4\,\text{sign}(\theta) \cdot \arctan\left(\sqrt{1 + 2\frac{\cos(\frac{|\theta|}{12} - \frac{2\pi}{3})}{\cos\frac{|\theta|}{4}}}\right).$$

Traveling along PQR in trigonometric direction induces a positive rotation angle, while traveling clockwise induces a negative rotation angle. For $|\theta| \leq \pi$, the above formula implies

$$\theta_0 \leq 4\arctan\sqrt{1 + 2\sqrt{2}\cos\frac{7\pi}{12}} = 4\arctan\sqrt{2 - \sqrt{3}} \approx 1.911.$$

From Equation (3.1), we deduce that the corresponding cutting angle satisfies

$$\lambda_0(\theta_0) \leq \arctan\frac{\sqrt{6 - 3\sqrt{3}}}{\sqrt{3} - 1} < \arctan\frac{49}{40}.$$

For further reference, we set

$$\lambda_0 := \arctan\frac{49}{40}.$$

Denote by s_0 the initial cross section of the helical twist, by s_1 the cross section at the end of the fourth bend, and by s_2 the initial cross section of the last bend. Refer to Figure 33.

Lemma 9. *Given any twist angle $\theta \in (-\pi, \pi]$ and any $h > 0$, we can construct a helical twist of angle θ so that its bends have cutting angle λ_0, and all its gaskets have height h, except the two gaskets between sections s_1 and s_2, which have height h' imposed by our construction. This helical twist is isometric to a right prism of length*

$$\ell_{twist} = 10a\tan\lambda_0 + 10\bar{h} + 2\bar{h}'$$

and the horizontal distance between the boundaries of the helical twist is bounded by

$$d_{twist} = 18(a\tan\lambda_0 + h).$$

Here, $\bar{h}$ and $\bar{h}'$ are given by Lemma 8. The height h' is moreover bounded by

$$2\sqrt{10}(2h + 3a\tan\lambda_0).$$

Proof. Let $a = 1/3$ be the length of a rib, i.e. of a side of the triangular cross-sections. The bending angle of the three first bends is equal to θ_0 and we know by the previous discussion that they can be realized with the cutting angle λ_0. We need to prove that the last two bends can be realized with this cutting angle. Define the **extent** e_{twist} of the helical twist as the horizontal distance between the centers of the sections s_0 and s_2.

We fix $e_{twist} = 16(h + a \tan \lambda_0)$. Let c_i be the center of s_i, $i = 0, 1, 2$. The last two bends have the same bending angle φ, which is the angle between the horizontal direction and the vector $\overrightarrow{c_1 c_2}$. We have $\tan \varphi = \delta_v / \delta_h$, where δ_v is the distance from c_1 to the horizontal line through c_2, and δ_h is the horizontal distance between c_1 and c_2. We estimate δ_v by adding the contributions of the eight gaskets and the four bends preceding s_1. Four of the eight gaskets are horizontal; it follows that they do not contribute to δ_v. The fourth bend turns towards the horizontal axis through c_2, it thus contributes negatively to δ_v. We infer that $\delta_v \le 4h + 6a \tan \lambda_0$. On the other hand, the horizontal distance d_{01} between c_0 and c_1 is bounded by $8h + 8a \tan \lambda_0$. We conclude that $\tan \varphi \le \frac{4h + 6a \tan \lambda_0}{8h + 8a \tan \lambda_0}$. Hence, for all h, $\tan \varphi < 3/4$. Using Equation (3.1) and the classical formula $\tan \varphi = 2 \tan \frac{\varphi}{2} / (1 - \tan^2 \frac{\varphi}{2})$, we deduce $\tan \lambda_0(\varphi) < \frac{1}{2\sqrt{3}}$. It follows that $\lambda_0(\varphi) < \lambda_0$ as desired.

The *intrinsic length* of the helical twist, i.e. the height of the corresponding isometric cylinder, is the sum of the intrinsic lengths of each constituting bend and gasket. We thus obtain the formula as in the lemma, where $\bar{h}$ and $\bar{h}'$ are given by Lemma 8. We now remark that the total horizontal extent of the helical twist is bounded by $e_{twist} + 2a \tan \lambda_0 + 2h$ to obtain the bound in the lemma.

We next remark that $d_{01} \ge 4h + 2a \tan \lambda_0$, taking into account the four horizontal gaskets and the two incident horieontal half bends. Hence, $\delta_h = e_{twist} - d_{01} \le 12h + a \tan \lambda_0$ and we finally conclude

$$h' = \sqrt{\delta_h^2 + \delta_v^2} \le \sqrt{(12h + 14a \tan \lambda_0)^2 + (4h + 6a \tan \lambda_0)^2}$$
$$\le 2\sqrt{10}(2h + 3a \tan \lambda_0).$$

$\square$

Universal triangulation for $\mathcal{M}_{long}$. Recall our variation of Zalgaller's embedding of flat tori as a prismatic rectangle shape where the upper branch is replaced by a helical twist as in Section 3.3 and Figure 33. In order to avoid intersection between the horizontal prism and the horizontal gaskets of the helical twist we choose the two vertical prisms of length $\frac{a}{3} > \frac{a}{2\sqrt{3}}$. We also choose the length of the horizontal prism to be equal to the total horizontal extent of the helical twist. We finally take the cutting angle of the four bends equal to $\lambda_0' := \arctan(9/10) > \lambda_0(\pi/2)$. The resulting torus has length

$$L < \ell_{twist} + 8a \tan \lambda_0' + 2a/3 + d_{twist},$$

where ℓ_{twist} and d_{twist} are given by Lemma 9. In other words,

$$L < 28a \tan \lambda_0 + 8a \tan \lambda_0' + 2a/3 + 18h + 10\bar{h} + 2\bar{h}'.$$

Using the bound for h' in Lemma 9 together with the inequality in Lemma 8, and the fact that $\tan \lambda_0 = 49/40$, and $\tan \lambda_0' = 9/10$, we get

$$L < \frac{253}{18} + 18h + 10\sqrt{h^2 + \frac{1}{9}} + 2\sqrt{40\left(2h + \frac{49}{40}\right)^2 + \frac{1}{9}}. \tag{5.1}$$

By taking $h = 0$, we thus obtain $L < \frac{253}{18} + \frac{10}{3} + 2\sqrt{\frac{49^2}{40} + \frac{1}{9}} < 33$. Note that any longer flat torus can be obtained by elongating the two vertical prisms. Hence, for h strictly positive
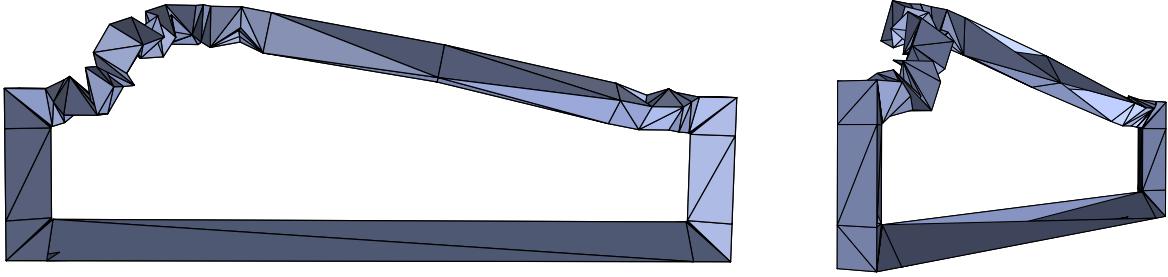
83

Figure 42: Rendering of the flat torus of length 18 and circular shift $2\pi/5$ corresponding to the modulus $0.2 + 18i$.
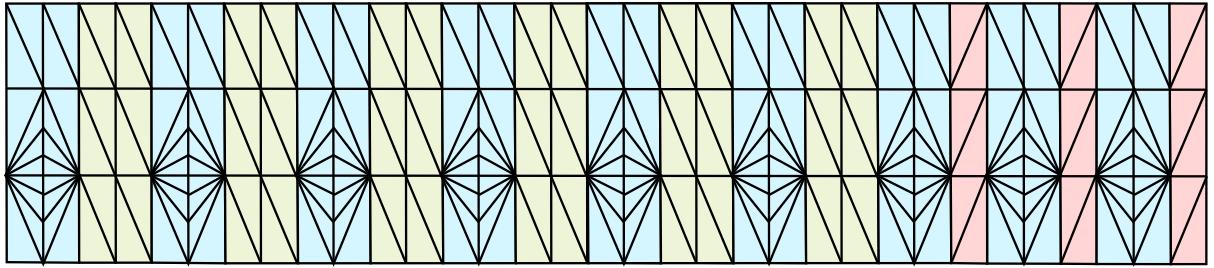

Figure 43: A universal triangulation for long flat tori.

and small enough, say smaller than 0.002, we can realize any flat torus of length at least 33. The bound for L in (5.1) is largely overestimated and our implementation shows that the same construction, taking $h = 1/15$, allows to embed tori of length much shorter than 33 even though the right member in (5.1) evaluates to more than 33. Some rendering is visible on Figure 42.

We remark that a prism can be triangulated as a gasket with turn 0, the whole construction thus corresponds to the pattern $(g^2b)^5g^2(bg)^3b$ and is composed of $15 \times 6 + 9 \times 20 = 270$ triangles. This ends the proof of Proposition 6. Figure 43 shows the resulting unfolded triangulation after cutting through a cross section and a longitude.

5.2 Three families of diplotori suffices to realize short flat tori

We now turn to the realization of short tori with modulus in $\mathscr{M}_{short} = \left\{ \tau : |\tau| \geq 1, |\Re\tau| \leq \frac{1}{2}, \Im\tau \leq 33 \right\}$.

Recall the diplotorus construction of Section 3.4. Arnoux, Lelièvre and Málaga showed the following realization theorem:

Theorem 10 (Arnoux, Lelièvre and Málaga - 2021)**.** *For $h, a \in \mathbb{R}$ and $n, d \in \mathbb{Z}$, $\mathcal{D}_{n,d}^{a,h}$ is an embedded flat torus if and only if*

$$h > 0, n > 4, 2 \leq |d| < n - 2 \text{ and } \begin{cases} d + 1 < a < n - 1 \text{ if } d > 0 \\ 1 - n < a < d - 1 \text{ if } d < 0 \end{cases}.$$

Moreover, the modulus of $\mathcal{D}_{n,d}^{a,h}$ *is* $\tau(n,d,a,h) = \tau_1(n,d,a) + i\tau_i(n,d,a,h)$ *with*

$$\tau_1(n,d,a) = d/n - \frac{\cos((a-d)\frac{\pi}{n})\sin(d\frac{\pi}{n})}{n\sin\frac{\pi}{n}} \quad and$$

$$\tau_i(n,d,a,h) = \left(\sqrt{h^2 + 4\sin^2(\frac{a+1}{2}\cdot\frac{\pi}{n})\sin^2(\frac{a-1}{2}\cdot\frac{\pi}{n})} + \right.$$
$$\left. \sqrt{h^2 + 4\sin^2(\frac{a-2d+1}{2}\cdot\frac{\pi}{n})\sin^2(\frac{a-2d-1}{2}\cdot\frac{\pi}{n})}\right) / (2n\sin(\pi/n))$$

The map τ_1 does not depend on h while τ_i is an increasing function of h. It follows that for n and d fixed, the moduli of the flat tori $\mathcal{D}_{n,d}^{a,h}$ form a subset of $\mathbb{H}^2$, which we denote by $\mathcal{M}_{n,d}$, that lies above the graph of the parametrized curve $a \mapsto (\tau_1(n,d,a), \tau_i(n,d,a,0))$, where a varies as in Theorem 10. For n and d fixed, the diplotori $\mathcal{D}_{n,d}^{a,h}$ have the same abstract triangulation. If one could cover the moduli space with a finite number of regions $\mathcal{M}_{n,d}$, this would therefore provide a universal triangulation. This is however impossible and one needs to let n grow to infinity in order to realize all the rectangular flat tori. We can nonetheless cover the moduli of short flat tori with only three regions $\mathcal{M}_{n,d}$.

The fundamental domain $F = \left\{z : |z| \geq 1, |\Re z| \leq \frac{1}{2}\right\}$ is symmetric with respect to the imaginary axis. Two symmetric points τ and $-\bar{\tau}$ actually represent isometric tori, but the isometry should reverse the orientation. Hence, if $\mathbb{T}_\tau$ has a PL isometric embedding in $\mathbb{R}^3$ so does $\mathbb{T}_{-\bar{\tau}}$: just take a reflected image of the embedding of $\mathbb{T}_\tau$. It is thus enough to realize the positive part $\mathcal{M}_{short}^+ := \{[\tau] \in \mathcal{M}_{short} : \tau_1 \geq 0\}$ of the short flat tori to ensure that we can realize all of them.

Remark 1. From Section 2.5.3, the moduli space of flat tori is the quotient of $\mathbb{H}^2$ by the action of $\text{PSL}_2(\mathbb{Z})$. To realize all the short flat tori, it is thus sufficient to realize their moduli in any image of $\mathcal{M}_{short}^+$ under the action of $\text{PSL}_2(\mathbb{Z})$. Figure 44 shows such an image. The top side $\tau_i = 33$ of $\mathcal{M}_{short}^+$ is transformed by $g_\delta = \begin{pmatrix} 0 & 1 \\ -1 & \delta \end{pmatrix} \in PSL_2(\mathbb{Z})$ to an arc of circle, called a **horocycle**, tangent at 0 to the real axis. In Figure 44, the blue and yellow lines are part of the *Dedekind tesselation* of the hyperbolic plane. It tiles $\mathbb{H}^2$ into hyperbolic triangles with one ideal vertex. Each such triangle is a fundamental domain for the action of the *extended modular group* $\text{PGL}_2(\mathbb{Z})$. This action includes orientation reversing transformations so that adjacent triangles have opposite orientations.

Lemma 11. *Any modulus in* $\mathcal{M}_{short}^+$ *can be geometrically realized by a diplotorus with parameters* $n = 19$ *and* $d \in \{2, 7, 13\}$.

We need to check that $\mathcal{M}_{short}^+$ is covered by the orbit of $\mathcal{M}_{19,2} \bigcup \mathcal{M}_{19,7} \bigcup \mathcal{M}_{19,13}$ under the action of $\text{PSL}_2(\mathbb{Z})$. Equivalently, writing $g \cdot \mathcal{M}_{short}^+$ for the image of $\mathcal{M}_{short}^+$ by $g \in \text{PSL}_2(\mathbb{Z})$, we must have that

$$\bigcup_{g \in \text{PSL}_2(\mathbb{Z})} g^{-1} \cdot \left((g \cdot \mathcal{M}_{short}^+)\bigcap(\mathcal{M}_{19,2}\bigcup\mathcal{M}_{19,7}\bigcup\mathcal{M}_{19,13})\right)$$

covers $\mathcal{M}_{short}^+$ (or any of its images). The regions $\mathcal{M}_{19,2}$, $\mathcal{M}_{19,7}$ and $\mathcal{M}_{19,13}$, deduced from the formulas of Theorem 10, are plotted in Figures 45 and 47.
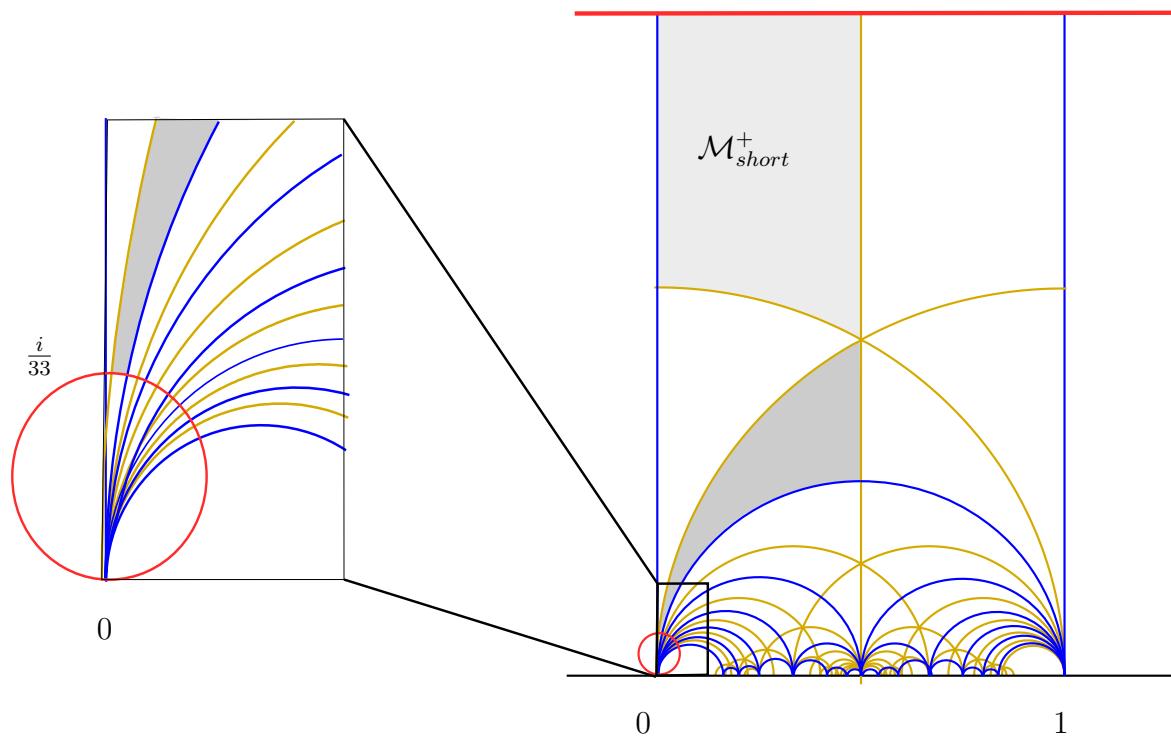
Figure 44: The image (in dark grey) of $\mathcal{M}^+_{short}$ by the action of $\begin{pmatrix} 0 & 1 \\ -1 & 1 \end{pmatrix} \in PSL_2(\mathbb{Z})$. The top horizontal line (in red) represents the horocycle $\tau_i = 33$ (not to scale). Its image by $\begin{pmatrix} 0 & 1 \\ -1 & 1 \end{pmatrix}$ is a circle (in red, not to scale) tangent at 0 to the real axis.
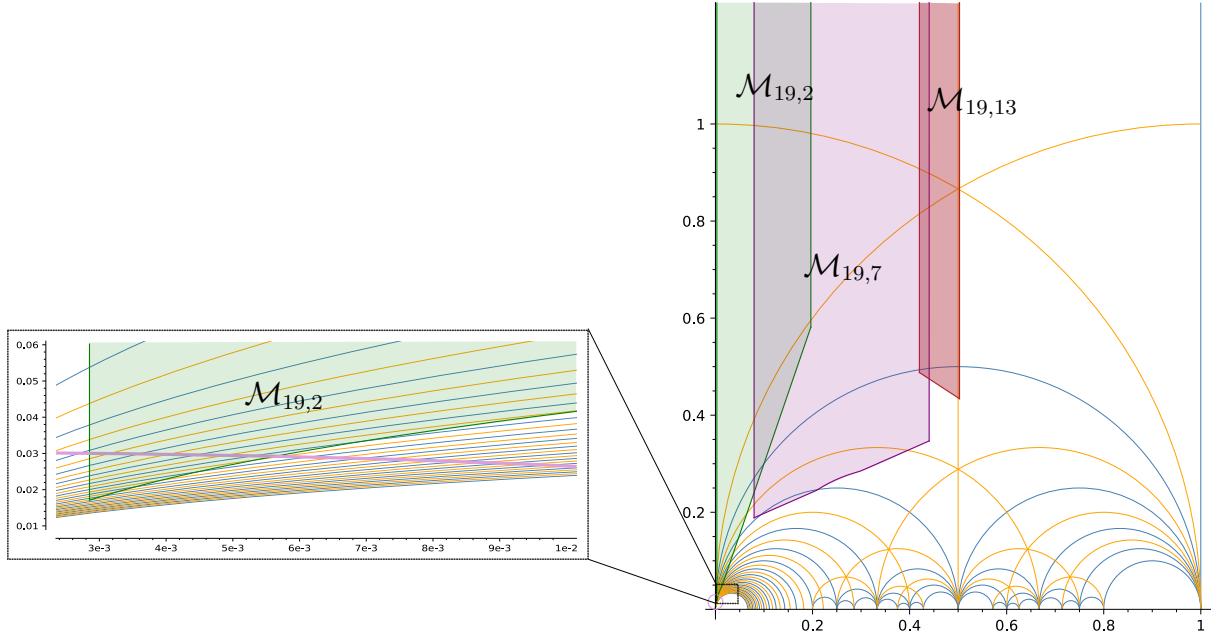
Figure 45: The moduli space for $\mathcal{M}_{19,2}$ (in green), $\mathcal{M}_{19,7}$ (in purple), and $\mathcal{M}_{19,13}$ (in red). The axes in the bottom enlargement have different scales; the horocycle (thick purple line), image of $\{\tau_i = 33\}$ by the elements of Δ, appear as an arc of ellipse.

Denote by $\mathcal{M}^+$ the part of the fundamental domain F with non-negative real part. $\mathcal{M}^+$ is bounded by the geodesic triangle with vertices $0, e^{i\pi/3}, \infty$. In particular, it contains $\mathcal{M}^+_{short}$. Consider the subset Δ of $\mathrm{PSL}_2(\mathbb{Z})$ composed of the matrices $g_\delta := \begin{pmatrix} 0 & 1 \\ -1 & \delta \end{pmatrix}$ with δ a positive integer. The elements in Δ transform $\mathcal{M}^+$ into a fan of triangular domains with positive real part, tangent at 0 to the imaginary axis. They moreover transform each horocycle $\{\tau_i = \text{constant}\}$ into a circle, independent of δ, and tangent at 0 to the real axis. Larger constants give rise to smaller circles. Two such circles cut the transforms of $\mathcal{M}^+$ by Δ into slices that are themselves transforms of a *same* slice in $\mathcal{M}^+$. Figure 46 and 47 demonstrate that we can slice $\mathcal{M}^+_{short}$ so that each slice has a transform by respectively g_1, g_3, g_5 (in yellow, blue, and red on the figure) covered by $\mathcal{M}_{19,2} \bigcup \mathcal{M}_{19,7} \bigcup \mathcal{M}_{19,13}$. It follows that

$$\mathcal{M}^+_{short} \subset \bigcup_{\delta \in \{1,3,5\}} g_\delta^{-1} \cdot \left((g_\delta \cdot \mathcal{M}^+_{short}) \bigcap (\mathcal{M}_{19,2} \bigcup \mathcal{M}_{19,7} \bigcup \mathcal{M}_{19,13}) \right),$$

which proves the lemma. This proof by picture can be made formal by computing the exact arrangement of the involved domains, whose boundaries are made of arcs of circles and line segments. The details are provided in Appendix A.

From Lemma 11 we can construct a universal triangulation for short tori. Indeed, all the diplotori with fixed parameters n, d have the same abstract triangulation, that we denote by $\mathcal{T}_{n,d}$. Hence, we just need a common subdivision of $\mathcal{T}_{19,2}, \mathcal{T}_{19,7}$ and $\mathcal{T}_{19,13}$ to obtain such a universal triangulation. In fact, we can replace $\mathcal{T}_{19,13}$ by $\mathcal{T}_{19,6}$ in the overlay. Indeed, considering the symmetric of a diplotorus with respect to a horizontal plane, we easily deduce the existence of an orientation reversing isomorphism between $\mathcal{T}_{n,d}$ and $\mathcal{T}_{n,n-d}$. It is thus enough to compute a common refinement of $\mathcal{T}_{19,2}, \mathcal{T}_{19,7}$ and
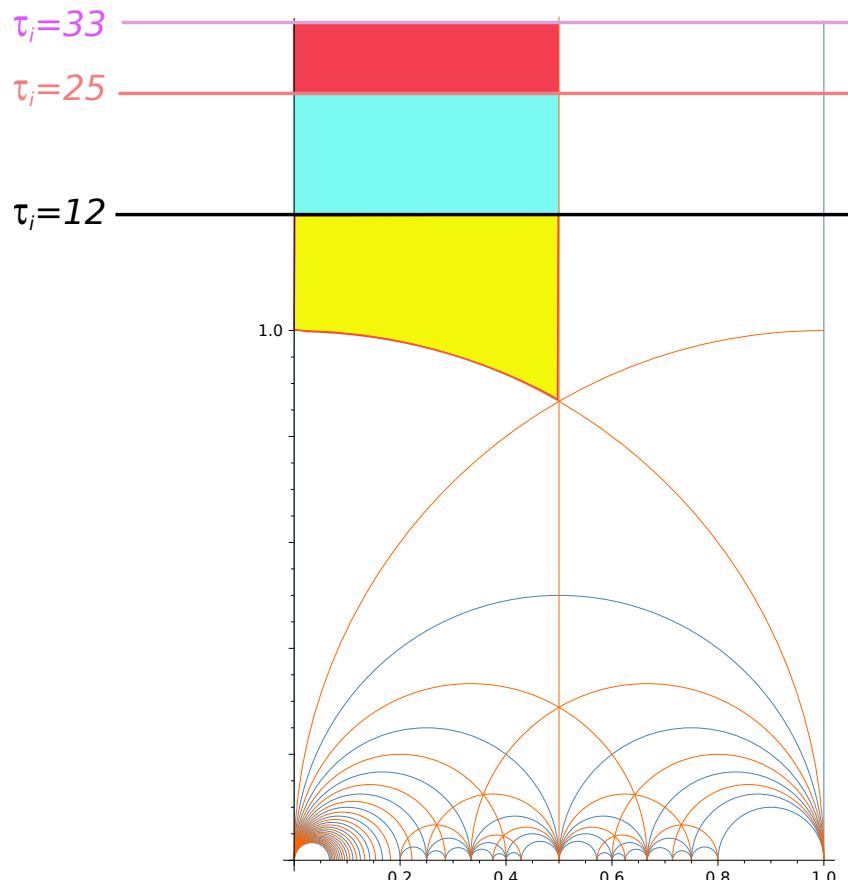
Figure 46: A slicing of $\mathcal{M}_{short}^{+}$ (not to scale) in three regions (yellow, blue and red) bounded by the horocycles $\tau_i = 33, 25, 12$ (respectively in purple, orange and black) and the (truncated) hyperbolic tesselation associated to the modular group.
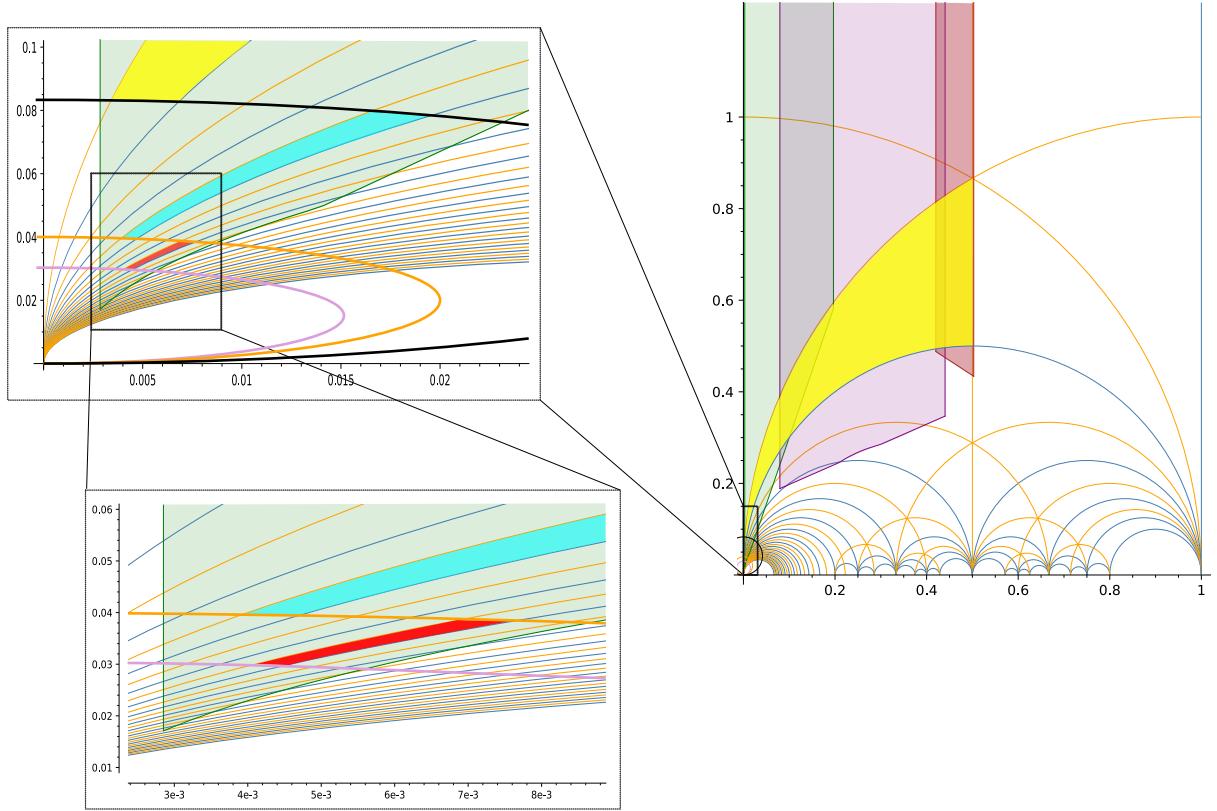
Figure 47: The three regions in red, blue and yellow are images of the corresponding slices in $\mathcal{M}^+_{short}$ by g_1, g_3, g_5, respectively.

$\mathcal{T}_{19,6}$ to obtain a universal triangulation for short flat tori. These three triangulations are obtained by identifying the boundaries of a same triangulated cylinder. However, they are not isomorphic, as one needs to apply distinct circular shifts before identification. We can nonetheless send them in a *same* torus as follows. For $k \in \mathbb{Z}$, consider the points

$$A_k = (k, -1), \quad B_k = (k, 0), \quad C_k = (k, 1)$$

in the infinite plane strip $\mathcal{B} := \mathbb{R} \times [-1, 1]$. Then $\mathcal{T}_{19,d}$ is isomorphic to the triangulation of $\mathcal{B}$ by the triangles $\{A_k A_{k+1} B_k, B_k A_{k+1} B_{k+1}, C_k C_{k+1} B_{k-d}, B_{k-d} C_{k+1} B_{k+1-d}\}_{k \in \mathbb{Z}}$ quotiented by the horizontal translations generated by the vector $(19, 0)$, further identifying the two boundaries according to the vertical translation $(0, 2)$. This quotient and identification being independent of d, the three triangulations for $d = 2, 6, 7$ are indeed embedded in a same torus, see Figure 44.

We overlay the three triangulated strips obtained for $d = 2, 6, 7$. We want to count the number of vertices of the resulting subdivision. We only have to care about the edges $B_k C_\ell$, the other ones being common to the three triangulations. The strip $\mathcal{B}$ being 1-periodic in the horizontal direction, it is sufficient to consider the number of intersections with the other edges of the 5 edges $B_0 C_k$ for $k \in I := \{2, 3, 6, 7, 8\}$. The edges $B_0 C_k$ and $B\ell C_{\ell+j}, j \in I$, intersect in their interior if and only if

- $\ell < 0$ and $\ell + j > k$, or equivalently $k - j < \ell < 0$, or

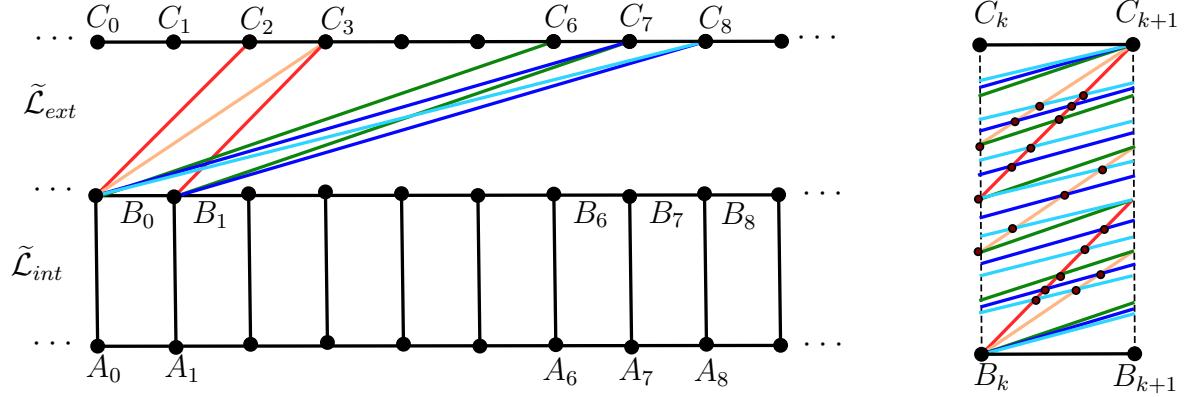- $\ell > 0$ and $\ell + j < k$, or equivalently $0 < \ell < k - j$.

89

Figure 48: Layout of the triangulations $\mathcal{T}_{19,2}, \mathcal{T}_{19,6}$ and $\mathcal{T}_{19,7}$. Left, the two sub-strips $\widetilde{L}_{int}$ and $\widetilde{L}_{ext}$ correspond to the (lift of the) overlay of the internal and external ploids. Right, a period of $\widetilde{L}_{ext}$ contains 20 intersection points from the overlay of the external ploids.

In this case, we compute $p_{\ell,j}^k := B_0 C_k \bigcap B_\ell C_{\ell+j} = \frac{\ell}{k-j}(k,1)$. All other intersection points are horizontal translates of the $p_{\ell,j}^k$ by an integral amount. The set of intersection points with x-coordinate in $[0,1)$ is thus given by $\left\{ \left(\mathrm{frac}\left(\frac{\ell k}{k-j}, \frac{\ell}{k-j}\right)\right)\right\}_{j,k,\ell}$ where j, k, ℓ vary as above and $\mathrm{frac}(x)$ is the fractional part of x. Eliminating the duplicates, we found 20 intersections leading to $n \times 20 = 380$ intersection points in total. See Figure 48. Adding the remaining points A_k, B_k (C_k and A_k should be identified) we find a total of $380 + 38 = 418$ vertices. It remains to triangulate the subdivision by adding diagonals in the non triangular faces. By Euler's formula on the torus, we conclude that the triangulated overlay has 836 triangles. We have thus proved

Proposition 12. *There exists an abstract triangulation with 836 triangles, which admits linear embeddings isometric to every short flat torus.*

5.3 Merging long and short flat tori

It remains to overlay our universal triangulations for long and short tori to obtain a universal triangulation for all flat tori. Before overlying the layouts of Figures 43 and 48, we perform some modifications. We first remove the diagonals introduced to triangulate the rectangular faces of the bends are they are not necessary to define the PL isometric embeddings of long tori. For the same reason, we remove the diagonals used to triangulate the three portions of right prisms. Compare Figure 43 and top Figure 49. Denote by $\mathcal{L}_{long}$ the resulting layout. It is composed of three horizontal strips, where the top one has no internal vertex. $\mathcal{L}_{long}$ also divides into 33 vertical bands corresponding to 9 bends (each made of two bands), 12 gaskets and 3 portions of right prisms. We squeeze the last 15 bands to the width of a single one. We now view $\mathcal{L}_{long}$ as composed of 19 bands of equal length, where the last one contains the 15 squeezed bands. See middle Figure 49. Denote by H the common height of the three horizontal strips of $\mathcal{L}_{long}$. We next consider the layout of the short tori, call it $\mathcal{L}_{short}$. It decomposes into two horizontal strips $\mathcal{L}_{int} \bigcup \mathcal{L}_{ext}$ corresponding to the internal and external ploids; compare Figure 48 with bottom of Figure 49. The bottom strip $\mathcal{L}_{int}$ decomposes into 19 vertical bands that we align with
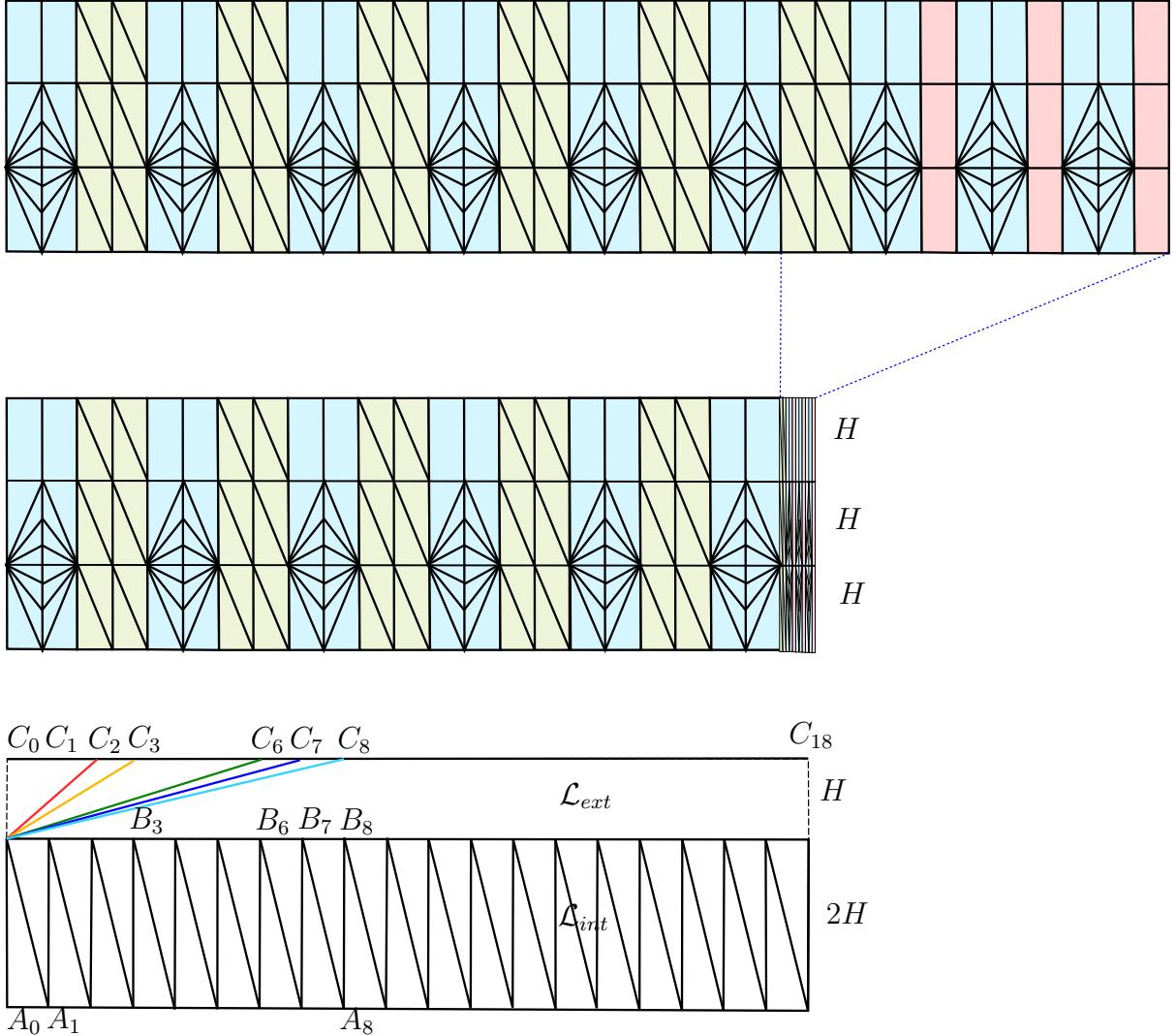
Figure 49: Modified layout of the universal triangulations for long and short flat tori.

the ones of $\mathcal{L}_{long}$. We also stretch $\mathcal{L}_{int}$ and $\mathcal{L}_{ext}$ vertically so that their heights becomes respectively $2H$ and H. We are now ready to overlay $\mathcal{L}_{short}$ and $\mathcal{L}_{long}$ as shown at the bottom of Figure 49. Note that the (universal) subdivisions for short and long flat tori are obtained from the corresponding layouts by applying the *same* identifications of their horizontal and vertical sides. Applying these identifications to the overlay of the layouts thus provides a common refinement of the subdivisions for short and long flat tori.

To enumerate the vertices of the overlay we consider adding the edges of $\mathcal{L}_{short}$ to the layout of $\mathcal{L}_{long}$. The horizontal and vertical edges of $\mathcal{L}_{short}$ can be mapped to the corresponding edges of $\mathcal{L}_{long}$ without introducing new vertices. Note that the three horizontal edges in the last band of $\mathcal{L}_{short}$ are each subdivided into 15 edges. The diagonals of $\mathcal{L}_{int}$ are inserted as follows. Among the 18 first diagonals, the ones inserted in a band corresponding to a bend in $\mathcal{L}_{long}$ introduce 6 crossings each, while the ones inserted in a band corresponding to a gasket introduce 1 crossing each. See bottom left of Figure 50. This introduces $6E_b + E_g$ vertices in total, where $E_b = 10$ and $E_g = 8$ are the respective numbers of bands of type bend and gasket. After subdivision, the 19th diagonal can be

inserted without introducing any vertex as shown at the bottom of Figure 50. Apart from their own intersections, the slanted edges of $\mathcal{L}_{int}$ cross the vertical and diagonal edges in the upper strip of $\mathcal{L}_{long}$. We deform these edges in the 18 first bands in order to minimize the number of new crossings . See the top part of Figure 50. This way, the slanted edges of $\mathcal{L}_{int}$ introduce 2 crossings per vertical edge and 16 crossings per diagonal of $\mathcal{L}_{long}$. In total, this leads to $2E_v + 16E_d$ crossings, where $E_v = 19$ and $E_d = 8$ stand for the respective numbers of verticals and diagonals in the 18 first bands of the upper strip. Finally, each vertical or diagonal in the interior of the squeezed part of $\mathcal{L}_{long}$ crosses all the slanted edges $B_l C_{l+j}$ of $\mathcal{L}_{int}$ that surround its extremities. Since the considered verticals and diagonals are squeezed in the interior of a band of width 1, this leads to $\sum_{j \in I} j = 26$ crossings each. In total, we thus get $26(E'_v + E'_d)$ crossings in the squeezed part, where $E'_v = 14$ and $E'_d = 4$ denote the respective numbers of vertical and diagonal edges. To sum up, the overlay contains

- $V_{long} = 270/2 = 135$ vertices from $\mathcal{L}_{long}$ as counted in Proposition 6,

- $V_\cap = 380$ vertices from the intersecting edges in $\mathcal{L}_{short}$ as computed in the proof of Proposition 12,

- $6E_b + E_g = 68$ vertices from the overlay of diagonals of $\mathcal{L}_{int}$ with $\mathcal{L}_{long}$,

- $2E_v + 16E_d = 166$ vertices from the overlay of the slanted edges of $\mathcal{L}_{ext}$ with the 18 first bands of $\mathcal{L}_{long}$,

- $26(E'_v + E'_d) = 468$ vertices from the overlay of the slanted edges of $\mathcal{L}_{ext}$ with squeezed part of $\mathcal{L}_{long}$.

In total the overlay thus contains

$$V_{long} + V_\cap + 6E_b + E_g + 2E_v + 16E_d + 26(E'_v + E'_d) = 135 + 380 + 68 + 166 + 468 = 1217$$

vertices. By Euler's formula this corresponds, after adding diagonals to triangulate the overlay, to 2434 triangles. this ends the proof of Theorem 5.
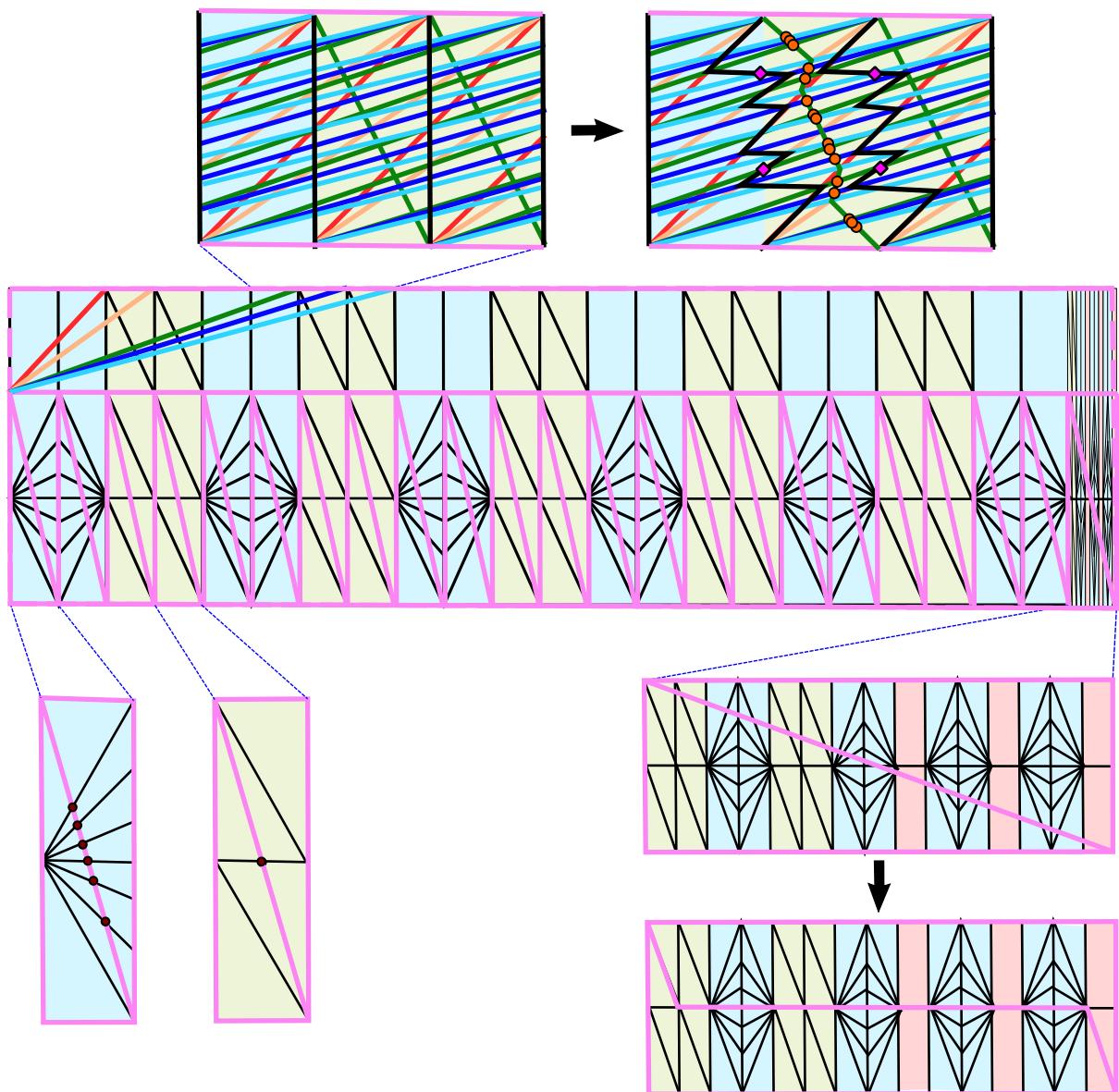
Figure 50: Overlay of the universal triangulations for long and flat tori.

Chapter 6

Realization of surfaces in $\mathcal{H}(2)$ and $\mathcal{H}(1,1)$

Résumé en français. L'existence d'une triangulation universelle pour les tores plats suggère l'existence de telles triangulations pour d'autres familles de surfaces. Nous avons vu, en genre 0, que l'existence de triangulations universelles pour les surfaces dont le nombre et le type des singularités sont fixés est une conséquence du théorème d'Alexandrov. Fort de ces résultats positifs en genre $g = 0$ et $g = 1$, nous nous intéressons au cas du genre $g = 2$. Nous nous concentrons dans ce chapitre sur les surfaces de translation de genre 2, et plus particulièrement sur la strate $\mathcal{H}(2)$, bien que nos modèles admettent des généralisations naturelles pour $\mathcal{H}(1,1)$ que nous évoquons succinctement. Bien que nos résultats ne permettent pas de conclure quant à l'existence d'une triangulation universelle pour $\mathcal{H}(2)$, nos modèles permettent de réaliser un ouvert assez important de $\mathcal{H}(2)$: un voisinage ouvert de la famille des surfaces de $\mathcal{H}(2)$ admettant une décomposition en L avec un parallèlogramme central rectangulaire et des parallélogramme périphérique dont la hauteur relative est assez importante. Ces modèles sont relativement simples et peuvent être utilisés à des fins de visualisation - réalisables par impression 3D ou pliage papier. L'idée est de réaliser la surface en deux temps. Tout d'abord, nous réalisons le parallélogramme central dans $\mathbb{R}^3$ en une sphère centrale PL admettant 4 bords triangulaires. Les parallélogrammes périphériques pouvant quant à eux être réalisés grâce aux travaux de Zalgaller sur les plongements de longs prismes droits. Ceci nous permet de réaliser la surface en entier : il suffit de recoller les prismes droits courbés et tordus, correspondant aux parallélogrammes périphériques, à la sphère centrale tout en prenant garde à ne pas introduire d'intersection.

In this chapter we present a family of relatively simple PL isometric embeddings of surfaces in $\mathcal{H}(2)$, whereas the author is not aware of a previous related work. While this family covers a hypersurface in $\mathcal{H}(2)$, our PL isometric embeddings underlie a single triangulation valid for all the elements in the family. We even succeeded in realizing an open neighborhood in $\mathcal{H}(2)$. Moreover, we manage to extend our method to embed surfaces in $\mathcal{H}(1,1)$.

Denote $\tau = a/b$ the ratio of the length longest side of the central parallelogram by the length of its smallest side. While we give a proof of the fact that our constructions are isometric embeddings in the rectangular case where the ratio τ is less than $\sqrt{3}$, we do not present a proof in the case $\tau \geq \sqrt{3}$ or in the more general skew case. Demonstrations of the embedding property are computationally intensive in the latter case, and do not appear in this document.

6.1   Result and idea of our approach

Recall that every surfaces in $\mathcal{H}(2)$ can be obtained from a gluing of parallel edges of a polygon with a L shape formed by three parallelograms as explained in Section 2.7.3, see Figure 51. In this decomposition, the central parallelogram gets its vertices identified by the gluing forming a central sphere with four boundary components joining at the singularity. Along these boundaries one should glue the two cylinders corresponding to the peripheral parallelograms of the L. To do so, we first restrict to a subspace of $\mathcal{H}(2)$ corresponding to the case where the central parallelogram is a rectangle. We describe a universal triangulation for this case, relying on Zalgaller's machinery described in Section 3.3, assuming that the peripheral parallelograms are long enough. We then extend our realization space to an open neighborhood of this subspace, thus covering a full dimensional part in $\mathcal{H}(2)$.

In the following, by a **geometric realization** of a simplicial complex K in $\mathbb{R}^3$, we mean an embedding $|K| \hookrightarrow \mathbb{R}^3$ whose restriction to any face is affine. The **relative height** of a right cylinder is the quotient of its height by its perimeter. We finally denote by $\mathcal{L}^{rect}_{\geq h}$ the subset of moduli in $\mathcal{H}(2)$ that admit an L decomposition whose central parallelogram is a rectangle and whose peripheral cylinders have relative height at least h. The following will be devoted to prove the following theorem.

Theorem 13. *There exists a triangulation $\mathcal{T}$ of the closed orientable surface of genus 2, a constant $h > 0$ and on open neighborhood $\mathcal{O} \subset \mathcal{H}(2)$ of $\mathcal{L}^{rect}_{\geq h}$, such that for each element $\sigma \in \mathcal{O}$ the triangulation $\mathcal{T}$ admits a geometric realization in $\mathbb{R}^3$ that is isometric to σ.*

In our geometric realizations of moduli in $\mathcal{L}^{rect}_{\geq h}$, each of the four boundaries of the central sphere is embedded as an equilateral triangle. This enables us to apply the building blocks developed by Zalgaller to connect each pair of opposite boundaries with a triangular prism, bended and twisted appropriately. The prisms, corresponding to geometric realizations of the peripheral parallelogram of the surface in L, must be long enough for this last construction to be feasible. Another relevant parameter of this construction is the **aspect ratio** $a/b \geq 1$ of a rectangle with long and short sides of respective lengths $3a$ and $3b$. When the central parallelogram is a rectangle, we consider two cases according to whether its aspect ratio τ is smaller or larger that $\sqrt{3}$
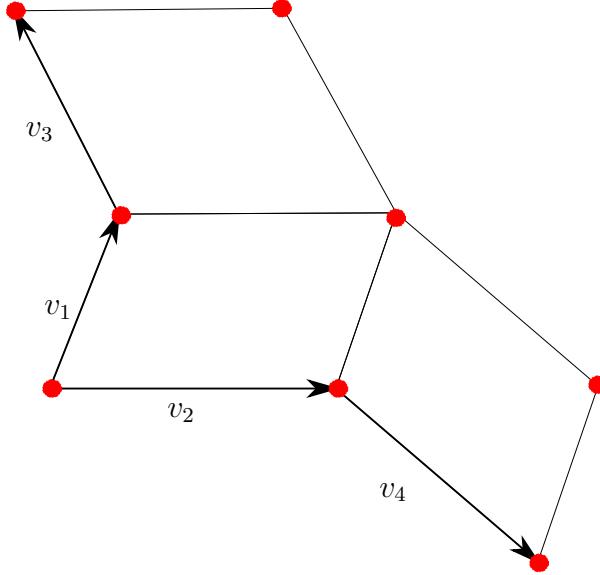
Figure 51: Standard L-decomposition of a surface of $\mathcal{H}(2)$ in three parallelograms (singularity in red). The one spanned by (v_1, v_2) is called the **central parallelogram**, while the other two are called **peripheral parallelograms**.

- In the case $\tau < \sqrt{3}$, which includes the square case, the semi-infinite prisms based at the four triangular boundaries of the central sphere are disjoint, allowing the peripheral parallelogram to be glued easily by bending.

- In the case $\tau \geq \sqrt{3}$, we need to be careful as the two semi-infinite prisms with smaller cross-section intersect. In order to prevent intersection of the corresponding glued cylinder, we rotate these two prisms and deform partly the central sphere by performing some bending at the level of their attaching boundaries using a construction reminiscent of Zalgaller's bending procedure.

The above constructions enable to cover $\mathcal{L}^{rect}_{\geq h}$, a sub-region of $\mathcal{H}(2)$ of real codimension 1, or real dimension 7. Indeed, apart from the fact that the peripheral parallelograms must be long enough, the only constraint of our construction is the rectangular shape of the central sphere. This amounts to fix one angle parameter of the L decomposition, whence the dimension. We show how to slightly modify the constructions in order to realize central parallelograms that are almost rectangular (i.e. with internal angles close to the right angle). Incidentally, by gluing each peripheral cylinder to *successive* triangular boundaries of the central sphere rather than to opposite boundaries, we obtain a realization of a flat surface of genus 2 with one singularity of conical angle 6π which is not a translation surface.

6.2 Embedding of the central parallelogram of a surface in $\mathcal{H}(2)$

As previously mentioned, we first embed the central sphere of a surface in L to be able to attach the two handles formed by the peripheral parallelograms. In this section, we

describe, how to do so in the case where the central parallelogram is a square, a rectangle, or a skew parallelogram close to be right.

6.2.1 Square case

When the central parallelogram is a square, we triangulate it as in Figure 52. The resulting triangulation is denoted by $\mathcal{T}$ and we name its vertices $S_0, ..., S_3, Q_0, ..., Q_3, P_0, ..., P_7$ as on Figure 52. Note that each side of the central square is cut into three equal parts whose length is denoted by a. We then define a map f, linear on each face of $\mathcal{T}$, which is an isometric embedding of the central sphere. By linearity, we can just define f on the vertices of $\mathcal{T}$. Our construction admits a rotational symmetry of order 4 about the z-axis, and a symmetry by reflexion across the xz-plane. More precisely let

- r be the rotation of $\mathbb{R}^2$ of angle $\pi/2$ about the origin O,

- s_x be the reflexion across the x-axis in $\mathbb{R}^2$,

- ρ be the rotation of angle $\pi/2$ about the z-axis in $\mathbb{R}^3$, and

- σ_{xz} be the reflexion across the xz-plane in $\mathbb{R}^3$.

The map f then satisfies:

$$f \circ r = \rho \circ f \quad \text{and} \quad f \circ s_x = \sigma_{xz} \circ f.$$

It thus suffices to specify the images of Q_0, S_0, P_0 and O in order to define f. Since S_0, S_1, S_2, S_3 are mapped to the same point by the identification of the L shape boundary, their common image must lie on the z-axis by rotational symmetry. We choose to place $f(S_0)$ at the origin Ω of $\mathbb{R}^3$. Note that, by the same rotational symmetry, the images of the five vertices S_0, Q_0, Q_1, Q_2, Q_3 form a pyramid with apex $f(S_0) = \Omega$ and horizontal square basis. The height of the pyramid must be $\sqrt{|Q_0 S_0|^2 - |OQ_0|^2} = a\sqrt{\frac{3}{2}}$ since f should preserve edge lengths. For the same reason, O must be sent to the center of the pyramid basis and the distance from $f(Q_0)$ to the z-axis is $|OQ_0| = \frac{a}{\sqrt{2}}$. It follows that $f(Q_0)$ lies on the horizontal circle of radius $\frac{a}{\sqrt{2}}$ with center $\left(0, 0, \sqrt{\frac{3}{2}}a\right)$. We choose $f(O) = \left(0, 0, -\sqrt{\frac{3}{2}}\right)$ and $f(Q_0) = \left(\frac{a}{2}, \frac{a}{2}, -\sqrt{\frac{3}{2}}a\right)$ so that the sides of the basis are aligned with the x and y-axes.

It remains to determine the coordinates of $f(P_0)$. For convenience, we denote X' the image $f(X)$ of a point X. Since f should be isometric, we must have $|S_0' P_0'| = |S_0 P_0| = a$, so that the spherical coordinates of P_0' are (a, θ, φ) for some angles θ and φ, meaning that P_0' has Cartesian coordinates $(a\cos\theta\cos\varphi, a\cos\theta\sin\varphi, a\sin\theta)$. By symmetry, we have that $P_7' = f(s_x(P_0)) = \sigma_{xz}(P_0')$ has spherical coordinates $(a, \theta, -\varphi)$. Moreover, the equations $|P_0' P_7'| = |P_0 P_7| = a$ and $|P_0' Q_0'| = |P_0 Q_0| = a$ lead to Equations (6.1) and (6.2) below.

$$\sin\varphi = \frac{1}{2\cos\theta}(\text{assuming } \varphi \in [0, \pi/2] \text{ and } \cos\theta > 0), \tag{6.1}$$

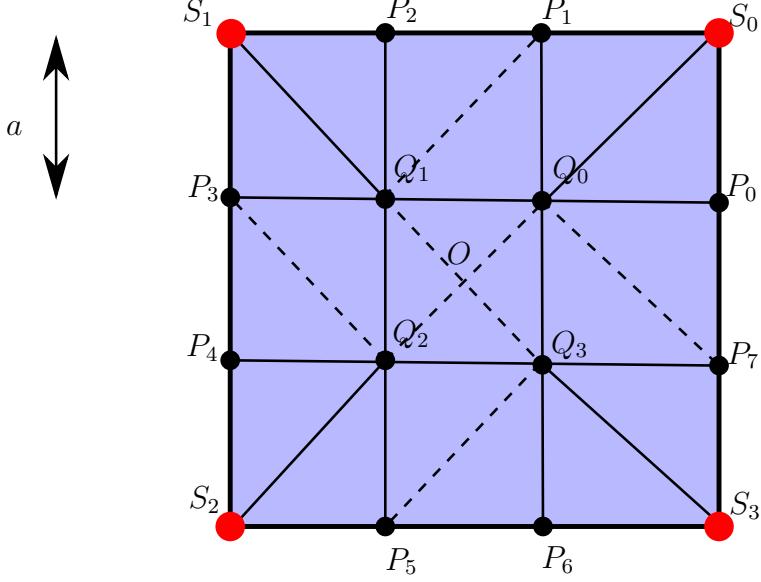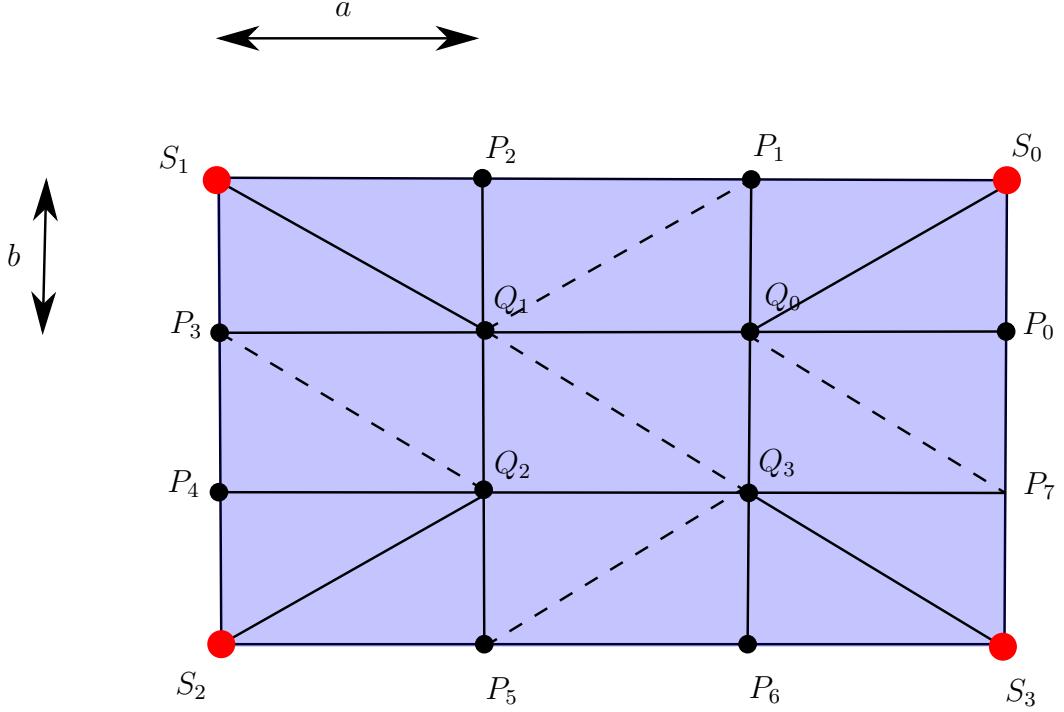$$\frac{3}{2} - \sqrt{\cos^2\theta - \frac{1}{4}} + \sqrt{6}\sin\theta = 0. \tag{6.2}$$

Figure 52: Triangulation of the central square. Dashed segments indicate coplanarity of the underlying squares in our embeddings.

Indeed, we compute $\overrightarrow{P'_0 P'_7} = (0, 2a\cos\theta\sin\varphi, 0)$, hence $|P'_0 P'_7|^2 = a^2$ is equivalent to (6.1).

For the second equality, we compute $\overrightarrow{P'_0 Q'_0} = a\left(\cos\theta\cos\varphi - \frac{1}{2}, \cos\theta\sin\varphi - \frac{1}{2}, \sin\theta + \sqrt{\frac{3}{2}}\right)$. Using simple trigonometric equalities and Equation (6.1) allows to infer Equation (6.2).

The second equation solves to

$$\sin\theta = -\frac{1}{7}\sqrt{\frac{33}{2} - 9\sqrt{2}} = \left(1 - \frac{3}{\sqrt{2}}\right)\frac{\sqrt{3}}{7}.$$

Together with (6.1), this allows us to determine the coordinates of P'_0. To summarize the above discussion, we set:

$$S'_0 = \Omega \text{ the origin of } \mathbb{R}^3,$$

$$O' = \left(0, 0, -\sqrt{\frac{3}{2}}a\right),$$

$$Q'_0 = \left(\frac{a}{2}, \frac{a}{2}, -\sqrt{\frac{3}{2}}a\right), \tag{C}$$

$$P'_0 = \left(\frac{3a}{7}\sqrt{\frac{9}{4} - \sqrt{2}}, \frac{a}{2}, \left(1 - \frac{3}{\sqrt{2}}\right)\frac{\sqrt{3}}{7}a\right).$$

6.2.2 Rectangle case

Let $3a, 3b$ denote the length of the sides of the central rectangle, with $a > b$. Analogously to the construction in the square case, we describe a map f linear on each triangle of the triangulation of the central rectangle depicted in Figure 53. It is thus enough to define

Figure 53: Triangulation of the central rectangle. Dashed segments indicate coplanarity of the underlying rectangular face in our embeddings.

f on the vertices of this triangulation. Our construction admits symmetry by reflexion across the xz-plane and the yz-plane. More precisely, denote by s_y the reflexion of $\mathbb{R}^2$ through the y-axis and by σ_{yz} the reflexion of $\mathbb{R}^3$ through the yz-plane and recall the definition of $r, s_x, \rho, \sigma_{xz}$ from the previous section. Then the map f satisfies:

$$f \circ s_x = \sigma_{xz} \circ f \quad \text{and} \quad f \circ s_y = \sigma_{yz} \circ f.$$

Since $r^2 = s_y \circ s_x$ and $\rho^2 = \sigma_{yz} \circ \sigma_{xz}$, the set of vertices also admits a rotational symmetry of order two about the z-axis. It is enough, to specify the images of S_0, Q_0, P_0 and P_1 to define f. By symmetry, S_0 is sent to the z axis and we choose $f(S_0) = \Omega$, the origin of $\mathbb{R}^3$. Also by symmetry, the images of the five vertices S_0, Q_0, Q_1, Q_2, Q_3 form a pyramid of apex S_0 with horizontal rectangular basis aligned with the x and y coordinates axes. Setting $\delta = \sqrt{a^2 + b^2}$, the height of the pyramid must be $\frac{\sqrt{3}}{2}\delta$ as f should preserve edge lengths. Moreover, the distance from $f(Q_0)$ to the z-axis must be half the length of the diagonal $Q_0 Q_2$, that is $\delta/2$. So $f(Q_0)$ lies on the horizontal circle of radius $\frac{\delta}{2}$ with center $\left(0, 0, -\frac{\sqrt{3}}{2}\delta\right)$ - we choose this center to lie below the xy-plane. Since the rectangular base $f(Q_0)f(Q_1)f(Q_2)f(Q_3)$ is aligned with the x and y axes in $\mathbb{R}^3$, each $f(Q_i)$ has coordinate $\left(\pm\frac{a}{2}, \pm\frac{b}{2}, -\frac{\sqrt{3}}{2}\delta\right)$. We choose $f(Q_0) = \left(\frac{a}{2}, \frac{b}{2}, -\frac{\sqrt{3}}{2}\delta\right)$.

It remains to determine the coordinates of $f(P_0)$ and $f(P_1)$. As previously, we write X' for $f(X)$. Since $|S_0'P_0'| = |S_0 P_0| = a$ and $|S_0'P_1'| = |S_0 P_1| = b$, the spherical coordinates of P_0' are (a, θ_0, φ_0) and those of P_1' are $\left(b, \theta_1, \frac{\pi}{2} - \varphi_1\right)$ for some angles $\theta_0, \varphi_0, \theta_1, \varphi_1$ (for symmetry reasons we write $\frac{\pi}{2} - \varphi_1$ for the azimuthal angle of P_1'). By symmetry, we must have that $P_7' = f(s_x(P_0)) = \sigma_{xz}(P_0')$ has spherical coordinates $(a, \theta_0, -\varphi_0)$ and that

99

$P_2' = f(s_y(P_1)) = \sigma_{yz}(P_1')$ has spherical coordinates $\left(b, \theta_1, \frac{\pi}{2} + \varphi_1\right)$. Finally, the constraints $|P_0'P_7'| = |P_0P_7| = b$ and $|P_1'P_2'| = |P_1P_2| = a$ lead to Equations (6.3) below while the equalities $|P_0'Q_0'| = |P_0Q_0| = a$ and $|P_1'Q_0'| = |P_1Q_0| = b$ lead to Equations (6.4) and (6.5) respectively.

To summarize the previous discussion, we set:

- $S_0' = \Omega$ the origin of $\mathbb{R}^3$,

- $Q_0' = \left(\frac{a}{2}, \frac{b}{2}, -\frac{\sqrt{3}}{2}\delta\right)$, where $\delta = \sqrt{a^2 + b^2}$,

- $P_0' = b(\cos\theta_0 \cos\varphi_0, \cos\theta_0 \sin\varphi_0, \sin\theta_0) = b\left(\cos\theta_0 \cos\varphi_0, \frac{1}{2}, \sin\theta_0\right)$,

- $P_1' = a(\cos\theta_1 \sin\varphi_1, \cos\theta_1 \cos\varphi_1, \sin\theta_1) = a\left(\frac{1}{2}, \cos\theta_1 \cos\varphi_1, \sin\theta_1\right)$,

where $\theta_0, \varphi_0, \theta_1$ and φ_1 satisfy Equations (6.3), (6.4) and (6.5) below (assuming $\varphi_i \in \left[0, \frac{\pi}{2}\right]$ and $\cos\theta_i > 0$).

$$\sin\varphi_i = \frac{1}{2\cos\theta_i}, \quad i \in \{0, 1\}, \tag{6.3}$$

$$\frac{3}{2}b + \sqrt{3}\delta\sin\theta_0 - a\sqrt{\cos^2\theta_0 - \frac{1}{4}} = 0, \tag{6.4}$$

$$\frac{3}{2}a + \sqrt{3}\delta\sin\theta_1 - b\sqrt{\cos^2\theta_1 - \frac{1}{4}} = 0. \tag{6.5}$$

Indeed, Equation (6.3) is obtained by a computation similar to the square case. For Equation (6.4), we compute $\overrightarrow{P_0'Q_0'} = \left(b\cos\theta_0\cos\varphi_0 - \frac{\delta}{2}\cos\frac{\alpha}{2}, b\cos\theta_0\sin\varphi_0 - \frac{\delta}{2}\sin\frac{\alpha}{2}, b\sin\theta_0 + \frac{\sqrt{3}}{2}\delta\right)$. Using simple trigonometric equalities, and Equation (6.3) as in the square case, Equation (6.4) follows. Similar computations permit to deduce Equation (6.5).

Setting $\tau = a/b$, the last two previous equations solve to

$$\sin\theta_0 = \frac{\sqrt{3}}{2}\frac{2a^2 - 3b\delta}{4a^2 + 3b^2} = \frac{\sqrt{3}}{2}\frac{2\tau^2 - 3\sqrt{1 + \tau^2}}{3 + 4\tau^2} \tag{6.6}$$

and

$$\sin\theta_1 = \frac{\sqrt{3}}{2}\frac{2b^2 - 3a\delta}{3a^2 + 4b^2} = \frac{\sqrt{3}}{2}\frac{2 - 3\tau\sqrt{1 + \tau^2}}{4 + 3\tau^2}. \tag{6.7}$$

By the symmetry of our construction, we infer

$$P_3' = \sigma_{yz}(P_0') = b\left(-\cos\theta_0 \cos\varphi_0, \frac{1}{2}, \sin\theta_0\right) \tag{6.8}$$

$$P_4' = \sigma_{xz}(P_3') = b\left(-\cos\theta_0 \cos\varphi_0, -\frac{1}{2}, \sin\theta_0\right) \tag{6.9}$$

$$P_7' = \sigma_{xz}(P_0') = b\left(\cos\theta_0 \cos\varphi_0, -\frac{1}{2}, \sin\theta_0\right) \tag{6.10}$$

and

$$P_2' = \sigma_{yz}(P_1') = a\left(-\frac{1}{2}, \cos\theta_1\cos\varphi_1, \sin\theta_1\right) \tag{6.11}$$

$$P_5' = \sigma_{xz}(P_2') = a\left(-\frac{1}{2}, -\cos\theta_1\cos\varphi_1, \sin\theta_1\right) \tag{6.12}$$

$$P_6' = \sigma_{xz}(P_1') = a\left(\frac{1}{2}, -\cos\theta_1\cos\varphi_1, \sin\theta_1\right) \tag{6.13}$$

6.2.3 Skew case

In this section, we extend the previous realization of the central parallelogram in the non rectangular case. In fact, it appears that the previous construction is not rigid and admits small deformations. Let $\theta \in (0, \pi)$ denote the angle in the bottom left corner of the central parallelogram rotated so that its longest side is aligned with the horizontal axis. Refer to Figure 54. Denote, as previously, $\tau = a/b$ the ratio of the length of the longest side of the parallelogram by the length of the shortest one. For a given τ, we are able to deform the triangulation of Figure 53 so that for every θ sufficiently close to $\pi/2$ (where sufficiently close depends on τ) the corresponding triangulation of the central sphere admits a linear isometric embedding. Actually, the previous construction in the rectangular case can be seen as the limit (when θ tends towards $\frac{\pi}{2}$) of the construction described in the present section.

Triangulation of the central parallelogram. The decomposition into polygons of the central parallelogram in $\mathbb{R}^2$ is combinatorially identical while it differs slightly from the previous rectangle case in its geometry.

We assume that the longest side of the parallelogram is aligned with the horizontal axis. Let $3a$ denotes the length of the longest side of the parallelogram, $3b$ the length of its shortest side, and $\theta \in (0, \pi)$ the angle in the bottom left corner. Refer to Figure 54. Without loss of generality, we can suppose $\theta < \frac{\pi}{2}$: if not, we can apply a vertical reflexion to the entire triangulation to ensure this condition. Divide in three each side of the parallelogram introducing this way the points P_i for $0 \leq i \leq 7$. Then draw the horizontal segments P_0P_3 and P_7P_4. Now define Q_0 as the intersection of the vertical line through P_1 and the horizontal segment P_0P_3. Similarly, define

- Q_1 as the intersection of the vertical line through P_2 and P_0P_3,

- Q_2 as the intersection of the vertical line through P_5 and the segment P_4P_7,

- and Q_3 as the intersection of the vertical through P_6 and P_4P_7.

All the vertices of the triangulation are now introduced, and it remains to link them with edges as in Figure 53 or 54

Iterative construction of the images of the vertices. We define the images of the vertices iteratively. First, we send the four points S_0, S_1, S_2, S_3 corresponding to the singularity to the origin Ω of $\mathbb{R}^3$. Then, noticing that the image of $S_1Q_1Q_3S_3$ is a triangle, we choose to realize this triangle in the Oxz plane of $\mathbb{R}^3$ with the image of Q_1Q_3 horizontal.
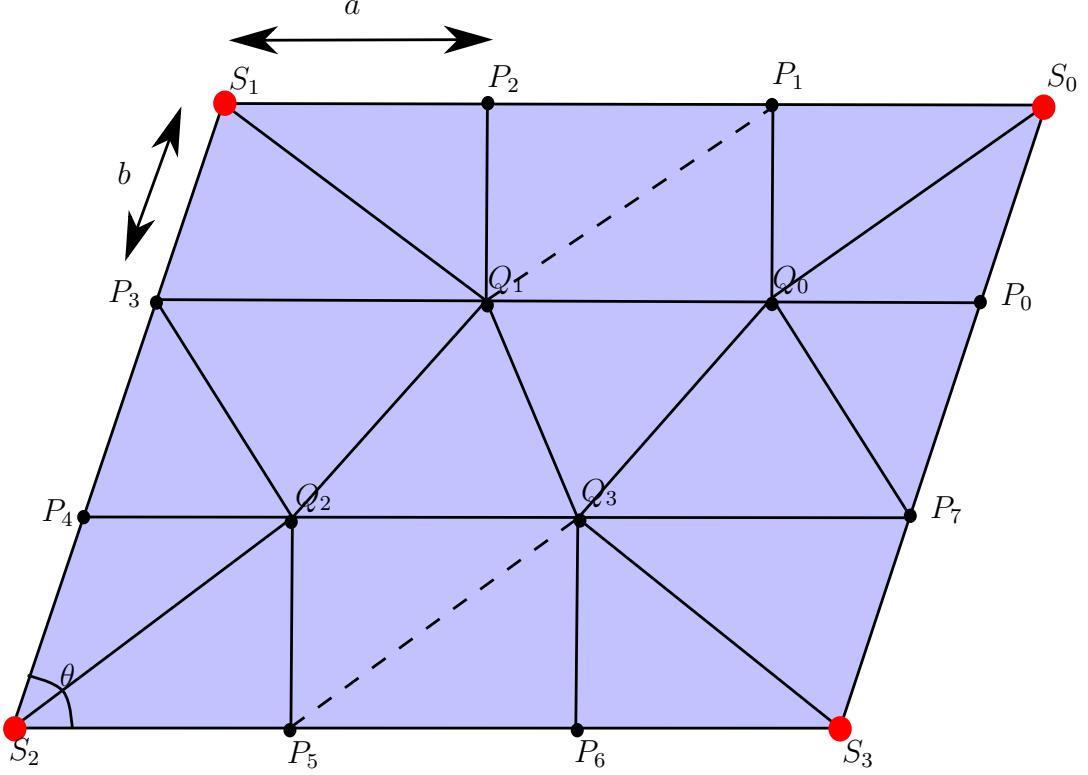
Figure 54: Triangulation of a skew central parallelogram.

This determines entirely the images of Q_1 and Q_3. We next construct the images of Q_0 and Q_2. As there is an edge from each $Q_i, i = 0, 2$, to Q_1, Q_3 and S_j, we have 3 distances that determines Q_i as the intersection of 3 spheres centered at Q_1, Q_3 and one of the S_j. Of course, the spheres have to intersect for the images of Q_0 and Q_2 to be well defined, and there is a choice to do as three spheres may intersect in several points, and generically intersect in two points. In fact, unless the three sphere centers are aligned, the spheres may only be disjoint or only have two intersection points. In the latter case, let us denote by $\iota(X_1, \rho_1, X_2, \rho_2, X_3, \rho_3, \varepsilon)$ - for $X_1, X_2, X_3 \in \mathbb{R}^3$, $\rho_1, \rho_2, \rho_3 > 0$ and $\varepsilon = \pm 1$ - the point at distance ρ_i from X_i, for $i = 1, 2, 3$, which lies in the half-space delimited by the plane $(X_1 X_2 X_3)$ towards the direction given by $\varepsilon \overrightarrow{X_1 X_2} \wedge \overrightarrow{X_1 X_3}$. For conciseness, we will drop the radii arguments of ι, as they can be deduced from the triangulation in Figure 54. The procedure to compute the images of the vertices is the following:

1. initialize $S_i' = \Omega$ the origin of $\mathbb{R}^3$, $Q_1' = \left(-\frac{1}{2}|Q_1 Q_3|, 0, -h\right)$ and $Q_2' = \left(\frac{1}{2}|Q_1 Q_3|, 0, -h\right)$ - where $h^2 = |S_1 Q_1|^2 - \frac{1}{4}|Q_1 Q_3|^2$,

2. compute $Q_0' = \iota(\Omega, Q_1', Q_3', 1)$ and $Q_2' = \iota(\Omega, Q_1', Q_3', -1)$,

3. compute $P_2' = \iota(\Omega, Q_0', Q_1', -1), P_6' = \iota(\Omega, Q_2', Q_3', -1), P_3' = \iota(\Omega, Q_1', Q_2', -1),$ $P_7' = \iota(\Omega, Q_0', Q_3', 1),$

4. Finally compute: $P_0' = \iota(\Omega, Q_0', P_7', 1), P_4' = \iota(\Omega, Q_2', P_3', 1), P_1' = \iota(\Omega, Q_0', P_2', -1),$ $P_5' = \iota(\Omega, Q_2', P_6', -1).$

102
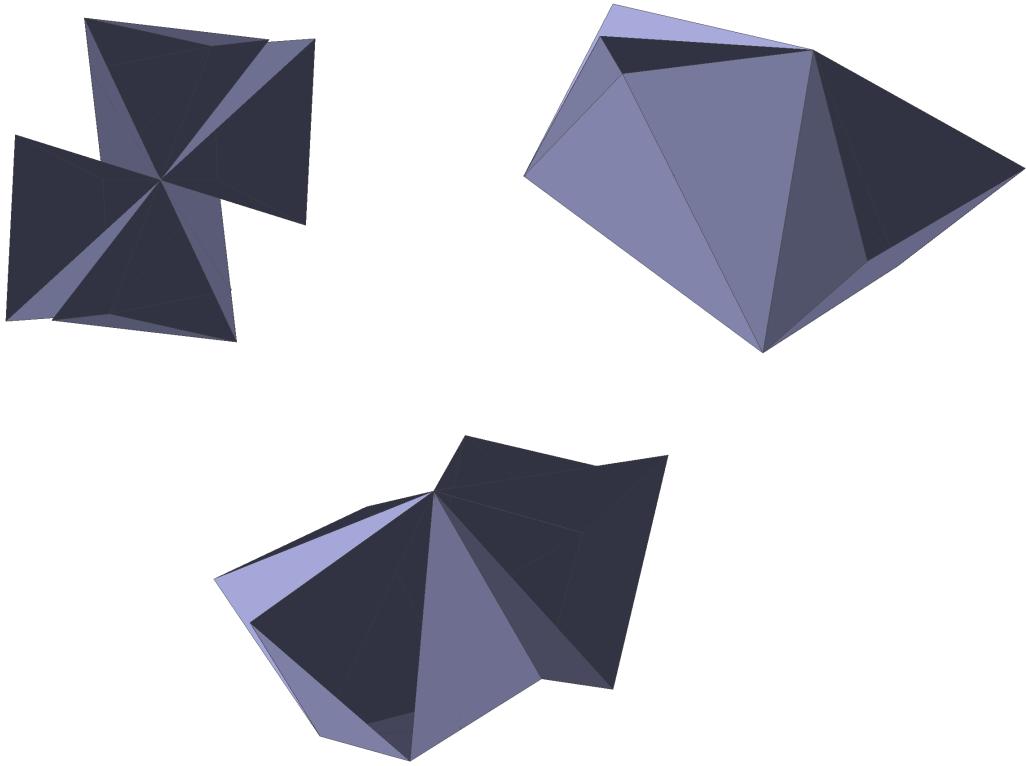
Figure 55: PL isometric embedding of a skew parallelogram with $\tau = 1$ and $\theta = 69°$.

We argue below that these constructions provide PL isometric embeddings for θ sufficiently close to $\pi/2$. An example of such an embedding is given in Figure 55.

Sketch of proof that the construction is well embedded. As previously noted, the triangulation of a central rectangle as in Section 6.2.2 is a deformation of the triangulation of a parallelogram which converges to the triangulation for the rectangular case when the angle θ tends toward $\pi/2$. The same is true for the global realization of the central parallelogram. Moreover, each intersection computation $\iota(X_1, X_2, X_3, \varepsilon)$ that appears in the above steps 2, 3, 4 is well defined in the limit rectangular case and remains so for θ sufficiently close to $\pi/2$. The embedded character of our PL map can be certified by a set of inequalities corresponding to the fact that each disjoint pairs of simplices in the central parallelogram have disjoint images. Indeed, in general a linear image of a simplicial complex is an embedding if and only if every pair of disjoint simplices in the complex have disjoint images [Laz20, Lemma 3.2.1]. At a given τ, these inequalities are strictly satisfied for $\theta = \pi/2$. Hence, since the skew triangulation converges to the triangulation in the rectangular case, the inequalities satisfying that any two disjoint simplices have disjoint images remain valid for θ sufficiently close to $\pi/2$.
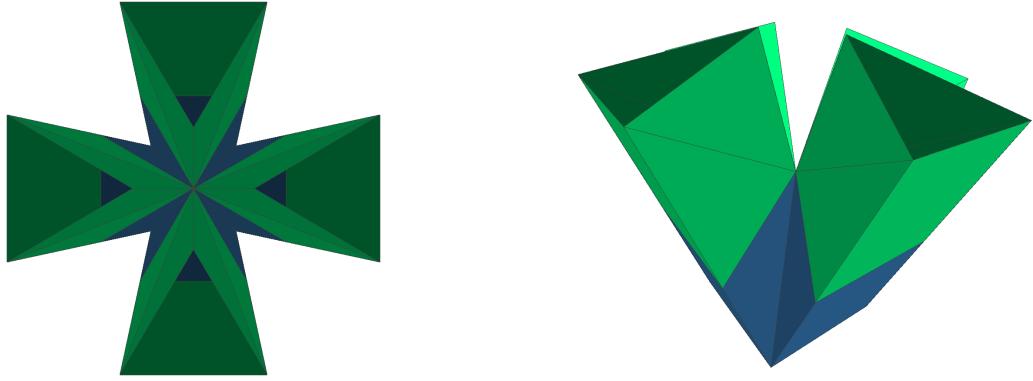
Figure 56: Embedding of a central square (corresponding to $\tau = 1$) in blue. The green "branches", corresponding to orthogonal continuations of the triangular boundaries, only intersect at the singularity.

6.3 Embedding of an entire surface of $\mathcal{H}(2)$ with long peripheral parallelograms

We saw in the last section how to embed the central parallelogram of a surface of $\mathcal{H}(2)$ close to $\mathcal{L}^{rect}$. We now explain how to extend this embedding to an embedding of the whole surface. We use Zalgaller's machinery, and derived tools from his work in [Zal00], to complete the construction by embedding the two remaining peripheral parallelograms as part of bended and twisted right prisms. In the rectangular case, there are two cases to consider, depending on the ratio $\tau = a/b$ of the length of the longest sides of the rectangles over the length of the smallest sides. Moreover, as in Zalgaller's paper, our method only works when the relative height of the peripheral parallelograms are sufficiently large.

Case where the ratio τ of the longer side of the rectangle with its smaller side is less than $\sqrt{3}$

This case is simpler, as there is no need to modify the central parallelogram to obtain an embedding. Indeed, in this case, the plane spanned by each boundary triangle is *supporting*: the embedding of the central rectangle lies on one side of this plane. See Figure 56. Hence, the interior of the orthogonal continuations of the triangular boundaries do not intersect. It suffices, and it is possible, to attach the two peripheral parallelograms to the central sphere without creating intersection. See Figure 57 for an example of embedding of such a surface with a square basis. We refer to Section 6.5 for proofs of the previous mentioned facts.

Case where the ratio τ of the longer side of the rectangle with its smaller side is greater or equal than $\sqrt{3}$

In this case, the previous method failed as the two planes spanned by the two small boundary components are not supporting anymore: the orthogonal continuation of the two thin branches intersect - see Figure 58. To remedy this situation, it is possible to apply a bending to the beveled part of right prisms corresponding to the two thin branches
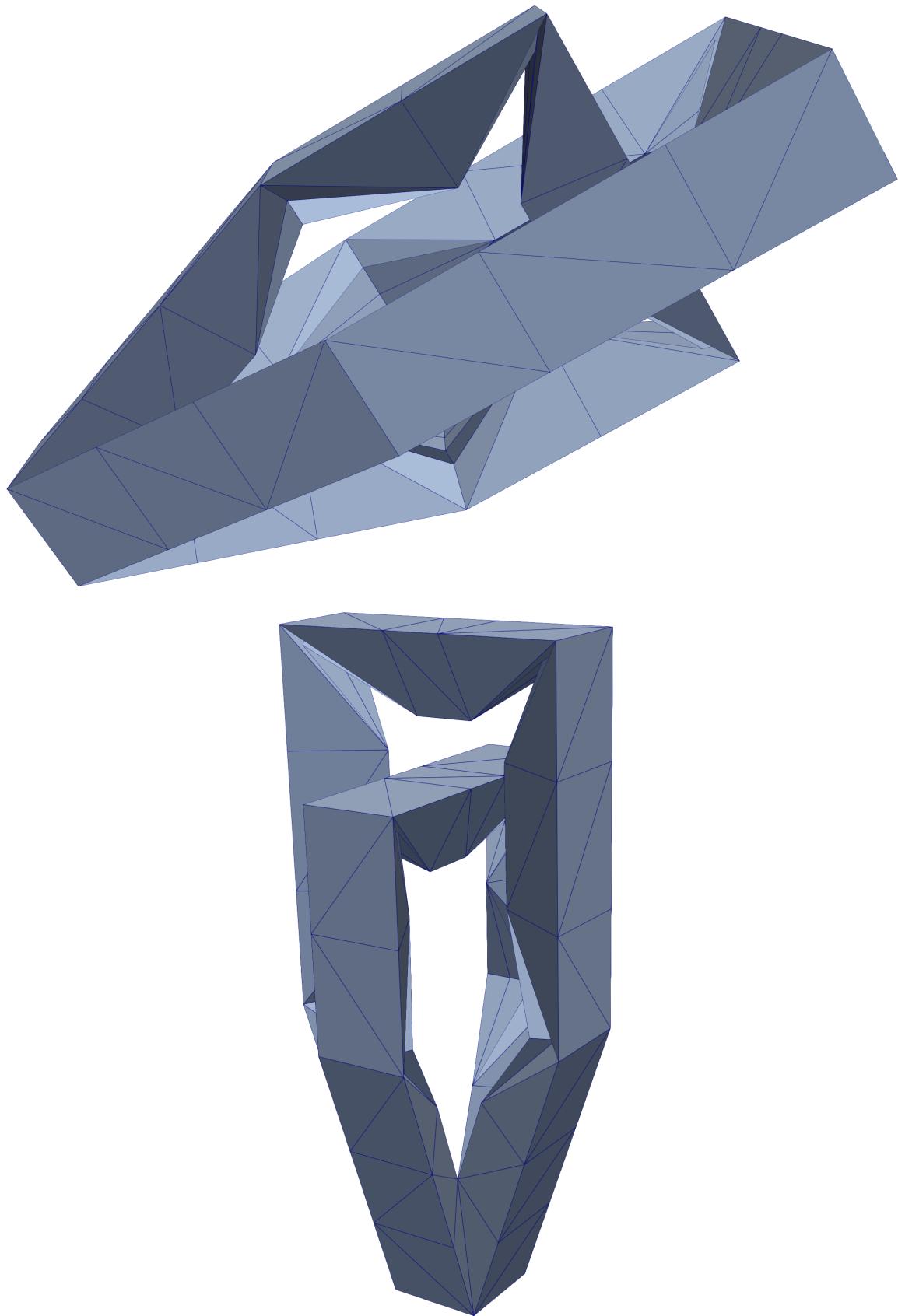
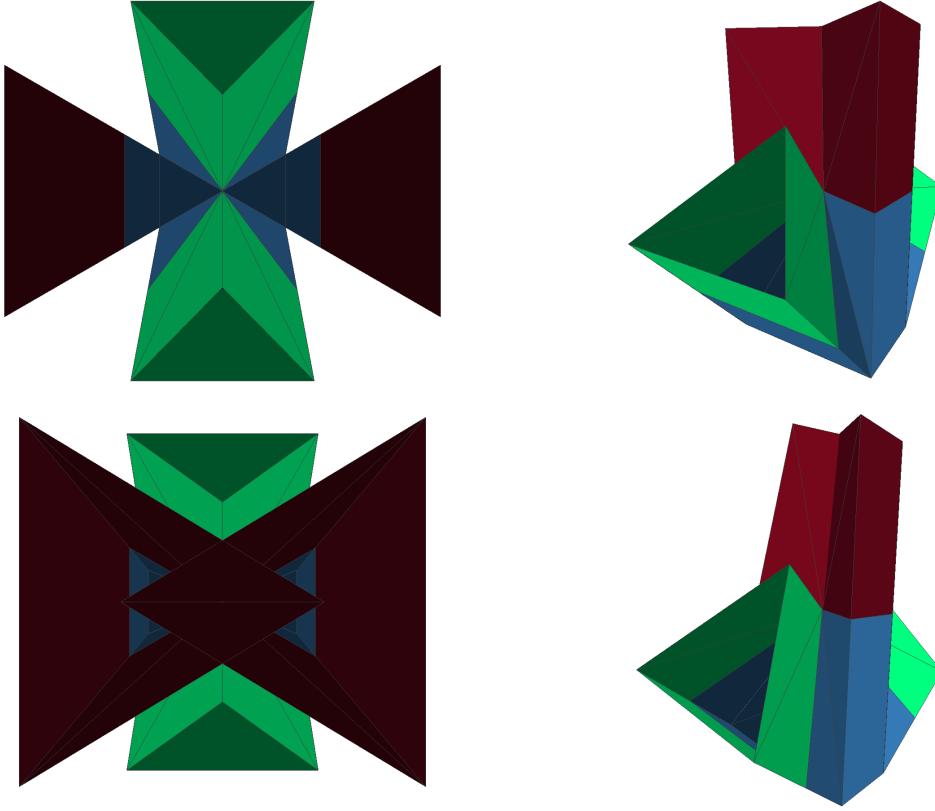Figure 57: Embedding of a surface of $H(2)$ with a square basis and long peripheral parallelograms.

Figure 58: Isometric realization of the central rectangle of a surface in $\mathcal{H}(2)$ that present self-intersection. The two top pictures represent the limit case ($\tau = \sqrt{3}$), while the two bottom pictures illustrates the case $\tau = \frac{7}{3}$.

of the central rectangle using opposed ribs, in order to make these two branches disjoint, see Figure 59. Doing so, we are able to glue the remaining peripheral parallelogram as a part of bended and twisted right prism as in the previous case, obtaining embedding of the entire surface. See Figure 60 for an example. As in the case $\tau < \sqrt{3}$, the proof relies on Appendix B, and the fact that the semi-infinite half-prisms bended as on Figure 59 do not intersect.

6.4 Alternative constructions to realize surfaces in $\mathcal{H}(2)$

In the previous sections we give a way to realize surfaces of $\mathcal{H}(2)$ with rectangle central parallelogram and long peripheral parallelograms. Here, we investigate two other methods to do so, introducing constructions that are interesting in their own rights. The first one amounts to bending the thin branches at a negative angle as opposed to the "positive" bending described in Section 3.3. The second method is to change the subdivision of the central rectangle, replacing the rectangle $Q_0Q_1Q_2Q_3$ in Figure 53 by an $c \times d$ rectangle with $0 < c \leq a$ and $0 < d \leq b$. When $c \neq a$ or $d \neq b$, the configuration imposes the boundary components of the central sphere to be isosceles but non equilateral triangles.
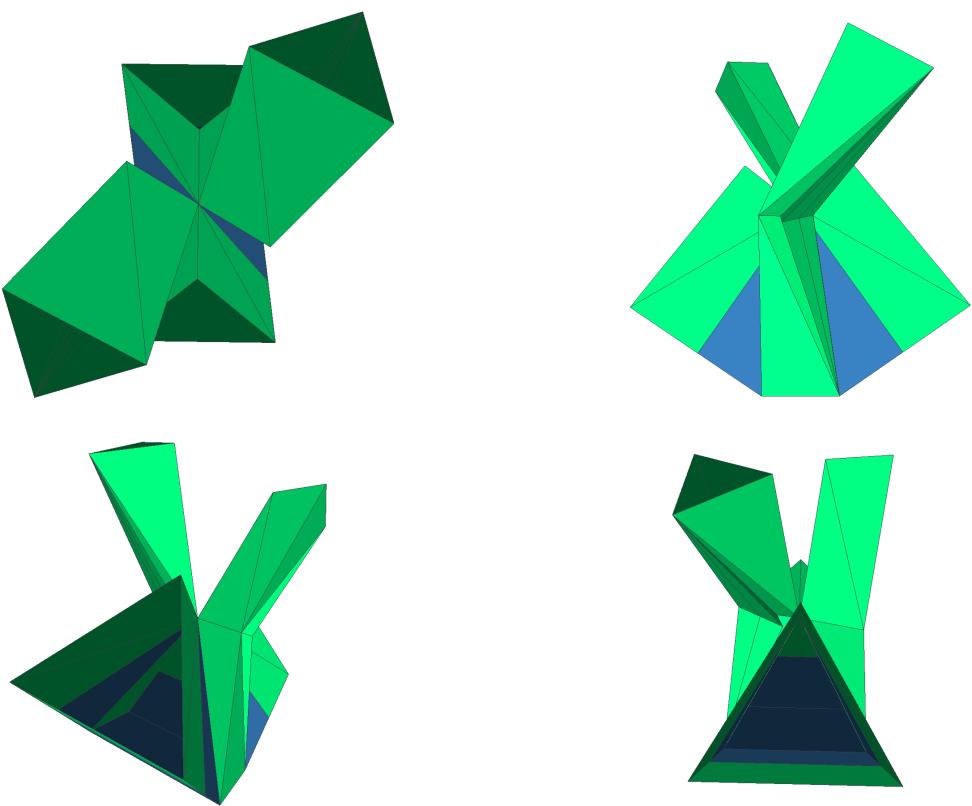
Figure 59: Bending of the two thin branches of an isometric realization of the central rectangle of a surface of $\mathcal{H}(2)$, resulting in an embedding. Here $\tau = \frac{7}{3}$ as in Figure 58.
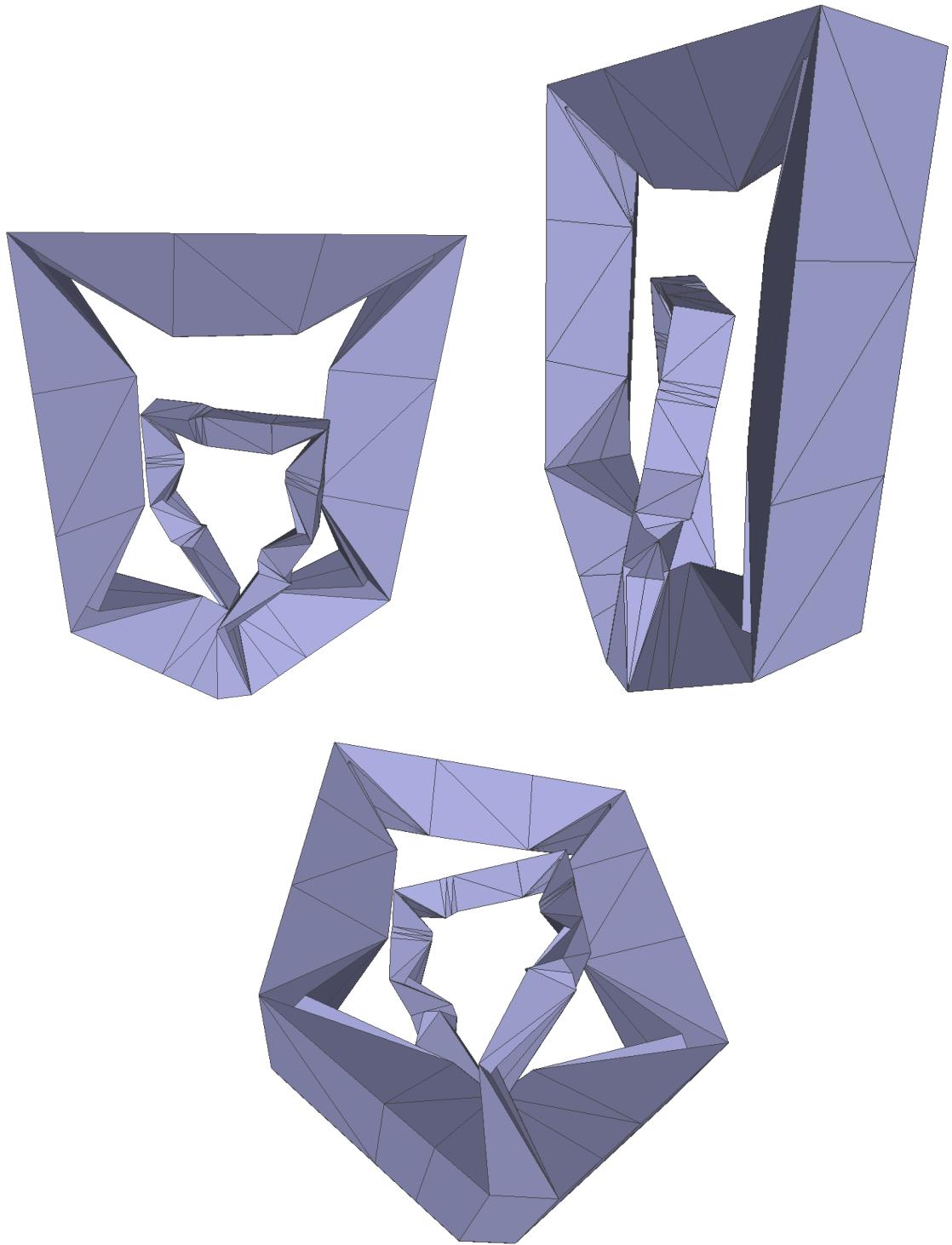
Figure 60: PL isometric embedding of a surface in $\mathcal{H}(2)$, with $\tau = \frac{7}{3}$ and long peripheral parallelograms.
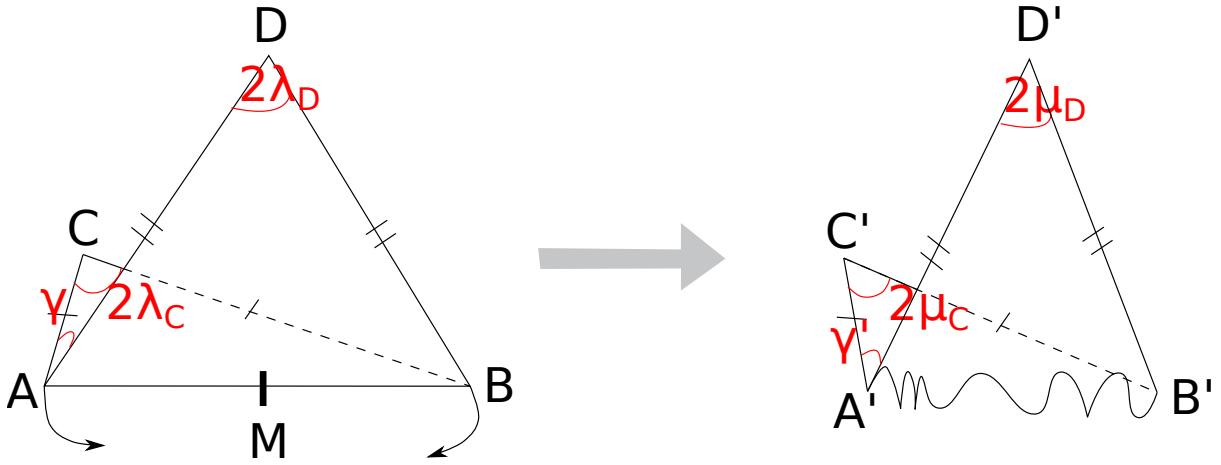
Figure 61: Left: the two initial isosceles triangles. Right: the two triangles after contraction of the common side AB.

Though it is possible to adapt Zalgaller's machinery of Section 3.3 in this context, we introduce a new original tool that permits to change the cross-section of a triangular right prism, going from isosceles to equilateral.

6.4.1 Bending at a negative angle

A preliminary construction. Consider two isosceles triangles ABC and ABD in $\mathbb{R}^3$ sharing a common side AB. Let $2\lambda_C$ be the angle at C of ABC, and let $2\lambda_D$ be the angle at D of ABD. We also denote by γ the dihedral angle between the two triangles. Refer to Figure 61. We view the four edges AC, CB, BD and DA as forming a rigid framework with idealized ball joints at each vertex. Our goal is to deform this framework while maintaining a PL isometric embedding of the union $ABC \cup ABD$. Denote by A', B', C', D' the vertices of the deformed framework and by $2\mu_C$ and $2\mu_D$ the angles of $A'B'C'$ and $A'B'D'$ at C' and D' respectively. Of course, A and B can only get closer in the deformation, for otherwise the shortest path distance between A' and B' would be larger than $|AB|$, preventing the deformation to be isometric. For analogous reasons we must have $\mu_C \leq \lambda_C$ and $\mu_D \leq \lambda_D$. We finally denote by γ' the angle between the two planes $(A'B'C')$ and $(A'B'D')$.

We construct the PL isometric embedding as follows. We first pleat the edge AB by moving its middle point M to a point M' in the plane through AB bisecting the angle γ'. The problem is now to pleat the triangle ABC (in an isometric way) to fit the new boundary $A'M' \cup M'B' \cup B'C' \cup C'A'$. For this, we rely on the preliminary construction elaborated by Zalgaller [Zal00, §2] (see also Section 3.3). It starts by folding ABC along its height MC until the distance between A and B equals $|A'B'|$. The resulting two-winged shape, call it Σ_C, may thus be moved rigidly so as to make its AC and BC sides coincide with $A'C'$ and $B'C'$ respectively. The point M reaches a position M'' and the goal is to further pleat Σ_C so as to rotate $A'M'' \cup M''B'$ about the axis $(A'B')$ and make M'' coincides with M'. This is obtained by cutting and reflecting parts of Σ_C using planes through $A'B'$. We refer to Figure 23. Note that there are two rigid motions applying Σ_C to $A'C' \cup B'C'$. Accordingly, the number of reflections used to pleat Σ_C may be chosen
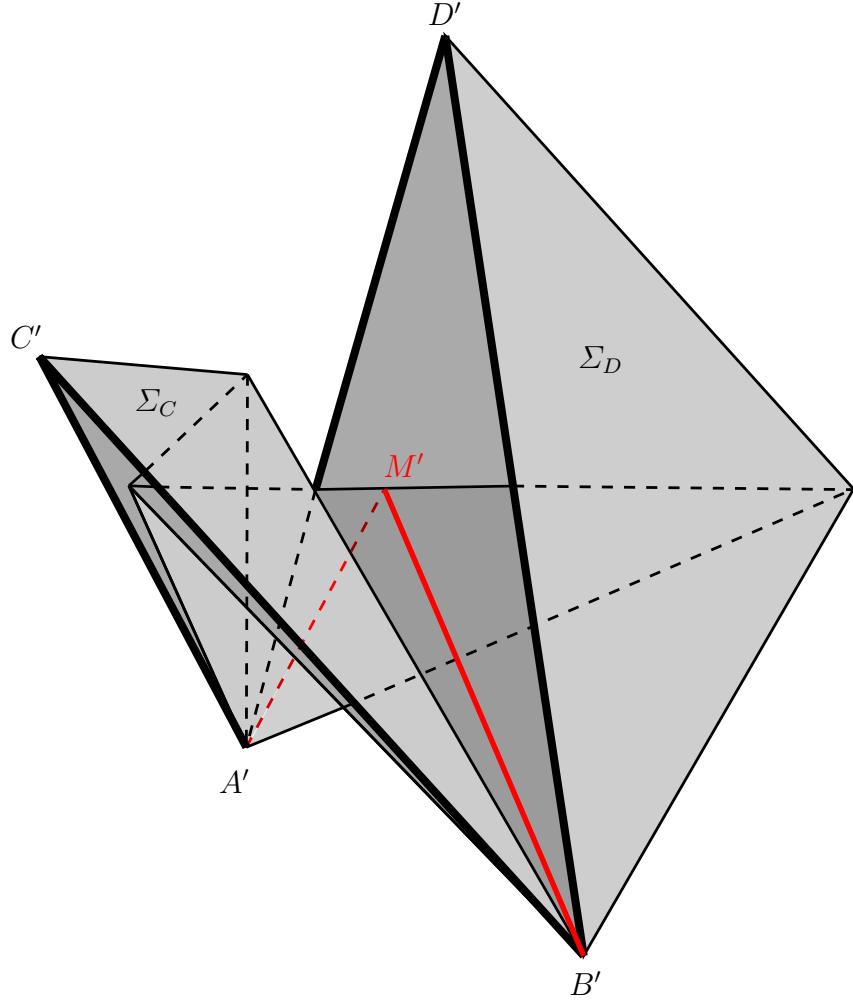
109

Figure 62: Final shape of our preliminary construction. Here, only one reflexion was applied to Σ_D, while two reflexions were applied to Σ_C.

even or odd. After pleating in a similar way the two-winged shape Σ_D corresponding to ABD, we obtain the desired PL isometric embedding of $ABC \cup ABD$ with boundary $A'C' \cup C'B' \cup B'D' \cup D'A'$. An example of the resulting pleating can be seen in Figure 62.

Bending at a negative angle. In this section, we adapt the bendings developed by Zalgaller in [Zal00] to handle negative angles. In the original construction of Zalgaller (see Section 3.3) the construction is rotated along a rib CC' towards the third point D of the corresponding cross-section. Considering this as a rotation of positive angle, a bending with negative angle would rotate the construction in the other direction, using the third point D as a pivot. Compare the diagrams in Figure 29 and Figure 63.

After choosing the rib CC' where we want to perform a negative bending, consider the pyramid $D * ABB'A'$ with apex D and square basis $ABB'A'$ centered at O as in Figure 64. To bend the prism at an angle $\varphi < 0$ along the rib CC', we do the following (see Figure 64 and 63):

(a) Remove from the right prims its intersection with the pyramid, leaving two half
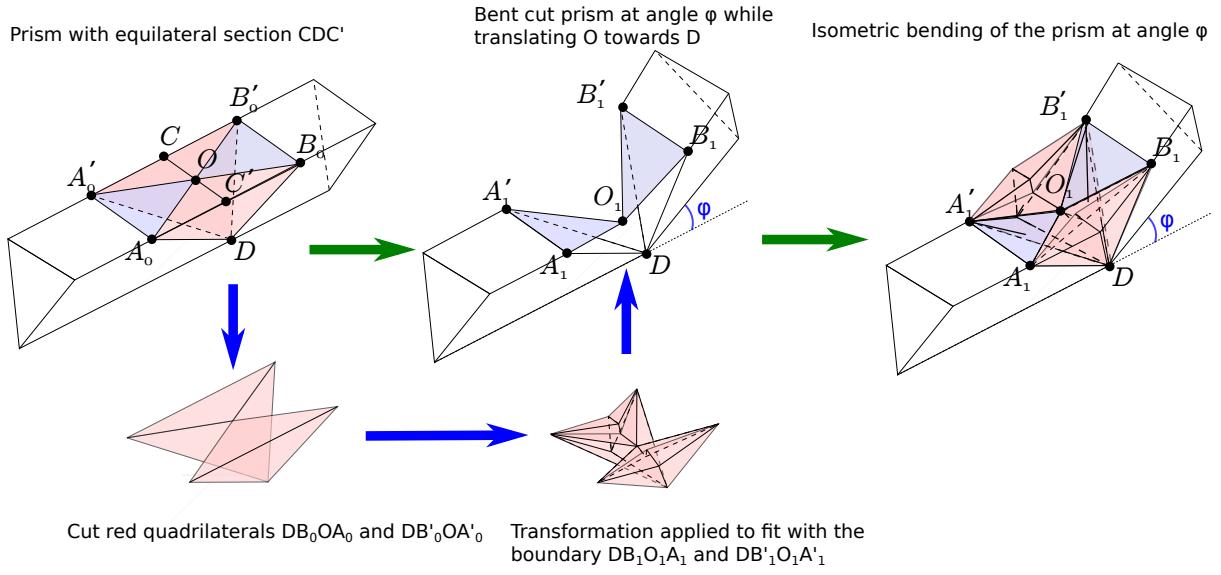
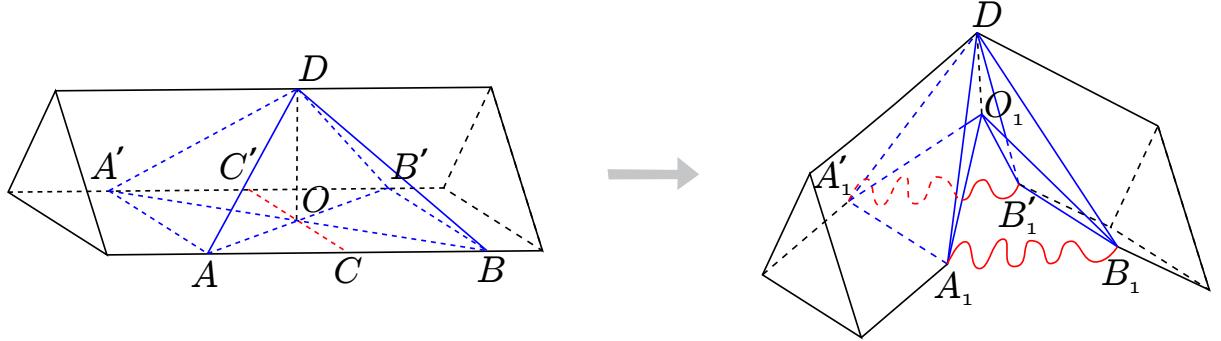Figure 63: The different steps to bend a prism at a negative angle.

Figure 64: Bending at negative angle. Left: the initial right prism. Right: the cut and bent prism, in red are indicated the contractions of the basis using the preliminary.

beveled prisms joined at D.

(b) Rotate one half prism at an angle $-\varphi$. The vertices A, B, A', B' are moved to A_1, B_1, A_1', B_1', respectively.

(c) Move the center O of the pyramid to a position O_1 towards D so that its distance to A, B, A', B' remains unchanged after rotation.

(d) Add the triangles $A_1 A_1' O_1$ and $B_A B_1' O_1$ to the construction. According to the previous move, they are isometric to $AA'O$ and $BB'O$.

(e) Finally, apply the preliminary construction of the previous paragraph to the quadrilaterals $ABO \cup ABD$ and $A'B'O \cup A'B'D$ in order to contract their respective basis AB and $A'B'$ to $A_1 B_1$ and $A_1' B_1'$, respectively.

An analysis analogous to the positive angle case shows that such a pleating is possible if the cutting angle $\lambda := \frac{1}{2}\angle ADB$ satisfies the inequality: $\lambda > \lambda_0(\varphi) := \arctan\left(\frac{\sqrt{3}}{2}\tan\frac{\varphi}{2}\right)$
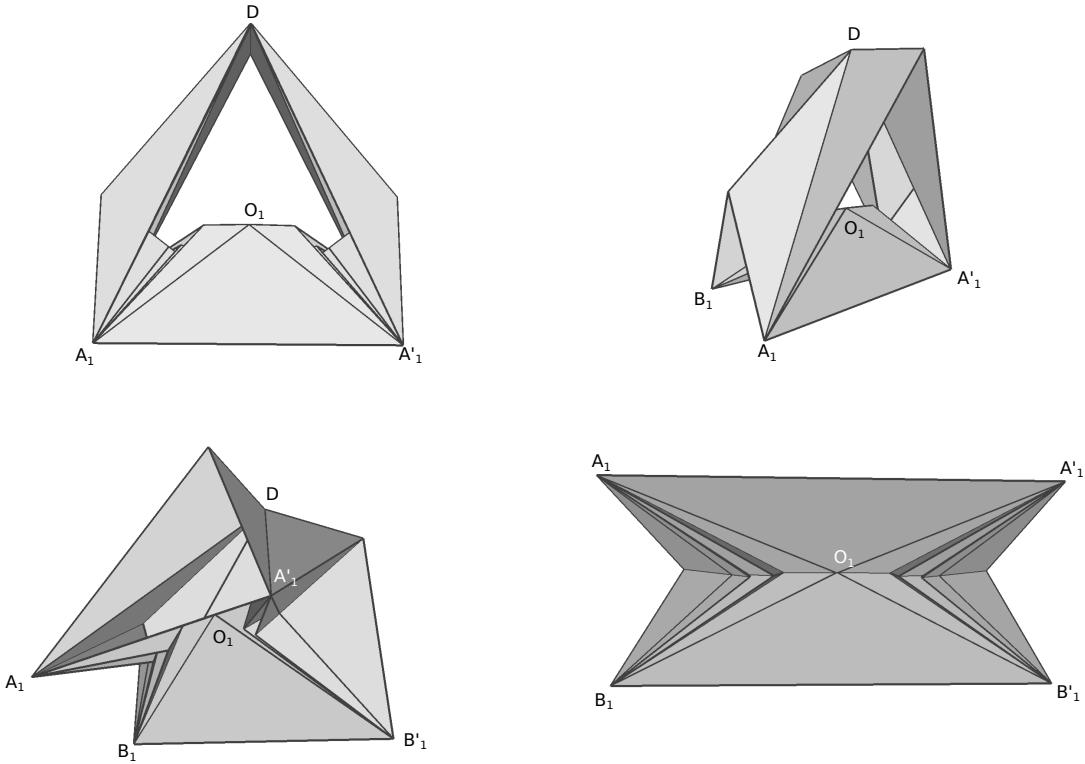
Figure 65: Some renderings of a bending at negative angle. It is composed of two preliminary constructions joining at O_1, and the two elevated triangles $A_1A'_1O_1$ and $B_1B'_1O_1$.

(this angle corresponds to the case where A_1B_1 and $A'_1B'_1$ coincide). Note that $|AO| < |AD|$, so that moving O to O_1 in step (c) lies inside the deformed pyramid $D * A_1B_1B'_1A'_1$.

Some renderings of the construction can be seen in Figure 65.

6.4.2 Modifying the bottom face of the central sphere with boundaries

We saw in Section 6.2 how to realize the central parallelogram of a surface in $\mathcal{H}(2)$ when this parallelogram is almost right angled. We now describe some variations of this model that allow to vary the obtained shapes. When $c, d \to 0$, the construction is well embedded as construction becomes closer and closer to a kind of cone with cross shape in a such a way that each triangular boundary becomes supporting. This way, we are able to uncross central spheres in the case $\tau \geq \sqrt{3}$ for all c, d sufficiently small by continuity. However, the exact bounds below which the construction becomes an embedding are difficult to compute.

Recall the setting of Section 6.2. We have a $3a \times 3b$ central rectangle of some surface in $\mathcal{H}(2)$ that we want to realize in $\mathbb{R}^3$ as a PL sphere with four triangular boundaries. In Section 6.2, we chose the four boundaries to be equilateral. Here, we relax this constraint and allow the boundaries to be isosceles. This allows us to slightly change the shape of the final construction, and enables to change the direction of the "branches".
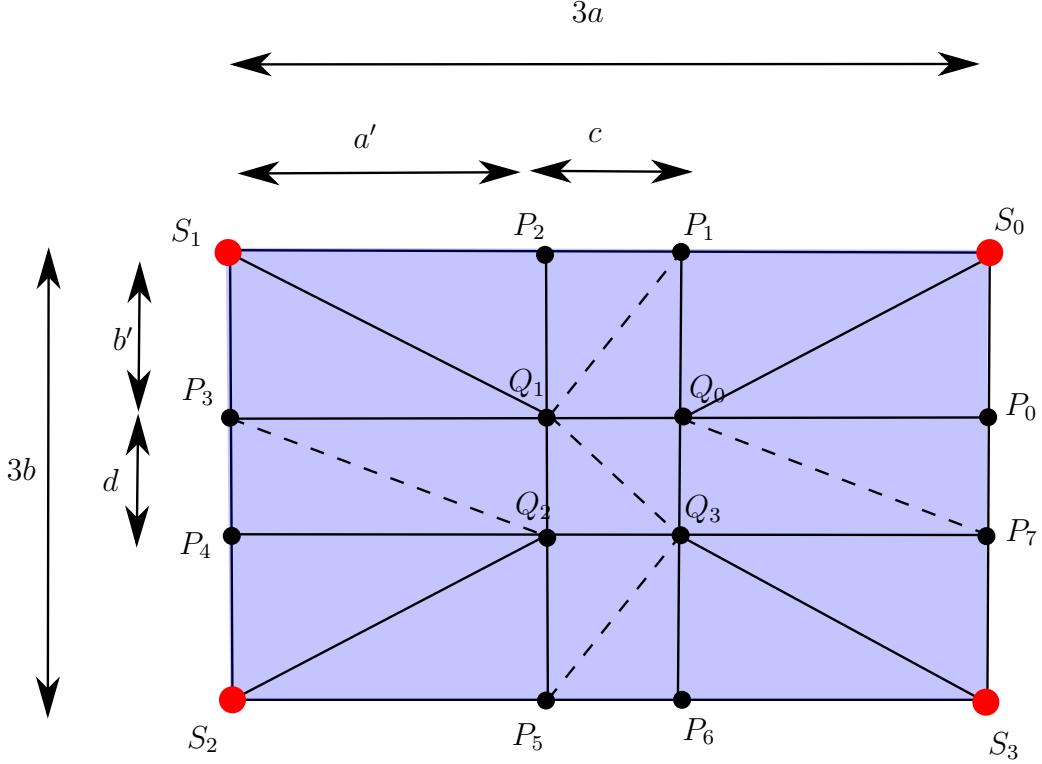
Figure 66: New triangulation of the central rectangle. Dashed segments indicate coplanarity of the corresponding rectangle in its final realization in $\mathbb{R}^3$.

Let $c, d > 0$ so that $c \leq a$ and $d \leq b$. In Section 6.2 we decompose the central rectangle into 9 isometric rectangles and add a diagonal in each of them to form a triangulation. In the modified construction we use the same combinatorial triangulation but we move the vertices Q_i and P_j. After subdividing the rectangles, this gives the desired triangulation as on Figure 66.

Given that new the triangulation, we proceed in a similar way as in Section 6.2 for the skew case. We first send S to the origin Ω of $\mathbb{R}^3$. Note that the images of the points Q_i and S_i form a pyramid with rectangular basis with $h = \frac{\sqrt{3}}{2}\sqrt{3(a^2 + b^2) - 2(ac + bd)}$. As usual, denote X' the image in $\mathbb{R}^3$ of a point X of the central rectangle by our realization. We chose to align the side $Q'_0 Q'_1$ with the Ωx axis, leading to the following coordinates: $Q'_0 = \left(\frac{c}{2}, \frac{d}{2}, -h\right)$, $Q'_1 = \left(-\frac{c}{2}, \frac{d}{2}, -h\right)$, $Q'_2 = \left(-\frac{c}{2}, -\frac{d}{2}, -h\right)$, $Q'_3 = \left(\frac{c}{2}, -\frac{d}{2}, -h\right)$.

Once the images of the singularity and the Q_i are determined, it is possible, step by step, to compute the coordinates of the remaining vertices of the central rectangle - the P_i - as intersections of spheres. As, by coplanarity, each P_i in the triangulation is incident via an edge to at least three points from $\{S_i, Q_i\}_{0 \leq i \leq 3}$, it is possible to compute their image for the final realization to be isometric.

Some example of such a modified realization is given in Figure 67.

6.4.3   Interpolating distinct isosceles sections with a cylinder

We saw in the preceding section how to modify the embeddings of Section 6.2 to avoid intersection of the orthogonal continuations of the beveled part of prism. However,
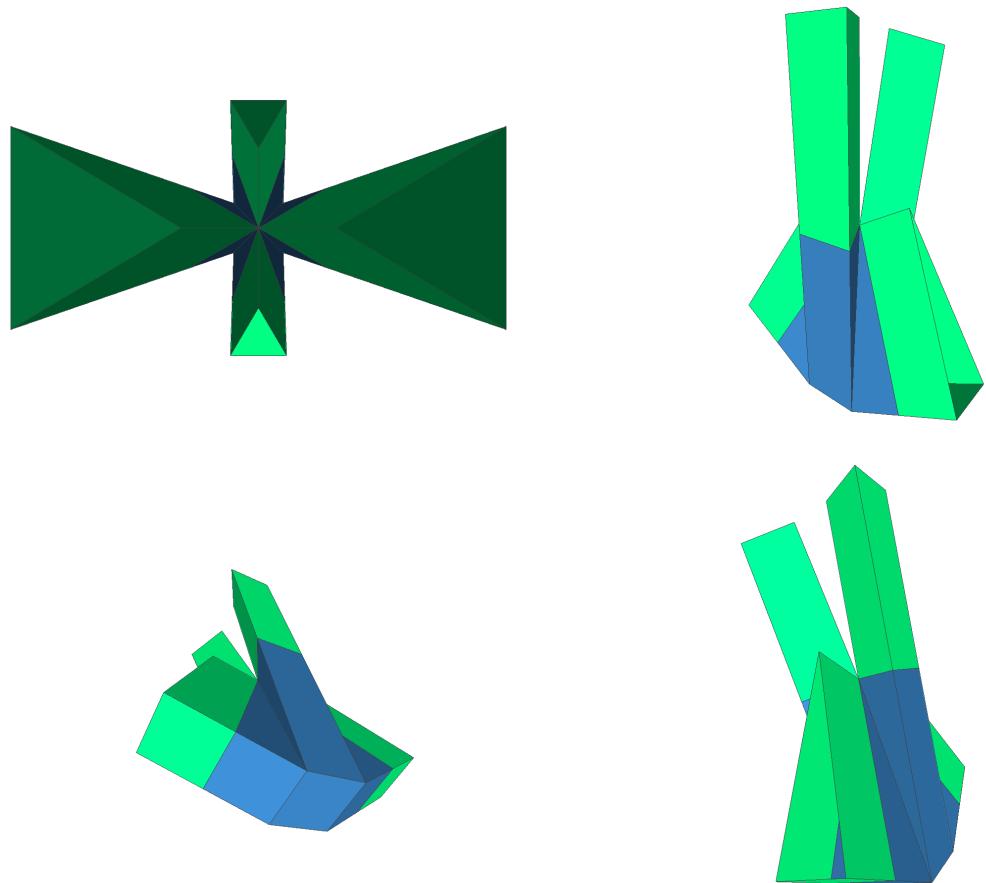
Figure 67: Variation of the realization of the central rectangle with $\tau = 7/3$, and $c/d = 1$ - more precisely $c = d = b$. The green branches do not intersect in this case. Compare with the bottom of Figure 59.

the present case where $Q_0Q_1Q_2Q_3$ has size $c \times d$ with $c, d \neq a, b$ makes the triangular boundaries of the realized central sphere isosceles non equilateral. Looking at the details of the bending procedure, it is not hard to see that Zalgaller's machinery can be adapted to the isosceles non equilateral case. Indeed, the very same bending procedure still works if the rib is chosen to be the base of the isosceles section. However, this requires longer prisms than in the equilateral case and would apply to fewer L shapes. These considerations motivate the introduction of a new tool that allows to modify the cross-section of a right prism.

Consider a triangle $C_0C_2C_4$, isosceles at C_0, with perimeter (length) L. The goal is to find a PL isometric embedding of the cylinder $C_0C_2C_4 \times [0, h]$ with one boundary equals to $C_0C_2C_4$ and the other one an equilateral triangle $C_1C_3C_5$ of perimeter L. To do so, we give a plane pattern for the pleating, see Figure 68. To compute the coordinates of the images C_i' of C_i by our linear embedding, we first assume that $L = 3$, i.e. that the equilateral has unit side. We then rotate the construction in $\mathbb{R}^3$ so that the equilateral triangle lies the xy-plane and more explicitly so that:

$$
\begin{aligned}
C_0' &= (0, 0), \\
C_2' &= (e^{i\pi/6}, 0) \text{ and} \\
C_4' &= (e^{-i\pi/6}, 0).
\end{aligned}
$$

where we identified $\mathbb{R}^3$ with $\mathbb{C} \times \mathbb{R}$ to denote the coordinates of the points.

Now, since the triangles $C_0C_1C_2$ and $C_0C_4C_1$ are right angled at C_0, the segment $C_0'C_1'$ must be orthogonal to both $C_0'C_2'$ and $C_0'C_4'$, hence must be vertical. We thus have $C_1' = (0, h)$ choosing to place the construction in the upper xy-halfspace.

In order to determine C_3', we remark that its distances to C_1', C_2', C_4' can be read on the unfolding in Figure 68. Indeed, the preservation of the edge lengths and the planarity of C_2', C_3', C_4', C_5' imply that:

$$
\begin{aligned}
C_3'C_1'^2 &= \left(\frac{3-\delta}{2}\right)^2, \\
C_3'C_2'^2 &= h^2 + \left(\frac{1-\delta}{2}\right)^2, \\
C_3'C_4'^2 &= h^2 + \left(\frac{1+\delta}{2}\right)^2
\end{aligned}
$$

where we denoted by δ the distance between C_3 and C_5.

Let $C_3' = (v, z)$ with $v = x + iy$. We must have:

$$
\begin{aligned}
|v|^2 + (h - z)^2 &= C_3'C_1'^2, \\
|v - e^{i\pi/6}|^2 &= C_3'C_2'^2, \\
|v - e^{-i\pi/6}|^2 &= C_3'C_4'^2.
\end{aligned}
$$

After expanding the equations, we obtain the equivalent system:

$$|v|^2 + h^2 - 2hz + z^2 = \left(\frac{3-\delta}{2}\right)^2, \tag{6.14}$$

$$|v|^2 + 1 - 2\Re(ve^{-i\pi/6}) + z^2 = h^2 + \left(\frac{1-\delta}{2}\right)^2 \tag{6.15}$$

$$|v|^2 + 1 - 2\Re(ve^{i\pi/6}) + z^2 = h^2 + \left(\frac{1+\delta}{2}\right)^2. \tag{6.16}$$

Subtracting (6.15) and (6.16), we deduce:

$$2\Re(v(e^{i\pi/6} - e^{-i\pi/6})) = \left(\frac{1-\delta}{2}\right)^2 - \left(\frac{1+\delta}{2}\right)^2,$$

which solves to

$$y = \frac{\delta}{2}. \tag{6.17}$$

Subtracting now (6.15) from (6.14), we obtain:

$$h^2 - 2hz - 1 + 2\Re(ve^{-i\pi/6}) = \left(\frac{3-\delta}{2}\right)^2 - \left(\frac{1-\delta}{2}\right)^2 - h^2.$$

After expanding and reordering the terms, we get:

$$z = z(x) = \frac{1}{2h}\left(\sqrt{3}x + 2h^2 + \frac{3}{2}\delta - 3\right). \tag{6.18}$$

Now, plugging (6.17) and (6.18) into (6.16), we get a quadratic equation for x given by $ax^2 + bx + c = 0$ with:

$$a = 1 + \frac{3}{4h^2}$$
$$b = \frac{3\sqrt{3}(\delta - 2)}{4h^2}$$
$$c = \frac{9}{4}\left(\frac{(1-\delta)^2}{h^2} + \frac{2}{3}\delta - 1\right).$$

We easily compute the discriminant

$$\Delta = 3(3 - 2\delta) - \frac{9}{4h^2}(4\delta^2 - 6\delta + 1) - \frac{3\delta}{16h^4}(27\delta - 36).$$

By the symmetry of the construction, and the fact that C_2', C_3', C_4', C_5' are coplanar, C_5' must be symmetric to C_3' with respect to the xz-plane. Moreover, h must be large enough for Δ to be nonnegative. In which case the solution for C_3' is given by $\left(x = \frac{-b+\sqrt{\Delta}}{2a}, y = \frac{\delta}{2}, z = z(x)\right)$. We can check that this solution leads to an embedding of the right cylinder $C_0C_2C_4 \times [0, h]$. The other solution with $x = \frac{-b-\sqrt{\Delta}}{2a}$ consists in reflecting the three faces $C_1'C_2'C_3'$, $C_2'C_3'C_5'C_4'$ and $C_4'C_5'C_1'$ with respect to the plane $C_1'C_2'C_4'$. This would have however introduced self-intersection in the corresponding surface.

Some rendering of the construction can be seen in Figure 69. Note that the two triangular boundaries are not parallel anymore. If necessary, it is possible to apply the multiple reflections technique of the Zalgaller's preliminary construction - see Section 5.1 - to make the triangular sections parallel as illustrated in Figure 70.
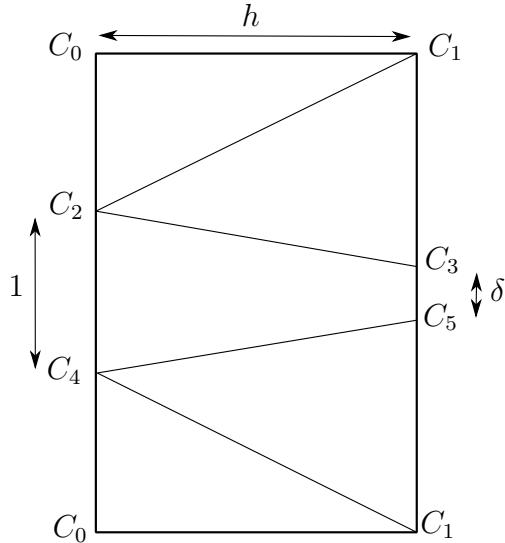
Figure 68: Pattern of our construction, that "interpolates" a triangle $C_0C_2C_4$ isosceles at C_0, and an equilateral triangle $C_1C_3C_5$ with same perimeter as $C_0C_2C_4$. The top and bottom edges should be glued to form a cylinder. Note that in our geometric realization, the four points C_2, C_3, C_4, C_5 have coplanar images.

6.5 Proof that the geometric realizations of surfaces of $\mathcal{H}(2)$ are well embedded in the case $\tau < \sqrt{3}$

6.5.1 Square case

Symmetry by rotation of angle $\frac{\pi}{2}$. By construction the candidate embedding f is invariant by the rotation ρ of angle $\frac{\pi}{2}$ and axis Oz. We have more precisely, recalling the notation $V' = f(V)$:

- $\rho(S_0') = S_0'$,

- $\rho(O') = O'$,

- $\rho(Q_i') = Q_{i+1}'$, $i \in [\![0, 3]\!]$ ($i \bmod 4$),

- $\rho(P_i') = P_{i+2}'$, $i \in [\![0, 7]\!]$ ($i \bmod 8$),

Isometric property. Since f is linear on the triangulation of the central square, checking that it is an isometry reduces to check that the length of the edges of the triangulation are preserved. In turn, using the rotational symmetry of order four of the construction, it is enough to check that f preserves the length of the following edges: Q_0Q_3, S_0P_0, P_0P_7, P_7S_3, Q_0P_0, Q_3P_7, OQ_0, Q_0S_0, Q_0P_7. From Figure 52, it is seen that the horizontal and the vertical edges have the same length a, that $|OQ_0| = \frac{a}{\sqrt{2}}$, and that the diagonal edges S_0Q_0 and Q_0P_7 have length $\sqrt{2}a$. As $Q_3' = \sigma_{xz}(Q_0')$ and $P_7' = \sigma_{xz}(P_0')$ we then verify using the point coordinates in (C) that:

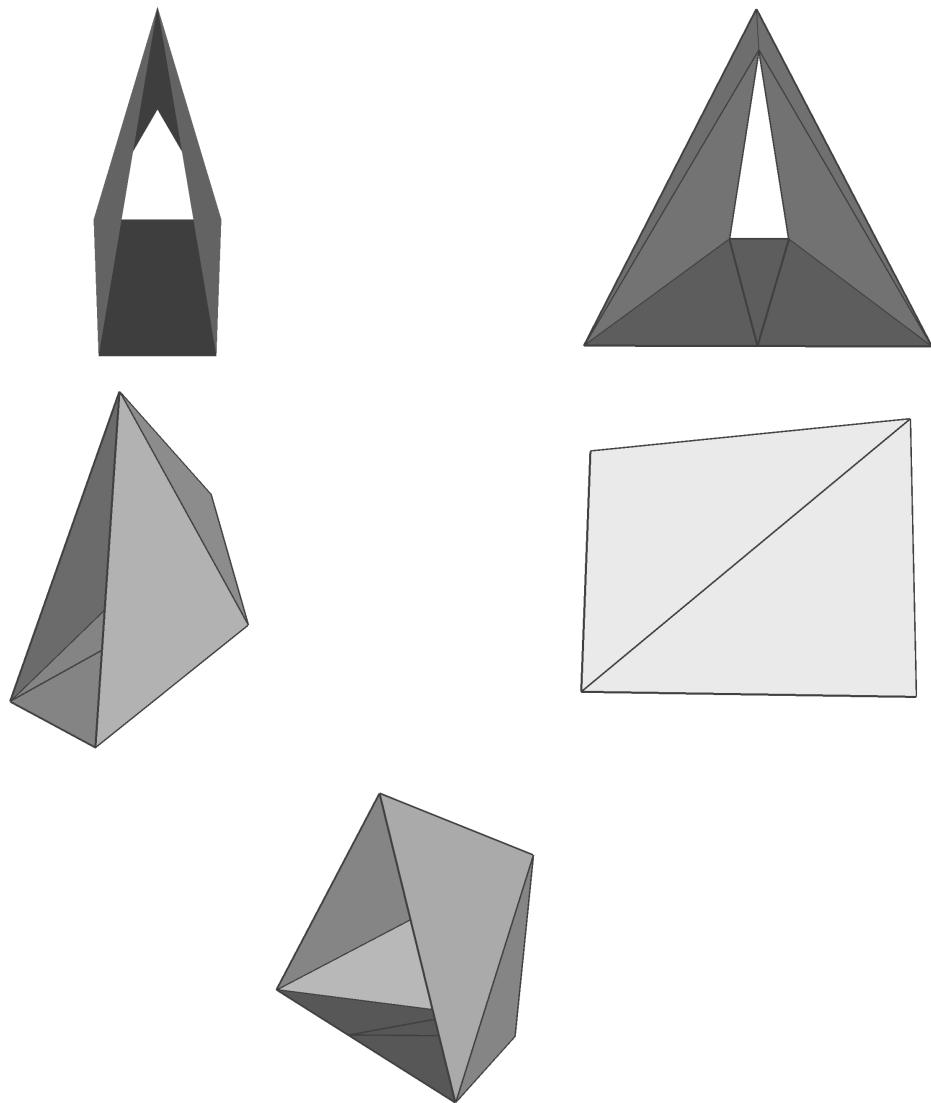- $Q_0'Q_3'$, $S_0'P_0'$, $P_0'P_7'$, $Q_0'P_0'$, $Q_3'P_7'$ and $S_3'P_7'$ have lenght a,

Figure 69: Our construction that interpolates the initial isosceles triangle, and the equilateral one. Observe that the two triangular boundaries are not parallel.
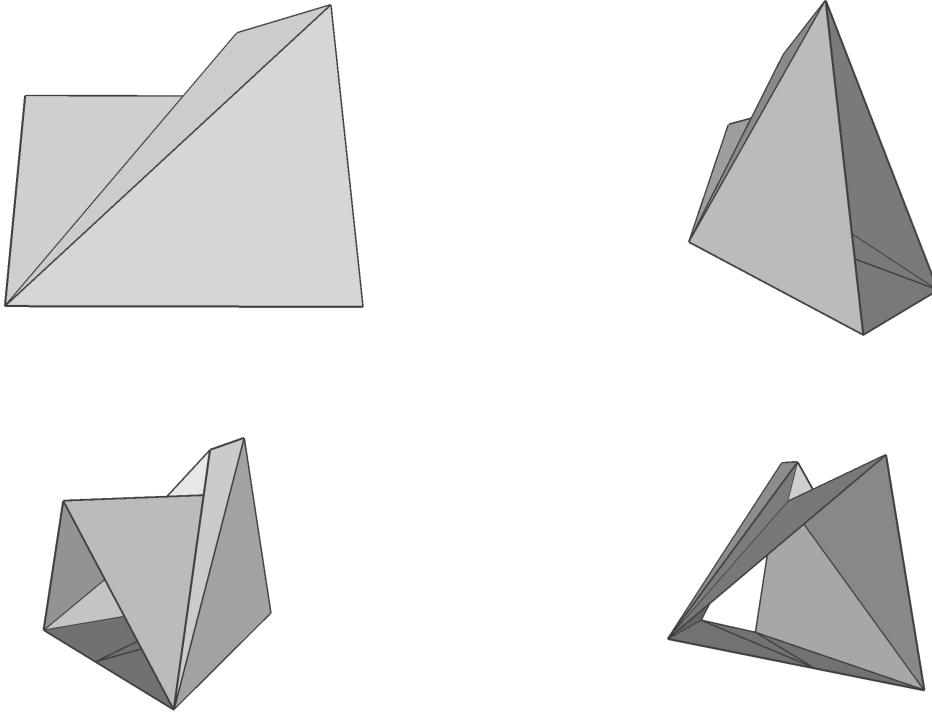
Figure 70: Modified construction for the triangular boundaries to be parallel.

- the image $O'Q'_0$ of the semi-diagonal OQ_0 has length $\frac{a}{\sqrt{2}}$,

- and the images $S'_0Q'_0$ and $Q'_0P'_7$ of the diagonals have length $\sqrt{2}a$.

It follows that f preserves the required edge lengths.

Embedding property. We now verify that f is an embedding. For further reference, we denote the central sphere by $\mathcal{S}_c$. We first use the rotational symmetry to restrict the verification to the dihedral sector, call it D, intersection of the two half-spaces $x \geq y$ and $x \geq -y$. From the point coordinates given by (C) and the fact that $P'_7 = \sigma_{xz}(P'_0)$, we readily check that $S'_0, O', Q'_0, Q'_3, P'_0$ and P'_7 are in D. By convexity, we deduce that D contains the triangles of the image $f(\mathcal{S}_c)$ of the central sphere induced by these vertices. Namely, D contains the triangles $O'Q'_0Q'_3, Q'_0P'_0P'_7, Q'_0P'_7Q'_3, Q'_0S'_0P'_0$ and $Q'_3P'_7S'_0$. We observe that the iterated images by r of the corresponding set of source triangles $\mathcal{T}_0 := \{OQ_0Q_3, Q_0P_0P_7, Q_0P_7Q_3, Q_0S_0P_0, Q_3P_7S_3\}$ cover the whole set of triangles of $\mathcal{S}_c$. By the symmetry of our construction, it follows that $f(r^i(\mathcal{T}_0))$ is included in $\rho^i(D)$. Hence, to show that f is an embedding, it is enough to show that the restriction of f to $\mathcal{T}_0$ is an embedding and that $f(\mathcal{T}_0) \cap \{x = y\}$ is a set of edges such that $f(\mathcal{T}_0) \cap \{x = y\} = \rho(f(\mathcal{T}_0) \cap \{x = -y\})$.

Only S'_0, O', P'_0 belong to $\{x = y\}$ among the vertices of $f(T)$. Since OS_0 is not an edge of $\mathcal{S}_c$, in particular S_0OP_0 is not a triangle of $\mathcal{S}_c$, we have that $f(T) \cap \{x = y\}$ is reduced to the edges $O'P'_0$ and $P'_0S'_0$. We similarly check that $f(T) \cap \{x = -y\} = O'Q'_3 \cup Q'_3S'_0$. In particular, $f(T) \cap \{x = y\} = \rho(f(T) \cap \{x = -y\})$ as desired.

We notice that $P'_7Q'_3 = \sigma_{xz}(Q'_0P'_0)$, so that the four vertices are coplanar and form a parallelogram isometric to $Q_0P_0P_7Q_3$. Hence $\mathcal{T}_0$ decomposes into a set of four faces $\Phi = \{OQ_0Q_3, Q_0S_0P_0, Q_3P_7S_3, Q_0P_0P_7Q_3\}$.

It remains to ensure that the restriction of f to Φ is an embedding. It is enough to exhibit a separating plane for the images of every pair of faces of Φ. Here, by a **separating plane** of two faces ϕ_1, ϕ_2, we mean a plane Π such that $\Pi \cap \phi_1$ is either empty or a common edge or vertex of ϕ_1 and ϕ_2, and that ϕ_2 is contained in the closed half-space bounded by Π that does not contain ϕ_1. We thus allow ϕ_2 to be entirely contained in Π. We now proceed to the verification that the faces of $f(\Phi)$ are pairwise separated in the above sense.

- The plane $\Pi_0 := \left\{ z = -\sqrt{\frac{3}{2}}a \right\}$ separates $O'Q'_0Q'_3$ from the other faces $Q'_0P'_0P'_7Q'_3$, $Q'_0S'_0P'_0$ and $Q'_3S'_0P'_7$. Indeed, from the coordinates of the points, we check that O', Q'_0 and Q'_3 belong to Π_0, while P'_0, P'_7, and S'_0 are located in the same open half-space $\left\{ z > -\sqrt{\frac{3}{2}}a \right\}$ bounded by Π_0. Moreover, the intersection of the face $Q'_0P'_0P'_7Q'_3$ with Π_0 is the edge $Q'_0Q'_3$ of $O'Q'_0Q'_3$, while the intersection of Π_0 with $Q'_0S'_0P'_0$ and $Q'_3S'_0P'_7$ is a vertex, respectively Q'_0 and Q'_3, that is also a vertex of $O'Q'_0Q'_3$.

- Let

$$\ell_1(x, y, z) = -\left(\sqrt{\frac{3}{2}} + \sin\theta_0 \right)x + \left(\sin\theta_0 + \sqrt{6}\cos\theta_0\cos\varphi_0 \right)y + \left(\cos\theta_0\cos\varphi_0 - \frac{1}{2} \right)z.$$

The plane $\Pi_1 := \{\ell_1(x, y, z) = 0\}$ separates $Q'_0P'_0S'_0$ from the faces $Q'_0P'_0P'_7Q'_3$ and $Q'_3P'_7S'_0$. Indeed, we have $Q'_0, P'_0, S'_0 \in \Pi_1$, while $\ell_1(Q'_3) < 0$ and $\ell_1(P'_7) < 0$. Moreover, the intersection of Π_1 and $Q'_0P'_0P'_7Q'_3$ is the edge $Q'_0P'_0$ common to $Q'_0P'_0S'_0$ and the intersection of Π_1 with $Q'_3P'_7S'_0$ is the vertex S'_0 shared with $Q'_0P'_0S'_0$.

- Let

$$\ell_2(x, y, z) = \left(\sqrt{\frac{3}{2}} + \sin\theta_0 \right)x + \left(\sin\theta_0 + \sqrt{6}\cos\theta_0\cos\varphi_0 \right)y + \left(-\cos\theta_0\cos\varphi_0 + \frac{1}{2} \right)z.$$

The plane $\Pi_2 := \{\ell_2(x, y, z) = 0\}$ separates $Q'_0P'_0P'_7Q'_3$ and $Q'_3P'_7S'_0$. Indeed, $Q'_3, P'_7, S'_0 \in \Pi_2$, while $\ell_2(Q'_0) < 0$ and $\ell_2(P'_0) < 0$. Moreover, $\Pi_2 \cap Q'_3P'_7S'_0 = Q'_3P'_7$ is an edge of $Q'_3P'_7S'_0$.

We have thus proved that every pair of faces in Φ is separated, allowing us to conclude that f is an embedding.

6.5.2 Rectangular case where $\tau < \sqrt{3}$

Arguments similar to those for the square case show that the PL realization described in Section 6.2.2 is isometric. Since our construction has a symmetry by rotation of angle π about the z axis, we only need to prove the existence of a separating plane for the images of each pair of faces in the triangular region $S_1S_3S_0$. The details of the proof
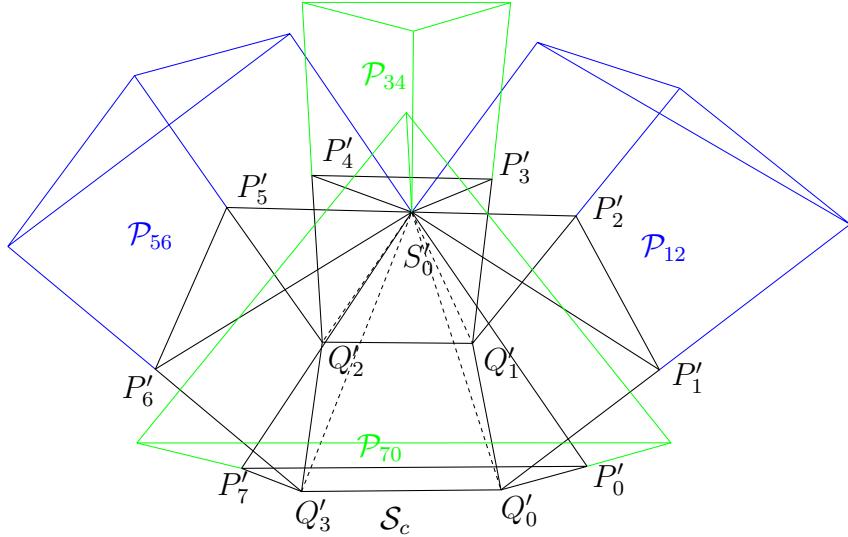
Figure 71: Realization of the black central rectangle with $\tau < \sqrt{3}$. In this case, the half-prisms $\mathcal{P}_{12}, \mathcal{P}_{56}$ (in blue) and $\mathcal{P}_{34}, \mathcal{P}_{70}$ (in green) generated by the four triangular boundaries do not intersect except at the image of the singularity, and only intersect the central sphere $\mathcal{S}_c$ at their common boundary.

are provided in Appendix B. Hence, in all case, the central sphere corresponding to the central rectangle is isometrically embedded.

It remains to show that, in the case $\tau < \sqrt{3}$, it is possible to glue the peripheral parallelograms without creating intersection. The following discussion is devoted to show this fact, summarizing in Proposition 14.

Proposition 14. *Let $\tau < \sqrt{3}$. Then every translation surface Σ in $\mathcal{H}(2)$, admitting a L decomposition with a central rectangle of aspect ratio τ and long enough peripheral parallelogram, has a PL isometric embedding in $\mathbb{R}^3$. Moreover, one can fix a triangulation of the underlying genus 2 topological surface S_2 that realizes all such surfaces.*

The central sphere $\mathcal{S}_c$ is bounded by its four boundary triangles $\partial S_0' P_1' P_2'$, $\partial S_0' P_3' P_4'$, $\partial S_0' P_5' P_6'$, and $\partial S_0' P_7' P_0'$. We consider each of these triangles as the initial cross-section of respective (semi-infinite) right prisms $\mathcal{P}_{12}, \mathcal{P}_{34}, \mathcal{P}_{56}$ and $\mathcal{P}_{70}$. We assume that the prisms extend infinitely from their initial cross-section in the direction opposite to the central sphere. We want to show that the central sphere and the four prisms only intersect at their common boundary points. Thanks to the symmetry of our construction it is enough to check that (see Figure 71)

1. $\mathcal{S}_c$ and $\mathcal{P}_{70}$ intersect along their common boundary $\partial S_0' P_7' P_0'$,

2. $\mathcal{S}_c$ and $\mathcal{P}_{12}$ intersect along their common boundary $\partial S_0' P_1' P_2'$,

3. The intersections $\mathcal{P}_{12} \cap \mathcal{P}_{56}$, $\mathcal{P}_{34} \cap \mathcal{P}_{70}$ and $\mathcal{P}_{12} \cap \mathcal{P}_{70}$ are each reduced to the point S_0'.

Hence, it becomes possible to cut, bend and join $\mathcal{P}_{12}$ and $\mathcal{P}_{56}$ away from $\mathcal{S}_c$ and from the two other prisms to form one of the peripheral cylinders, and similarly for $\mathcal{P}_{34}$ and $\mathcal{P}_{70}$.

1. $\mathcal{S}_c$ and $\mathcal{P}_{70}$ intersect along their common boundary $\partial S_0' P_7' P_0'$. It is enough to show that the plane $(S_0' P_7' P_0')$ separates $\mathcal{S}_c$ from the interior of $\mathcal{P}_{70}$ with $(S_0' P_7' P_0') \cap \mathcal{S}_c = (S_0' P_7' P_0') \cap \mathcal{P}_{70} = \partial S_0' P_7' P_0'$. An equation for $(S_0' P_7' P_0')$ is given by $\ell_3(x, y, z) = 0$ with

$$\ell_3(x, y, z) = 2x \sin \theta_0 - z\sqrt{3 - 4\sin^2 \theta_0}.$$

We just need to check that all the vertices of $\mathcal{S}_c$, except S_0', P_7' and P_0', strictly lie on the same side of $(S_0' P_7' P_0')$ since, by definition, $\mathcal{P}_{70}$ lies on the other side of this plane. We actually prove that for $1 \leq \tau < \sqrt{3}$ we have $\ell_3(X) > 0$ for $X \in \{P_1', P_2', P_3', P_4', P_5', P_6', Q_0', Q_1', Q_2', Q_3'\}$.

- **Proof that $\ell_3(X) > 0$ for $X \in \{Q_0', Q_1', Q_2', Q_3'\}$.** We have from Section 6.2.2:

$$Q_0' = \frac{b}{2}(\tau, 1, -\sqrt{3(1 + \tau^2)}) \qquad\qquad Q_1' = \frac{b}{2}(-\tau, 1, -\sqrt{3(1 + \tau^2)})$$

$$Q_2' = \frac{b}{2}(-\tau, -1, -\sqrt{3(1 + \tau^2)}) \qquad\qquad Q_3' = \frac{b}{2}(\tau, -1, -\sqrt{3(1 + \tau^2)})$$

Using (6.6), we compute

$$\ell_3(Q_0')\ell_3(Q_2') = b^2 \left(3(1 + \tau^2)(\frac{3}{4} - \sin^2 \theta_0) - \tau^2 \sin^2 \theta_0 \right) = 3b^2 \frac{2\tau^4 + 3\tau^2(1 + \sqrt{1 + \tau^2})}{3 + 4\tau^2}$$

It immediately follows that $\ell_3(Q_0')\ell_3(Q_2')$ is strictly positive for any $\tau > 0$. We infer that $\ell_3(Q_0') + \ell_3(Q_2') = b\sqrt{3(1 + \tau^2)(3 - 4\sin^2 \theta_0)}$ has the same sign as $\ell_3(Q_0')$ and $\ell_3(Q_2')$, implying that this sign is positive.

Now, we have $\ell_3(Q_3') = \ell_3(Q_2')$ and $\ell_3(Q_1') = \ell_3(Q_0')$, so that $\ell_3(Q_i')$ is positive for $i = 0, 1, 2, 3$.

- **Proof that $\ell_3(X) > 0$ for $X \in \{P_3', P_4'\}$.** Recall from (6.8) and (6.9) that

$$P_3' = b \left(-\cos \theta_0 \cos \varphi_0, \frac{1}{2}, \sin \theta_0 \right) \qquad \text{and} \qquad P_4' = b \left(-\cos \theta_0 \cos \varphi_0, -\frac{1}{2}, \sin \theta_0 \right).$$

By (6.3), it is easily seen that

$$\cos \theta_0 \cos \varphi_0 = \frac{1}{2}\sqrt{3 - 4\sin^2 \theta_0}. \tag{6.19}$$

We thus compute $\ell_3(P_3') = \ell_3(P_4') = -2b \sin \theta_0 \sqrt{3 - 4\sin^2 \theta_0}$. Since $\sin \theta_0$ is negative, we immediately infer that $\ell_3(P_2')$ is positive.

- **Proof that $\ell_3(X) > 0$ for $X \in \{P_1', P_6'\}$.** We first claim that $0 > \sin \theta_0 > \sin \theta_1$ for $\tau > 1$. From (6.6) and (6.7) this is equivalent to

$$(2\tau^2 - 3\sqrt{1 + \tau^2})(4 + 3\tau^2) > (2 - 3\tau\sqrt{1 + \tau^2})(3 + 4\tau^2).$$

After expanding and regrouping this is equivalent to

$$6(\tau^4 - 1) > 3\sqrt{1 + \tau^2}(4 - 3\tau + 3\tau^2 - 4\tau^3).$$

The last inequality is trivially true since the left hand side is positive while the right hand side is negative as can be seen by factoring $4-3\tau+3\tau^2-4\tau^3 = (1-\tau)(4\tau^2+\tau+4)$. This proves the claim. Now, recalling from Section 6.2.2 that

$$P_1' = a\left(\frac{1}{2}, \cos\theta_1\cos\varphi_1, \sin\theta_1\right) \qquad \text{and} \qquad P_6' = a\left(\frac{1}{2}, -\cos\theta_1\cos\varphi_1, \sin\theta_1\right),$$

we compute $\ell_3(P_1') = \ell_3(P_6') = a(\sin\theta_0 - \sin\theta_1\sqrt{3-4\sin^2\theta_0})$. By the above claim, this is larger than $a\sin\theta_0(1 - \sqrt{3-4\sin^2\theta_0})$. Dividing Equation (6.4) by b, we obtain

$$\frac{3}{2} + \sqrt{3(1+\tau^2)}\sin\theta_0 - \frac{\tau}{2}\sqrt{3-4\sin^2\theta_0} = 0. \tag{6.20}$$

Together with (6.6), we deduce

$$\frac{1}{2}\sqrt{3-4\sin^2\theta_0} = \frac{3}{2}\tau\frac{1+2\sqrt{1+\tau^2}}{3+4\tau^2}. \tag{6.21}$$

It easily follows that $\sqrt{3-4\sin^2\theta_0} > 1$ for any $\tau \geq 1$. We deduce that $\sin\theta_0(1 - \sqrt{3-4\sin^2\theta_0})$ is positive, and in turn $\ell_3(P_1')$ and $\ell_3(P_6')$ are positive.

- **Proof that $\ell_3(X) > 0$ for $X \in \{P_2', P_5'\}$.** From (6.11) and (6.12):

$$P_2' = a\left(-\frac{1}{2}, \cos\theta_1\cos\varphi_1, \sin\theta_1\right) \qquad \text{and} \qquad P_5' = a\left(-\frac{1}{2}, -\cos\theta_1\cos\varphi_1, \sin\theta_1\right).$$

Since the first and third coordinates of P_2' and of P_5' are negative, and since their multiplicative coefficients in ℓ_3 are also negative it ensues that $\ell_3(P_2')$ and $\ell_3(P_5')$ are positive.

2. $\mathcal{S}_c$ and $\mathcal{P}_{12}$ intersect along their common boundary $\partial S_0'P_1'P_2'$. As opposed to $(S_0'P_7'P_0')$, the plane $(S_0'P_1'P_2')$ is not a supporting plane of $\mathcal{S}_c$ for some $1 \leq \tau < \sqrt{3}$. It is however a supporting plane of $\mathcal{P}_{12}$, as are the planes $(S_0'Q_0'P_1')$ and $(S_0'P_2'Q_1')$. We thus show that each face of $\mathcal{S}_c$ is separated from (the relative interior of) $\mathcal{P}_{12}$ by one of these planes and intersects this separating plane along a possibly void subset of $\partial S_0'P_1'P_2'$. By the symmetry of our construction with respect to the yz-plane, it is enough to prove that the triangles $S_0'Q_0'P_0'$, $S_0'P_7'Q_3'$, $S_0'Q_3'P_6'$, $S_0'P_5'Q_2'$ and the quadrangles $P_0'Q_0'Q_3'P_7'$ and $P_6'Q_3'Q_2'P_5'$ are separated from $\mathcal{P}_{12}$ by either $(S_0'P_1'P_2')$ or $(S_0'Q_0'P_1')$, and that the intersections of these faces with their separating plane is contained in $\partial S_0'P_1'P_2'$. Let $\ell_4 = 0$ and $\ell_5 = 0$ be respective equations for the planes $(S_0'P_1'P_2')$ and $(S_0'Q_0'P_1')$, such that $\mathcal{P}_{12}$ lies in $\{\ell_4 \leq 0\} \cap \{\ell_5 \leq 0\}$. The required separation conditions now reduce to

1. $\ell_4(X) > 0$ for $X \in \{Q_0', Q_1', Q_2', Q_3', P_5', P_6'\}$,

2. $\ell_5(X) > 0$ for $X \in \{Q_3', P_0', P_7'\}$

We easily compute an equation for $(S_0'P_1'P_2')$:

$$\ell_4(x, y, z) = 2y\sin\theta_1 - z\sqrt{3-4\sin^2\theta_1}$$

123

and an equation for $(S_0'Q_0'P_1')$: $\ell_5(x, y, z) = c_x' x + c_y' y + c_z' z$, with

$$c_x' = \sqrt{3}$$

$$c_y' = -\tau \sin \theta_1 - \frac{\sqrt{3(1 + \tau^2)}}{2} = -\sqrt{3}\frac{\tau + 2\sqrt{1 + \tau^2}}{4 + 3\tau^2}$$

$$c_z' = \frac{\tau\sqrt{3 - 4\sin^2\theta_1} - 1}{2} = \frac{3\tau\sqrt{1 + \tau^2} - 2}{4 + 3\tau^2}$$

- Since $P_1'Q_0'$ and $P_2'Q_1'$ are orthogonal to the plane $(S_0'P_1'P_2')$, we easily infer

$$\ell_4(Q_1') = \ell_4(Q_0') = \sqrt{3}|P_1'Q_0'| = \sqrt{3}|P_2'Q_1'| = b\sqrt{3} > 0.$$

- $\ell_4(Q_3') = \ell_4(Q_2') = \frac{b}{2}(\sqrt{3(1 + \tau^2)}\sqrt{3 - 4\sin^2\theta_1} - 2\sin\theta_1)$. This quantity is positive since $\sin\theta_1$ is negative for $1 \le \tau < \sqrt{3}$.

- From (6.3) we get $\cos\theta_1 \cos\varphi_1 = \frac{1}{2}\sqrt{3 - 4\sin^2\theta_1}$. Using this equality to express the coordinates of P_5' and P_6', we compute
$\ell_4(P_5') = \ell_4(P_6') = -2a\sin\theta_1\sqrt{3 - 4\sin^2\theta_1}$. This is again positive for the same reason as above.

Concerning the plane $(S_0'Q_0'P_1')$, we compute

- $\ell_5(Q_3') = b\sqrt{3}\dfrac{\tau + 2\sqrt{\tau^2 + 1}}{3\tau^2 + 4}$. This is clearly positive for $\tau \ge 1$.

- $\ell_5(P_0') = \dfrac{\sqrt{3}b}{2}\dfrac{q_0(\tau)}{(3 + 4\tau^2)(4 + 3\tau^2)}$ where, using that $1 \le \tau^2 < 3$,

$$q_0(\tau) = 4\tau\left(2\sqrt{1 + \tau^2}\left(3\tau^2 - \tau + 3\right) - \tau\left(1 + \tau\right)\right)$$
$$> 4\tau\left(2\sqrt{2}(6 - \sqrt{3}) - \sqrt{3}(1 + \sqrt{3})\right) > 0$$

- Finally, we have $\ell_5(P_0') - \ell_5(P_7') = bc_y'$. Since c_y' is negative, it follows that $\ell_5(P_7') = \ell_5(P_0') - bc_y' > \ell_5(P_0') > 0$.

3. The right prisms pairwise intersect at S_0' only. Thanks to the symmetry of the construction with respect to the xz-plane and yz-plane we only need to check that $\mathcal{P}_{12} \cap \mathcal{P}_{56}$, $\mathcal{P}_{34} \cap \mathcal{P}_{70}$ and $\mathcal{P}_{12} \cap \mathcal{P}_{70}$ are each reduced to the point S_0'.

- To see that $\mathcal{P}_{12} \cap \mathcal{P}_{56} = \{S_0'\}$, it is enough to exhibit a separating plane Π so that

  - the initial cross-sections $S_0'P_1'P_2'$ and $S_0'P_5'P_6'$ of respectively $\mathcal{P}_{12}$ and $\mathcal{P}_{56}$ are contained in the (open) opposite half-spaces bounded by Π, except for their common vertex S_0' contained in Π,

  - the normals to the initial cross-sections, in the direction opposite to $\mathcal{S}_c$, are contained in the vectorial counterpart of the corresponding opposite half-spaces.

These conditions are easily satisfied by taking for Π the xz-plane.

- An analogous verification applies to $\mathcal{P}_{34} \cap \mathcal{P}_{70}$ using the yz-plane for Π.

- For the last case concerning $\mathcal{P}_{12} \cap \mathcal{P}_{70}$ we set $\Pi = (S_0'Q_0'P_1')$. Its equation is given by $\ell_5 = 0$. We already checked that $\ell_5(P_0')$ and $\ell_5(P_7')$ are positive. Let $n_{70} = \frac{1}{b}S_0'P_7' \wedge S_0'P_0' = (-\sin\theta_0, 0, \cos\theta_0\cos\varphi_0)$ be a normal to $(S_0'P_7'P_0')$ directed outside $\mathcal{S}_c$. We compute

$$\ell_5(n_{70}) = -\sin\theta_0\sqrt{3} + \cos\theta_0\cos\varphi_0 \frac{3\tau\sqrt{1+\tau^2}-2}{4+3\tau^2}.$$

Using (6.6), (6.19) and (6.21), we obtain

$$
\begin{aligned}
\ell_5(n_{70}) &= -\frac{3}{2}\frac{2\tau^2 - 3\sqrt{1+\tau^2}}{3+4\tau^2} + \frac{3}{2}\tau\frac{1+2\sqrt{1+\tau^2}}{3+4\tau^2}\frac{3\tau\sqrt{1+\tau^2}-2}{4+3\tau^2} \\
&= \frac{3}{2}\frac{(3\sqrt{1+\tau^2}-2\tau^2)(4+3\tau^2)+\tau(1+2\sqrt{1+\tau^2})(3\tau\sqrt{1+\tau^2}-2)}{(3+4\tau^2)(4+3\tau^2)} \\
&= 3\frac{2\sqrt{1+\tau^2}(3\tau^2 - \tau + 3) - \tau^2 - \tau}{(3+4\tau^2)(4+3\tau^2)} \\
&> 3\frac{2\tau(3\tau^2 - \tau + 3) - \tau^2 - \tau}{(3+4\tau^2)(4+3\tau^2)} = 3\frac{\tau(6\tau^2 - 3\tau + 5)}{(3+4\tau^2)(4+3\tau^2)} > 0
\end{aligned}
$$

It ensues that $\mathcal{P}_{70} \setminus \{S_0'\}$ is contained in the half-space $\{\ell_5 > 0\}$.

We now check that $\mathcal{P}_{12}$ is contained in the closed half-plane $\{\ell_5 \le 0\}$. This will allow us to conclude that $\mathcal{P}_{12}$ and $\mathcal{P}_{70}$ indeed intersect at S_0' only. First note that $\ell_5(P_1') = 0$ since $P_1' \in \Pi$. Next, we have

$$\ell_5(P_2') = a\left(-\frac{1}{2}c_x' - \cos\theta_1\cos\varphi_1 c_y' + \sin\theta_1 c_z'\right).$$

Since c_x' and c_z' are positive, while c_y is negative, we immediately infer that $\ell_5(P_2')$ is negative. The triangle $S_0'P_1'P_2'$ thus satisfies $\ell_5 \le 0$. Finally, since $S_0'P_1'P_2'$ is normal to the plane $(S_0'Q_0'P_1')$, the prism $\mathcal{P}_{12}$ is indeed contained in $\{\ell_5 \le 0\}$.

6.6 The Nguyen's moves on L decompositions

In [Ngu14], Nguyen exhibits a group Γ that acts on L decompositions of surfaces of $\mathcal{H}(2)$ with the property that the L decompositions in a same Γ orbit correspond to a same flat surface. Γ is generated by three elements T, S, R. They correspond to gluing and pasting of the initial L decomposition.

Let (Σ, ω) be a flat surface of genus 2 with one singularity, and denote by S_2 the underlying topological surface. Fix a basis $\mathcal{B} = (\alpha_1, \alpha_2, \alpha_3, \alpha_4)$ of $\pi_1(S_2)$, and denote $\Phi_{\mathcal{B}}(\omega) = (z_1, z_2, z_3, z_4)$ the periods of ω on the basis $\mathcal{B}$ as in Section 2.7.2.

First we have to make precise the notion of L decomposition. Let z_1, z_2, z_3, z_4 denote four complex numbers such that the "cross products" $\Im(\bar{z}_1 z_2), \Im(\bar{z}_2 z_3), \Im(\bar{z}_3 z_4)$ are strictly positive. In particular, the parallelograms $\mathrm{Conv}(0, z_1, z_2, z_1 + z_2), \mathrm{Conv}(0, z_2, z_3, z_2 +$
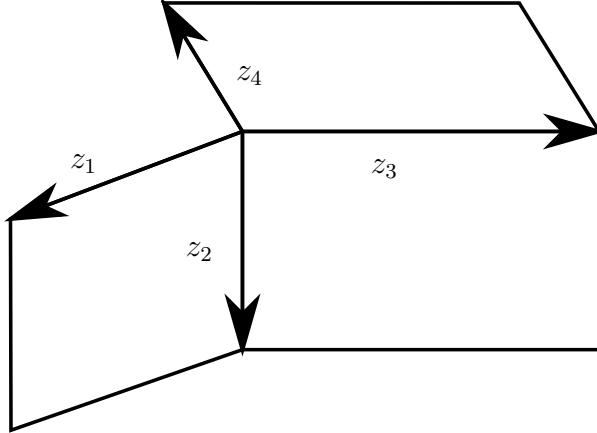
Figure 72: L shape pattern $\mathcal{L}(z_1, z_2, z_3, z_4)$ associated to four complex numbers z_1, z_2, z_3, z_4 defining three non degenerated non overlapping parallelograms. The gluing of this polygon along parallel edges results in a surface in $\mathcal{H}(2)$.

z_3), $\mathrm{Conv}(0, z_3, z_4, z_3 + z_4)$ are non degenerate. Gluing the sides corresponding to z_2 and z_3, one obtains a L shape denoted $\mathcal{L}(z_1, z_2, z_3, z_4)$. This L shape defines a flat surface of genus 2 in $\mathcal{H}(2)$ by gluing its parallel sides - see Figure 72.

We now explain the T, S and R moves. T is defined by

$$T(\mathcal{L}(z_1, z_2, z_3, z_4)) = \mathcal{L}(z_1, z_2, z_3, z_3 + z_4),$$

see Figure 73. While S is defined by

$$S(\mathcal{L}(z_1, z_2, z_3, z_4)) = \mathcal{L}(-z_4, z_3, -z_2, z_1),$$

see Figure 74. Finally,

$$R(\mathcal{L}(z_1, z_2, z_3, z_4)) = \mathcal{L}(z_1, -z_1 + z_2 + z_3, z_3, z_4)$$

which is only possible in certain cases, cf Figure 75. As we can obtain the images of each move by cutting and pasting the initial L shape, they define indeed the same flat surface. Let us look closer at the R move. This move is only possible if the segment joining the extremities of z_3 and z_1 lies inside the $\mathcal{L}(z_1, z_2, z_3, z_4)$ for the cutting and pasting to be feasible. The limit case of possible patterns is thus when the segment joining these extremities passes through the extremity of z_2, which corresponds to the case where $z_1 - z_3$ is proportional to $z_2 - z_3$. The R move possible cases correspond then to the situation where $z_1 - z_3$ points above the direction of $z_2 - z_3$ in Figure 72, or in short when $\Im((\overline{z_1 - z_3})(z_2 - z_3)) \geq 0$. We claim that, given z_1, z_2, z_3, z_4, there always exists a L shape pattern $\mathcal{L}$ that is $< S, T >$-equivalent to $\mathcal{L}(z_1, z_2, z_3, z_4)$ such that the R move is feasible on $\mathcal{L}$. Indeed, we compute $(ST^k) \cdot \mathcal{L}(z_1, z_2, z_3, z_4) = \mathcal{L}(-z_4 - kz_3, z_3, -z_2, z_1) =: \mathcal{L}(z'_1, z'_2, z'_3, z'_4)$ and we have $\Im((\overline{z'_1 - z'_3})(z'_2 - z'_3)) = (k+1)\Im(\bar{z}_2 z_3) - \Im(\bar{z}_3 z_4) + \Im(\bar{z}_4 z_2)$ which becomes positive for all k great enough as $\Im(\bar{z}_2 z_3) > 0$.

Nguyen showed that every two L decompositions of the same translation surface are related by a move in $\Gamma = < T, S, R >$.

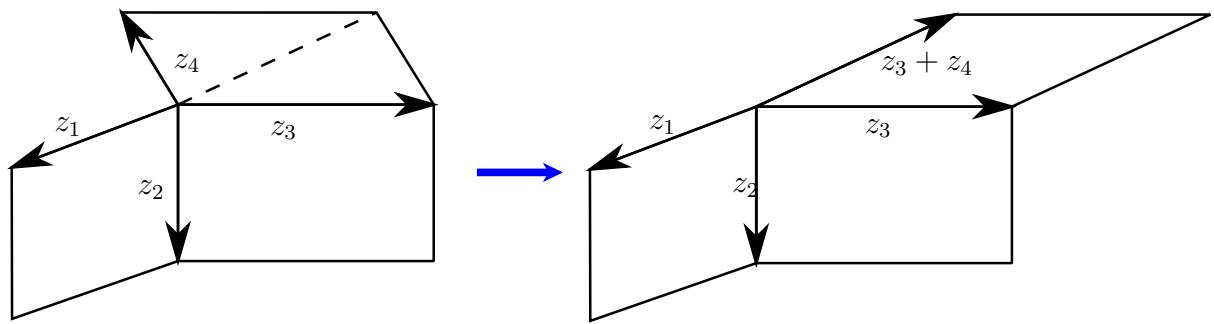This moves permit to understand better the realization space for our constructions.
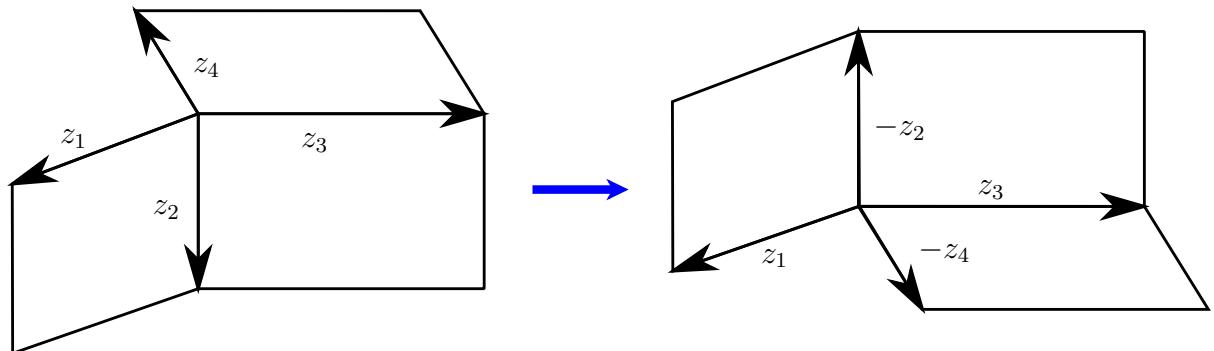
126

Figure 73: The T move.
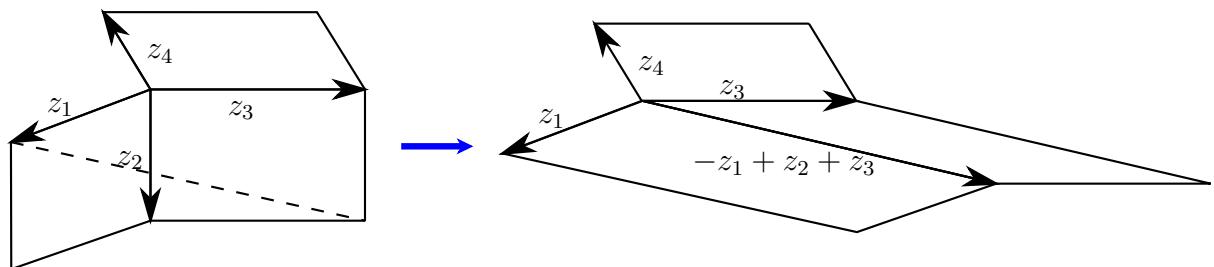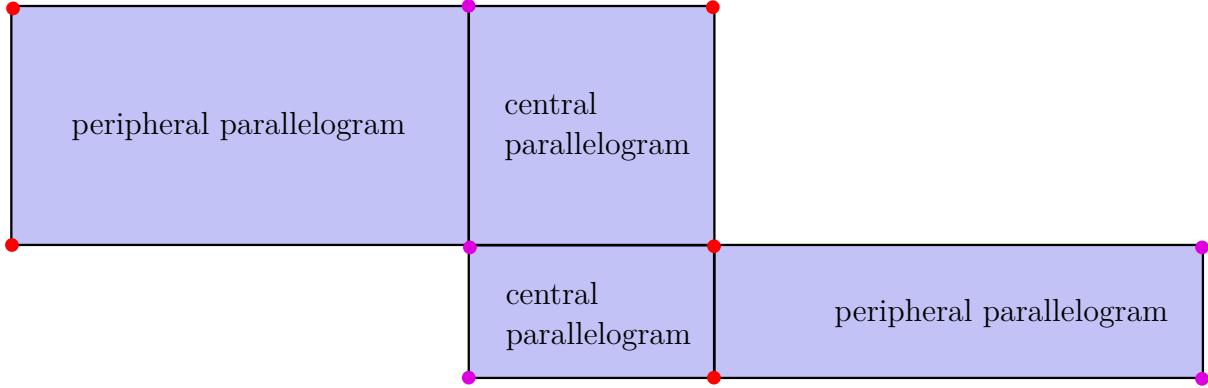

Figure 74: The S move.

Figure 75: The R move.

Figure 76: Z decomposition of a surface in $\mathcal{H}(1,1)$. Singularities are in red and purple.

6.7 The case of surfaces in $\mathcal{H}(1,1)$

We now give the ideas to adapt the previous method in the case of a surface in $\mathcal{H}(1,1)$.

As we saw in Section 2.7.3, every surface in $\mathcal{H}(1,1)$ can be obtained by gluing two slitted flat tori as explained in Figure 15. We use a slightly different viewpoint. Refer to Figure 76. Cutting out the two peripheral parallelograms from the surface, there remains the two central parallelograms which form a topological sphere with four boundary components. Based on our experience with surfaces of $\mathcal{H}(2)$, we can use a similar approach. First we find a PL and isometric realization of this central sphere in $\mathbb{R}^3$, with equilateral triangular boundaries. Then, we embed the two remaining peripheral parallelograms as part of bent and twisted right prism in order to glue them on the boundaries of the sphere.

We only sketch of the construction.

Consider the triangulation of the two central parallelograms depicted in Figure 77, and we refer to this Figure 77 for the naming of the vertices. We suppose the central parallelogram to be rectangles. This triangulation can be realized in $\mathbb{R}^3$ the following way, see Figure 78. Denote S_1 and S_2 the two singularities. We send S_1 to the origin Ω of $\mathbb{R}^3$. Note that, by adding the Q_i's, we obtain a prism with apex S_1. Realize this prism in the half-space $\{z \geq 0\}$ so that the axis Ωz is a symmetry axis, and denote θ the angle between Ωz and $\Omega Q_0'$, where Q_0' is the image of Q_0 in $\mathbb{R}^3$. We then send S_2 at height $a + 2a\sin\theta$ on the Ωz axis, and we build the symmetric construction for S_2 and the P_i's. It remains to paste the topological cylinder made by the Q_i's and P_i's to obtain an isometric realization of the two central parallelograms, which is an embedding. Figure 79 shows an example.

Nevertheless, the central axis of the four triangular boundaries are directed so that the four branches continuing the boundaries intersect pairwise as shown in Figure 79. In order to avoid such intersections, we can apply gaskets on each branch. This way, we can realize the two remaining peripheral parallelograms as shown in Figure 80 and Figure 81.
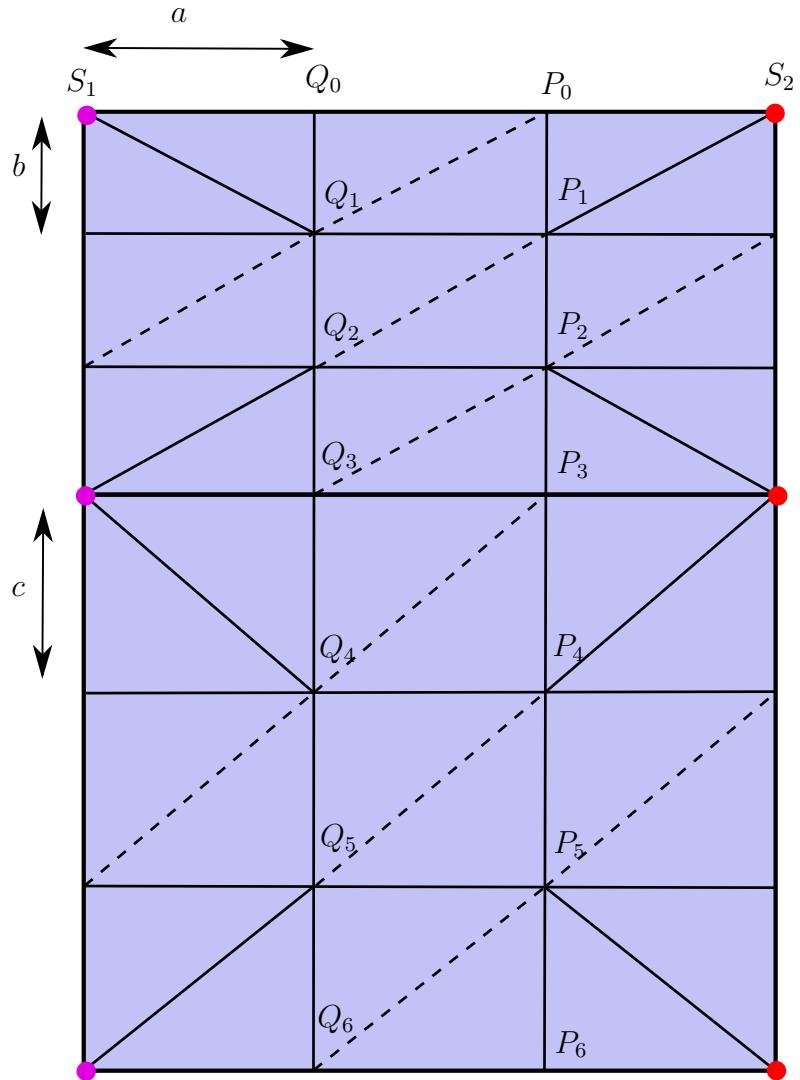
Figure 77: Triangulation of the two central parallelograms that can be used to infer a realization as a PL sphere with four triangular boundaries.
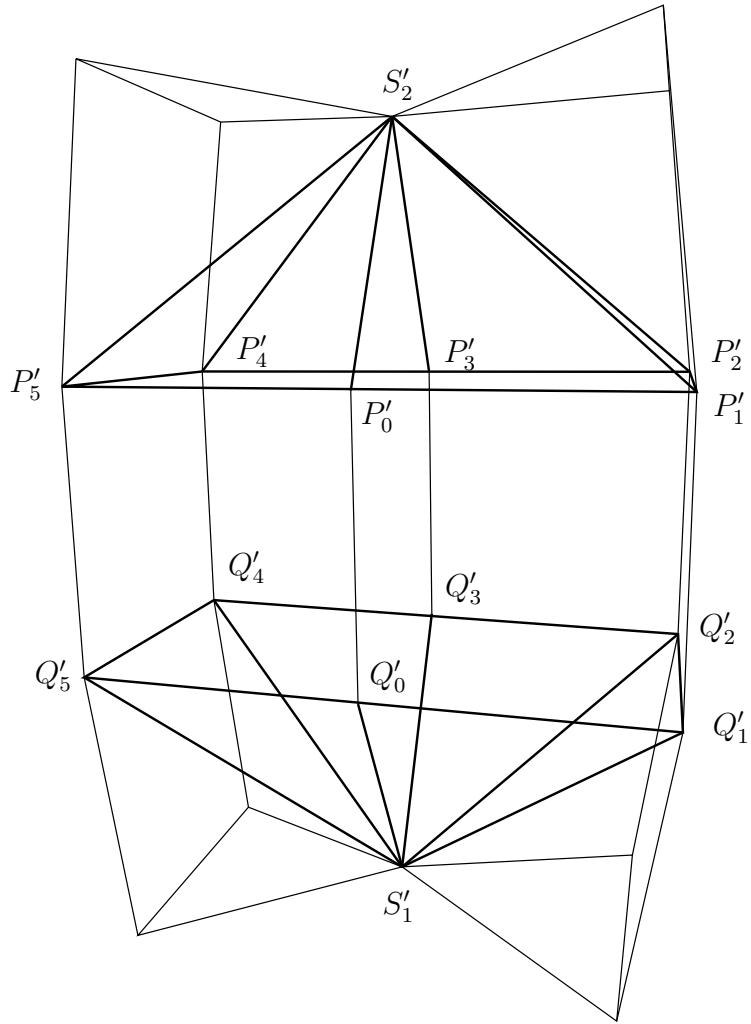
Figure 78: Scheme of our construction. $S_1' * Q_0'Q_1'Q_2'Q_3'Q_4'Q_5'$ and $S_2' * P_0'P_1'P_2'P_3'P_4'P_5'$ form symmetric conical prisms. The Q_i' and P_j' make a right prism.
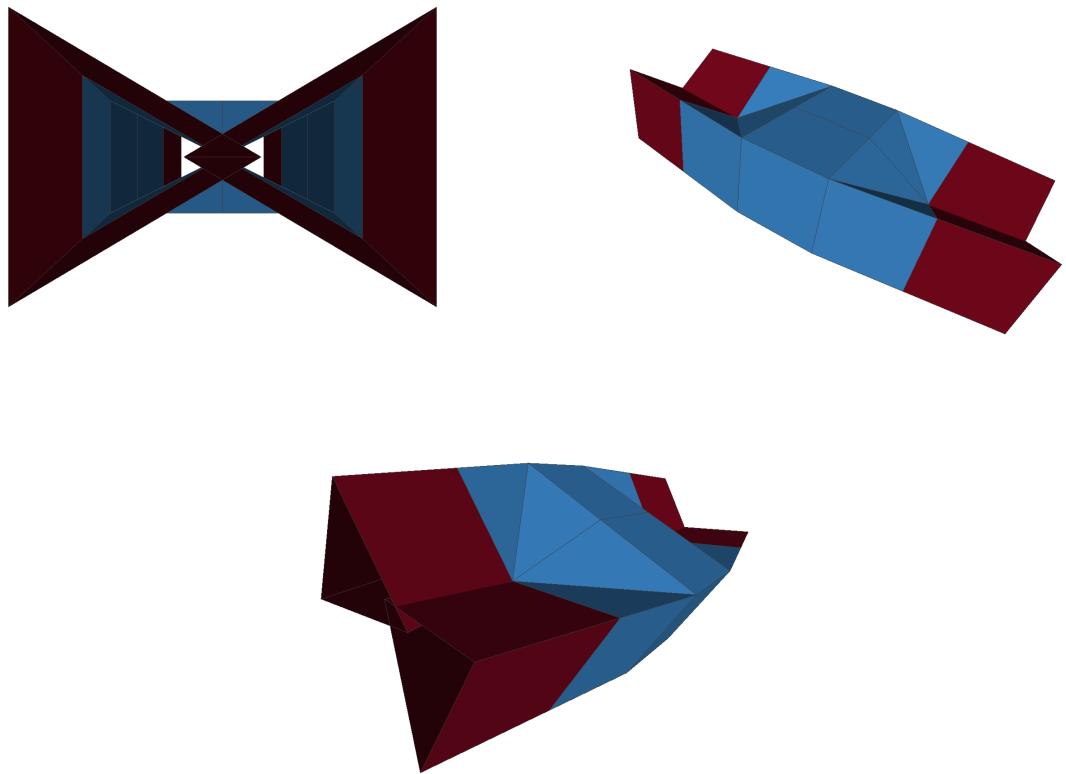
Figure 79: Our isometric embedding (in blue) of the two central rectangles of a surface in $\mathcal{H}(1,1)$. Here, the red orthogonal continuation of the four boundaries intersect. Gaskets can be made to avoid them.
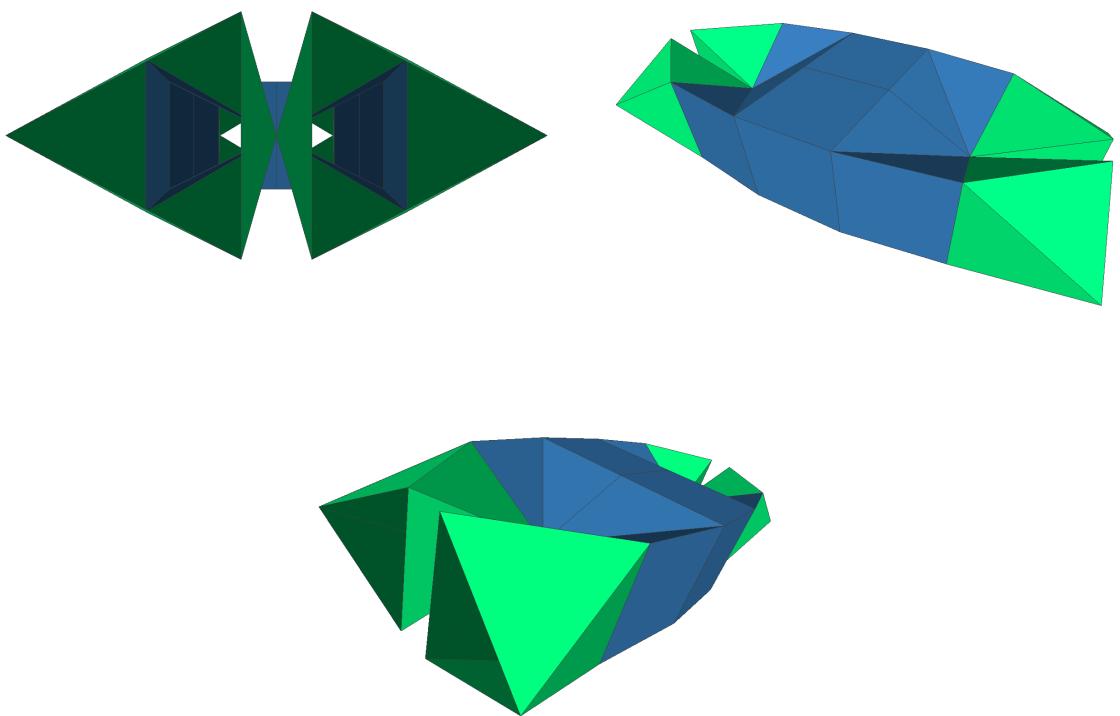
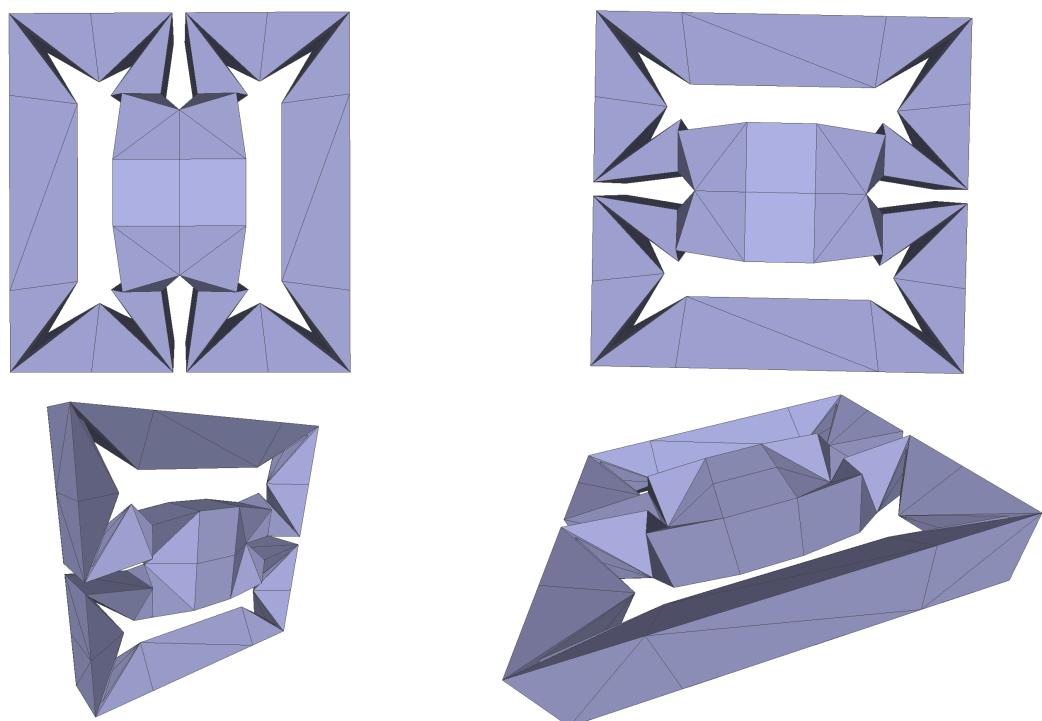Figure 80: Gaskets are applied on the construction to avoid intersections on the four branches.

Figure 81: The final isometric embedding of a surface in $\mathcal{H}(1, 1)$.

Conclusion

We showed three results in this thesis. To conclude, we recall the description of each one, and we indicate open questions related to it if any.

Effective implementation of the method of Burago and Zalgaller

Though the procedure of Burago and Zalgaller allows to embed PL isometrically any polyhedral surface, it relies on the non constructive Nash-Kuiper process. Nonetheless, in the case of flat tori, the different steps of the method of Burago and Zalgaller described in 3.2 greatly simplify. Indeed, as flat tori present no singularity, we can take $U = U_{>2\pi} = \emptyset$ in 3.2. Next, one can compute easily an acute triangulation of a flat torus, and even an almost equilateral one. Then, by the articles [Pin85] and [Ban88], one can find conformal embeddings of a given flat torus. It remains to apply the elementary construction described in the first paragraph of Section 3.2 to obtain the desired PL isometric embedding.

Universal triangulation for flat tori

In order to obtain some uniformity in the previous realizations, we asked if it is possible to realize all flat tori with a bounded number of vertices. As, for $N \in \mathbb{N}$, there are only finitely many combinatorial triangulation of the torus with at most N vertices, the existence of such realizations amounts to the existence of a fixed combinatorial triangulation $\mathcal{T}$ that is **universal**. In turn, a **universal triangulation** $\mathcal{T}$ for the moduli space $\mathcal{M}_1$ of flat tori is a combinatorial triangulation of the torus, which admits for each $\tau \in \mathcal{M}_1$ a geometric realization that is isometric to $\mathbb{T}_\tau$ and that is linear in restriction to each triangle of $\mathcal{T}$.

    We give a constructive proof for the existence of a universal triangulation of flat tori. We chose to rely on two constructions. The first one is a construction due to Zalgaller that allows to realize all long enough flat torus. By a precise study of the construction, we were able to conclude that all modulus with imaginary part greater or equal to 33 is realizable thanks to this construction. It remained to find models for the complementary of such flat tori in $\mathcal{M}_1$, call it the family of short flat tori. We then rely on the diplotori of Arnoux, Lelièvre and Málaga. We exhibit 3 families of diplotori that cover the family of short flat tori, that we superimpose to obtain a universal triangulation for short tori. The merging of the two previous triangulations gives the desired universal triangulation for $\mathcal{M}_1$.

Some problems naturally occur with the existence of such a universal triangulation for flat tori.

The first one, the most natural, is the size - in terms of vertices - of a minimal universal triangulation for $\mathcal{M}_1$. By Theorem 5, it is less or equal to 2434. To our knowledge, the only lower bound is 7 and comes from the fact that it is the size of a minimal simplicial triangulation of the torus. There exists PL (not necessarily isometric) embeddings realizing this triangulation, such as the Császár torus, which were studied by Bokowski and Eggert. Again, to our knowledge, it is not even known what is the minimal number of vertices that realize a fixed torus.

Another open problem is about the connectedness of the realization space for our universal triangulation $\mathcal{T}$. We know that individually, every flat torus of modulus τ can be realized by $\mathcal{T}$, thanks to a PL isometric embedding f_τ linear on each triangle of $\mathcal{T}$. But, given $\tau, \tau' \in \mathcal{M}_1$, is it possible to continuously deform f_τ so as to obtain $f_{\tau'}$ and staying a PL isometric embedding during the process? More formally, is there an isotopoy H such that $H(0, \cdot) = f_\tau, H(1, \cdot) = f_{\tau'}$ and $H(t, \cdot)$ is a PL isometric embedding for all t. The answer seems to be yes for $\Im\tau, \Im\tau' \geq 33$, as Zalgaller's construction seems to allow for such a modularity. Indeed, if a long modulus is given, it suffices to decrease the angle made by the helical twist in order to reach the null angle. That gives a continuous path from any long modulus to some right modulus. It is now easy to reach any modulus by varying the length of the sides of Zalgaller's construction. However, for a long modulus τ and a short modulus τ', the answer is far less clear. It is even not clear if, for two short moduli τ, τ' realized by two distinct families of diplotori, f_τ and f'_τ can be connected. Finally, the last and most interesting question which is linked with our last result, is to know if the existence of universal triangulations can be extended to other moduli spaces. This is the object of the second "part" of this thesis.

PL isometric embeddings of some surfaces in $\mathcal{H}(2)$ and $\mathcal{H}(1,1)$

Comforted by our result in genus 1, we investigated the genus 2 case. We focused on the moduli space $\mathcal{H}_2$ of translation surfaces of genus 2. It decomposes into two strata $\mathcal{H}(2)$ and $\mathcal{H}(1,1)$. We gave models, i.e. PL realizations, for subsets of both $\mathcal{H}(2)$ and $\mathcal{H}(1,1)$, with details of the fact that they realize isometric embeddings in the case of the subset of $\mathcal{H}(2)$. Although our constructions do not realize the entire stratum $\mathcal{H}(2)$ (nor $\mathcal{H}(1,1)$), they realize, for $h > 0$ big enough, an open neighborhood of the family $\mathcal{L}^{rect}_{\geq h}$ of translation surfaces in $\mathcal{H}(2)$ that admits an L decomposition with a rectangular central parallelogram and peripheral parallelograms with relative height greater or equal to h. Our models are relatively easy to understand. We first realize the central parallelogram as a PL sphere with four triangular boundaries. Next, we glue the peripheral parallelograms as part of bent and twisted right prisms. We actually propose two realizations of the central parallelogram: the first one leads to equilateral boundaries while the second only provides isosceles boundaries. In the former case, we saw that, doing this way, it is possible to realize elements of $\mathcal{L}^{rect}$ whose central rectangle has aspect ratio $\tau < \sqrt{3}$ and long enough peripheral parallelograms. When $\tau \geq \sqrt{3}$, we also show how to realize the corresponding surface of $\mathcal{L}^{rect}$ by introducing bending possibly with negative angle. In the other case

of central parallelogram with isosceles boundaries, we introduced a simple construction that allows to interpolate from an isosceles to an equilateral boundary, leading to other realizations of elements of $\mathcal{L}^{rect}$. In order to circumvent this rigidity, we introduce modular models, at the cost of relaxing the equilateral property of the boundaries while keeping isosceles triangular boundaries.

We have also shown how to deform our constructions of the central spheres to realize skew parallelograms. In the end, we are able to exhibit a single model that allows to realize a reasonably "large" open subset of $\mathcal{H}(2)$.

However, the existence of a universal triangulation for $\mathcal{H}(2)$ (or $\mathcal{H}(1,1)$) still remains open. In particular one should find models to realize surfaces in $\mathcal{H}(2)$ with one (or both) of the peripheral parallelograms arbitrarily short. Note that our approach does not seem to adapt in this case. Indeed, it is always possible to realize the central parallelogram if this latter is close to be right. However, to realize the remaining two peripheral parallelograms, as soon as they are not right, a twist has to be applied in order to shift the boundary of the cylinder before gluing. This twist, as we saw in Section 5.1, requires enough "material" to be realized. This fact - among others - prevent us to realize, with our method, surfaces with too short peripheral parallelograms. To go further, recall though that it is only sufficient to find models that covers a subdomain $\mathcal{R}$ of $\mathcal{H}(2)$ whose complementary region is compact. According to Mumford's compactness criterion, it is thus enough for this complementary region that the saddle connections, corresponding to some period coordinates, have upper and lower bounded lengths. Indeed, the constructions in the theorem of PL isometric embedding Burago and Zalgaller allows for some flexibility for $\mathcal{H}(2)$. Hence we can cover the compact complementary region of $\mathcal{R}$ by open subsets, each realized by a fixed triangulation. By compactness, we can select a finite number of such open sets to cover the complementary region. Overlaying all these triangulations, and the one for $\mathcal{R}$, would thus result in a universal triangulation for $\mathcal{H}(2)$.

One approach to build a universal triangulation for $\mathcal{R}$, is to rely on some compactification of $\mathcal{H}(2)$ in order to identify "directions" to infinity and, for each of them, to find a single model that realizes it. There are several compactification candidates, such as the Deligne-Mumford compactification, or the more recent WYSIWYG compactification, the Incidence Variety compactification, and the Multi-scale differentials compactification. Identifying a good candidate that leads to a convenient stratification of the boundary of $\mathcal{H}(2)$ so as to structure our efforts seems to be a prerequisite. Up to now, only the case when the sides of the central parallelogram become smaller and smaller, corresponding to longer and longer peripheral parallelograms, has been achieved. A challenging task would be to find models for the case where the sides of the central rectangle remain large, but the peripheral parallelograms become shorter and shorter. To do so, a very useful problem related to this thesis is the problem of PL isometric embedding with given boundary. Given a polyhedral surface Σ with boundary, and a PL isometric embedding $\partial f : \partial \Sigma \to \mathbb{R}^3$ of the boundary of Σ in $\mathbb{R}^3$, can ∂f be extended to the entire Σ into a PL isometric embedding $f : \Sigma \to \mathbb{R}^3$? It is a difficult question which could help in the construction of polyhedral models for large family of surfaces and in particular surfaces in $\mathcal{H}(2)$.

Moreover, obvious generalizations to other strata and genera appear. Such a program, started from a combinatorial problem: to know if an entire moduli space can be realized by a fixed triangulation, and appeared to have deep connection with complex geometry

and analysis that we studied in this document. However, the links with algebraic geometry and dynamics was not fully considered and it would be very interesting to see if some progress can be achieved with such viewpoints.

Appendix A

Proof of Lemma 11

Here, we provide the details for the proof of Lemma 11. From Theorem 10, simple computations show that the region $\mathcal{M}_{19,2}$ is bounded by the following parametrized curves:

- $\lambda_2(t) = z_2 + it$ with $t \in [0, +\infty[$ and $z_2 = \frac{2 - \sin\frac{2\pi}{19}\cot\frac{\pi}{19} + i\sin\frac{2\pi}{19}}{19}$,

- $\beta_{2,1}(t) = \frac{2}{19} - \frac{\sin\frac{2\pi}{19}}{19\sin\frac{\pi}{19}}e^{-it}$ with $t \in [\frac{\pi}{19}, \frac{3\pi}{19}]$,

- $\beta_{2,2}(t) = \frac{2 + i\cot\frac{\pi}{19}}{19} - \frac{e^{i\frac{15\pi}{38}}}{19\sin\frac{\pi}{19}}t$ with $t \in [\cos\frac{16\pi}{19}, \cos\frac{3\pi}{19}]$,

- $\rho_2(t) = w_2 + it$ with $t \in [0, +\infty[$ and $w_2 = \beta_{2,2}\left(\cos\frac{16\pi}{19}\right)$.

While $\mathcal{M}_{19,7}$ is bounded by:

- $\lambda_7(t) = z_7 + it$ with $t \in [0, +\infty[$ and $z_7 = \frac{7 - \sin\frac{7\pi}{19}\cot\frac{\pi}{19} + i\cot\frac{\pi}{19}\left(1 - \cos\frac{7\pi}{19}\right)}{19}$,

- $\beta_{7,1}(t) = \frac{7 + i\cot\frac{\pi}{19}}{19} - \frac{e^{i\frac{5\pi}{38}}}{19\sin\frac{\pi}{19}}t$ with $t \in [\cos\frac{6\pi}{19}, \cos\frac{\pi}{19}]$,

- $\beta_{7,2}(t) = \frac{7}{19} - \frac{\sin\frac{7\pi}{19}}{19\sin\frac{\pi}{19}}e^{-it}$ with $t \in [\frac{6\pi}{19}, \frac{8\pi}{19}]$,

- $\beta_{7,3}(t) = \frac{7 + i\cot\frac{\pi}{19}}{19} - \frac{e^{i\frac{5\pi}{38}}}{19\sin\frac{\pi}{19}}t$ with $t \in [\cos\frac{11\pi}{19}, \cos\frac{8\pi}{19}]$,

- $\rho_7(t) = w_7 + it$ with $t \in [0, +\infty[$ and $w_7 = \beta_{7,3}\left(\cos\frac{11\pi}{19}\right)$.

And $\mathcal{M}_{19,13}$ is bounded by:

- $\lambda_{13}(t) = z_{13} + it$ with $t \in [0, +\infty[$ and $z_{13} = \frac{13 - \sin\frac{13\pi}{19}\cot\frac{\pi}{19} + i\cot\frac{\pi}{19}\left(1 - \cos\frac{13\pi}{19}\right)}{19}$,

- $\beta_{13,1}(t) = \frac{13 + i\cot\frac{\pi}{19}}{19} - \frac{e^{-i\frac{7\pi}{38}}}{19\sin\frac{\pi}{19}}t$ with $t \in [\cos\frac{5\pi}{19}, \cos\frac{\pi}{19}]$,

- $\rho_{13}(t) = w_{13} + it$ with $t \in [0, +\infty[$ and $w_13 = \beta_{13,1}\left(\cos\frac{5\pi}{19}\right)$.
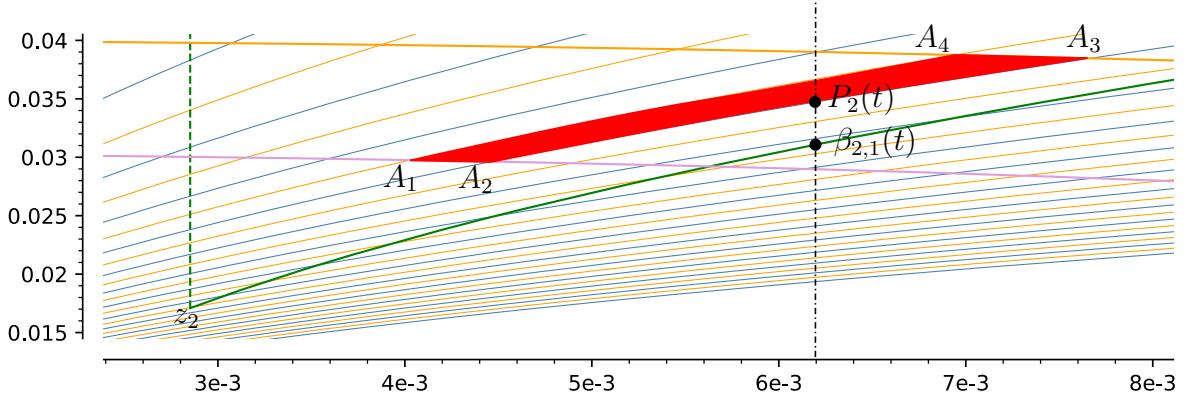
Figure 82: The red quadrilateral $A_1A_2A_3A_4$.

In the sequel we denote by $\mathcal{B}(z,r)$ the closed disk of radius r centered at z and by $\mathcal{C}(z,r)$ its boundary circle. Recall that each $g_\delta : z \mapsto \frac{1}{-z+\delta}$ sends the horizontal line $\{\Im(z) = h\}$ onto the circle $\mathcal{C}\left(\frac{i}{2h}, \frac{1}{2h}\right)$. Furthermore, for $\delta \geq 1$, g_δ sends the imaginary axis onto the circle $\mathcal{C}\left(\frac{1}{2\delta}, \frac{1}{2\delta}\right)$, and the line $\{\Re(z) = \frac{1}{2}\}$ onto the circle $\mathcal{C}\left(\frac{1}{2\delta-1}, \frac{1}{2\delta-1}\right)$. We denote the red, blue and yellow slices of $\mathcal{M}_{short}^+$ on Figure 46 by respectively $\mathcal{S}_r, \mathcal{S}_b$ and $\mathcal{S}_y$.

From these facts, we deduce that $g_5(\mathcal{S}_r)$, the image of the red slice by g_5 (see Figure 47), is bounded by four arcs of circles; one form respectively $\mathcal{C}\left(\frac{1}{9}, \frac{1}{9}\right), \mathcal{C}\left(\frac{i}{66}, \frac{1}{66}\right), \mathcal{C}\left(\frac{1}{10}, \frac{1}{10}\right)$ and $\mathcal{C}\left(\frac{i}{50}, \frac{1}{50}\right)$. Similarly, the image $g_3(\mathcal{S}_b)$ of the blue slice is bounded by arcs from the circles $\mathcal{C}\left(\frac{1}{5}, \frac{1}{5}\right), \mathcal{C}\left(\frac{i}{50}, \frac{1}{50}\right), \mathcal{C}\left(\frac{1}{6}, \frac{1}{6}\right)$ and $\mathcal{C}\left(\frac{i}{24}, \frac{1}{24}\right)$. Finally, the image $g_1(\mathcal{S}_y)$ of the yellow slice is bounded by arcs of the circles $\mathcal{C}(1, 1), \mathcal{C}\left(\frac{i}{24}, \frac{1}{24}\right), \mathcal{C}\left(\frac{1}{2}, \frac{1}{2}\right)$ and a segment of the line $\{\Re(z) = \frac{1}{2}\}$. For this last slice, we note that g_1 sends the arc of circle $\{e^{it} \mid \frac{\pi}{3} \leq t \leq \frac{\pi}{2}\}$ to the vertical line segment $\{\frac{1}{2} + it \mid t \in [\frac{1}{2}, \frac{\sqrt{3}}{2}]\}$.

We now proceed to prove that the three curvilinear quadrilaterals $g_5(\mathcal{S}_r), g_3(\mathcal{S}_b)$ and $g_1(\mathcal{S}_y)$ shown in Figure 47 lie above the lower boundary of $\mathcal{M}_{19} := \mathcal{M}_{19,2} \cup \mathcal{M}_{19,7} \cup \mathcal{M}_{19,13}$ - a point lie above another point w with same real part if $\Im(z) \geq \Im(w)$. Let us remark that for showing that such a quadrilateral lies above some boundary, it suffices to show that the bottom side and the right most side of the quadrilateral lie above this boundary as the quadrilateral is completely included in the region of the plane above these two sides.

The red quadrilateral $g_5(\mathcal{S}_r)$ Denote the vertices of this quadrilateral as in Figure 82. From the above description, one computes $A_1 = \frac{6+44i}{1479}, A_2 = \frac{5+33i}{1114}, A_3 = \frac{1+5i}{130}, A_4 = \frac{18+100i}{2581}$. By the previous remark, it is enough to show that the curvilinear sides $\overset{\frown}{A_1A_2}$ and $\overset{\frown}{A_2A_3}$ lie above the lower boundary of $\mathcal{M}_{19}$.

  – Arc $\overset{\frown}{A_1A_2}$.

    The vertical line through $\beta_{2,1}(t)$ cuts $\mathcal{C}\left(\frac{i}{66}, \frac{1}{66}\right)$ (the circle containing $\overset{\frown}{A_1A_2}$) in two points. We denote by $P_1(t)$ the highest of this two points. Remark that $\overset{\frown}{A_1A_2}$

is indeed in the upper half part of $\mathcal{C}\left(\frac{i}{66}, \frac{1}{66}\right)$. We compute $P_1(t) = \frac{i+e^{i\tau}}{66}$ with $0 \leq \tau \leq \pi$, where $\frac{\cos \tau}{66} = \frac{2}{9} - \frac{\sin \frac{2\pi}{19}}{19 \sin \frac{\pi}{19}} \cos t$. Thus:

$$\Im(P_1(t)) = \frac{1 + \sin\tau}{66} \geq \Im(\beta_{2,1}(t)) = \frac{\sin \frac{2\pi}{19}}{19 \sin \frac{\pi}{19}} \sin t$$

$$\Longleftrightarrow \frac{\sin^2 \tau}{66^2} \geq \left(-\frac{1}{66} + \frac{\sin \frac{2\pi}{19}}{19 \sin \frac{\pi}{19}} \sin t\right)^2$$

$$\Longleftrightarrow f_1(\cos t) \geq 0,$$

where

$$f_1(x) := \frac{8x}{361} \cos \frac{\pi}{19} + \frac{2\sqrt{1-x^2}}{627} \cos \frac{\pi}{19} - \frac{6 + 2 \cos \frac{2\pi}{19}}{361}.$$

A study of f_1 shows that it is non negative on $[0.96, 1]$, so that $f_1(\cos t)$ is non negative for $t \in [0, t_{red}^1 := 0.283]$. Note that $0 < \pi/19 < t_{red}^1 < 3\pi/19$. Moreover[1], $\Re(z_2 = \beta_{2,1}(\frac{\pi}{19})) \approx 0.002 < \Re(A_1) = \frac{6}{1479}$ and $\Re(\beta_{2,1}(t_{red}^1)) \approx 0.0055 > \Re(A_2) = \frac{5}{1114}$. This shows that the arc $\overset{\frown}{A_1 A_2}$ entirely lies above $\beta_{2,1}$.

- Arc $\overset{\frown}{A_2 A_3}$.

  The vertical line through $\beta_{2,1}(t)$ cuts $\mathcal{C}\left(\frac{1}{10}, \frac{1}{10}\right)$ (the circle containing $\overset{\frown}{A_2 A_3}$) in two points. Denoting by $P_2(t)$ the highest of these two points, similar computations as above lead to:

$$\Im(P_2(t)) \geq \Im(\beta_{2,1}(t)) \iff f_2(\cos t) := \frac{1}{1805} \frac{\sin \frac{2\pi}{19}}{\sin \frac{\pi}{19}} \cos t + \frac{18}{1805} - \frac{\sin^2 \frac{2\pi}{19}}{361 \sin^2 \frac{\pi}{19}} \geq 0.$$

  Since f_2 is non negative on $[0.55, 1]$, we have that $f_2(\cos t)$ is non negative for $t \in [0, 0.9]$. Note that this interval contains the interval of definition $[\frac{\pi}{19}, \frac{3\pi}{19}]$ of $\beta_{2,1}$. Since $\Re(z_2) < \Re(A_2)$ and $\Re(\beta_{2,1}(\frac{3\pi}{19})) \approx 0.014 > \Re(A_3) = \frac{1}{130}$, the arc $\overset{\frown}{A_2 A_3}$ is included in the region above $\beta_{2,1}$. We thus conclude that $A_1 A_2 A_3 A_4$ lies entirely above $\beta_{2,1}$.

The blue quadrilateral $g_3(\mathcal{S}_b)$. Denote the vertices of this quadrilateral B_1, B_2, B_3, B_4 in analogy with what precedes (B_1 is the bottom left vertex of the quadrilateral, B_2 the bottom right one, B_3 the top right one and B_4 the top left one). We compute $B_1 = \frac{2+20i}{505}, B_2 = \frac{3+25i}{634}, B_3 = \frac{1+4i}{51}, B_4 = \frac{10+48i}{601}$. Again, it is enough to show that the curvilinear sides $\overset{\frown}{B_1 B_2}$ and $\overset{\frown}{B_2 B_3}$ lie above the lower boundary of $\mathcal{M}_{19}$.

- Arc $\overset{\frown}{B_1 B_2}$.

  The vertical line passing by $\beta_{2,1}(t)$ cuts $\mathcal{C}\left(\frac{i}{50}, \frac{1}{50}\right)$ (the circle containing $\overset{\frown}{B_1 B_2}$ in two points. Let $Q_1(t)$ denotes the highest of this points. We have

$$\Im(Q_1(t)) \geq \Im(\beta_{2,1}(t)) \iff$$

$$f_3(\cos t) := \frac{4 \sin \frac{2\pi}{19}}{361 \sin \frac{\pi}{19}} \cos t + \frac{\sin \frac{2\pi}{19}}{475 \sin \frac{\pi}{19}} \sqrt{1 - \cos^2 t} - \frac{4}{361} - \frac{\sin^2 \frac{2\pi}{19}}{361 \sin^2 \frac{\pi}{19}} \geq 0.$$

---

[1] Here and in the sequel, we write $x \approx y$, where $y = \sum_{i=k}^{l} d_i 10^i$ is a decimal with $d_k \neq 0$, to mean that $|x - y| < 10^k$.

Furthermore, f_3 is non negative on $[0.94, 1]$, so that $f_3(\cos t)$ is non negative on $[0, t^1_{blue} := 0.3]$. Note that $0 < \pi/19 < 0.3 < 3\pi/19$. Moreover, $\Re(z_2) \approx 0.002 < \Re(B_1) = \frac{2}{505}$ and $\Re(\beta_{2,1}(t^1_{blue})) \approx 0.008 > \Re(B_2) = \frac{3}{634}$, which implies that $\overset{\frown}{B_1 B_2}$ lies entirely above $\beta_{2,1}$.

- Arc $\overset{\frown}{B_2 B_3}$. Denote by $Q_2(t)$ the highest intersection point of the vertical line passing through $\beta_{2,1}(t)$ with $\mathcal{C}\left(\frac{1}{6}, \frac{1}{6}\right)$ (the circle containing $\overset{\frown}{B_2 B_3}$). We have

$$\Im(Q_2(t)) \geq \Im(\beta_{2,1}(t)) \iff f_4(\cos t) := -\frac{7\sin\frac{2\pi}{19}}{1083\sin\frac{\pi}{19}}\cos t + \frac{26}{1083} - \frac{\sin^2\frac{2\pi}{19}}{361\sin^2\frac{\pi}{19}} \geq 0.$$

Since f_4 is non negative on $[-1, 1]$ and $\Re(z_2) < \Re(B_2)$, it follows that $\overset{\frown}{B_2 B_3}$ is above $\beta_{2,1}$ over the interval $[\Re(B_2), \Re(\beta_{1,2}(\frac{3\pi}{19}))]$. Let $\bar{\beta}_{2,2}$ be the supporting line of $\beta_{2,2}$. The point of $\bar{\beta}_{2,2}$ on the same vertical as B_2 is $Q_3 := \beta_{2,2}\left(\frac{1211\sin\frac{\pi}{19}}{634\cos\frac{15\pi}{38}}\right)$, while the point of $\beta_{2,2}$ in the same vertical line as B_3 is $Q_4 := \beta_{2,2}\left(t^2_{blue} := \frac{83\sin\frac{\pi}{19}}{51\cos\frac{15\pi}{38}}\right)$. Observe that $t^2_{blue} \in [\cos\frac{16\pi}{19}, \cos\frac{3\pi}{19}]$. We compute $\Im(Q_3) \approx 0.02 < \Im(B_2) = \frac{25}{634}$ and $\Im(Q_4) \approx 0.06 < \Im(B_3) = \frac{4}{51}$. By concavity of $\overset{\frown}{B_2 B_3}$, we deduce that $\overset{\frown}{B_2 B_3}$ lies above $\beta_{2,2}$ over $[\Re(\beta_{2,2}(\cos\frac{3\pi}{19})), \Re(B_3)]$. We conclude that $\overset{\frown}{B_2 B_3}$ lies above $\beta_{2,1} \cup \beta_{2,2}$.

The yellow quadrilateral $g_1(\mathcal{S}_y)$. Denote the vertices of this quadrilateral analogously to what precedes. One computes

$$C_1 = \frac{2 + 48i}{577}, C_2 = \frac{1 + 12i}{145}, C_3 = \frac{1 + i}{2}, C_4 = \frac{1 + \sqrt{3}i}{2} = e^{i\frac{\pi}{3}}.$$

We show that the curvilinear sides $\overset{\frown}{C_1 C_2}$ and $\overset{\frown}{C_2 C_3}$ lie above the lower boundary of $\mathcal{M}_{19}$.

- Arc $\overset{\frown}{C_1 C_2}$. Let $R_1(t)$ be the highest intersection point of the vertical line through $\beta_{2,1}(t)$ with $\mathcal{C}\left(\frac{i}{24}, \frac{1}{24}\right)$ (the circle containing $\overset{\frown}{C_1 C_2}$). We have

$$\Im(R_1(t)) \geq \Im(\beta_{2,1}(t)) \iff$$
$$f_5(\cos t) := \frac{8\cos\frac{\pi}{19}}{361}\cos t + \frac{\cos\frac{\pi}{19}}{114}\sqrt{1 - \cos^2(t)} - \frac{6 + 2\cos\frac{2\pi}{19}}{361} \geq 0.$$

Since f_5 is non negative on $[0.8, 1]$, it ensues that $f_5(\cos t)$ is non negative for t in $[0, 0.6]$. This interval contains $[\frac{\pi}{19}, \frac{3\pi}{19}]$. As $\Re(z_2) \approx 0.002 < \Re(C_1) = \frac{2}{577}$ and $\Re(\beta_{2,1}(\frac{3\pi}{19})) \approx 0.02 > \Re(C_2) = \frac{1}{145}$, we conclude that $\overset{\frown}{C_1 C_2}$ lies entirely above $\beta_{2,1}$.

- Arc $\overset{\frown}{C_2 C_3}$. First we note that if a point z with $\Re(C_3) \leq \Re(z) \leq \frac{1}{2}$ belongs to $\mathcal{B}\left(\frac{1}{2}, \frac{1}{2}\right)$, then it lies below the arc $\overset{\frown}{C_2 C_3}$. Thus to show that $\beta_{i,j}(t)$ is below $\overset{\frown}{C_2 C_3}$ it is sufficient to show that $|\beta_{i,j}(t) - \frac{1}{2}| \leq \frac{1}{2}$.
We have

$$|\beta_{1,2}(t) - \frac{1}{2}| \leq \frac{1}{2} \iff f_6(\cos t) := \frac{15\sin\frac{2\pi}{19}}{361\sin\frac{\pi}{19}}\cos t + \frac{\sin^2\frac{2\pi}{19}}{361\sin^2\frac{\pi}{19}} - \frac{34}{361} \geq 0.$$

Since f_6 is non positive on $[-1, 1]$, it follows that $f_6(\cos t)$ is always non positive. Hence $\overset{\frown}{C_2 C_3}$ is above $\beta_{2,1}$ over $[\Re(C_2), \Re(\beta_{2,1}(\frac{3\pi}{19}))]$.

Next, we show that $\overset{\frown}{C_2 C_3}$ lies above $\beta_{2,2}$ in the strip $\{z \mid \Re(z) \in [\Re(\beta_{2,1}(\frac{3\pi}{19})), \Re(z_7)]\}$. Let $R_{2,7}$ be the point on $\beta_{2,2}$ with real part $\Re(z_7)$. We have

$$R_{2,7} = \beta_{2,2}\left(\tau_{2,7} := \frac{(-5 + \cos\frac{5\pi}{38} \cot\frac{\pi}{19}) \sin\frac{\pi}{19}}{\sin\frac{2\pi}{19}}\right)$$

and we verify that $\tau_{2,7} \in [\cos\frac{16\pi}{19}, \cos\frac{3\pi}{19}]$ and $\Im(R_{2,7}) \approx 0.24 > \Im(z_7) \approx 0.18$. Then, to show that $\overset{\frown}{C_2 C_3}$ lies above $\beta_{2,2}$ in the above strip, it suffices by concavity of $\mathcal{B}\left(\frac{1}{2}, \frac{1}{2}\right)$ (as $\beta_{2,2}$ is a line segment) to show that $\beta_{2,2}(\cos\frac{3\pi}{19}), R_{2,7} \in \mathcal{B}\left(\frac{1}{2}, \frac{1}{2}\right)$. We indeed compute: $|\beta_{2,2}(\cos\frac{3\pi}{19}) - \frac{1}{2}|^2 \approx 0.23 < \frac{1}{4}, |R_{2,7} - \frac{1}{2}|^2 \approx 0.23 < \frac{1}{4}$.

It remains to show that the lower boundaries of $\mathcal{M}_{19,7}$ and $\mathcal{M}_{19,13}$ lie below $\overset{\frown}{C_2 C_3}$ in the strip $\{z \mid \Re(z) \in [\Re(z_7), \Re(C_3) = 1/2]\}$.

We have

$$|\beta_{7,1}(t) - \frac{1}{2}|^2 = |\beta_{7,3}(t) - \frac{1}{2}|^2 \leq \frac{1}{4} \iff$$
$$f_7(t) := \frac{\cos^2\frac{5\pi}{38}}{361\sin^2\frac{\pi}{19}}t^2 + \frac{5\cos\frac{5\pi}{38}}{361\sin\frac{\pi}{19}}t - \frac{84}{361} + \frac{\cos^2\frac{\pi}{19} + \cos\frac{\pi}{19}\sin\frac{5\pi}{38} + \sin^2\frac{5\pi}{38}}{361\sin^2\frac{\pi}{19}} \leq 0.$$

As f_7 is non positive on the interval $[-1, 1]$, which contains the domains of $\beta_{7,1}$ and $\beta_{7,3}$, we deduce that these two curves lie entirely below $\overset{\frown}{C_2 C_3}$.

We then have

$$|\beta_{7,2}(t) - \frac{1}{2}|^2 \leq \frac{1}{4} \iff f_8(\cos t) := \frac{5\cos\frac{5\pi}{38}}{361\sin\frac{\pi}{19}}\cos t - \frac{84}{361} + \frac{\cos^2\frac{5\pi}{38}}{361\sin^2\frac{\pi}{19}} \leq 0.$$

Since f_8 is non positive on $[-1, 1]$, it follows that $f_8(\cos t)$ is non positive for all t, which shows that $\beta_{7,2}$ lies below $\overset{\frown}{C_2 C_3}$.

Finally, as previously noted, since $\beta_{13,1}$ is a line segment, it suffices to show that its extremities lies below $\overset{\frown}{C_2 C_3}$ by concavity. We compute: $|z_{13} - \frac{1}{2}|^2 \approx 0.244 < \frac{1}{4}$ and $|w_{13} - \frac{1}{2}| \approx 0.1 < \frac{1}{4}$. Thus $\overset{\frown}{C_2 C_3}$ lies above $\beta_{13,1}$, and as $\Re(w_{13}) \approx 0.502 > \frac{1}{2} = \Re(C_3)$, we deduce that $\overset{\frown}{C_2 C_3}$ is included in $\mathcal{M}_{19}$.

This ends the proof of Lemma 11.

Appendix B

Proofs that the planes mentioned in section [6.5.2] are separating

First recall that the faces $Q_1'Q_0'P_1'$ and $P_1'P_2'Q_1'$ are coplanar as well as $Q_0'Q_3'P_7'$ and $P_7'P_0'Q_0'$.

$S_0'P_2'Q_1'$ **and the other faces:** Let

$$\Pi_0 := (S_0'P_2'Q_1')$$
$$= \left\{ \left(\ell_0(x,y,z) := \left(\lambda_0\tau - \lambda_1\tau^2 + \lambda_2\lambda_3 \right) x + \left(\frac{\lambda_2}{2} + \lambda_0\tau^2 - \lambda_1\tau^3 \right) y + \left(\frac{\tau}{4} - \frac{\tau^2}{2}\lambda_3 \right) z \right) = 0 \right\},$$

where $\lambda_0 = \frac{\sqrt{3}}{8+6\tau^2}, \lambda_1 = \frac{3\sqrt{3}\sqrt{1+\tau^2}}{16+12\tau^2}, \lambda_2 = \frac{\sqrt{3}}{2}\tau\sqrt{1+\tau^2}$ and $\lambda_3 = \sqrt{\frac{3}{4} - \frac{(2\sqrt{3}-3\sqrt{3}\tau\sqrt{1+\tau^2})^2}{(8+6\tau^2)^2}}$.
Then Π_0 separates $S_0'P_2'Q_1'$ and $P_2'P_1'Q_0'Q_1'$. Indeed, we check that

$$\ell_0(Q_0') = \ell_0(P_1')$$
$$= \frac{\sqrt{3}\tau^2}{16+12\tau^2} \left(2 + 3\sqrt{1+\tau^2} \left(4\sqrt{\frac{1}{4+5\tau^2-4\tau\sqrt{1+\tau^2}}} + \tau \left(-1 + 3\tau\sqrt{\frac{1}{4+5\tau^2-4\tau\sqrt{1+\tau^2}}} \right) \right) \right)$$
$$> 0$$

as $4 + 5\tau^2 - 4\tau\sqrt{1+\tau^2} < 9\tau^2$ for all τ.

Let $\Pi_1 := (Q_0'Q_1'Q_3') = \{z = -\frac{\sqrt{3}}{2}\sqrt{a^2+b^2}\}$. Then Π_1 separates the faces $S_0'P_2'Q_1'$ and $Q_0'Q_1'Q_3'$. Indeed, $z(S_0') = 0 > -\frac{\sqrt{3}}{2}\sqrt{a^2+b^2}$ while $z(P_2') = a\sin\theta_1 > -\frac{\sqrt{3}}{2}\sqrt{a^2+b^2}$ is equivalent to $(4+3\tau^2)(\tau+2\sqrt{1+\tau^2}) > 0$ which is true for all τ.

Let $\Pi_2 := \{x = 0\}$. Then Π_2 separates $S_0'P_2'Q_1'$ from all the remaining faces. Indeed, those faces have only vertices in the set $V_0 := \{P_1', Q_0', Q_3', S_0', P_0', P_7'\}$. But, we have $x(P_2') = x(Q_1') = -\frac{a}{2} < 0$, $S_0' \in \Pi_2$ while $x(P_1') = x(Q_0') = x(Q_3') = \frac{a}{2} > 0$ and $x(P_0') = x(P_7') = b\sqrt{\cos^2\theta_0 - \frac{1}{4}} > 0$.

$S_0'Q_3'P_7'$ **and the other faces:** Let

$$\Pi_3 := (S_0'Q_3'P_7')$$
$$= \left\{ \left(\ell_1(x,y,z) := \left(\frac{\lambda_2'}{2} + \lambda_0'\tau^2 - \lambda_1' \right) x + \left(\lambda_0'\tau^3 - \lambda_1'\tau + \lambda_2'\lambda_3' \right) y + \left(\frac{\tau}{4} - \frac{\lambda_3'}{2} \right) z \right) = 0 \right\},$$

with $\lambda_0' = \frac{\sqrt{3}}{6+8\tau^2}$, $\lambda_1' = \frac{3\sqrt{3}\sqrt{1+\tau^2}}{12+16\tau^2}$, $\lambda_2' = \lambda_2 = \frac{\sqrt{3}}{2}\sqrt{1+\tau^2}$, $\lambda_3' = \sqrt{\frac{3}{4} - \frac{(2\sqrt{3}\tau^2 - 3\sqrt{3}\sqrt{1+\tau^2})^2}{(6+8\tau^2)^2}}$.

Then Π_3 separates $S_0'Q_3'P_7'$ and $Q_3'Q_0'P_0'P_7'$. Indeed, $S_0', Q_3', P_7' \in \Pi_3$ while

$$\ell_1(Q_0') = \ell_1(P_0')$$
$$= \frac{\sqrt{3}}{8}\left(6\tau\sqrt{1+\tau^2}\sqrt{\frac{1}{5+4\tau^2-4\sqrt{1+\tau^2}}} + \frac{4\tau^3 - 6\tau\sqrt{1+\tau^2}}{3+4\tau^2}\right) > 0$$

as $3 + 4\tau^2 > \sqrt{5 + 4\tau^2 - 4\sqrt{1+\tau^2}}$.

The plane Π_1 separates $S_0'Q_3'P_7'$ from $Q_0'Q_1'Q_3'$. Indeed, $Q_0', Q_1', Q_3' \in \Pi_1$ while $z(S_0') = 0 > -\frac{\sqrt{3}}{2}\sqrt{a^2 + b^2}$ and $z(P_7') = b\sin(\theta_0) > -\frac{\sqrt{3}}{2}\sqrt{a^2 + b^2}$ is equivalent to $\tau^2(3 + 4\tau^2)(1 + 2\sqrt{1+\tau^2}) > 0$ which is true for all τ.

Finally, the plane $\Pi_4 := \{y = 0\}$ separates $(S_0'Q_3'P_7')$ from all the remaining faces. Indeed, all the other faces have vertices inside the set $V_1 := \{S_0', P_2', P_1', Q_1', Q_0', P_0'\}$. But, $y(Q_3') = y(P_7') = -\frac{b}{2} < 0$, $S_0' \in \Pi_4$ while $y(P_0') = y(Q_0') = y(Q_1') = \frac{b}{2} > 0$ and $y(P_1') = y(P_2') = a\sqrt{\cos^2\theta_1 - \frac{1}{4}} > 0$.

$Q_0'Q_1'Q_3'$ and the other faces: We show that the plane $\Pi_1 = (Q_0'Q_1'Q_3')$ is separating, by showing that all the vertices distinct from Q_0', Q_1' and Q_3' are on the same side of Π_1. We indeed already checked that: $z(S_0') > 0$, $z(P_1') = z(P_2') = a\sin\theta_1 > -\frac{\sqrt{3}}{2}\sqrt{a^2 + b^2}$ and $z(P_0') = z(P_7') = b\sin\theta_0 > -\frac{\sqrt{3}}{2}\sqrt{a^2 + b^2}$.

$P_1'P_2'Q_1'Q_0'$ and the other faces: Let

$$\Pi_5 = (P_1'P_2'Q_1'Q_0')$$
$$= \left\{\left(\ell_2(x,y,z) := \left(-\lambda_2 - 2\lambda_0\tau^2 + 2\lambda_1\tau^3\right)\left(y - \frac{1}{2}\right) + \left(-\frac{\tau}{2} + \tau^2\lambda_3\right)\left(z + \frac{\sqrt{3}}{2}\sqrt{1+\tau^2}\right)\right) = 0\right\}.$$

Then Π_5 separates $P_1'P_2'Q_1'Q_0'$ from $Q_0'Q_3'P_7'P_0'$. Indeed, $P_1', P_2', Q_1', Q_0' \in \Pi_5$. Moreover,

$\ell_2(Q_3') = \frac{\sqrt{3}\tau(\tau + 2\sqrt{1+\tau^2})}{4+3\tau^2} > 0$, $\ell_2(P_0') = \frac{\sqrt{3}\tau^3(1+2\sqrt{1+\tau^2})\left(-1+3\tau\sqrt{\frac{1}{4+5\tau^2-4\tau\sqrt{1+\tau^2}}}\right)}{6+8\tau^2} > 0$ as $4 + 5\tau^2 -$

$4\tau\sqrt{1+\tau^2} < 9\tau^2$, and $\ell_2(P_7') = \frac{\sqrt{3}}{2}\tau\left(\frac{2\tau + 4\sqrt{1+\tau^2}}{4+3\tau^2} + \frac{\tau^2(1+2\sqrt{1+\tau^2})\left(-1+3\frac{\tau}{\sqrt{4+5\tau^2-4\tau\sqrt{1+\tau^2}}}\right)}{3+4\tau^2}\right) > $

0.

Π_5 separates also $P_1'P_2'Q_1'Q_0'$ from $P_1'Q_0'S_0'$ and $S_0'Q_0'P_0'$. Indeed, $P_1', Q_0' \in \Pi_5$, $\ell_2(P_0') > 0$ as seen previously and $\ell_2(S_0') = \frac{\sqrt{3}\tau^2\left(2+3\sqrt{1+\tau^2}\left(\frac{4}{\sqrt{4+5\tau^2-4\tau\sqrt{1+\tau^2}}} + \tau\left(-1+3\frac{\tau}{\sqrt{4+5\tau^2-4\tau\sqrt{1+\tau^2}}}\right)\right)\right)}{16+12\tau^2} > $

0.

$P_1'Q_0'S_0'$ and $S_0'Q_0'P_0'$: We have to check that some determinant is of constant sign, namely $\det(Q_0', P_0', P_1')$. After dividing the determinant by $\frac{ab^2}{8}$, we obtain:

$$\Delta = \begin{vmatrix} \tau & \sqrt{3 - 4\sin^2\theta_0} & 1 \\ 1 & 1 & \sqrt{3 - 4\sin^2\theta_1} \\ -\sqrt{3(1+\tau^2)} & 2\sin\theta_0 & 2\sin\theta_1 \end{vmatrix}.$$

Let us first do the change of variable $x = \sqrt{1 + \tau^2}$. Then we have $\sin \theta_0 = \sqrt{3} \frac{x-2}{4x-2}$ and $\sin \theta_1 = \sqrt{3} \frac{-3x\sqrt{-1+x^2}+2}{6x^2+2}$. The determinant of interest takes then the following shape: $\Delta = \frac{2(x^2-1)}{2x-1} + \frac{2\sqrt{x^2-1}}{2x-1} \left(\frac{(2-3x\sqrt{x^2-1})(x-2)}{1+3x^2} - \frac{3(x+1)}{\sqrt{5x^2-4x\sqrt{x^2-1}-1}} \right)$. We want to show that $\Delta < 0$, that is to say $\frac{\sqrt{x^2-1}(6x+1)+2(x-2)}{1+3x^2} < \frac{3(x+1)}{\sqrt{5x^2-4x\sqrt{x^2+1}-1}}$. As the two members of the inequality are positive, we can square the inequality, and obtain:

$$(1 + 3x^2)^2 \left(-8(-3 + \sqrt{-1 + x^2}) + (22 - 11x + 16\sqrt{-1 + x^2})x \right) > 0.$$

It is equivalent to: $(16x - 8)\sqrt{-1 + x^2} > 11x^2 - 22x - 24$. Setting $f(x) = \sqrt{1 - \frac{1}{x^2}}$, we have by taking the order two Taylor expansion of f at ∞: $5x^2 + 14x + 16 + \frac{4}{x} + x(16x - 8)R_2(f)(\frac{1}{x}) > 0$ where $R_2(f)(\frac{1}{x}) = -\frac{1}{8x^4} - \frac{1}{16x^6} - \dots$ is the order two rest in the Taylor expansion of f at ∞. But $R_2(f) = R_3(f)$, and we have: $|R_3(f)| \le \frac{1}{24x^4}$ by Taylor-Lagrange inequality as $|f| \le 1$. Now the desired inequality is implied by: $5x^2 + 14x + 16 + \frac{4}{x} > \frac{16x^2+8x}{24x^4} = \frac{2}{3x^2} + \frac{1}{3x^3}$ which is clearly true for $x \ge \sqrt{2}$ (that corresponds to $\tau \ge 1$).

$Q_0'Q_3'P_7'P_0'$ **and the two faces** $P_1'Q_0'S_0'$ **and** $S_0'Q_0'P_0'$: We see that the plane $(S_0'Q_0'P_0')$ separates at the same time $Q_0'Q_3'P_7'P_0'$ from $P_1'Q_0'S_0'$ and $S_0'Q_0'P_0'$. We have already checked that, denoting $[P_0', Q_0', X]$ the determinant of the three vectors $\overrightarrow{S_0'P_0'}, \overrightarrow{S_0'Q_0'}$ and $\overrightarrow{S_0'X}$, $[P_0', Q_0', P_1'] < 0$. It remains to show that $[P_0', Q_0', P_7'] > 0$ and $[P_0', Q_0', Q_3'] > 0$.

Denote by $\omega := [P_0', Q_0', P_7']$. We have:

$$\Delta' = \frac{b^2}{2} \begin{vmatrix} a & \sqrt{\frac{3}{4} - \sin^2\theta_0} & \sqrt{\frac{3}{4} - \sin^2\theta_0} \\ b & \frac{1}{2} & -\frac{1}{2} \\ -\sqrt{3(a^2 + b^2)} & \sin\theta_0 & \sin\theta_0 \end{vmatrix} = \frac{b^2}{2} \left(a\sin\theta_0 + \sqrt{3(a^2 + b^2)}\sqrt{\frac{3}{4} - \sin^2\theta_0} \right).$$

Hence:

$$\omega := \frac{\Delta'}{b^2/2} = \tau \sin\theta_0 + \sqrt{3(1 + \tau^2)(\frac{3}{4} - \sin^2\theta_0)}.$$

Using formula (6.6), we deduce that:

$$\omega = \frac{\sqrt{3}\tau \left(2\tau^2 - 3\sqrt{1 + \tau^2} \right)}{8\tau^2 + 6} + \frac{3}{2} \frac{\sqrt{(1 + \tau^2)(12\tau^4 + 15\tau^2 + 12\sqrt{1 + \tau^2})}}{4\tau^2 + 3}.$$

Applying the change of variable $x = \sqrt{1 + \tau^2}$ gives us:

$$\omega = \frac{1}{8x^2 - 2} \left(\sqrt{3(x^2 - 1)}(2x^2 - 3x - 2) + 3x\sqrt{12x^4 - 9x^2 + 12x - 3} \right).$$

We easily check that $(8x^2 - 2)\omega$ is increasing in x, with strictly positive value in $x = \sqrt{2}$ (corresponding to $\tau = 1$). Thus, $\omega > 0$.

Now, for Q_3', we compute:

$$[Q_0', P_0', Q_3'] = b \begin{vmatrix} a & \sqrt{\frac{3}{4} - \sin^2 \theta_0} & a \\ b & \frac{1}{2} & -b \\ -\sqrt{3(a^2 + b^2)} & \sin \theta_0 & -\sqrt{3(a^2 + b^2)} \end{vmatrix}$$

$$= 2b^2 \left(a \sin \theta_0 + \sqrt{3(a^2 + b^2)} \sqrt{\frac{3}{4} - \sin^2 \theta_0} \right)$$

that is proportional to Δ'. Hence, $[Q_0', P_0', Q_3'] > 0$, and $(S_0' Q_0' P_0')$ separates both $Q_0' Q_3' P_7' P_0'$ and $P_1' Q_0' S_0'$ from $S_0' Q_0' P_0'$.

Index

Nomenclature

$\Im z$ imaginary part of a complex number z

$\mathbb{E}^n$ $\mathbb{R}^n$ endowed with its canonical Euclidean structure

$\mathbb{H}^2$ Poincaré's half-plane

$\mathbb{T}_\tau$ flat torus with modulus τ: $\mathbb{C}/\left(\mathbb{Z}+\mathbb{Z}\tau\right)$

$\mathcal{D}_{n,d}^{a,h}$ diplotorus of parameter (n,d,a,h)

$\mathcal{H}(\mu=(m_1,...,m_n))$ Moduli space of translation surfaces with n singularities of order $m_1,...,m_n$; typically $\mu=(2)$ or $\mu=(1,1)$ in this thesis

$\mathcal{H}_g$ moduli space of translation surfaces of genus g

$\mathcal{M}_g$ moduli space of closed Riemann surfaces of genus g

$\mathcal{T}_g$ Teichmüller space of Riemann surfaces of genus g

$\mathscr{M}$ modular curve or moduli space for flat tori, identified with $\mathbb{H}^2/\mathrm{PSL}_2(\mathbb{Z})$

$\mathscr{Q}(S_g, Z, \mu)$ Teichmüller space of translation surfaces of genus g, set of singularities Z and multi-index μ representing the orders at singularities

$\Phi_\mathcal{B}(\omega)$ period coordinates of the translation surface (Σ, ω) in the homology basis $\mathcal{B}$

$\pi_1(X, x)$ Fundamental group of loops in X based at x

$\Re z$ real part of a complex number z

$\mathrm{MCG}(S_g)$ mapping class group of the topological surface of genus g

$\widehat{\mathbb{C}}$ Riemann sphere

$\widetilde{X}$ universal cover of a topological space X

f^* pull-back morphism associated to a smooth map f

f_* morphism induced in homology by a continuous map f, or push-forward morphism associated to a smooth map f

$J_z f$ Jacobian of a map f

S_g closed orientable topological surface of genus g

Bibliography

[Ale06]   A.D. Alexandrov. *Intrisic Geometry of Convex Surfaces.* Chapman and Hall/CRC Taylo and Francis Group, 2006. (translation of the 1948 Russian original).

[ALM21]   Pierre Arnoux, Samuel Lelièvre, and Alba Málaga. Diplotori: a family of polyhedral flat tori. In preparation, 2021.

[Ban88]   Thomas F. Banchoff. Geometry of the Hopf mapping and Pinkall's tori of given conformal type. In Martin C. Tangora, editor, *Computers in algebra*, volume 111 of *Lecture notes in pure and applied mathematics*, pages 57–62. M. Dekker, 1988.

[BBI⁺01]   Dmitri Burago, Yuri Burago, Sergei Ivanov, et al. *A course in metric geometry*, volume 33. American Mathematical Society Providence, 2001.

[BJLT13]   Vincent Borrelli, Saïd Jabrane, Francis Lazarus, and Boris Thibert. Isometric embeddings of the square flat torus in ambient space. *Ensaios Matemáticos*, 24:1–91, 2013.

[BZ60]   Yuriy Dmitrievich Burago and Viktor Abramovich Zalgaller. Polyhedral realizations of developments (in Russian). *Vestnik Leningrad. Univ*, 15:66–80, 1960.

[BZ95]   Yuriy Dmitrievich Burago and Viktor Abramovich Zalgaller. Isometric piecewise-linear imbeddings of two-dimensional manifolds with a polyhedral metric into $\mathbb{R}^3$. *Algebra i analiz*, 7(3):76–95, 1995. Transl. in St Petersburg Math. J. (7)3:369–385.

[DHV24]   Vincent Delecroix, Pascal Hubert, and Ferrán Valdez. Infinite translation surfaces in the wild. *arXiv preprint arXiv:2403.05424*, 2024.

[DM68]   PH Doyle and Daniel A Moran. A short proof that compact 2-manifolds can be triangulated. *Inventiones mathematicae*, 5(2):160–162, 1968.

[FM13]   Giovanni Forni and Carlos Matheus. Introduction to teichmüller theory and its applications to dynamics of interval exchange transformations, flows on surfaces and billiards. *arXiv preprint arXiv:1311.2758*, 2013.

[GX⁺13]   Jean H Gallier, Dianna Xu, et al. *A guide to the classification theorem for compact surfaces.* Springer, 2013.

[Hat13]   Allen Hatcher. The kirby torus trick for surfaces. *arXiv preprint arXiv:1312.3518*, 2013.

[Hub06]   John H Hubbard. *Teichmüller theory and applications to geometry, topology, and dynamics*, volume 1. Matrix Editions, 2006.

[iIY09]   Jin ichi Itoha and Liping Yuan. Acute triangulations of flat tori. *European journal of combinatorics*, 30:1–4, 2009.

[IT12]   Yoichi Imayoshi and Masahiko Taniguchi. *An introduction to Teichmüller spaces.* Springer Science & Business Media, 2012.

[JS87]   Gareth A Jones and David Singerman. *Complex functions: an algebraic and geometric viewpoint.* Cambridge university press, 1987.

[Kui55]   Nicolaas Kuiper. On C^1-isometric imbeddings. *Indagationes Mathematicae*, 17:545–555, 1955.

[Laz20]   Francis Lazarus. Some Algorithmic Aspects of PL Embeddings, 2020.

[Mas19]   William S Massey. *A basic course in algebraic topology*, volume 127. Springer, 2019.

[Mas22]   Daniel Massart. A short introduction to translation surfaces, veech surfaces, and teichmüller dynamics. In *Surveys in geometry I*, pages 343–388. Springer, 2022.

[McM]   Curtis McMullen. Complex analysis on Riemann surfaces.

[Moi13]   Edwin E Moise. *Geometric topology in dimensions 2 and 3*, volume 47. Springer Science & Business Media, 2013.

[Mum71]   David Mumford. A remark on Mahler's compactness theorem. *Proceedings of the American Mathematical Society*, 28(1):289–294, 1971.

[Nas54]   John F. Nash. C^1-isometric imbeddings. *Annals of Mathematics*, 60(3):383–396, 1954.

[Ngu14]   Duc-Manh Nguyen. On the topology of $\mathcal{H}(2)$. *Groups, Geometry, and Dynamics*, 8:513–551, 2014.

[Pak06]   Igor Pak. Inflating polyhedral surfaces. *Preprint, Department of Mathematics, MIT*, 326, 2006.

[Pet24]   Bram Petri. Introduction to Teichmüller theory, 2024.

[Pin85]   Ulrich Pinkall. Hopf tori in S^3. *Inventiones mathematicae*, 81(2):379–386, 1985.

[Qui20]   Tanessi Quintanar. An explicit PL-embedding of the square flat torus into $\mathbb{E}^3$. *Journal of Computational Geometry*, 11(1):615–628, 2020.

[Sik18]   Jean-Claude Sikorav. Advanced geometry, 2018.

[Tho92]   Carsten Thomassen. The jordan-schönflies theorem and the classification of surfaces. *The American Mathematical Monthly*, 99(2):116–130, 1992.

[Tro86]   Marc Troyanov. Les surfaces euclidiennes à singularités coniques.(euclidean surfaces with cone singularities). *L'enseignement Mathématique*, 32:79–94, 1986.

[Tsu20]   Takashi Tsuboi. On origami embeddings of flat tori. *arXiv preprint arXiv:2007.03434*, 2020.

[Vee86]   William A Veech. The teichmuller geodesic flow. *Annals of Mathematics*, 124(3):441–530, 1986.

[Vee90]   William A Veech. Moduli spaces of quadratic differentials. *Journal d'analyse mathématique*, 55(1):117–171, 1990.

[Wel16]   Jean-Yves Welschinger. Surfaces de Riemann, May 2016.

[Wri15]   Alex Wright. Translation surfaces and their orbit closures: An introduction for a broad audience. *EMS Surveys in Mathematical Sciences*, 2:63–108, 2015.

[Yoc10]   Jean-Christophe Yoccoz. Interval exchange maps and translation surfaces. *Homogeneous flows, moduli spaces and arithmetic*, 10:1–69, 2010.

[Zal00]   V. A. Zalgaller. Some bendings of a long cylinder. *Journal of Mathematical Sciences*, 100(3):2228–2238, 2000.

[Zam13]   Carol T. Zamfirescu. Survey of two-dimensional acute triangulations. *Discrete Mathematics*, 313(1):35–49, 2013.